CONCEPTS NREC

TECHNICAL MEMORANDUM NO. 1761
Concepts NREC Project No. 10274
Prepared for: The Department of Energy (DOE)
Award Number: DE-SC0001692
Project Director: Dan Hinch
Project Manager: Francis A. Di Bella
By: Francis A. Di Bella
August 29, 2014

PHASES I AND II
FINAL REPORT
DE-SC0001692

SELF-ADAPTIVE AIR TURBINE FOR WAVE ENERGY CONVERSION USING TURBINE SHUTTER VALVE AND OWC HEIGHT CONTROL SYSTEM

Corporate Headquarters:
217 Billings Farm Road
White River Jct., VT 05001-9486 USA
Tel: (802) 296-2321 Fax: (802) 296-2325

www.conceptsnrec.com
sales@conceptsnrec.com

Boston Office:
285 Billerica Road, Suite 102
Chelmsford, MA 01824-4174 USA
Tel: (781) 935-9050 Fax: (978) 596-0622

TECHNICAL MEMORANDUM NO. 1761
PHASES I AND II FINAL REPORT:
SELF-ADAPTIVE AIR TURBINE FOR WAVE ENERGY CONVERSION USING TURBINE SHUTTER VALVE AND OWC HEIGHT CONTROL SYSTEM

TABLE OF CONTENTS

TABLES

FIGURES

TECHNICAL MEMORANDUM NO. 1761
Concepts NREC Project No. 10274
Prepared for: The Department of Energy (DOE)
Award Number: DE-SC0001692
Project Director: Dan Hinch
Project Manager: Francis A. Di Bella
By: Francis A. Di Bella
August 29, 2014

PHASES I AND II FINAL REPORT: SELF-ADAPTIVE AIR TURBINE FOR WAVE ENERGY CONVERSION USING TURBINE SHUTTER VALVE AND OWC HEIGHT CONTROL SYSTEM

1.0 CONTRACT INFORMATION

Project Title: Development of Self-Adaptive Air Turbine for Wave Energy Conversion Using an Oscillating Water Column

Topic Number: 19. Advanced Water Power Technology Development

Subtopic Letter: a. Wave and Current Energy Technologies

Covering Period: Phases I and II Final Report; Reporting Period: 08/2009 to 08/2012

Date of Report: August 29, 2014

Recipient: Concepts ETI, Inc., d.b.a. Concepts NREC (*CN*), 217 Billings Farm Road, White River Junction, VT 05001

Principal Investigator: Francis A. Di Bella, PE, Chelmsford, MA Office; 781-937-4718

Award Number: DE-SC0001692

2.0 PROJECT SIGNIFICANCE, BACKGROUND INFORMATION, AND TECHNICAL RESULTS OF THE PHASE I EFFORT TO IMPROVE WAVE ENERGY RECOVERY EFFICIENCY

2.1 Identification and Significance of Initial Problem and Technical Approach

An oscillating water column (OWC) is one of the most technically viable options for converting wave energy into useful electric power. The OWC system uses the wave energy to "push or pull" air through a high-speed turbine, as illustrated in Figure 1. The turbine is typically a bi-directional turbine, such as a Wells turbine or an advanced Dennis-Auld turbine, as developed by Oceanlinx Ltd. (Oceanlinx), a major developer of OWC systems and a major collaborator with Concepts NREC (*CN*) in Phase II of this STTR effort. Prior to awarding the STTR to *CN*, work was underway by *CN* and Oceanlinx to produce a mechanical linkage mechanism that can be cost-effectively manufactured, and can articulate turbine blades to improve wave energy capture. The articulation is controlled by monitoring the chamber pressure. Funding has been made available from the U.S. Department of Energy (DOE) to *CN* (DOE DE-FG-08GO18171) to co-share the development of a blade articulation mechanism for the purpose of increasing energy recovery. However, articulating the blades is only one of the many effective design improvements that can be made to the composite subsystems that constitute the turbine generator system.

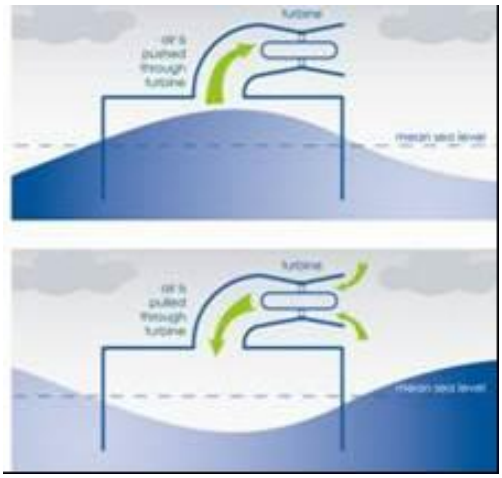

Figure 1. Conceptual Layout of the OWC Demonstrating Functionality

The energy conversion step from the water column to pneumatic power in an OWC system is affected by the turbine volume flow rate and OWC chamber pressure transients, which are also affected by the relative motions of the OWC structure and the water wave at any instant. Several other methods for improving wave energy capture have been reported in the technical literature. One such example is the use of bypass valves (used in a process called latching) that are in parallel or in series with the turbine; another example is the use of power absorption devices (Falnes [1]) that can pressurize the air chamber and result in improved and more consistent power delivery. In a very early phase of its research, and first publicly identified in its Phase I proposal, CN identified an important parameter, a system time constant, T_c (units: seconds) that analytically can be shown to characterize the optimum design point for an OWC as a function of wave period. The flow characteristics of the turbine, along with other parameters of the OWC that define a time constant (T_c), are given in Equation 1. The time constant is a characteristic time parameter, which represents the pneumatic pressure decay within the OWC chamber. Using several simplifying assumptions that enable a "closed-form" classic analytical solution, the percentage (%) of recoverable wave energy pneumatic power was presented for the first time by CN, as graphically displayed in Figure 2.

$$T_c = \Delta P / P_o \times V / Q \text{ , or} \tag{1}$$

$$T_c = \sqrt{(\Delta P)} \times V / (P \times C_v) \tag{2}$$

where:

$$Q = C_v \times \sqrt{\Delta P} \tag{3}$$

and, for the first time in the Phase I proposal, C_v was identified as the flow coefficient for the OWC air chamber-turbine as an integrated system.

Figure 2 illustrates the graphical relationship of the time constant, wave period, and recoverable wave energy for a given wave amplitude. The technical literature up to this time had reported similar results using an entirely different optimizing parameter called a damping coefficient. However, what is discernible from CN's Figure 2 using the time constant, T_c, which is not discernible from using a damping coefficient, is the very conclusive observation that the optimum power recovery is always achieved when the time constant (T_c) is 1/6 x the wave period. It is also clear from Figure 2 that when the time constant, T_c, is small or very large, there is less potential for pneumatic energy recovery. When the time constant is very large, the OWC acts essentially as a very stiff gas spring, as evidenced by very high air chamber pressures that cause the OWC to "ride" the incident wave; thus, without relative motion

between the OWC structure and the wave, high recovery of the available wave energy is not possible. With very low time constants, there is very little pressure generated within the OWC, and thus little or no power generated.

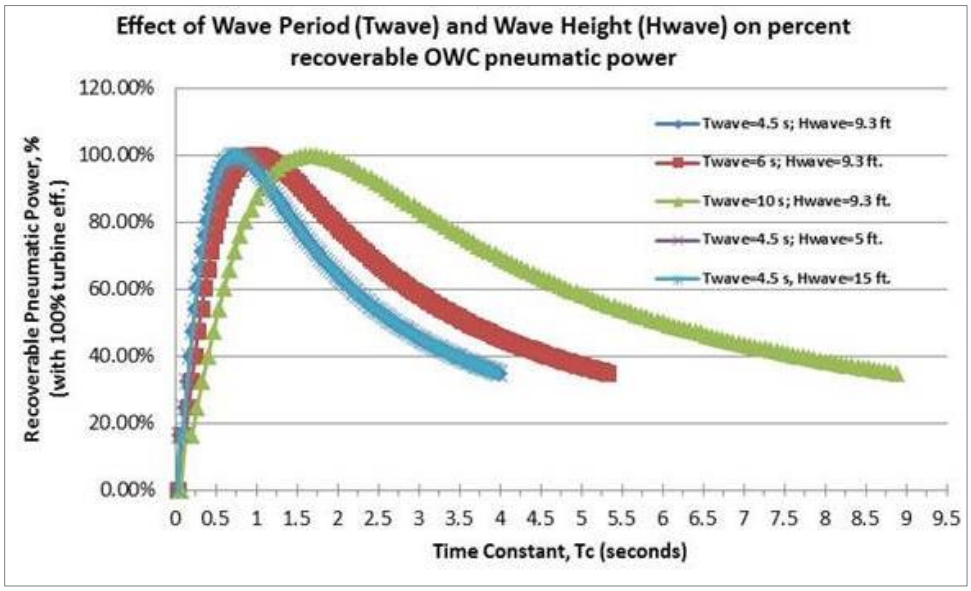

Figure 2. Relationship of the Time Constant, Wave Period, and Recoverable Wave Energy for a Given Wave Amplitude

OWC systems typically operate at low time constants that are to the left of the optimum, usually less than 1.0 seconds. Also apparent from Figure 2 is the effect of different wave periods on the amount of energy that can be recovered once the design point of the OWC system has been selected. For example, if the OWC system is designed for a 4.5-second wave period, the maximum energy recovery is 4.5/6 = .75 second. The turbine size and speed, as well as the OWC chamber size, would be designed to accommodate this time constant. However, as the incident wave energy is changed corresponding to a wave period of 10 seconds, it is clear that the optimum time constant is now 10/6 = 1.7 seconds. More importantly, however, the OWC must continue to operate at a time constant of .75 second, because all of the system's physical parameters have been fixed by the initial design point. Thus, the recoverable energy is reduced from 100% for the 4.5-second wave to approximately 60% when the 10-second wave is incident to the OWC. Thus, as may be seen from Figure 2, there is considerable unrecovered potential wave energy at time constants of 1–1.5 seconds. In summary, proceeding to the left or the right of the optimum 100% recoverable energy design point, the recovery energy is less than 100%. It was the goal of the Phase I STTR effort to identify ways of "tuning" the OWC system in an attempt to recover this otherwise lost wave energy potential. The Phase I STTR study has succeeded in identifying how much of this heretofore unrecovered energy can be returned to the power turbine, and with a means that is entirely affordable and not inherently prone to engineering risk.

With this analytical revelation and to more easily discern which mechanical and electrical subsystems can provide improvements in OWC wave energy recovery for Oceanlinx's OWC systems, *CN* identified two categories of these OWC systems: MACRO Wave Energy Dynamics (WED) and MICRO WED.

MACRO WED (pertaining to magnitude of wave period and amplitude):

1. "Tuning" the OWC turbine system so that the system operates at the theoretical maximum power recovery with respect to the OWC system's time constant, T_c; the design of a diffuser at the inlet and discharge of the bi-directional turbine

that can have a variable aspect ratio, so as to optimize the diffuser's pressure recovery efficiency through the range of changing air flow rate and chamber pressure profiles. Once again, this will effect a change in the C_v for the composite turbine generator system.

2. Adjusting the oscillation of the OWC structure so that it is 180 degrees out of phase, with the incident wave using adaptive controls; this can be affected by, for example, damping the OWC via varying the projected area of the stabilizer-heave plates by adjusting the orientation of the plates. This is an interesting area for future research but is not part of the turbine generator composite system options that was considered in Phase I of the project.

MICRO WED (pertaining to effects of wave cycles in the OWC chamber)

1. The design of a variable aperture that works similarly to the iris in the human eye to open and close the flow through the turbine and thus affect the velocity through the turbine blades, which would then affect the overall flow coefficient, C_v, for the turbine system. The aperture would be installed at the hub of the turbine and open from the outer radius to admit flow into the turbine, thus controlling the chamber pressure by maintaining flow control of the air though the turbine, which would affect the variable flow coefficient for the turbine system.

2. The design of flexible blade profiles (along the blade axis) that self-adapt to the instantaneous pressure in the OWC chamber, and thus to the pressure at the leading edge of the turbine blade.

3. The design of an effective means of articulating the blade in order to continually optimize the aerodynamics of the turbine blade during each intake and discharge "stroke" of the wave. This is currently being explored via DOE funding.

MICRO WED system improvements are associated closely with how the ascending and descending wave fronts affect the chamber pressure and air volume flow rates. The MACRO WED system improvements are closely associated with how the amplitude and periods of the wave energy affect the dynamics of the OWC structure. Improvements in subsystems that involve the turbine generator being treated as a composite system can have origins in the MICRO or MACRO WED. As an example of one such modification, consider the Dennis-Auld turbine that is being designed by Oceanlinx with contributions made by *CN*. This turbine utilizes a mechanical mechanism to vary the pitch of the blades through a feedback control loop that measures the velocity, direction of the airflow, and inlet pressure.

In order to quantify the improvements that can be achieved in each of these areas within each MACRO or MICRO category, it was necessary for *CN* to develop an "engineering-friendly" numerical model of an OWC wave energy conversion system that could be used as an effective engineering tool to determine the design of the OWC subsystems and predict the integrated performance as a complete system. The STTR awarded by the DOE provided an opportunity to perfect this numerical model. As a result, *CN* has developed a new means of modeling an OWC performance that was previously unknown, or at least unreported in the technical literature. The basis for this numerical model is as straightforward as is its ability to provide greater physical insight into the behavior of an OWC system as it is acted upon by incident waves of fluctuating wave amplitudes and frequency. This improved insight leads to improved engineering solutions on how to increase wave energy capture. The algorithms used in the numerical model are based on the Conservation of Energy principle applied to the potential energy content of waves. The solution technique, henceforth identified in this final report as the Energy Conservation Methodology, is thought to be a vast improvement over the published technical studies for the modeling of OWC system performance, in that it eliminates the dependency on mathematical series solutions and the use of computational fluid dynamics

modeling of the interaction of the wave and the OWC device. Of particular importance to the use of this algorithm is the ability to use only the energy content of the wave, as defined by kW/meter or energy per area, without the need to stochastically account for the variation of the wave frequency and amplitude over time.

As a direct result of the Phase I STTR effort, two methods were identified as enabling the improvement of wave energy recovery by as much as 30%, as shown in Figure 3: 1) the cyclic starting and stopping of air flow to the turbine, and 2) controlling the OWC height in the water. The magnitude of the improvement has been determined and quantified by *CN*'s numerical model. The numerical model has been validated by wave-tank experiments conducted by the Maine Maritime Academy (MMA) under the supervision of Professor Patrick Lorenz, Project Collaborator during the Phase I effort. This improvement can be affected by the integration of a single device, identified as a "turbine shutter valve" (shown schematically in Figure 4), along with the control of the buoyancy of the OWC system (i.e., affecting the height of the air chamber above the mean water level as a function of the wave's period (T_{wave}).

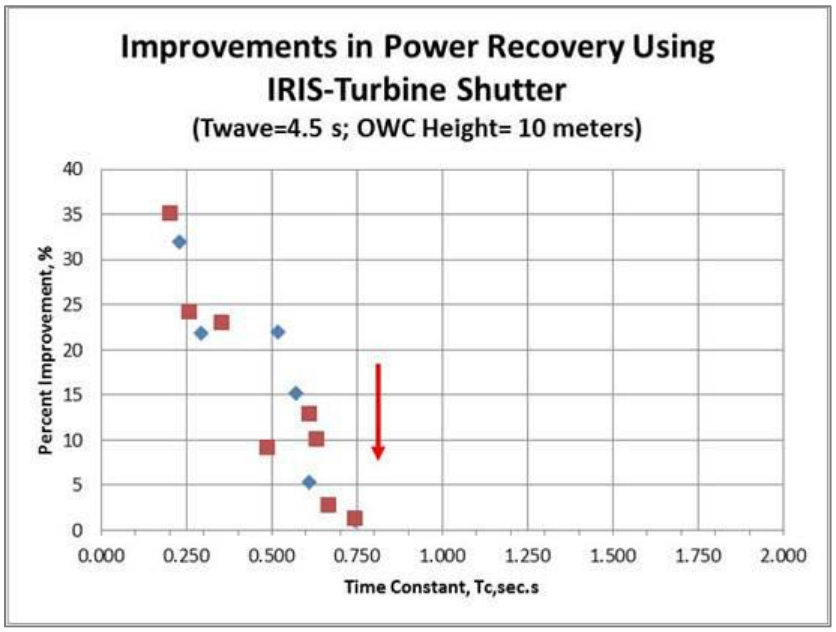

Figure 3. Wave Energy Recovery

The turbine shutter valve is a mechanical subsystem that is designed to quickly shut off the air flow to the turbine during the initial ascension (or "up stroke") of the wave into the OWC chamber and during the last moments of its descension (or "down stroke"). The turbine shutter valve can also affect the control of the relative phasing of the OWC, with the incident wave causing the OWC to be 180 degrees out-of-phase with the incident wave. The OWC phasing results in the OWC descending as the wave ascends, and this increases the relative speed between the wave and the OWC device, and in turn, enables higher operating pressures within the OWC chamber. The innovation discovered from the Phase I STTR effort includes the correct initiation of the ON/OFF timing and the duration of the turbine shutter valve, as well as when to adjust the height of the OWC above the mean water line via the existing OWC buoyancy system as a function of the wave frequency and amplitude.

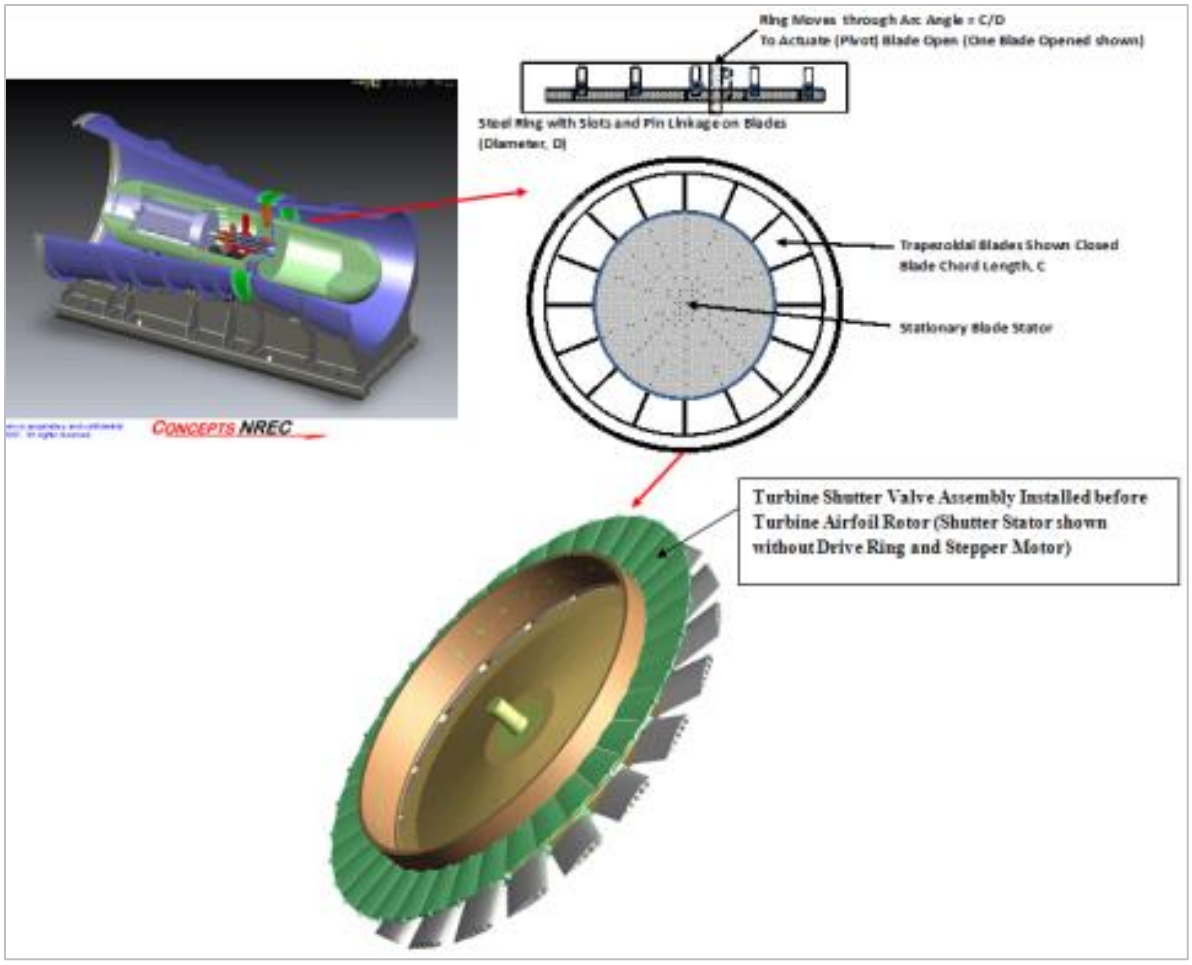

Figure 4. Turbine Shutter Valve

The cost of prototype-level OWC systems is relatively high, at $8,000 per kW, while future economy of scale units rated up to 23 MW are estimated to have a projected capital cost of $4,000 per kW [2]. Increasing the capture efficiency has the largest impact on decreasing the cost per kW ($/kWe) for the OWC system. A 2003 study [2] by The Carbon Trust, entitled "Oscillating Water Column Wave Energy Converter Evaluation Report," suggested that the goal of reaching a competitive price for the generated electric power from an OWC system would require "… a combination of capture efficiency being increased by 10% to a (net) of 52%" after considering the electric power turbine generator efficiency. *CN*'s innovations that have been outlined above, and are explained in this report, are seen as important contributions to the OWC design field of study and ultimately enable more wave energy to be recovered from incident waves that have a wider range of wave frequency and amplitudes. The net consequence is a reduction in the cost per kW ($/kW) of the system by as much as 22%, as summarized in Table I. Table I correctly accounts for the energy savings that can be attributed to an OWC subsystem, but then also accounts for any costs (or savings) for additional (or fewer) components needed to affect these savings.

TABLE I. COST SAVINGS

Ref: # 41; page 283 averages from 3 OWC systems

			Component Costs			$cost adder for Additional	
			$present	% reduction	$final cost	Component(s)	% Improvement Energy Recover
System Availability, %	85%						
OWC Base Cost , $/kWe	6000						
Kwe=	350						
OWC Cost	$2,100,000						
Mechanical & Electric Systems, %	0.3		$ 630,000				
Generator		0.07	$ 147,000	0.00%	$ 147,000	$ -	2.0%
Turbine		0.075	$ 157,500	5.00%	$ 169,625	$ 20,000	25.0%
Diffuser & Inlet Guide Vanes		0.025	$ 52,500	7.50%	$ 48,563	$ -	0.0%
Structural Framework		0.05	$ 105,000	0.00%	$ 115,000	$ 10,000	0.0%
Controls		0.08	$ 168,000	5.00%	$ 159,600	$ -	1.0%
Installation, %	0.15		$ 315,000				
Mechanical		0.1	$ 210,000	0.0%	$ 210,000	$ -	0.0%
Electrical		0.05	$ 105,000	0.0%	$ 105,000	$ -	0.0%
Vessel Construction, %	0.25		$ 525,000	0.0%	$ 525,000	$ -	
Electrical Trans., %	0.05		$ 105,000	10.0%	$ 94,500	$ -	0.0%
Contingencies, %	0.1		$ 210,000	0.0%	$ 210,000	$ -	
Transportation, %	0.15		$ 315,000	0.0%	$ 315,000	$ -	0.0%
	1.00		$ 2,100,000		$ 2,099,288	$ 30,000	

NET OWC Cost Savings,%	0.03%	Energy Improv.=	28.0%
NET Effective $/kWe=	4,686		
Net Improvement, $/kWe %=	22%		
$O&M=	0.02	$/kwH	
$finance=	0.06	$/kwH	
$/kWh)income=	0.15	$/kWh	
Yearly Income=	$ 229,242		
Simple Payback=	0.47	years	

The reduction in the first-time cost $/kWe is essential if the economics of a wave energy conversion device using the OWC principle is to be high enough for its adaptation. The overall wave-to-electric efficiencies of conventional OWC systems are often less than 25% [2], which results in an increase in the effective cost per kW ($/kWe) for the OWC system.

A large number of OWC water wave energy recovery systems have been constructed over the past 30 years, either on the shoreline, near the shoreline, or in the breakwater in a number of countries [2]. There are over 60 companies currently engaged in the development of ocean wave energy devices [3]. These systems include subsurface hydroturbines, oscillating buoys, OWCs, and many other devices. In general, near-shore OWCs have an overall efficiency of wave energy to electric power of 10% to 25% [2] consisting of: 42% of the wave energy converted to pneumatic power, 65% of the pneumatic power converted to mechanical power, and 91% of the mechanical power converted to electric power. In the 1980s, relatively small demonstration systems with ratings under 100 kW [2] were conducted by several companies, but most were installed on coast lines and thus stationary with respect to the wave vertical velocity. However, in the early 2000s, interest in OWC technology significantly increased, with Oceanlinx (Sydney, Australia) taking a leading role and moving aggressively towards the development of multi-megawatt wave farms. Their first 300-kW unit (Figure 5) is shown operating in Port Kembla, Australia, in 2000, followed by the 2012 demonstration of the Mark3 Prototype OWC (Mk3PC) in Figure 6.

Figure 5. First 300-kW Unit by Oceanlinx

Figure 6. Demonstration of the Oceanlinx Mark3 (Mk3PC) Prototype OWC

The Mk3PC was designed to accommodate multiple turbines, each with its own OWC air chamber. This system was designed and installed by Oceanlinx to be an in-water test. *CN* has worked with Oceanlinx on a privately funded project, as well as a DOE-funded project that involved researching improvements in OWC technology. Unfortunately, the original plan to use the Mk3PC in-water test facility had to be cancelled due to the destruction of the Mk3PC system after the Phase II Statement of Work (SOW) was submitted. The damage to the OWC system occurred in an unrelated test conducted by Oceanlinx before the start of the Phase II effort. The in-water testing of the advanced OWC turbine developed in the Phase II effort was then coordinated with the University of Maine and the MMA. The necessary change in the original Statement of Work is identified in Section 3.2 of this final report.

2.2 Anticipated Public Benefits

2.2.1 Technical, Economic, and Social Benefits of the Project

The purpose of the proposed research was to increase the energy recovery from a wider range of incident wave energies by optimizing the performance of the OWC system. The increase in energy recovery was estimated to be as high as 30%, depending on the wave energy intensity (which is a function of where the OWC system is sited) and the design point selected for the OWC components. This increase in energy recovery is in effect a reduction in the cost per kW for an OWC system. This cost reduction improves the economics of the OWC application and thus makes the system more attractive to entrepreneurial commercial

developers and/or governmental or institutional funding agencies. The net benefit to the world is to make available another economically attractive and viable alternative, renewable energy resource that can be used to recover the projected 1.3 x 10^{12} kW-hr energy that is available from the world's deep water oceans [3]. Assuming even a 0.1% utilization factor of the world's ocean energy, this is enough energy to power an additional 70 million households throughout the world.

2.3 Federal and Commercial Benefactors of Technology

The DOE, major energy companies, and local power utilities will gain important benefits towards the advancement of this renewable technology. This technology has the potential to provide at least as much affordable clean energy as present wind turbines, with negligible environmental impact. The OWC systems are considered to be the most viable means of recovering the world's wave energy resource, and many have been prototyped and are under testing, either on the coast lines where wave energy content is high or as floating vessels. An improvement of up to 30% in the energy recovery would effectively reduce the cost per kW for the systems and make the economics of their application much more viable.

The final product from the development effort was the turbine shutter valve assembly that enables a "next-generation, advanced adaptive OWC" method to recover more energy from incident waves that have a wider range of incident wave amplitudes and periods interacting with the OWC. The net result was more energy to recover and thus a more economic OWC on a per-kWe and per-annual kWh basis than existing systems. The market opportunity for this technology is very significant given the increased interest in the use of large-scale, renewable energy in the face of depleting fossil fuel supplies. It has been estimated by the World Energy Council that the world's oceans can provide an annual energy equivalent of 17,500 TW-hrs. The 30% projected increase in recoverable energy per kWe rating for an OWC, if the proposed subsystem redesigns are implemented, translates directly into a 30% decrease in the cost per kWe for the system. This should enable the Return on Investment for an OWC system to be even more attractive for the entrepreneurial investor, governmental world body, or private funding agency. Wave energy is much more predictable using advanced weather warnings, and is more continuously available over a span of 24 hours, even when compared to wind energy. The low-profile OWC design also does not obstruct the view of the horizon, even when used close to shore. Based on a 0.1% utilization of the available ocean energy and a marketable 1% with nominal 10-MWe OWC modules, a market of 150 OWC systems per year can be substantiated and projected.

2.4 A Summary of Phase I STTR Demonstrated Technical Feasibility of Proposed Innovations: Turbine Shutter Valve and Active Control of OWC Height

The following section of this report provides a detailed summary of *CN*'s efforts for the STTR entitled "Development of Self-Adaptive Air Turbine for Wave Energy Conversion Using an Oscillating Water Column (OWC)." This effort is in collaboration with The MMA (c/o Applied Mathematics Professor Patrick Lorenz [207-326-2145], and Mechanical Engineering Professor Richard Kimball).

2.4.1 Technical Problem Statement

The principal objective of this STTR was to improve the power recovery from a wider range of incident wave energy that may interact with an OWC system and thus effectively reduce the cost per kWe for an OWC Wave Energy Recovery System. This primary objective was further delineated into three specific objectives:

1. What are the critical design parameters and mathematical relationships for each subsystem that impact the overall system performance and can be useful in constructing a controls strategy for improving energy recovery from wave energies?

2. Which of the OWC subsystems in the MICRO WED and MACRO WED opportunities are the most viable to redesign in order to effect a change in the time constant, T_c?

3. What are the net cost savings ($/kWe) for an OWC that uses these robust designs?

These three objectives were completed by the fabrication and testing of a laboratory-size prototype OWC system that was to be deployed in the wave tank facilities maintained by the MMA, and/or by using the wave tank facilities available at the University of Maine, a companion university site. The testing of the scaled OWC system in water helped to validate the computer models that were developed in this project. Based on these validated computer and mathematical models that served as engineering design tools, the controls methodology strategy for directing the operation of the turbine shutter valve and/or the OWC height changes was better understood, and determined to be effective in maintaining the OWC at its optimum power recovery for a varying wave climate.

Present OWCs, if not all wave energy conversion (WEC) systems, are constrained in their ability to recover a range of incident wave energies by the need to select a system design point that is fixed on a nominal wave power specification. This nominal rating is then used to determine the physical size, and hence, the turbine generator system power rating. This power rating is often chosen to be somewhat higher than the expected nominal power recovery potential from the incident wave, in an attempt to recover more of the energy from a wider range of wave amplitudes. The result is a system that is often oversized, and therefore more expensive on an effective cost per kWe ($/kWe) basis.

The analysis of the dynamics between the OWC system and the incident water waves continues to evolve and mature with the research effort of many academic researchers. The Phase I STTR effort was successful in developing a unique computational (numerical) solution to the equations of energy and motion which has served to guide the feasibility analysis of the turbine generator subsystems that can best facilitate the tuning of the OWC to improve wave energy recovery over a broader spectrum of wave energy.

The *CN*-MMA collaboration produced two advanced OWC engineering computer models that have been used to identify which of the turbine generator and OWC chamber subsystems can be modified to effect an improvement in the energy capture of a wider range of ocean waves. The magnitude of the improvement of the energy recovery over time and the costs associated with these improvements, including an estimate of the operation and maintenance costs, has also been determined. The OWC engineering model also aided in defining a controls strategy based on the validation of the model's results using three independent derivations. For example, it was shown that the measurement of the changing pressure and air volume flow rates during the waxing and waning of the wave within the OWC can serve as a controls methodology and is predictable by the OWC models that were developed.

Technology Background, Concept Description, and Work Performed

There is considerable technical literature concerning the mathematical analysis and numerical modeling of an OWC system that is subject to incident water wave energy. A short list of some of the more relevant technical papers that can provide the quickest introduction to the relevant mathematical models is given in the reference section at the end of this final report (Appendix 3). This research continues to be performed by university researchers from the Departments of Applied Mathematics, Physics, and Mechanical Engineering. The review of these technical papers was conducted by MMA for this STTR. This classical formulation of a solution was complemented by the development of a computer model by *CN* that enables a basic physical insight, and thus engineering understanding, of how the component parameters can best affect the improvement of the energy capture effectiveness of the overall OWC-type of WEC system. This is particularly true when these technical articles are viewed from the

perspective of what remains to be mathematically developed that can be easily integrated into the thermo-fluid models that *CN* had already started prior to the Phase I STTR award.

CN's thermo-fluids theoretical, analytical, and numerical models of an OWC continue to be improved, but in their present form, it does appear that they provide some insight into the operation of an OWC to affect power recovery from a range of wave energies. For example, by knowing the physical size (length, width, and height) of the OWC and the relationship between the turbine's volume flow rate and chamber pressure, *CN*'s thermo-fluids models can calculate the optimum power output from the OWC for a given water wave energy; an energy which is a function of the water wave's amplitude and frequency.

However, both models depend on knowing the magnitude of the relative velocity of the water wave's free surface with respect to the OWC structure. The water's free surface velocity is also a function of the fraction of the incident wave's energy that is partitioned into useful radiant energy or that is otherwise diffracted energy, and thus cannot be captured via[1] the OWC system. These assumptions are required due to a lack of precise mathematical solution of the water wave hydrodynamics, which should lead to closed-form mathematical formula(s) or algorithm(s) that could be used to complete the engineering model(s) of the OWC. This proportionment is, in turn, very much dependent upon the physical design of the OWC structure, as well as whether this structure is fixed on the shore (and thus has a zero relative speed with respect to the inertia reference [the ground]), or whether it is allowed to float in the water (and thus may have a non-zero relative velocity with respect to the ground). For example, it has been well-established mathematically by University researchers, such as Falnes [1]; Evans and Porter [4]; Suzuki and Arakawa [5]; Sarmento and de O. Falcão [6]; de O. Falcão and Justino [7]; and Tease, Lees, and Hall [8] that an OWC without a refracting wall (see the larger, left-side vertical wall in Figure 7) will be able to recover only 50% of the wave's potential and kinetic energies; and this is before the efficiency of the power turbine is considered. The use of a reflecting wall will increase the potential recovery efficiency to 100%. The precise maximum theoretical recovery efficiency of the OWC depends on several factors; chief among these are length of the wall into the water, the width of the chamber with respect to the incident water wave length, and the water wave frequency. It has also been established that these physical parameters for the OWC can be combined with the linear or non-linear relationship between the volume flow rate (cfm) – pressure differential (ΔP) of the air turbine to determine an effective damping coefficient. Whether the damping coefficient is represented by C, D, or Beta (β) by different authors or with different system variables, all of the various forms for the damping coefficient can be reduced to:

$$(\Delta P_{avg}\ A_{owc}{}^2 / Q_{avg}) \tag{4}$$

Where: ΔP_{avg} is the turbine pressure differential (i.e., chamber pressure minus ambient pressure).

A_{owc} is footprint area.

Q_{avg} is the volume flow rate through the turbine.

Research into the modeling of OWC systems continues, and researchers have agreed that the damping coefficient is a key parameter in optimizing the power output of the OWC for a given wave energy source, and that the energy absorbed by the damping of the radiated fraction of the incident wave energy is equivalent to what potentially may be recovered by the pneumatic, oscillating column, and then by an efficient, well-engineered power recovery subsystem. With the successful development of *CN*'s energy methodology-based numerical

[1] The diffracted wave energy is that portion of the incident wave energy that is redirected away from the OWC structure, and thus, the energy content cannot be recovered by the OWC power system. The radiated energy or reflected wave energy is that portion of the incident wave energy that is available for recovery by the OWC power subsystems. Only a fraction of this radiated energy is recovered as useful energy depending on the efficiency of the type of wave energy converter and the efficiencies of the prime mover (turbine, hydraulic pumps, etc.) power subsystem.

model of OWC performance, it is now known that a more practical design parameter is the system's time constant, T_c = (units: seconds).

Figure 7 provides another simplified illustration of an OWC power conversion system. The OWC-based wave energy conversion system uses a high-speed wind turbine to recover the energy of the wave via the pressurized air that is trapped between the ascending and receding water wave front and the inlet to the turbine that is situated at the top of the OWC chamber. As the wave crest ascends within the closed chamber, the air is pushed through the turbine. As the wave recedes, the ambient air is drawn back through the wind turbine in the reverse direction driven by the differential pressure between atmospheric pressure and the partial vacuum created by the receding wave. The wind turbine is designed to rotate in the same direction regardless of the direction of the air stream. Thus, the wind turbine is generating power during both the ascending and receding actions of the water wave.

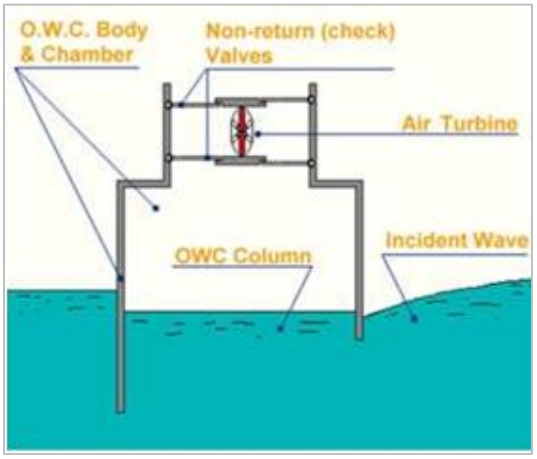

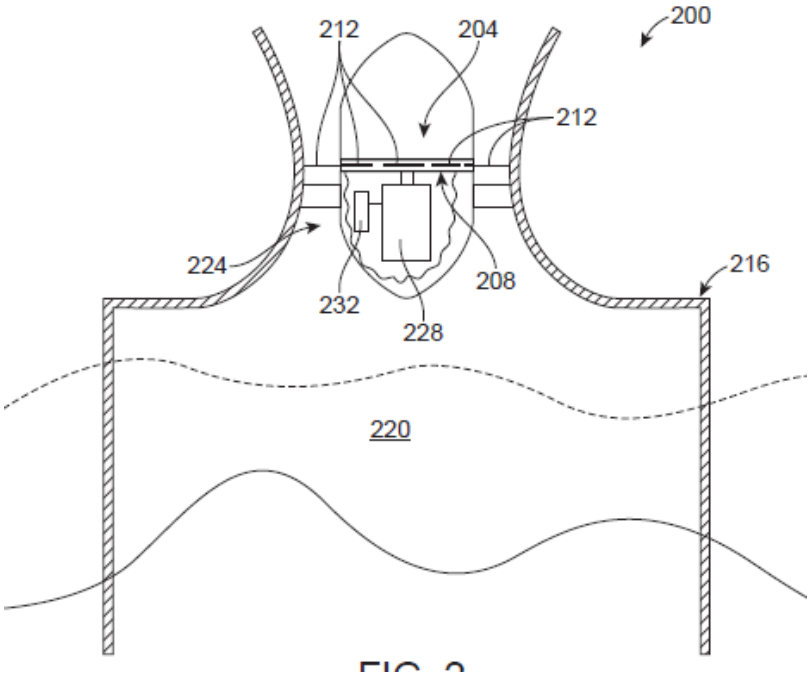

Figure 7. Schematic of a Basic OWC System

The OWC, like any fixed-sized power generating system, must be designed for a very specific design point power in order to determine the physical size and power rating for the

wind turbine, diffuser, electric generator and power conditioning systems, and the balance of the OWC chamber structural support systems. Thus, it is necessary to mechanically and thermodynamically design the OWC for a specific wave amplitude and frequency. Unfortunately, the ultimate source of the wave energy is local weather conditions (as well as remote), which can cause wave amplitudes and frequencies to vary depending on the severity of the ocean storms. In most instances, the system design point must be selected for power generation that is recoverable from a wave that has nominal energy. The wind turbine must then be feathered or a bypass valve implemented (as suggested by some researchers) to reduce the chamber pressure to safer operating levels when incident waves are considerably above the nominal wave energies that can be safely handled by the OWC mechanical structure.

One other complication is that the OWC power system must maintain a relative constant horizontal position with respect to the ocean floor, as one point of reference, in order for the air that is trapped within the OWC chamber to be pushed through the wind turbine, rather than having the OWC system rise buoyantly with the surge of the water wave. In order for the OWC to remain relatively fixed with respect to an inertial reference, the OWC is designed with heave plates attached to the four vertical "legs" that help stabilize the system by imposing a drag restraining force on the entire structure, dampening the buoyant forces caused by the incident waves. It is also important to note that the OWC chamber pressure, and hence the inlet pressure to the wind turbine, is a function of the initial volume of the chamber above the water line and the volume ratio after the large or small water wave has completed its ascension in the chamber. Clearly, the magnitude of the power output from an ocean wave power system is very much dependent upon the "tuning" of the wave machine to the amplitude and frequency of the incident water wave.

The mass dynamics equation that models the time-dependent motion of an OWC system, and thus how much energy can be recovered from the wave, is the subject of many research papers. Several of the most useful of these papers are given in Appendix 3 of the report. A major objective of these papers appears to be the matching of the damping coefficient (D) of the OWC system with the power output that can be generated by the wind turbines. A relationship between the damping coefficient and the relative velocity of the free surface of the wave front has been determined to be a critical parameter in the OWC power output. This damping helps to stabilize the wave machine by synchronizing the effects of buoyant and dynamic forces on the OWC that tend to lift the wave machine as the wave swells and recedes, thus always leaving a relatively large volume of air before the turbine that can be pushed through the air turbine by the wave.

The extent of the system dampening is a function of the magnitude of the drag imposed on the heave plates by the water, as well as the relationship between the volume flow rate through the turbine and the chamber pressure. Once the water wave machine is designed and in the water, the system damping is somewhat limited in its ability to capture all of the incident water wave energy, in that the OWC volume and "footprint" areas have been established, but the wave frequencies and heights (i.e., wave energies) are constantly changing during the seasonal operation of the water wave machine. The result is a water machine that is not always optimally tuned, that is, in proper resonance with the incident wave energy (wave height and frequency). The consequence is a loss of recoverable energy over the year, since changes in the wave magnitude and frequency inevitably change during the year.

For example, researchers (i.e., Budal and Falnes [9]) have analytically shown that the maximum power per OWC chamber volume is related to the wave height and period by the relationship shown here:

$$(\text{OWC POWER}_{optimum}/V_t) = \pi/4\ \rho_w\ (g_q/g_c)\ H/T \qquad (5)$$

However, this equation is not useful for the engineering design of OWC systems. At best, the formulation presents the absolute maximum in power recovery available from an incident water wave, much as the Carnot efficiency describes the maximum efficiency that a

heat engine can attain; however, it does little to provide an intuitive sense of what parameters and to what extent these parameters can improve the energy recovery efficiency.

CN has introduced a new parameter to the literature of water wave energy research, the OWC time constant (T_c):

Where:

$$T_c = (\Delta P_{avg}/P_0)\ (\ V_t\ ) / Q_{avg} \quad (6)$$

The results of the Phase I and II study by *CN* show that the use of the time constant provides a simplified approach to understanding how the OWC design parameters are related, and thus can provide a means of determining how to maintain the peak power from an OWC. It was determined analytically, and then confirmed by two additional independent models, that the OWC maximum power recovery is attained when the system has a time constant equal to 1/6 the wave period (T_{wave}). This result is new to the field of study, and more importantly, the time constant, T_c, provides some new insight into how to capture more of the energy available from a wide range of water wave profiles or spectrums. For example, it is clear from the wave energy equations developed by various researchers that the optimum OWC power varies with wave height and period. However, the numerical and analytical solutions developed by *CN* have shown that the percent of recoverable pneumatic power available from the incident wave energy is only a function of the wave period, T_{wave}, and not the height of the wave.

This non-intuitive result ultimately leads to two proposed suggestions: 1) using a turbine shutter valve, and 2) varying the OWC height above the mean water line as a means of improving energy recovery for a fixed-size OWC system. More specifically, the bi-cyclical opening and closing of the air flow to the turbine in sequence with the ascending and descending of the water wave front can increase the chamber pressure and increase the air flow rate through the turbine, letting the turbine operate in a high-efficiency zone. Also, changing the height of the OWC as a function of the wave frequency can tune the OWC to the different wave periods, and in effect, change the time constant (T_c) for a fixed OWC structure. The air flow rate (Q_{avg}) through the turbine is either a linear or non-linear relationship, depending on the type of OWC turbine in use (e.g., a Wells or Dennis-Auld type), and/or whether a diffuser, or fixed or variable inlet guide vanes are used, or if a bypass valve is in use with the chamber. *CN*'s numerical model has been successfully used in the Phase I STTR with both linear and non-linear pressure-flow-rate relationships and has given the same quantitative energy recovery improvement results.

Using the validated energy conservation methodology-based numerical model, *CN* identified the turbine shutter subsystem as the best method for enabling more energy capture from the ocean waves.

2.4.2 *CN*'s Analytical Theoretical Thermo-Fluid Model

CN derived a closed-form, analytical solution for the amount of power that is potentially recoverable from incident wave energy. This derivation was developed in part to quickly develop a basic, useful model of an OWC system, with simplified assumptions of time-invariant parameters, so as to make the solution solvable via calculus. This served as the first means of validating the later numerical model using an energy conservation methodology that allows OWC parameters, such as air flow rate, chamber pressure, and OWC height, to be functions of time, and thus not constant. The analytical solution was derived more from the point of view of using the basic engineering formula for power generation based on volume flow rate and pressure differential across a wind turbine, and less from actually solving the water wave equations from which the velocity potential, and hence, the free surface velocities could be determined. For OWC applications, the volume flow rate and chamber pressure are transient functions with respect to time and can be determined from the simultaneous application of the Ideal Gas Law (Equation of State) (Eq. 7) for air in a chamber that has a variable volume (due to the ascension or retraction of the wave front within the chamber), a loss (or gain) of air due

to the pressure-flow relationship that is an inherent characteristic of the type of air turbine that is used with the OWC (Eq. 8), heat transfer to or from the ambient (Eq. 9), and the conservation of energy (Eq. 11).

The power output of an OWC system can be determined for a given water column oscillation, $L(t)$, by numerically integrating volume flow rate and pressure as functions of time, with Equations 15, 16, and 17, using the development shown below.

Equation of state (i.e., ideal gas law):

$$P = (k\, M_{air}\, T) / V \text{ Turbine Flow/Pressure Equation} \tag{7}$$

$$\dot{M} = \text{Function } (P, \rho, \text{variable geometry}(t)) \tag{8}$$

$$Q_{dot} = \text{Function } (T\text{- Ambient Temperature}) \tag{9}$$

Equation of state differentiated:

$$(dP/dt)/P = [\dot{M}_{in} - \dot{M}_{out}]/ M_{air} + (dT/dt)/T - (dL/dt)/L \tag{10}$$

Conservation of energy:

$$\begin{aligned} d(M_{air}U)/dt &= (\dot{M}_{in}H_0 - \dot{M}_{out}H) + Q_{dot} - P\, A_{owc}\, dL/dt \\ M_{air}\, C_v\, dT/dt &= (\dot{M}_{in}H_0 - \dot{M}_{out}H) + Q_{dot} - P\, A_{owc}\, dL/dt - \dot{M}\, U \end{aligned} \tag{11}$$

Substituting Equation 5 into Equation 4:

$$(dP/dt)/P = [\dot{M}_{in} - \dot{M}_{out}]/ M_{air} + [(\dot{M}_{in}H_0 - \dot{M}_{out}H) - \dot{M}\, U + Q_{dot}]/(M_{air}C_vT) - \kappa\, (dL/dt)/L \tag{12}$$

Conservation of mass:

$$\dot{M} = dM_{air}/dt = \dot{M}_{in} - \dot{M}_{out} \tag{13}$$

These equations result in an expression for the OWC chamber pressure:

$$P(t) = - P_0\, (K')/L_0 \int e^{(s-t)/Tc}\, (dL/dt)\ ds, \text{ integrated from } -\infty \text{ to } t \tag{14}$$

and by using the pressure function (Eq. 8) together with the volume flow rate function:

$$Q(t) = A_{owc}\, (dL/dt) \tag{15}$$

the pneumatic power recovered from air chamber can be found from:

$$\text{Pneumatic Power} = \int \{A_{owc}\, (dL/dt)\, P(t) \tag{16}$$

where a simplifying assumption is made for the vertical, free surface wave velocity:

$$dL/dt = V_y\, \cos(2\pi\, t\, /T) \tag{17}$$

with $V_y = 2\pi\, (a/2)$ being the magnitude of the oscillating wave velocity, thus:

$$\text{Pneumatic Power} = P_0\, A_{owc}\, (K')\, (a\pi/T)^2/(2L_0)\ [T_c/(1+4\pi^2 T_c^2/\, T^2)] \tag{18}$$

$T_c = (\Delta P_{avg}/P_0)\ (A_{owc}\ \ L_0)\ /\ Q_{avg}$ is introduced for the first time in the literature by <u>CN</u> and identified as the OWC system's time constant. The time constant has time (seconds) as its units, and thus is different from the damping coefficient (D) that is typically used to correlate the OWC system chamber pressure, footprint area, and volume flow rate into a single parameter that can be used to characterize the OWC performance.

Where:
- a = peak-to-peak wave amplitude
- P = pressure, absolute
- M_{air} = mass of air in OWC chamber
- T = temperature, absolute
- T = wave period, seconds

$\dot{M}_{in}$ = rate of mass entering OWC
V = volume of OWC air chamber
$\dot{M}_{out}$ = rate of mass leaving OWC
L_o = height of air column in OWC
C_v = constant volume specific heat = 716 J/kg-k
U = internal energy in OWC; k = ideal gas constant = 286.9 J/kg-K
H = enthalpy in OWC
H_0 = ambient enthalpy – $P_{turb}/\dot{M}in$
A_{owc} = OWC area
Q_{dot} = heat transfer into OWC
T_c = OWC time constant
Q_{avg} = average turbine flow rate
ΔP_{avg} = average turbine pressure
P_{turb} = turbine power recovery
Q_{avg} = average volume flow rate into or out of the OWC chamber
K' = $(1+ K/C_v)$; K = gas constant $(R_u/Mole.Wt_{air})$

Figure 8 presents the results from using Eq. 10 to calculate OWC power as a function of the system time constant, T_c, and parameterized with the wave period and amplitude shown. Figure 8 serves to quickly identify the optimum performance of an OWC given the amplitude of the wave and its period, and to offer some clarity as to how to improve the OWC performance. It is interesting to note that the power generation is higher for a wave with a shorter wave period but the same wave height. This is not an intuitive result and is due to the wave energy content being delivered by a wave with a short wave period. This is also the reason why an OWC system, sized for energy recovery with a short wave period, is oversized with respect to power generation capacity when a wave with a larger wave period is incident upon the OWC system.

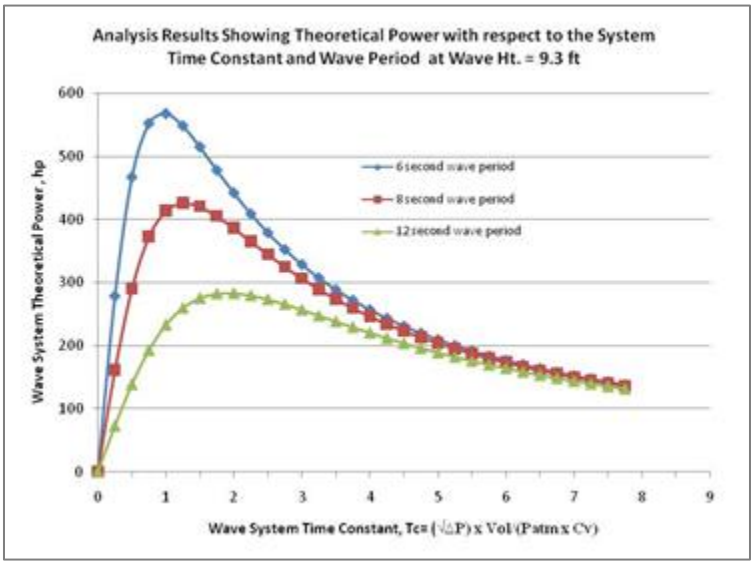

Figure 8. OWC Power as a Function of the System Time Constant

The OWC systems are typically designed to operate with time constants between ½ to 1 second, compared to a typical wave period of 6 to 12 seconds. As can be observed from Figure 8, the time constant, T_c, which enables the OWC to achieve maximum power output, is closer

to 2 to 3 seconds for larger, low-frequency waves. Unfortunately, with a fixed turbine flow curve, it would be problematic to operate at a time constant this high. A system designed with a 3-second time constant would act more like a gas spring in smaller, high-frequency waves of 6 seconds, as opposed to an energy converter. Thus, a turbine system with an adjustable time constant has tremendous benefits to improve the wave-to-pneumatic energy capture efficiency.

2.4.3 *CN*'s Numerical Spreadsheet Thermo-Fluid Model

CN's input page of the numerical thermo-fluid model is shown in Figure 9. The OWC is shown to have an overall length, width, and height of 10 meters x 15 meters x 7 meters. The OWC width of 15 meters was not arbitrary, but rather was exactly ½ of the wave length, according to the classically derived formula that relates deep sea wave periods and wave lengths: $\lambda = T^2_{wave}\, g_c/2/\pi$.

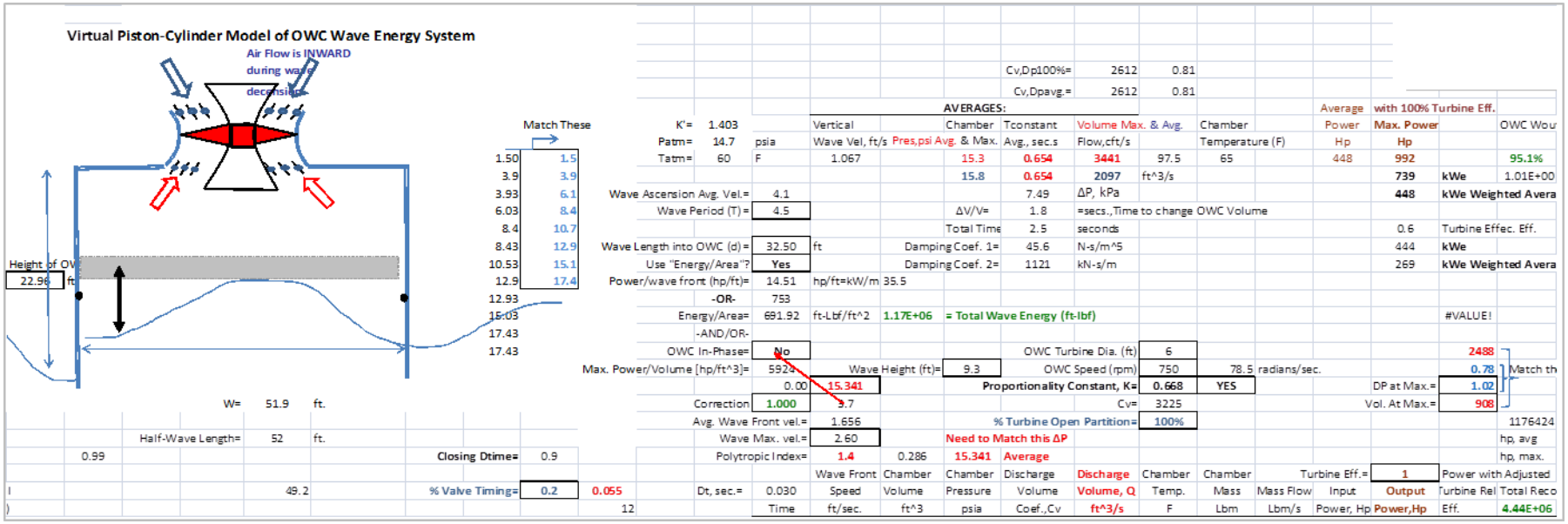

Figure 9. Input Page of Numerical Thermo-Fluid Model

The incident wave has a wave period of 4.5 seconds and a wave height of 9.3 ft for a power density of 35.5 kW/meter, or an energy flux of 692 ft-lbf/ft^2. This may be considered the "baseline" OWC dimensions for all of the parametric studies that followed during the Phase I STTR effort. The model uses the same basic engineering thermodynamics and fluid dynamic principles as used in the analytical models, but uses these principles in very small time increments. Thus, the integrations of these relationships are simulated by simple algebraic expressions that are solved for each moment in time. That is, each row of the spreadsheet is a step-in-time, enabling a numerical integration of the second order, non-linear equations. The transient progressions of the chamber pressure and volume flow rate are incremented through each time step using the initial conditions of these parameters from the time step before. However, the numerical model must also use several simplifying assumptions concerning the energy absorbing capability of the OWC and the non-linear relationship between the volume flow rate through the turbine and the chamber pressure. For example, both models have determined the pressure and volume flow rate transients for the OWC system by assuming that 100% of the wave energy is recoverable. This essentially assumes that all of the incident wave energy is radiated into the pneumatic air column, and that none of the incident energy is radiated away from the OWC system.

The key to the development of this numerical model is the adaptation of a physical analogy between the ascending and descending wave in the OWC chamber to a piston moving up and down in a cylinder, except that there is an aperture on top of the cylinder, where the power turbine is placed. Thus, as the piston (wave) ascends into the cylinder (OWC chamber), it compresses the air and also pushes some of the air out of the cylinder through the turbine. The amount of air that can be pushed out of the turbine is dependent upon whether the aperture can be considered a simple orifice, or if it must be more correctly represented by a spinning obstruction or turbine. For a simple aperture, the flow coefficient, C_v is typically used in fluid dynamics as the ratio of the volume flow rate (Q, cft/s) to the square of the pressure drop through the aperture. The turbine flow-rate-pressure drop relationship is most adequately and conventionally represented by aerodynamic terms: φ, flow coefficient = $Q,cfs/(ND^3)$ and load coefficient $\Psi = \Delta P/\rho/(ND)^2$ in the formula: $\varphi = K \times \Psi$, where K is a proportionality constant that depends on the type of turbine in use. For this study, both methods were used and determined to give the same wave energy recovery improvement results.

The wave power density (kW/meter) or wave energy flux (E/ft^2) is the primary wave characterization that is needed for this numerical model. Certainly, the energy flux and power density are determined from the classical wave energy derivations that consider the wave height and period as given in Eq. 19 and Eq. 20. For this reason, the <u>*CN*</u> numerical model developed in the Phase I STTR is identified as the energy conservation methodology to discern it from the analytical classical solution presented in the previous section. The major link between the wave energy content and the piston-cylinder analogy is the calculation of an average piston velocity. The piston average velocity is determined from knowing the energy content of the water wave and iterating on the weighted average of the piston–cylinder (i.e., OWC chamber) pressure using the relationship:

$$Avg.\ velocity\ (V_{avg}) = (Wave\ Energy\ per\ A_{owc})/Avg.\ chamber\ pressure\ (\Delta P_{avg.})/T \quad (19)$$

or

$$Avg.\ Velocity\ (V_{avg}) = (Power\ per\ wave\ front)/\ \Delta P_{avg.})/(\lambda/2) \quad (20)$$

where the energy content of the wave is equivalently expressed as either:

$$Energy\ per\ area\ (E/A_{owc}) = \rho \times g_g/g_c \times a^2/8 \quad (21)$$

or

$$Power/wave\ front\ length\ (Power/L) = \rho \times g^2_g/g_c \times a^2 \times T^2/(32 \times \pi) \quad (22)$$

Where: λ is the (deep sea) wave length and is determined from [10]: $T^2 \times g_g/(2\pi)$

These are classical expressions for water wave energy derived in any good text on ocean wave energy by integrating the potential and kinetic energy of the water particles, assuming a sinusoidal wave shape in three dimensions.

The velocity of the free-surface wave front (similar to *DL/Dt* expressed in Eq. 10) is then determined to be a function of time according to the following equation:

$$V(t) = \pi (V_{avg})/2 \sin (2\pi/T \times t);\ \text{where } T \text{ is the wave period} \quad (23)$$

With the velocity of the free-surface wave front known, and assuming a relationship between the volume flow rate through the turbine as a function of chamber pressure (i.e., $Q = C_v \times \sqrt{\Delta P}$), it is possible to model the transient behavior of the chamber pressure and volume flow rate during the ascension (or descension) of the wave. The transient power of the wind turbine can then be determined from the conventional turbine power calculations or:

$$Power(t) = \Sigma \{\Delta P(t) \times Q(t) \times \eta_{turbine} \times Constant\ (for\ unit\ conversions)\} \quad (24)$$

An example of the comparison of the theoretical analytical solution and this numerical solution is shown in Figure 10, using the C_v relationship between flow rate and pressure, and in Figure 11 when the turbine relationship $\varphi = K \times \Psi$ is used. This virtually identical result is even more remarkable due to the fact that the expressions used for the vertical, free surface velocity in both models are different, although both are ultimately dependent on the energy content of the wave. That is, the numerical model uses the classical expression for wave energy (Eq. 14 and Eq. 15) to determine the vertical velocity of the free surface of the water, whereas the theoretical solution uses only the entire wave height and wave period in its derivation. However, the integration performed in Eq. 16 must essentially calculate the same water wave energy content in the process.

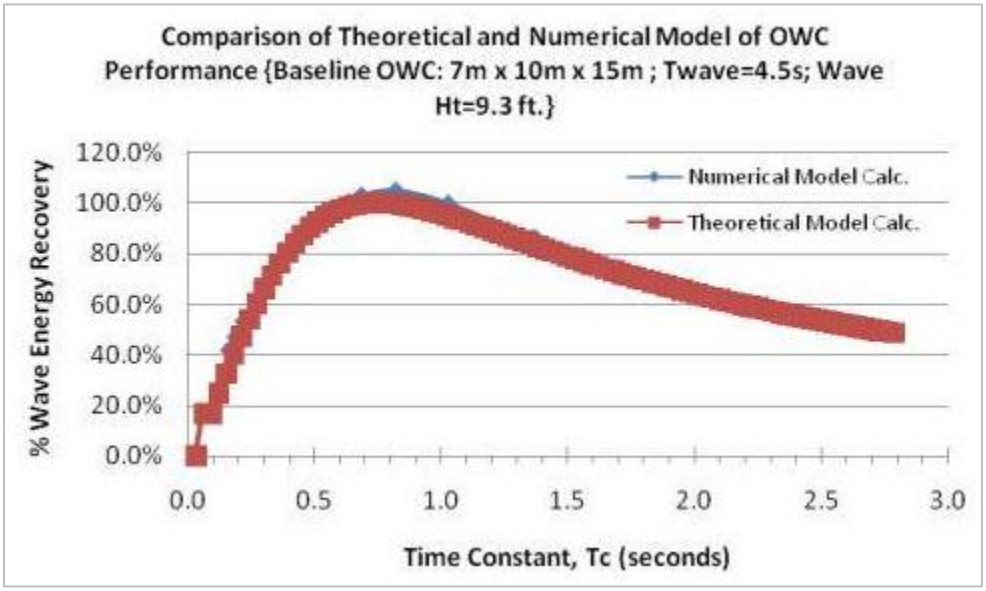

Figure 10. Comparison of Theoretical Analytical Solution and Numerical Solution

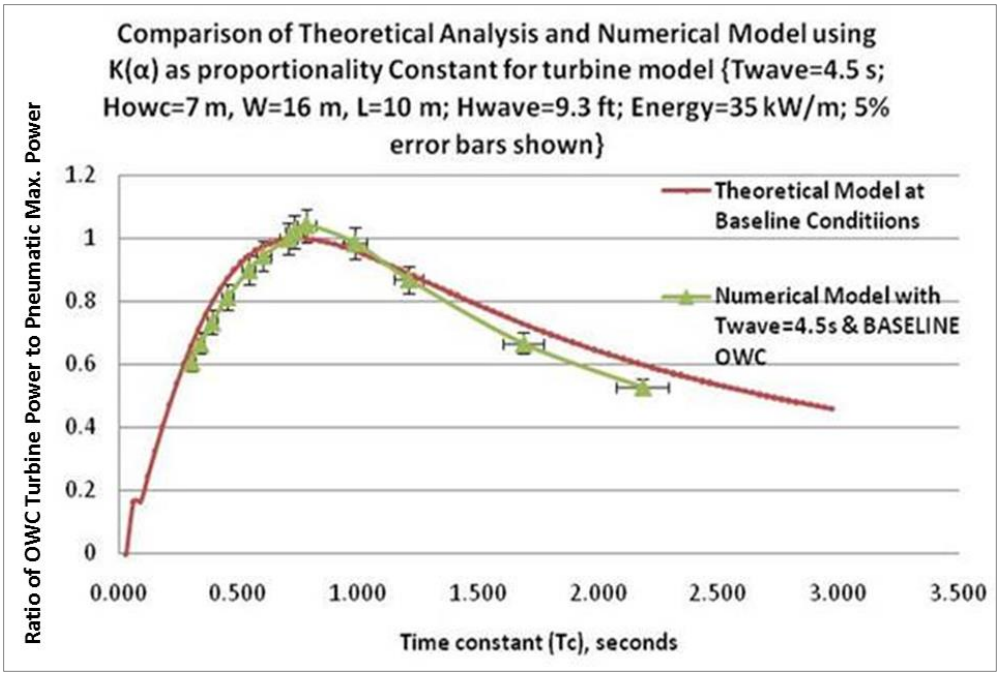

Figure 11. Comparison of Theoretical Analytical Solution and Numerical Solution

2.5 Numerical Model Validation

The simplicity of this energy conservation methodology and its ability to provide time variant, numerical solutions was extremely welcome, as it easily enabled changes to several critical OWC design parameters, in order to calculate any energy recovery improvements as a result of these changes. However, the strong dependency on the validity of the numerical model to provide credible and reproducible results also required extensive validation of the numerical model. For this purpose, several validations of this numerical model are given in this section, using independently published studies obtained from the technical literature. Figure 12 presents a comparison of the results obtained using the *CN* numerical model, compared to the reported measured performance results for a coastline-based OWC system. The measured results were presented in a research paper prepared by Tease, Lees, and Hall [8]. The comparison is particularly striking given that the coastline OWC was 100 meters long and consisted of 16 individual OWC turbines. The numerical model used the same overall dimensions, except for an unreported depth from the coastline, where a length of 10 ft was used in the model. It was also assumed that the Wells turbine had an overall efficiency of 50%, and that the flow rate vs. turbine pressure drop was linear; this is a typical and valid assumption for a Wells turbine.

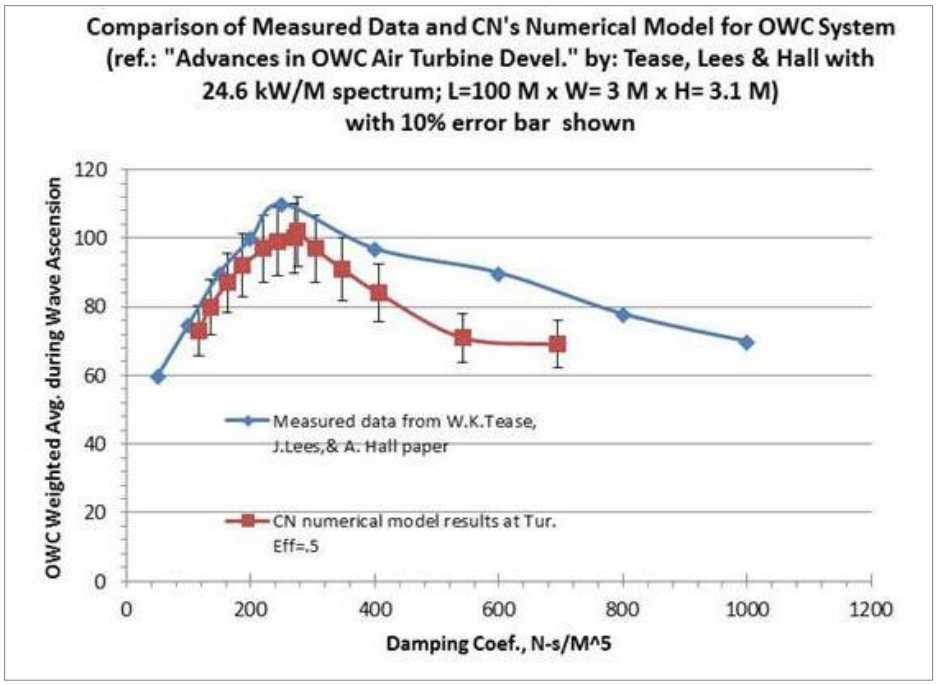

Figure 12. Comparison of Measured Data and *CN*'s Numerical Model

A comparison of the results shown in Figure 13 from a study by Anand et al. [11] indicates agreement of the power calculation using the energy conservation methodology model, but using the more conventional damping coefficient as the independent variable. The similar shape of the curve is particularly noticeable, indicating that an optimization is physically true and possible to discern.

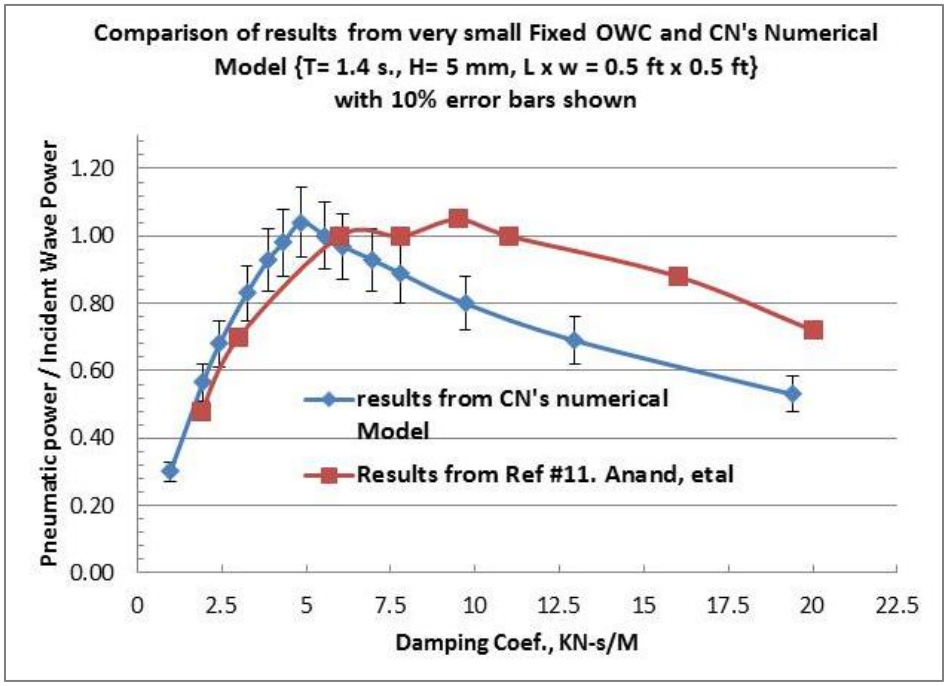

Figure 13. Comparison of Results from a Small, Fixed OWC and *CN*'s Numerical Model

A dissertation by Corsini and Rispoli [12] offers a simplified analytical expression for the changes in pressure in the OWC chamber as a function of time using independent variables associated with the size of the OWC system and the turbine that would be used with the OWC. The comparison of the results of pressure variation, as predicted by Mr. Corsini in his OWC Transient System Computer Model: TRNSYS and by *CN*'s energy conservation methodology numerical model, is shown in Figure 14.

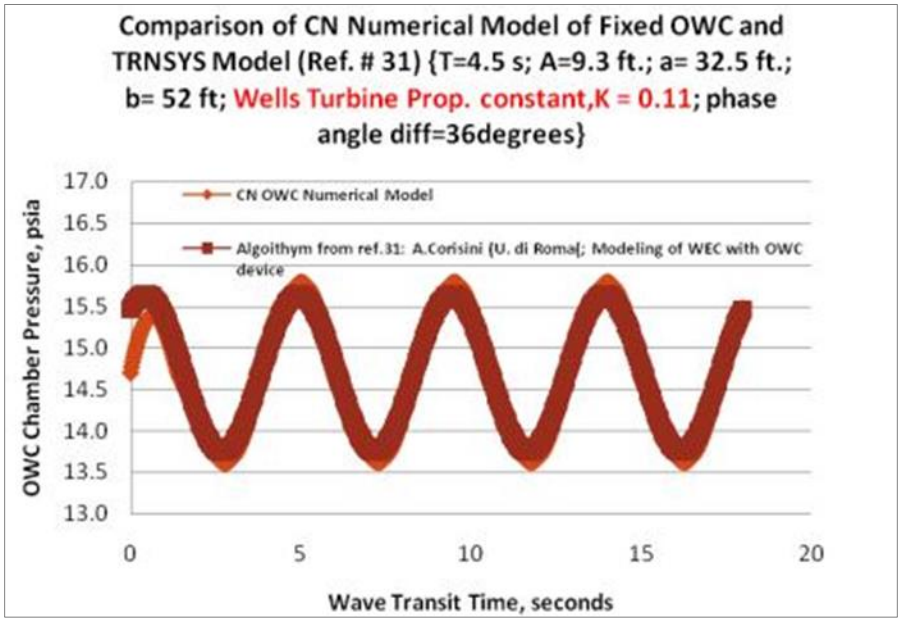

Figure 14. Comparison of *CN*'s Numerical Model of a Fixed OWC and the Model Developed by Mr. Corsini

The most definitive validation of *CN*'s numerical model was only recently determined from testing conducted by the MMA engineering professors and students as part of their collaboration in Phase I of the STTR. A small-scale OWC chamber was used, fabricated, and tested in the MMA wave tank. The MMA OWC chamber is shown in Figure 15 as it is readied for a test. The dimensions of the chamber are 12" x 12" x 14" tall and it is instrumented with a pressure transducer to record the chamber pressure changes as the water wave ascends and descends in the OWC chamber. This OWC prototype was built without a reflector wall, and thus only ½ of the available wave energy could be potentially recovered.

A series of tests were performed using 6-inch and 12-inch tall waves with a wave period of 3 seconds. The output from this test is shown in Figure 16, compared to the predicted performance according to the energy conservation methodology numerical model. The match between predicted and actual test measurements is particularly strong in the model's ability to display an inflection of the pressure as it changes sign. These inflections are noticeable when modeling a very small OWC chamber and not as apparent, or perhaps not existing, in larger systems, as may be witnessed from the comparison shown in Figure 16.

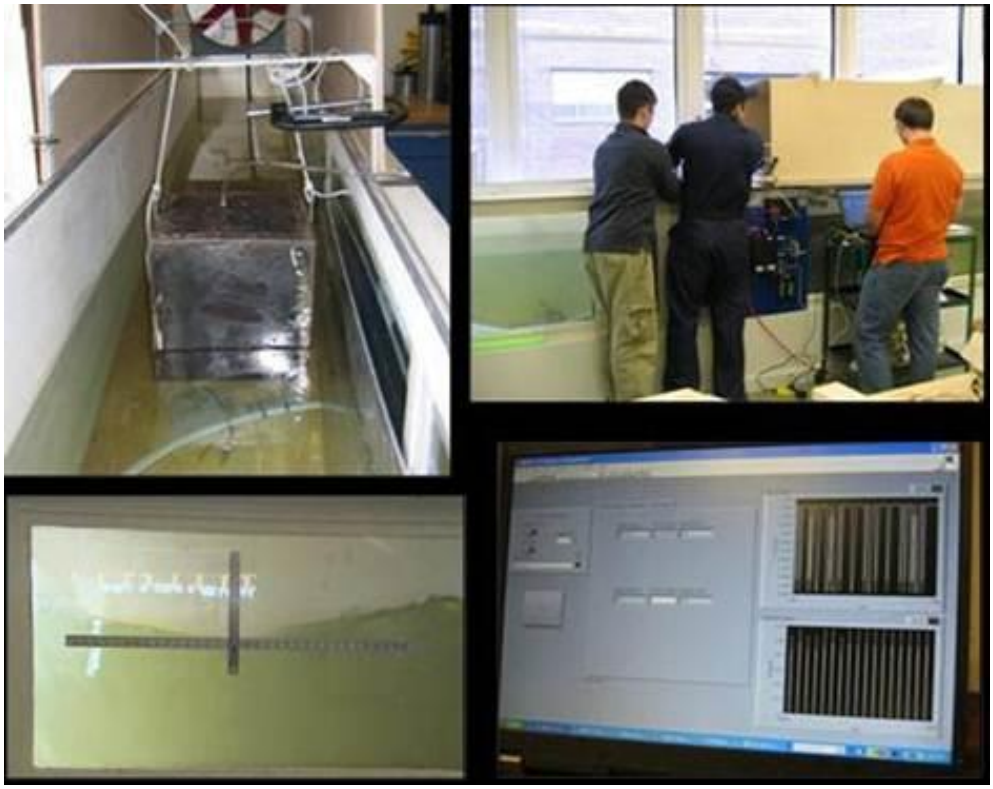

Figure 15. MMA OWC Chamber

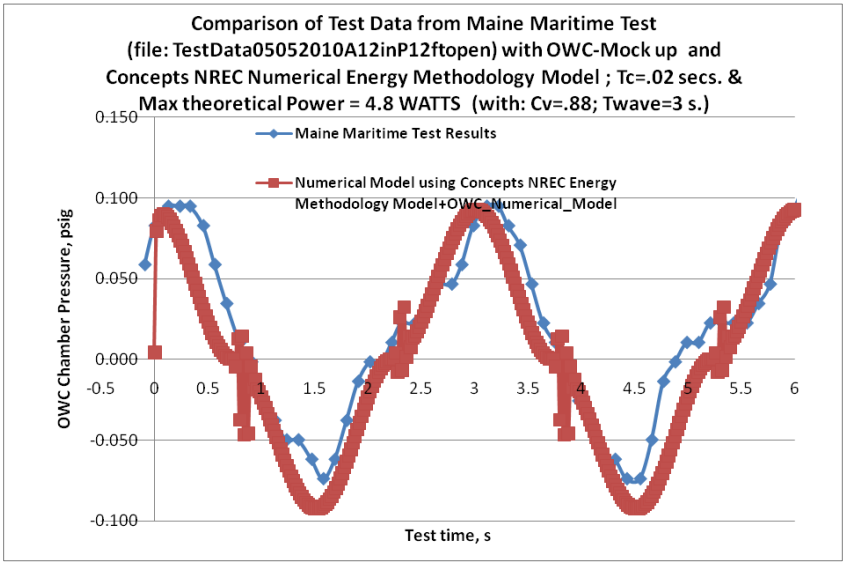

Figure 16. Test Output

2.6 Results from the Application of *CN*'s OWC Numerical Model

2.6.1 Identification of Innovations that Improve Energy Recovery Efficiency

The success in demonstrating the equivalency of the analytical and numerical models in calculating the performance of an OWC system was and is encouraging. It was encouraging because it validates the "water wave piston-in-a-cylinder" approach for modeling the interaction of the water wave with the OWC structure. The numerical model was found to

match the measured performance of an OWC system as presented by independent researchers (with reasonable assumptions made), which increased CN's confidence in the results obtained when the model was used to evaluate the relative performance of the OWC, particularly when time-variant changes were made to the turbine and OWC chamber subsystem design parameters. Given the model's dependency only on the need for an accurate wave ascension speed (i.e., piston), confidence is high that the model would be even more accurate once mathematically precise solutions for the relative velocity of the free surface of a radiant water wave were made available from MMA's research. However, until the more mathematically precise solution for the wave ascension speed (i.e., the piston speed) was known, it was possible to more easily determine the effect of transient behaviors on the performance of the OWC for such design parameters as $C_v(t)$, wave height(t) and wave frequency(t), OWC buoyancy(t), heave plate drag(t), etc. This is facilitated by entering the values of these parameters at each time step during the numerical integration.

The simplifying assumption of having 100% of the water wave energy available for OWC recovery is a poor assumption in both the theoretical and the numerical solutions. The amount of incident wave energy that diffracts away from the OWC, and is thus not available for energy recovery, is dependent upon the details of the OWC structural design, and the water wave lengths and periods. Thus, a major objective of the mathematical analysis that needed to be completed was to determine the mathematical equations for the relative velocity (i.e., the wave front with respect to the OWC vessel) of the free surface of only the radiant wave energy, i.e., the wave that actually enters the OWC chamber and that is thus available for OWC recovery. With these reduced water wave velocities and/or reduced water wave energy, the CN thermo-fluids model would be complete and would provide the mathematical relationships between OWC design parameters and power output.

However, even as these algorithms were being developed by Professor Lorenz, CN proceeded to assume that 100% of the wave energy content was available to the OWC device, and proceeded to determine how the turbine subsystem and the OWC chamber design could be altered to "tune" the OWC performance to improve the recovery of the water waves.

The first major result from the use of the analytical solution, and then validated by the model, was the discovery that the wave period, T_{wave}, and an OWC system parameter labeled by CN as the time constant, T_c, were direct functions of each other. The time constant is defined by the following equation, as derived from a purely analytical description of the interrelated behavior of the piston (wave)-cylinder (OWC chamber) and the fluid dynamics of flow rate through an orifice:

$$T_c = (\Delta P_{avg}/P_0)\,(A_{owc}\ L_0)/Q_{avg} \quad \textit{(units: seconds)} \tag{25}$$

A further relationship between the fluid flow rate through an orifice is governed by either: $Q = C_v\, x\, \sqrt{\Delta P}$ or $\varphi = K\, x\, \Psi$ (where: ϕ flow coefficient = $Q,cfs/(ND^3)$ and load coefficient $\Psi = \Delta P/\rho/(ND)^2$). The latter equation is used to model the aerodynamics of the air turbine. The proportionality constant, K, in the turbine governing relationship is dependent on whether the turbine is a Wells or Dennis-Auld-type turbine, and is usually constant through a wide operating range, until turbine stall is caused by a flow rate that is too high. It is the need to prevent stall due to high flow rates in OWC systems that has caused many researchers to advocate for the use of bypass or blowout valves that are in parallel with the OWC turbine(s).

It is clear from optimizing by use of calculus in the analytical expression presented in Equation 14, that the optimum power occurs when $T_c = T_{wave}/6$. This was clearly demonstrated upon the first application of the numerical model, as shown in Figure 17.

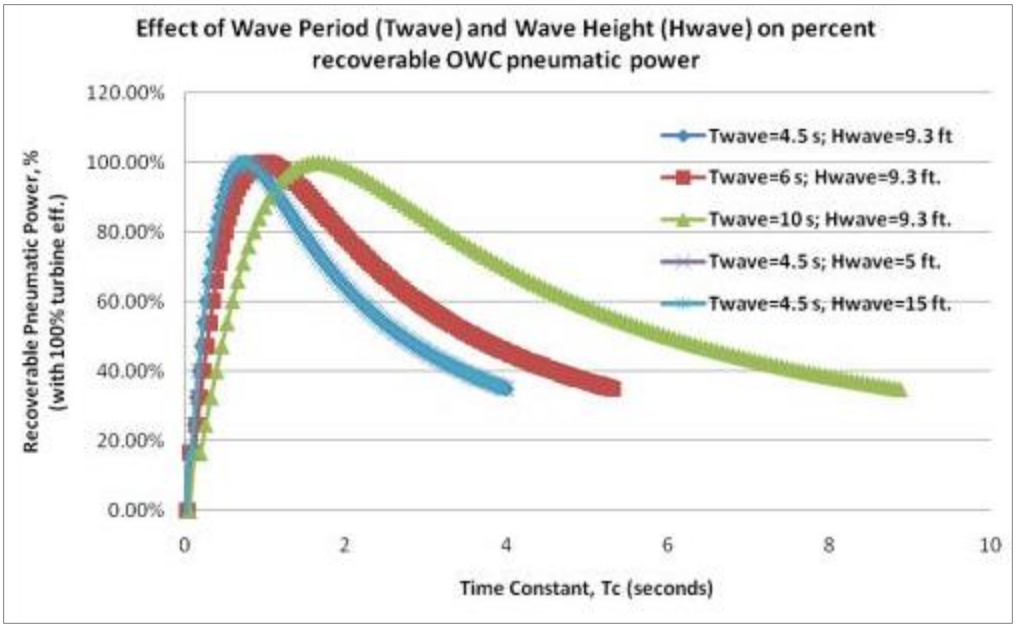

Figure 17. Effect of Wave Period and Wave Height on Percent Recoverable OWC Pneumatic Power

This optimization is not intuitive, but can become more so when one visualizes the piston-cylinder analogy that is offered (and that has been demonstrated as accurate) by the energy conservation methodology numerical model. That is, as a piston (the wave front) is moving upward in the cylinder (the OWC chamber), the chamber air is both compressed and also leaked from the enclosure. The rate of pressure change can be fast or slow, depending on both the speed of the ascending piston (the wave front) and the amount of air flow that can be pushed out of the cylinder (the OWC chamber). The system time constant is small if the flow rate is high, which causes a low chamber pressure. A large time constant indicates a low flow rate, but at a high chamber pressure. However, the product of flow rate and chamber pressure (equal to the ΔP across the turbine) determines the actual power developed. Therefore, there must be a maximum power determined by the correct pressure and flow rate.

The analogy is complicated by the fact that, during the ascension or descension of the wave inside the OWC chamber, the chamber pressure and flow rate are constantly changing, as may be observed in Figure 18 (a and b). Note the rectangular shapes are superimposed on the graph to identify the times when pressure is at atmospheric. This will be an important reference when the turbine shutter innovation is introduced, but can be ignored when observing only the pressure change in the OWC chamber. The volume flow rate through the turbine is even more dramatic, as shown in Figure 18 (b). Close observation of the pressure and volume flow rate changes across and through the turbine, respectively, and quickly hints at the need for finding a means of keeping the flow rate and the pressure more constant in order to achieve and maintain a high turbine efficiency, as well as to eliminate the possibility of stalling the turbine due to very high flow rates. Thus, as may be seen in Figure 18 (c), the goal is to maintain more constant turbine efficiency.

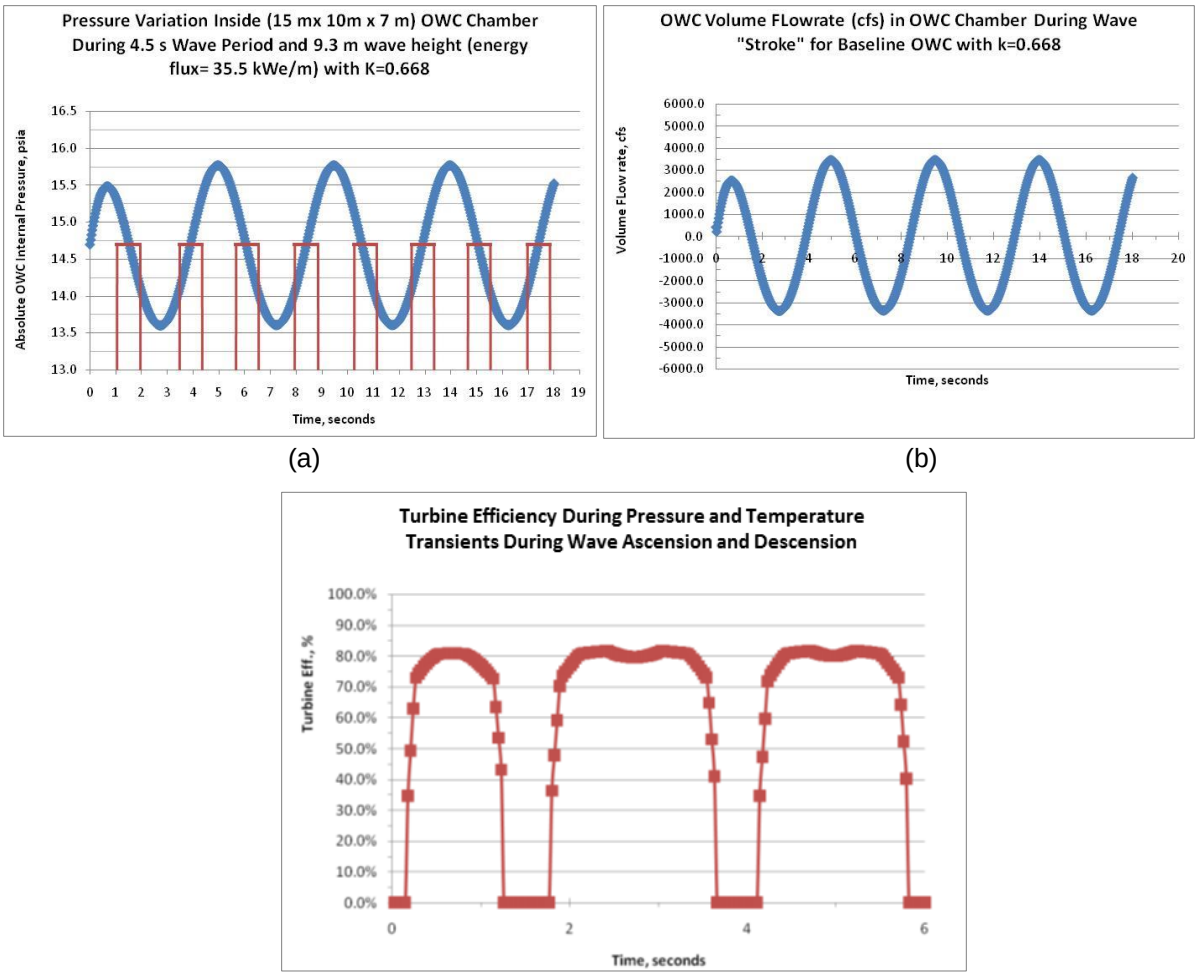

Figure 18. Chamber Pressure and Flow Rate

By algebraically combining these several relationships, it is easy to show several important equations that provide more insight into the operating characteristics of an OWC system's performance. These equations are:

$$C_v = (144\ g_c/\rho)\ x\ (D/\omega)\ x\ \sqrt{\Delta}P\ x\ \ K(\alpha) \tag{26}$$

Where: D is the rotor diameter; ω is the rotor speed (radian/s); ρ is air density; $\sqrt{\Delta P}$ is the square root of the rotor pressure drop; and $K(\alpha)$ is the turbine proportionality constant (which can be a function of blade pitch as well as turbine type).

$$(T_{wave}/6)\ x\ (144\ g_c\ Patm/\rho)\ =\ (A_{owc}\ L\ x\ o)\ x\ (\omega/D)/\ K(\alpha) \tag{27}$$

Where: A_{owc} and $L\ x\ o$ are the projected area and the height of the OWC chamber, respectively.

$$Q = K(\alpha)\ x\ [\Delta P\ 144\ g_c/\rho]\ x\ (D/\omega) \tag{28}$$

$$OWC\ Power = (\omega/D)/\ K(\alpha)\ \ x\ (\rho/gc)\ x\ Q2\ x\ \eta_t\ x\ \eta_{owc}\ x\ \eta_{gen} \tag{29}$$

These equations gave insight to the following conclusions that have since been demonstrated through the application of the energy conservation methodology numerical

model, as may be witnessed by the figures or tables that accompany each statement. Note that the "baseline" case as called out in these figures is as defined (see Figure 19).

1. The turbine proportionality constant, $K(\alpha)$, can be used to "tune" the OWC performance by changing the magnitude of the OWC time constant for a given incident wave energy. A literature survey of technical articles concerning the benefit of using a Wells-type variable pitch turbine rotor revealed a consensus of the independent researchers that a variable pitch turbine can increase the efficiency of the turbine; but also important, variable pitch blades can increase the operating range of the turbine.

   From Reference [13], one learns that variable-pitched turbines can increase the range by 20% to 40%. The increase in operating range before airfoil stall is encountered has been verified by *CN*'s numerical modeling using the Wells turbine data shown in Table II. The development of a self-actuating blade articulation system that uses the aerodynamic forces of the air stream that is driving the turbine has been completed by *CN* during turbine research conducted in a separate Phase I SBIR. The detailed results of that research were the subject of another final report (*CN*'s Technical Memorandum No. 1560 for DOE Project #DE-SC0003571). An illustration of *CN*'s self-actuated blade articulation turbine assembly is shown in Figure 19. Thus, variable-pitched blades not only can increase the efficiency of the turbine as the air flow rate varies through the turbine, but also control of the pitch can change the system's time constant, T_c.

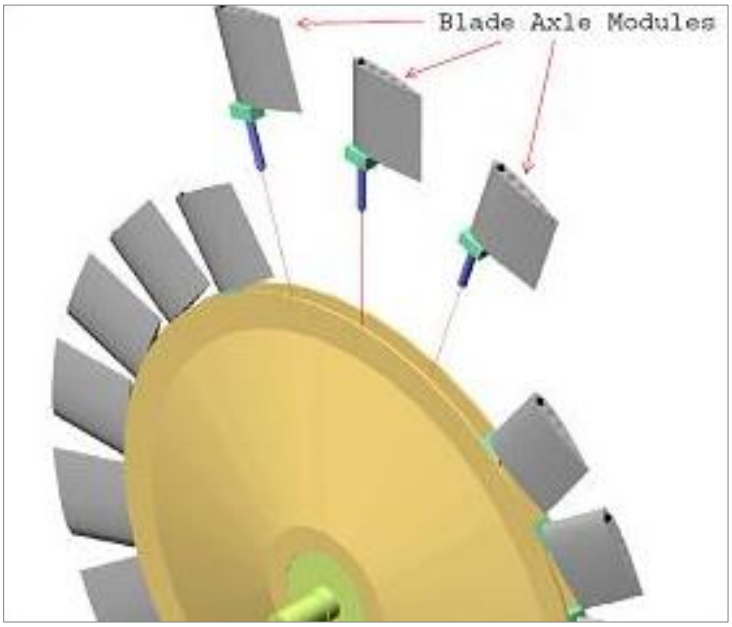

Figure 19. Baseline of Self-actuated, Blade Articulation System

TABLE II. RESULT OF *CN*'S MODEL OF WELLS TURBINE DATA SHOWING INCREASE IN OPERATING RANGE

11152	Actual Vol. MAX. Flow rate=		7535		0.4442	ϕ,actual max
	Actual MAX. Δpressure=		16.1	1.41	0.3916	Ψ,actual, max.
	Max Base Vol. Flow rate=		1109	cfs	1.134	
	Max Base ΔPressure =		0.341	psia		
	K= 0.6882					
Corrected FActors=	0.243		0.147			
	Ψ	Π	ϕ		η	
0	0.01	0	0.006882	1	0.000	0.00688
0.2	0.02	0.0002	0.013764	2	0.727	0.01376
0.5	0.03	0.0005	0.020646	3	0.807	0.02065
0.9	0.04	0.0009	0.027528	4	0.817	0.02753
1.3	0.05	0.0013	0.03441	5	0.756	0.03441
1.85	0.06	0.00185	0.041292	6	0.747	0.04129
2.15	0.065	0.00215	0.044733	7	0.739	0.04473
2.25	0.067	0.00225	0.0461094	8	0.728	0.04611
2.1	0.07	0.0021	0.048174	9	0.62274	0.04817
0.98	0.075	0.00098	0.051615	10	0.253	0.05162
0.8	0.08	0.0008	0.055056	11	0.182	0.05506
0.55	0.087	0.00055	0.0598734	12	0.106	0.05987
0.25	0.09	0.00025	0.061938	13	0.045	0.06194
0.15	0.095	0.00015	0.065379	14	0.024	0.06538
0.08	0.124	0.00008	0.085	15	0	0.085

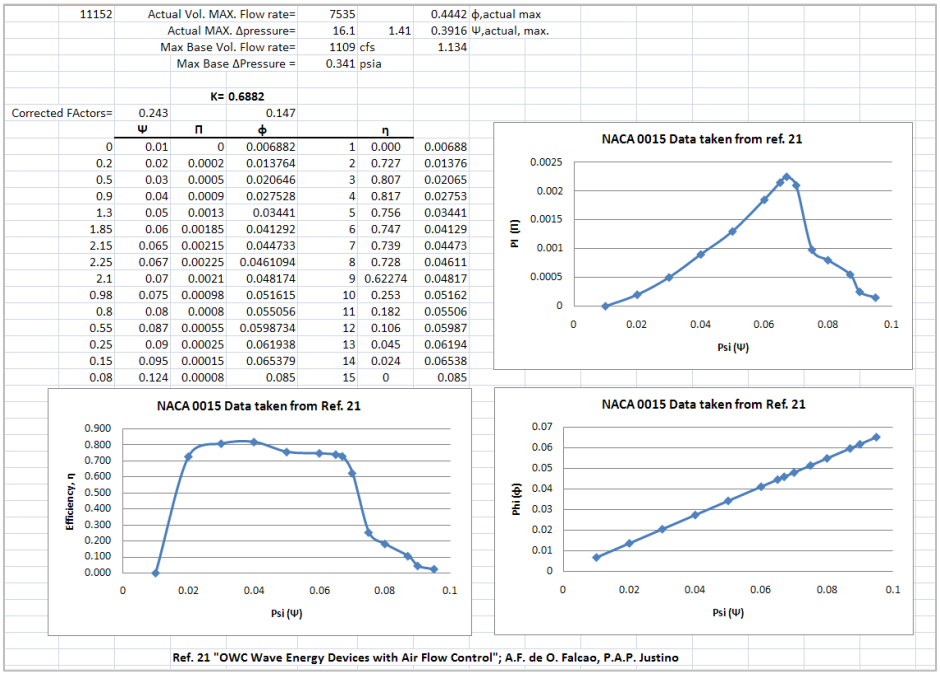

2. The wave period (not the wave amplitude) has an effect on the potential for energy recovery improvement. This result is demonstrated by the results from the numerical model in Figure 20, as well as in Figure 17, which was developed from the purely analytical solution for the energy recovery potential of an OWC system.

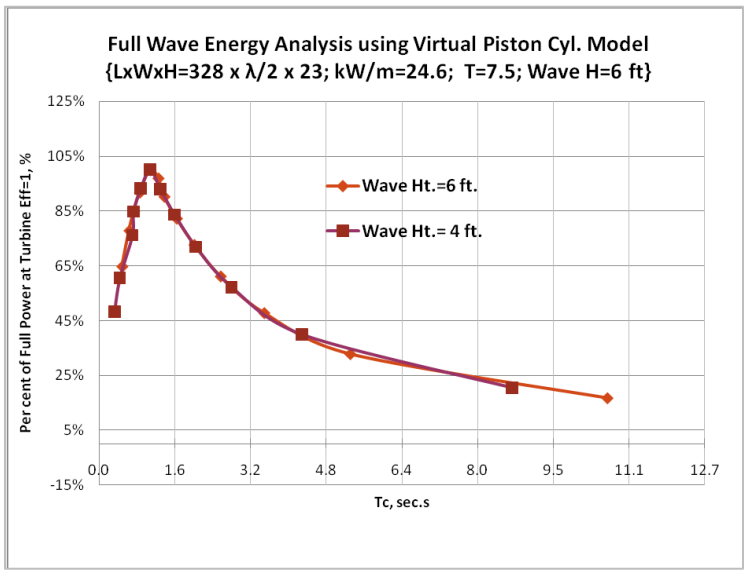

Figure 20. Results from Numerical Model

3. The OWC chamber pressure ΔP is increasing almost linearly, as shown in Figure 21, with an increase in the time constant until the optimum time constant (equal to $T_{wave}/2\pi$) is reached, at which time the OWC system no longer continues to

produce power with the increasing chamber pressure, but rather starts to lift the OWC, causing it to ride the wave.

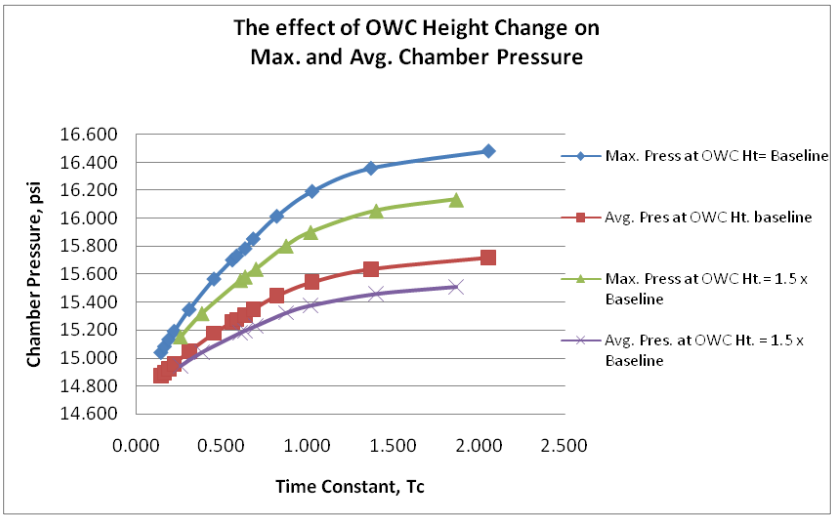

Figure 21. Effect of OWC Height Change on Chamber Pressure

4. The OWC height, with the same OWC footprint area and **constant incident wave energy flux**, does not affect the percent of incident wave energy that can be recovered for a given system time constant. This may be observed in the output from the numerical model presented in Figure 22. The emphasis is given only to distinguish this non-effect of the OWC height on energy recovery potential from the case where the height of the OWC ***does*** affect the ability to improve energy recovery from an incident wave when the wave period, T_{wave}, has changed. This observation of an improvement in recoverable energy leads to one of the proposed innovations that is a major result from the Phase I STTR research. This proposed benefit is explained in Item 5.

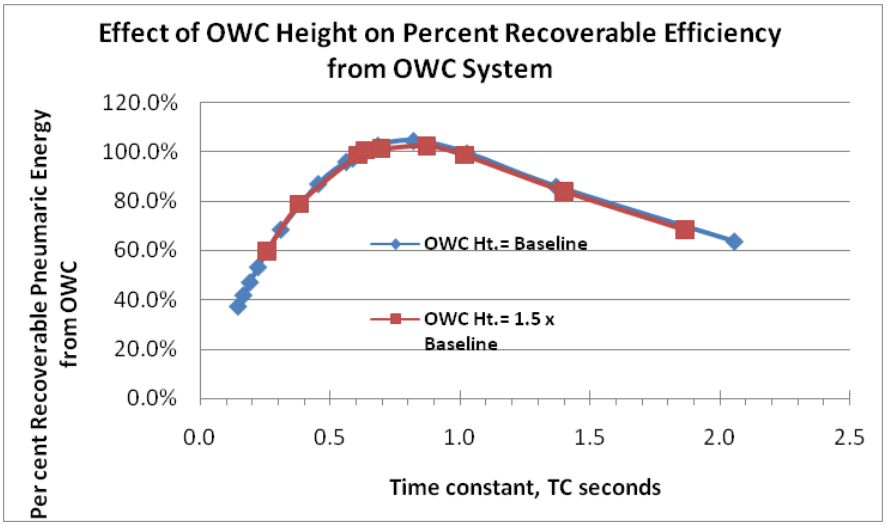

Figure 22. Effect of OWC Height on Percent Recoverable Efficiency

5. A proposed innovation to affect the "tuning" of the OWC system for different incident wave intensities is to raise or lower the chamber height with respect to the wave's meanline level. This is a direct consequence of the relationship

between T_{wave} and the volume of the OWC chamber as shown in Eq. 16. The innovation is to decrease the height of the OWC chamber by means of ballast controls that are already onboard the OWC seaworthy vessel in inverse proportion to the change in the wave period. Thus, as the wave period increases, the OWC chamber should be decreased. This is a reasonable innovation that also has the result of selecting the initial design point for the OWC system based on the highest probability for the presence of waves with the **lowest** wave period. Thus, a climate of waves with a wave period of 4.5 seconds (this is the baseline period selected for the STTR study) should be selected as the starting point for the design of the OWC chamber size and the turbine rating.

As can be observed in Figure 23, when the completed OWC structure is in the presence of waves that have a higher period (for example, 6 or 10 seconds were used in the numerical model), the time constant for the (4.5-second wave period) OWC system will still recover energy from the higher period waves, *but* at a lower potential energy recovery effectiveness, *unless* the height of the OWC chamber is reduced. By reducing the height to its optimum level, as determined by iterations using the OWC numerical model, an improvement of energy-capture effectiveness of 20% is possible. This result is summarized in Figure 24.

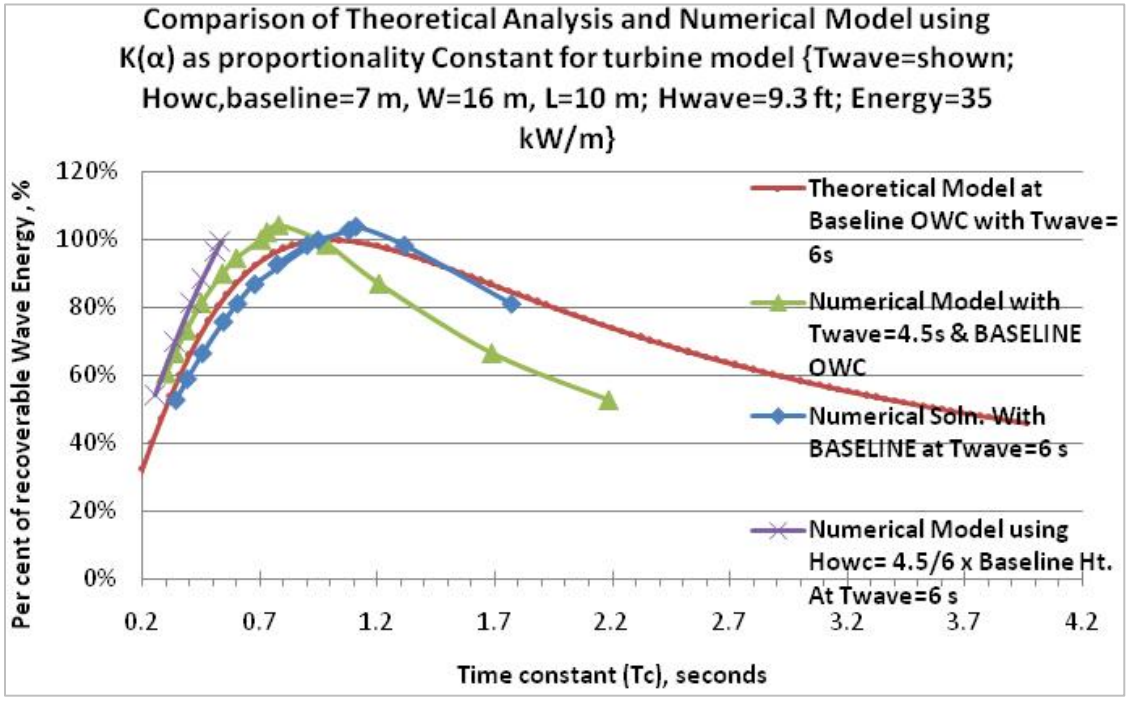

Figure 23. Comparison of Theoretical Analysis and Numerical Model

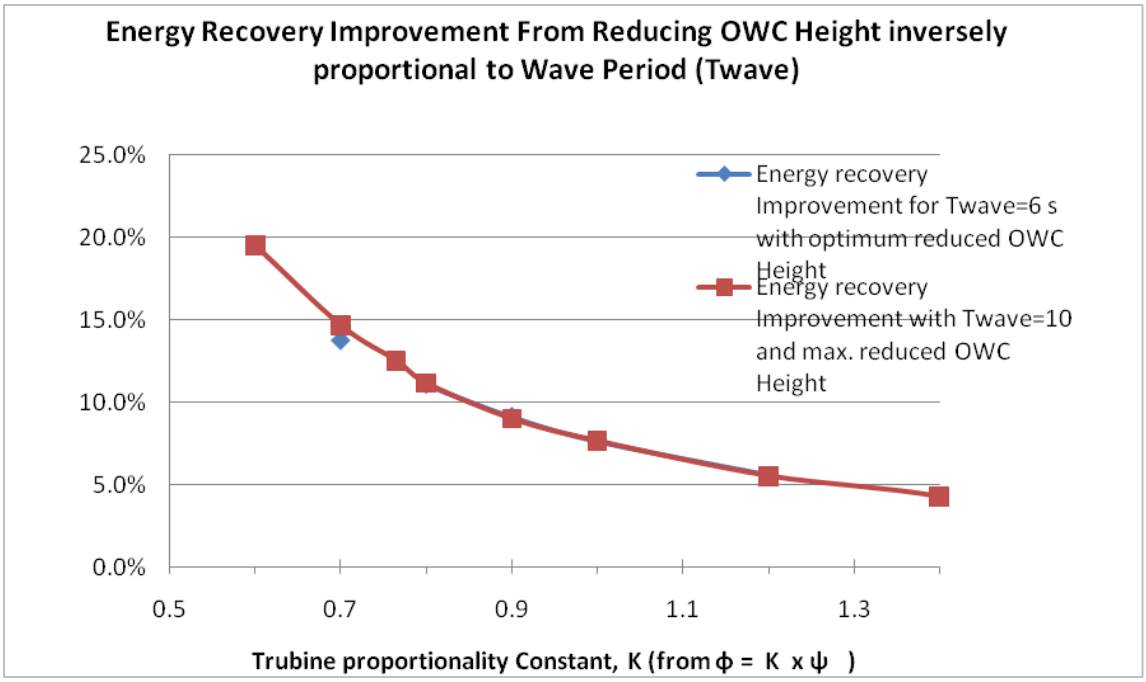

Figure 24. Results of Energy Recovery Improvement

It is essential to note that this innovation is not intended to be applied through active feedback control of the buoyancy system in place on the OWC system for rapidly changing wave frequencies. Instead, the intent is to be able to monitor the imminent wave climate for long-term availability of higher frequency waves, i.e., durations measured in hours and not minutes, or days and not hours, and adjust the operating height of the OWC chamber according to this modeling algorithm. The actual demonstration of this effect on a scaled OWC chamber is proposed as one of the major Phase II STTR efforts by using the wave tank testing facility available to the faculty, students, and staff project collaborators at the MMA. The MMA collaboration includes access to the wave tank facilities at their sister institution, the University of Maine, which like the MMA, is part of Maine's public higher education system.

As this benefit comes at little to no change to the buoyancy control mechanism of the OWC system, it will eventually be tried on the Oceanlinx Mk3PC OWC prototype system; a system that was designed by Oceanlinx precisely for demonstrating the benefit of innovations that improve the effectiveness of OWC systems.

6. The major innovation resulting from the Phase I research was the proposed use of a turbine "shutter" valve system. That is, at the beginning and at the end of the wave ascension and descension, it is suggested that the air flow to the turbine be momentarily interrupted in order to enable the chamber pressure. Upon its sudden release, the OWC airflow rate is increased but is also made more constant, resulting in more power from the net energy from the turbine, even at its design point wave period specification.

   To demonstrate the benefit of this innovation, the energy conservation methodology model was used to affect a time-variant air flow rate through the turbine (effectively modeling a sudden closing and opening of a turbine "shutter" valve). The timing of the valve closing and opening was controlled, as was its

duration and the amount of air that was allowed to leak through the turbine. For this study, a time duration of 30% of the wave period and an 80% reduction in the flow rate through the turbine were modeled. The location of the valve closing and opening is shown in Figure 25. The effect on the flow rate is dramatically displayed in Figure 27. The efficiency of the turbine may be observed in Figure 25 to be steadier for a longer range of time.

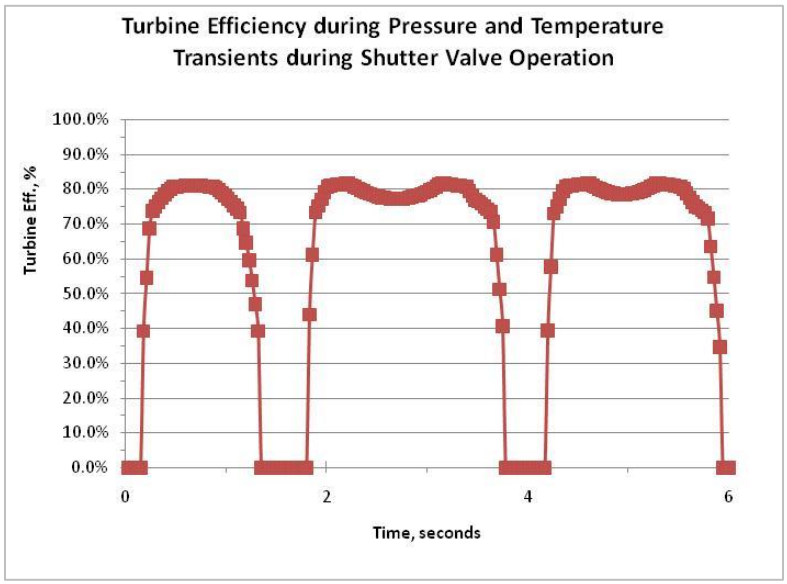

Figure 25. Location of Valve Opening and Closing

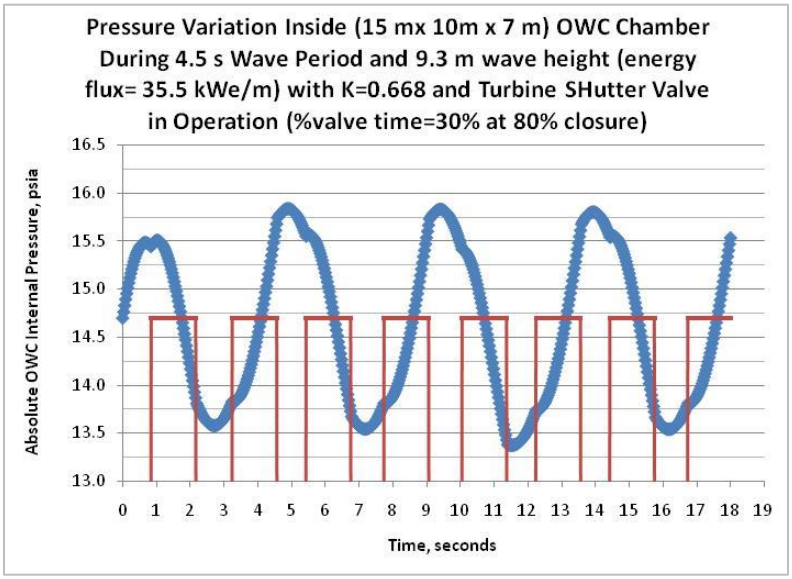

Figure 26. Effect on Flow Rate

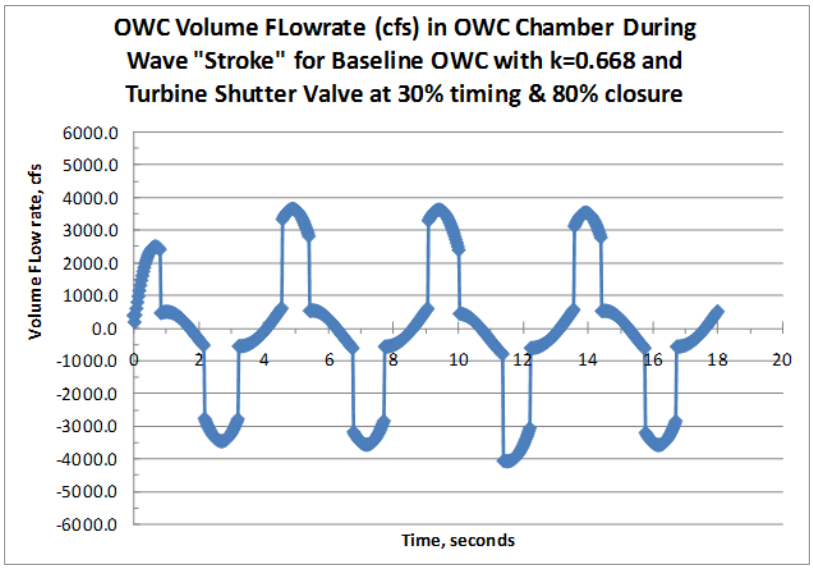

Figure 27. Efficiency of the Turbine

The energy recovery improvement is displayed in two ways, as shown in Figures 28 and 29. Figure 28 displays the improvement as a function of the time constant, T_c, as defined in this report. The arrow shown in Figure 28 identifies the optimum time constant for a wave period of 4.5 seconds. Thus, improvements are shown to increase at smaller time constants. This is as expected because the amount of wasted, non-recoverable energy for a given wave period and OWC system size was observed to increase at smaller values of the time constant (see Figure 24). Figure 29 displays a similar result, but is presented as a function of the turbine proportionality constant, which as described in Item 1, can be made to effect change in the time constant for a fixed system. Figure 30 illustrates that resuts from *CN*'s numerical model also provide evidence that the the volume of the OWC air space above the wave enables a means of optimizing the recovery of the wave power relative to the OWC system time constant.

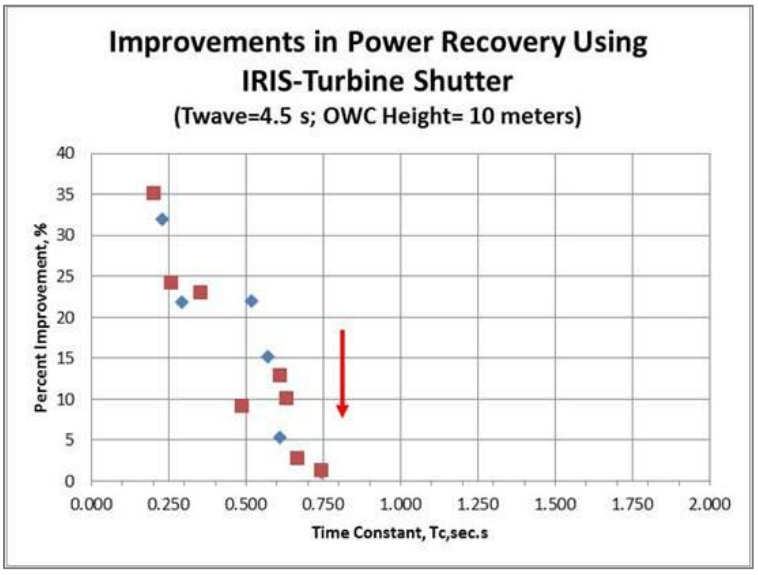

Figure 28. Energy Recovery Improvement as a Function of Time Constant

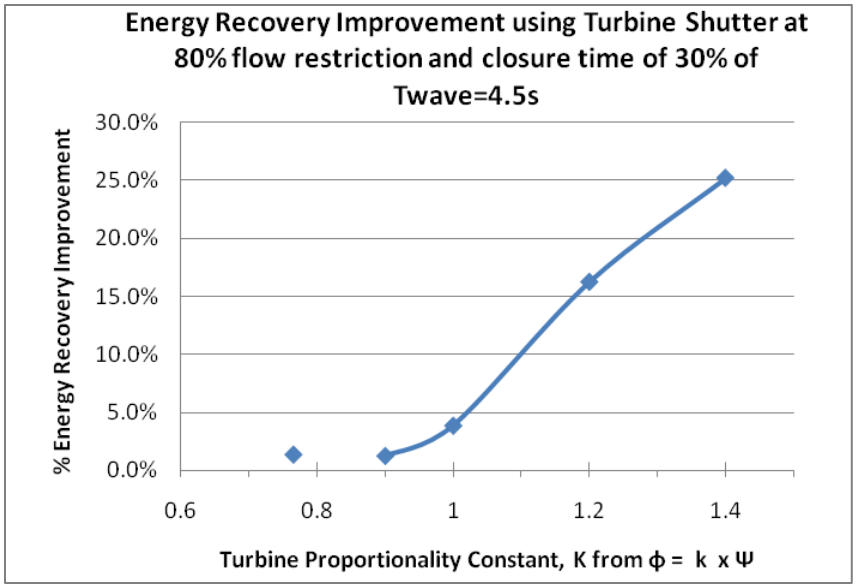

Figure 29. Energy Recovery Improvement as a Function of the Turbine Proportionality Constant

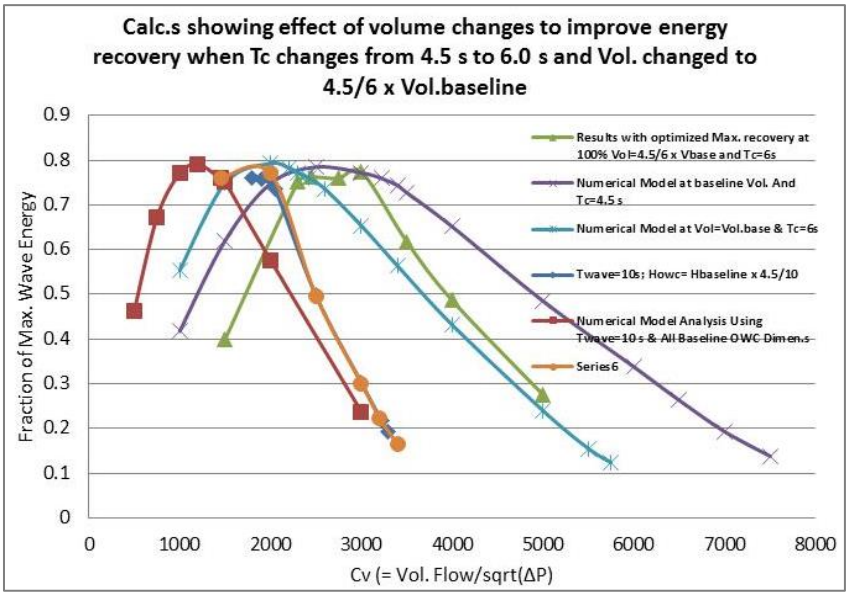

Figure 30. Results from *CN*'s Numerical Model that Provide Evidence that the Change in the Volume for the Air Space Above the Wave Enables an Optimization of the Wave Power Relative to the OWC System Time Constant

It is interesting to note that *CN*'s modeling does concur with several very relevant results by researchers identified in References [10, 14, and 15]. This independent research tended to validate *CN*'s numerical results and thus provides confidence in *CN*'s proposal to use a turbine shutter valve. For example, de O. Falcão [15] analytically identifies a 37% increase in the power output from an OWC system if a bypass valve is used in the OWC chamber. The bypass valve provides this improvement by simply eliminating the stalling of the turbine, and thus allowing the turbine to continue to generate power at a higher overall efficiency. However, what is not clear from de O. Falcão's analysis is how much more power could have been achieved if the air flow that is forced to

bypass the turbine could drive the turbine, while the turbine is operating at a higher efficiency. Also, it is important to note that de O. Falcão's study was more of a focus on how to improve turbine performance as a means of improving wave energy recovery when using an OWC device, as opposed to a focus on the operational mechanics of the OWC device as a way of identifying characteristics of all of the OWC subsystems that can help improve wave energy recovery.

7. The turbine shutter valve can also contribute to the phase shifting of the OWC system. Independent researchers such as Falnes [1] and de O. Falcão [15] dominate the area of OWC optimization and control. Independently, these researchers proposed the use of "latching" to correct the motion of the OWC, so that it can be 180 degrees "out-of-phase" with the incident wave. This will help to increase the relative velocity between the OWC structure and the motion of the wave. However, the latching as recommended by Falnes and others is to add a bypass valve to the OWC structure that is in parallel to the turbine, or to add power through various pneumatic means during parts of the wave's cyclic motion. It is relevant here to indicate that the proposed turbine shutter valve concept presents a much simpler means of affecting OWC control and, at a controllable moment during the incident wave motion, uses the wave energy to "capture" the OWC structure via the increase in OWC chamber pressure (i.e., increasing the air spring stiffness) and releasing the OWC when it is in the correct 180-degree out-of-phase relationship with the subsequent incident wave activity.

   Using the turbine shutter valve to enable the wave energy to be used to manipulate the OWC structure is an advantage over the suggestion of previous researchers to employ hydraulic or pneumatic power input to the OWC chamber air and thus bring the OWC in step. In summary, the proposed turbine shutter valve system can contribute to correcting the OWC motion by increasing the stiffness of the air column, and thus have the OWC structure heave with the wave until the shutter valve is opened to allow the vessel to fall into a 180-degree phase shift. This feature would not be controlled instantaneously via an active feedback control of the OWC motion, but rather a periodic adjustment of the structure when the wave climate changes significantly and the changes are predictable and expected to be prolonged.

   It is also interesting to observe a conclusion from Falnes' technical paper, wherein he suggests that "…to obtain the optimum oscillatory motion for maximizing the absorbed energy or the converted useful energy, it may be necessary to return some of the energy back to the sea." Falnes proposed (but like de O. Falcão, did not implement the proposals) that mechanical power be input into the OWC system in the form of pneumatic or hydraulic energy "… during some small fractions of each oscillation cycle and profit from this during the remaining part of the cycle."

   The turbine shutter valve, as conceived in the Phase I STTR study, can provide this power input by utilizing the incident wave energy during the moments of the ascension and descension of the wave front, as described above. That is, by trapping the air volume in the OWC chamber, the effective spring constant that models this trapped air causes the OWC to be raised or lowered with the wave front; literally having the wave energy content stored in the mass of the OWC in the form of potential energy. Some or all of this potential energy can then be restored to the water when the OWC "rides" the wave downward. Whether some or all of the waste energy is dissipated in this manner is dependent on when the turbine shutter valve is closed or opened during the wave cycle. As mentioned

above, the timing of the turbine shutter valve operation would be guided by keeping the OWC 180 degrees out-of-phase with the incident water wave.

2.7 Turbine Shutter Valve System

A conceptual design for the turbine shutter valve system was completed in Phase I, with a cost estimate prepared based on the purchase of 64 shutter valve systems. The feasibility study indicated that in order to minimize the starting torque required from the electric or pneumatic driver to actuate the shutters in one second, it would be necessary to reduce the rotating mass as much as possible. Thus, the design requirement was constrained to concepts that would have only the shutters of the turbine shutter valve move to interrupt the air flow to the turbine, and not the entire rotor assembly. Two options were selected among the many different conceptual designs that were studied. The best of several options considered is shown in Figure 31. The detailed design of the turbine shutter valve is completed in Phase II; however, the basic design consists of a stationary wheel or stator that is constructed with pivotal shutters. The shutters have roller pins on the shutter edges that protrude through the slots in the outer ring. The slotted ring guides the shutter pins through their 70-degree motion as it is rotated through (approximately) 20 degrees. The slotted ring can be motored by a stepper motor for precise control.

The shutter valve is intended to impede only 80–90% of the flow to the turbine rotor, and thus, the shutters are expected to be at least as tall as the blades of the turbine. An aerodynamic study of a Wells-type turbine that could provide 300 to 350 kWe power indicated a hub rotor diameter of 4 ft plus 1 ft long turbine blades (i.e., 6 ft overall diameter) with a speed of 750 rpm. The cost to manufacture the shutter assembly, shown as Option 2 in Figure 31, has been estimated, and the summary is given in Table III.

These estimates are based on manufacturing cost studies for a mechanical system associated with air turbine construction and on *CN*'s experience in manufacturing similar systems for other projects. For example, a ½-scaled blade articulation system included the construction of a similar blade support stator but included a sophisticated blade articulation system, as shown in Figures 32. The stator has a diameter of 26 inches, and the cost to manufacture a single prototype system was commissioned at $8,000. Therefore, the cost estimate for a much simpler, albeit larger diameter, stator of $14,743 is considered reasonable. However, this cost was conservatively increased to $20,000 for the purpose of determining the simple payback for the turbine shutter valve integration into an OWC system (as shown in Table IV).

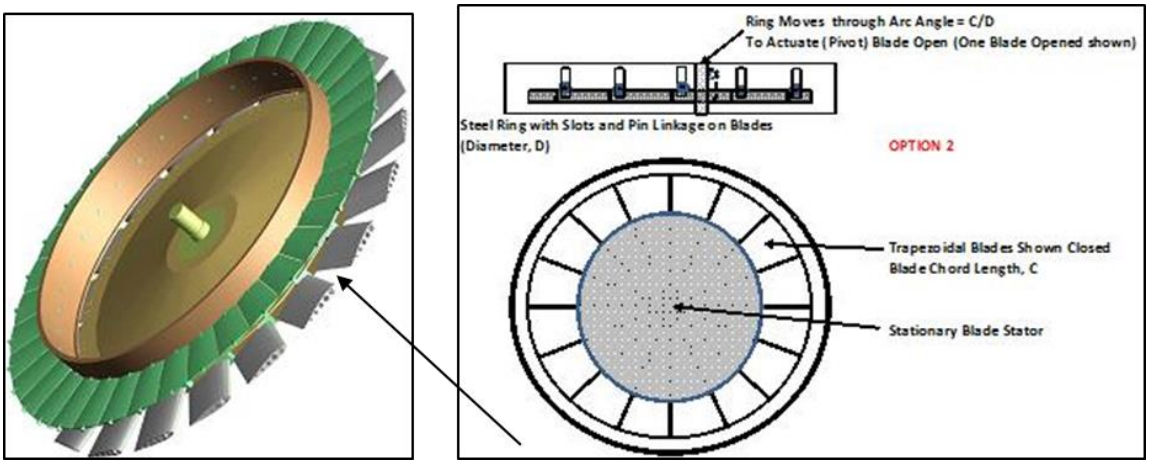

Figure 31. Turbine Shutters Shown Closed in Front of Turbine Airfoil Blades (slotted drive ring and stepper motor not shown)

TABLE III. COST TO MANUFACTURE OPTION 2 SHUTTER ASSEMBLY

No. of Mark 3 Oceanlinx Systems			**8**			
No. of Turbines per Mk3 OWC			**8**			
Single Turbine Power=			**350**	kW		
Shutter Mfg. Costs (64 systems - 22.4 MWe OWC)						
Hub Dia= 4 ft	**per Unit**	**No. req.d**	**Single Assy.**	**Multiple Assy per Unit**		
Shutter Length= 1 ft	**Cost**	**per Assy.**	**Cost**	**Cost**	**Weight (lbf)**	
Shutter Plates	$ 125	18	$ 2,250	$ 1,800	148	
Shutter Plate Pin and bearings	$ 50	18	$ 900	$ 855	3	
Hub & Rotor Stamping	$ 7,500	1	$ 7,500	$ 5,625	124	
Slotted Rim & gear rack (20 deg. Arc)	$ 4,500	1	$ 4,500	$ 3,600	384	
Rim Bearing	$ 750	1	$ 750	$ 713	250	
8 Hp Elec. Motor & Control	$ 1,000	1	$ 1,000	$ 850	175	
Misc. (10% of total)				$1,300.0	100	
				$ 14,743	1,184	

Using this manufacturing cost for the proposed turbine shutter valve system and the published cost estimates [2] for the subsystems that constitute the OWC-type water energy conversion system, a net simple payback for adding the proposed turbine shutter valve system to an OWC system has been calculated, and the result is shown in Table IV. The analysis considered the present costs per kW for an OWC system, the O&M costs for producing the electric power, and the value of the electric power that is produced to determine a very reasonable payback for the proposed new shutter valve system that can improve the cost per kW for the OWC system by 22%.

TABLE IV. SIMPLE PAYBACK FOR INTEGRATION INTO OWC SYSTEM

Ref: # 41; page 283 averages from 3 OWC systems

			Component Costs			$cost adder for Additional Component(s)	% Improvement Energy Recover
System Availability, %	85%						
OWC Base Cost ,$/kWe	6000						
Kwe=	350						
OWC Cost	$ 2,100,000		$present	% reduction	$final cost		
Mechanical & Electric Systems, %	0.3		$ 630,000				
Generator		0.07	$ 147,000	0.00%	$ 147,000	$ -	2.0%
Turbine		0.075	$ 157,500	5.00%	$ 169,625	$ 20,000	15.0%
Diffuser & Inlet Guide Vanes		0.025	$ 52,500	7.50%	$ 48,563	$ -	0.0%
Structural Framework		0.05	$ 105,000	0.00%	$ 115,000	$ 10,000	0.0%
Controls		0.08	$ 168,000	5.00%	$ 159,600	$ -	1.0%
Installation, %	0.15		$ 315,000				
Mechanical		0.1	$ 210,000	0.0%	$ 210,000	$ -	0.0%
Electrical		0.05	$ 105,000	0.0%	$ 105,000	$ -	0.0%
Vessel Construction, %	0.25		$ 525,000	0.0%	$ 525,000	$ -	
Electrical Trans., %	0.05		$ 105,000	10.0%	$ 94,500	$ -	0.0%
Contingencies, %	0.1		$ 210,000	0.0%	$ 210,000	$ -	
Transportation, %	0.15		$ 315,000	0.0%	$ 315,000	$ -	0.0%
	1.00		$ 2,100,000		$ 2,099,288	$ 30,000	
			NET OWC Cost Savings, %		0.03%	Energy Improv.=	28.0%
			NET Effective $/kWe=		4,686		
			Net Improvement, $/kWe %=		22%		
			$O&M=		0.02	$/kwH	
			$finance=		0.06	$/kwH	
			$/kWh)income=		0.15	$/kWh	
			Yearly Income=		$ 229,242		
			Simple Payback=		0.47	years	

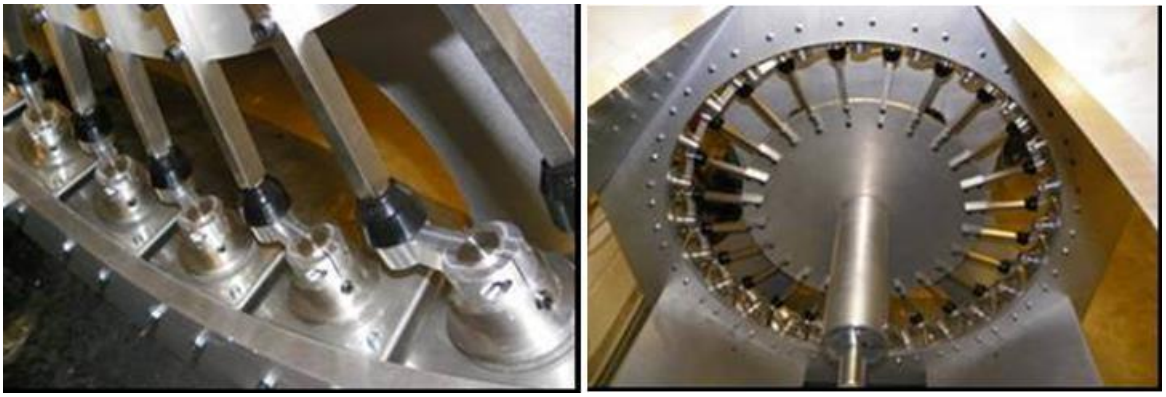

Figure 32. Construction of a Blade Stator Including a Blade Articulation System

2.8 Mathematical Algorithm Development Efforts by MMA (Professor Pat Lorenz)

It is clear from CN's theoretical and numerical OWC performance models that the vertical, free surface, relative velocity of the radiated portion of the incident wave energy must be known accurately if the models are to be successful to help optimally "tune" the OWC systems. That is, equally important to the efficient transfer of the wave energy into the pneumatic OWC column, is controlling the motion of the OWC platform relative to the incident wave.

The essence of the problem is that the vertical motion of the water column within the OWC must act to absorb incoming wave energy, essentially having the damping characteristics (D or β) of the OWC perform the same function that a damper in a classical mass-spring system performs to absorb the unwanted vibratory energy. It is essential, however, that the damping does not exceed the critical damping for the system, which would start to cause the OWC to heave upward with the water wave and thus not compress the air column to produce power by the turbine. The damping energy is found to be the product of the damping coefficient, $\Delta P_{avg}\, A_{owc}^2/Q_{avg}$, and one-half the square of vertical velocity of the water wave's free surface (i.e., Eq. 10). Therefore, it is necessary to solve for this DL/Dt for the water wave energy that is radiated from the primary incident water wave energy.

At the beginning of the Phase I research effort for the STTR, CN and the MMA researcher, Professor Pat Lorenz, summarized the subtasks that would most benefit CN's numerical modeling. These subtasks were as follows:

1. Derive the mathematical equations that determine the fraction of the incident wave energy that is separated into radiated and diffracted parts. The radiant energy is the recoverable portion of the incident wave energy that can be recovered by the OWC system to generate power.
2. Derive the mathematical equations that determine the velocity (Vy) of the free surface of only the radiant wave energy portion of the incident wave energy. This is the wave that actually enters the OWC chamber, and that is therefore available for OWC recovery.
3. The mathematical relationships will be a function of the OWC structural parameters that can be used to develop engineering design specifications for the OWC, much like what is accomplished in Reference [17]. Among these engineering specifications is the damping coefficient (D) which is defined as: $\Delta P \times A_{owc}/Q$, and for which the mathematical relationships derived in Items 1 and 2 will determine an optimization criterion. For example:
    a. According to Reference [18], the optimum conversion potential occurs with: $(D/A_{owc})\, x\, V_y = 1$ and at repetitive integer frequencies that correspond to the ratio of the breadth of the OWC to the wave length (L).

b. According to References [15] and [17], the maximum energy efficiency for a simple OWC system that does not use a reflecting wall will be limited to 50%.

c. Most of the references noted above remind the reader that the energy absorbed in the pneumatic air column is essentially the amount of energy that is required to damp the OWC system. Thus, if damping power is equal to: $D\,(V_y^2)/2$, then the power generated by the OWC turbine is: $Power = \{D\,(V_y^2)/2\} \times \eta_{turbine}$ (where the V_y is a relative velocity between the water wave and the vertical motion of the OWC motion)[2]. This is an interesting insight into the behavior of the OWC and is an approach used to determine the amount of potential energy that can be captured without needing to define the wind turbine subsystem, except for assumptions made of the linear or nonlinear nature of the relationship between the chamber pressure and the volume flow rate through the turbine.

   The approach essentially uses the well-known and understood engineering principle of a damping system that can absorb the energy of a harmonically oscillating system (usually represented by a mass (*M*) suspended by a spring, with a spring constant, *k*, and a damper (*C* or *D*) that is used to absorb the mass-spring energy. Although not stated in these technical references, but inferred, is the need to design the damping system parameter (which is a function of the geometry of the OWC and the performance characteristics of the OWC turbine) such that the system is, in the limit, critically dampened and thus optimally enabling the water wave energy to be completely absorbed for each periodic incident wave, without allowing the system to decay over several cycles. A proposed expression for the critical damping coefficient is: $D_c = 2\,[D\,Q\,\rho/g_c]^{0.5}$ based on classical harmonic mass-damping theory.

4. The ability to keep the OWC structure in negative phase (i.e., 180 degrees opposite relative motion with respect to the wave frequency) may achieve the maximum in power recovery from the pneumatic column. Thus, a solution to the overall dynamics of the OWC structure with respect to the incident wave frequency at any time is of interest to <u>*CN*</u>.

The mathematical solution should proceed by solving the equations governing linear water waves with slightly different boundary conditions. The two boundary conditions for Laplace's equation at the free surface are typically linearized into one equation by applying the conditions at y = 0 rather than at the free surface, $P(t,x_1,x_2)$. For linear wave theory, the pressure at the free surface, $P(t,x_1,x_2)$, is assumed to be a constant. In the case of an OWC, the pressure inside the OWC is a function of time and is strongly influenced by the time constant of the OWC system determined by the turbine flow characteristics, as seen in Eq. 10. The geometry of the OWC places additional boundary conditions as well by dictating that the velocity normal to any surface on the OWC must be zero.

Water Wave Equations (References [4, 6, 18–20]):

Laplace's Equation: $\partial^2\varphi/\partial x^2 + \partial^2\varphi/\partial y^2 + \partial^2\varphi/\partial z^2 = 0$ $\qquad -h_0<y<0$

Boundary Conditions:

$\delta\eta/\delta t + (\delta\varphi/\delta x_1)(\delta\eta/\delta x_1) + (\delta\varphi/\delta x_2)(\delta\eta/\delta\chi_2) = \delta\varphi/\delta y$ $\qquad y = \eta(x_1,y_1,t)\sim 0$

$P(t,x_1,x_2) = P_0 - \rho_{H2O}[\partial\varphi/t\,\partial + 0.5(\partial\varphi)^2 + g\eta]$ $\qquad y = \eta(x_1,y_1,t)\sim 0$

$\partial\varphi/\partial y + (\partial\varphi/\partial x_1)(\partial h_0/\partial x_1) + (\partial\varphi/\partial x_2)(\partial h_0/\partial x_2) = 0$ $\qquad y = -h_0$

Free Surface: $\eta(x_1,y_1,t) = -1/g\,\delta\varphi(x_1,x_2,0,t)/\delta t$

[2] It is noted that the use of a relative velocity is not mentioned in any of the papers referenced thus far and perhaps only because most OWC applications are for land-based systems, and not for systems that are floating on the water.

Fluid Velocity Vector: $U = \nabla \varphi$

Pressure: $P = P_0 - \rho_{H2O} [\delta \varphi / \delta t + 0.5(\nabla\varphi)^2 + gy]$

Linear Wave Theory Dispersion Relationship: $\omega^2(k) = g\, k\, tanh\, (kh_0)$

The focus of this STTR effort is on developing an actively tunable OWC system which will allow real time control and synchronization of the OWC pressure $P(t,x_1,x_2)$, and hence, the ability to produce an optimized water column motion within the OWC in order to absorb and cancel the incident wave energy. Given enough range and control of the time constant, the OWC designer will be able to optimize the OWC geometry by solving the water wave equations, which will determine both the motion of the water column and the freedom motion of the OWC.

In some of the previous literature, there has been a temptation to over-simplify the problem by reducing the equations of motion to a linear damped harmonic oscillator, as shown in the following equation.

$$m\, d^2z/dt^2 + ß\, dz/dt + k\, z = f(t)$$

Unfortunately, the predicted results compared to the actual performance tests are typically disappointing when a simple harmonic oscillator model is used to design the OWC system. The result is that, in order to optimize an OWC design and take full advantage of an actively tunable turbine system, the water wave equations outlined above need to be understood and solved for the particular geometry of the OWC design, but by taking advantage of the prior research performed by several university researchers identified in References **[4, 6, 18–20]]**.

A review of the technical literature concerning the mathematical and numerical modeling of OWC system performance with their interaction with water waves continued even as MMA's models matured. Due to the extensive amount of literature and the variations on the OWC modeling theme that each of these technical papers provides, the review can never be exhausted, but simply must be prioritized to accomplish the work at hand for the current STTR, namely to determine how an OWC can be "tuned" to achieve the highest possible energy recovery for a variety of water wave energies that are incident upon it. This objective necessarily must have the interaction of the water wave hydraulics and the OWC structure understood in order to determine how the OWC can be tuned, i.e., the OWC structure, and particularly how the wind turbine subsystem can be adjusted in a cost-effective manner to modulate with changes in the incident water wave energy.

Many other research papers that have been studied are listed at the end of this report. These papers are also useful for modeling the Wells turbine in its application of OWC systems, but were given lower priority for their review than the several technical papers listed in the references given at the end of this final report.

The accomplishment of the following objectives for the MMA mathematical analysis would be most beneficial for improving the OWC thermo-fluid computer model. This analysis has also been studied by many researchers, as noted in the references provided in this report. Some of this analysis was thought to be very applicable to the necessary mathematical solutions that can be applied to *CN*'s thermo-fluid model.

In the most relevant references (such as those listed above), the objective is to satisfy all of the boundary conditions for this velocity potential (φ) that are constrained by the physical parameters of the OWC system and to determine the diffracted and radiated parts of the incident wave energy, along with their subsequent shorter wave heights and thus lower energy content. Unfortunately, given the typical length constraint of a technical paper, the derived equations often have missing links and the results of the calculations are usually summarily displayed in graphs without displaying the step-by-step calculations that produce those results. Therefore, the equations that are presented do not lend themselves to direct programming. In addition, only the mathematical developments shown in Reference No. 19

come close to producing results that can be directly applied to a floating OWC, which would be the most applicable to the OWC system that is of interest to this STTR.

Thus, the mathematical analysis that was performed by MMA generally followed along the same lines of thought as noted in these studies. That is in these studies, the water wave dynamics are represented by a velocity potential (φ) that satisfies the Laplace equation, assuming that the linear water wave theory applies, i.e., that one of the boundary conditions is the horizontal free surface of the water (i.e., $y = 0$) when no motion is present[3]. The MMA results are provided in Appendix 1. A major objective of the completed mathematical analysis was to determine the mathematical equations for the relative velocity (i.e., the wave front with respect to the OWC vessel) of the free surface of only the radiant wave energy, (i.e., the wave that actually enters the OWC chamber and that is thus available for OWC recovery). In order to determine this velocity, it will be necessary to determine the fraction of the incident water wave energy that partitions into the radiated and diffracted portions.

3.0 PHASE II STTR PROJECT TECHNICAL OBJECTIVES AND WORK PLAN: DESIGN AND INTEGRATION OF A TURBINE "SHUTTER" VALVE TO AFFECT INCREASED WAVE ENERGY RECOVERY IN OWC SYSTEMS

3.1 Technical Objectives

The principal objective of this research has been to improve the power recovery from a wider range of incident wave energy that may interact with an OWC system, and thus effectively reduce the cost per kWe for an OWC wave energy recovery system. The primary objectives may be summarized into four specific objectives.

1. Experimentally validate the use of a turbine shutter and an OWC height control methodology that has been analytically determined by *CN* to improve the energy capture from incident water waves. The turbine "shutter" valve system (shown in Figure 31) is a major innovation resulting from the research. The turbine shutter closes the turbine from air flow at the beginning and at the end of the wave ascension and descension. The momentary interruption of the turbine flow has the effect of storing the kinetic energy. Upon its sudden release, the OWC airflow rate and pressure is increased, but is also made more constant, resulting in more power from the net energy from the turbine, as it now operates closer to its design point specification. *CN* has been able to analytically identify energy improvements of as much as 20% for conventional OWC wave energy conversion systems.
2. The shutter vane described in Section 2.7 may also serve as a means of continuously controlling the airflow through the turbine in order to maintain a relatively constant velocity across the turbine rotor airfoils. The control of the shutter assembly is to be based on the continuous monitoring of the OWC chamber pressure. The objective of modulating the shutter vanes is to reduce the inherent transient nature of the air flow and hence velocity through the turbine. The controls methodology strategy for timing the operation of the turbine shutter, the OWC height and/or the reflector plate extension will be perfected as a result of actual water wave tank tests and summarized via suitable controls algorithms.
3. The OWC system can also be better "tuned" to provide increased energy capture from waves that are of a wide range of amplitude and frequency (i.e., different energy density, kW/meter) that are incident upon the OWC by changing the height of the OWC above the water line. This is not anticipated to be done on a continuous feedback basis, but rather only when a known wave climate is

[3] Reference [21] is actually a tutorial for defining the terms that are often used in these other research papers. The reference includes an excellent primer on the solution of the velocity potential (φ) for the water wave dynamics. However, this reference does not develop the necessary equations for modeling an OWC or any other water wave energy system.

expected to reach the OWC system and extend for many hours or days. A conceptual sketch of a proposed lab prototype OWC structure (shown in Figure 33) has been designed with adjustable wall lengths and reflector plate extensions that will enable the manual adjustment of these dimensions in order to determine their benefit in tuning the OWC system for a wide range of wave amplitudes and frequencies.

4. Continue to develop the mathematical model the OWC system in order to identify additional critical design parameters for the OWC turbine and OWC structure. For example, as a result of the continued mathematical modeling, it is suggested that a wave reflector plate that is installed on the OWC system, and designed to have a variable length extension and surface area, can "tune" the OWC to improve the energy capture effectiveness of the OWC structure when incident upon by water waves of different amplitudes and periods.

In a concurrent effort, a scaled WEC OWC that can test these system modifications is planned to be fabricated for testing at the MMA and University of Maine, using their wave tank facilities. A functional mock-up of an OWC was fabricated by MMA during the Phase I of the STTR project and is shown in Figure 17 (a), but was redesigned similar to Figure 33. The MMA development test facility is part of the Tidal Energy Demonstration and Evaluation Center (TEDEC; c/o Mr. Richard Armstrong, 207-326-2186) that is in place at the Maritime campus for such purposes.

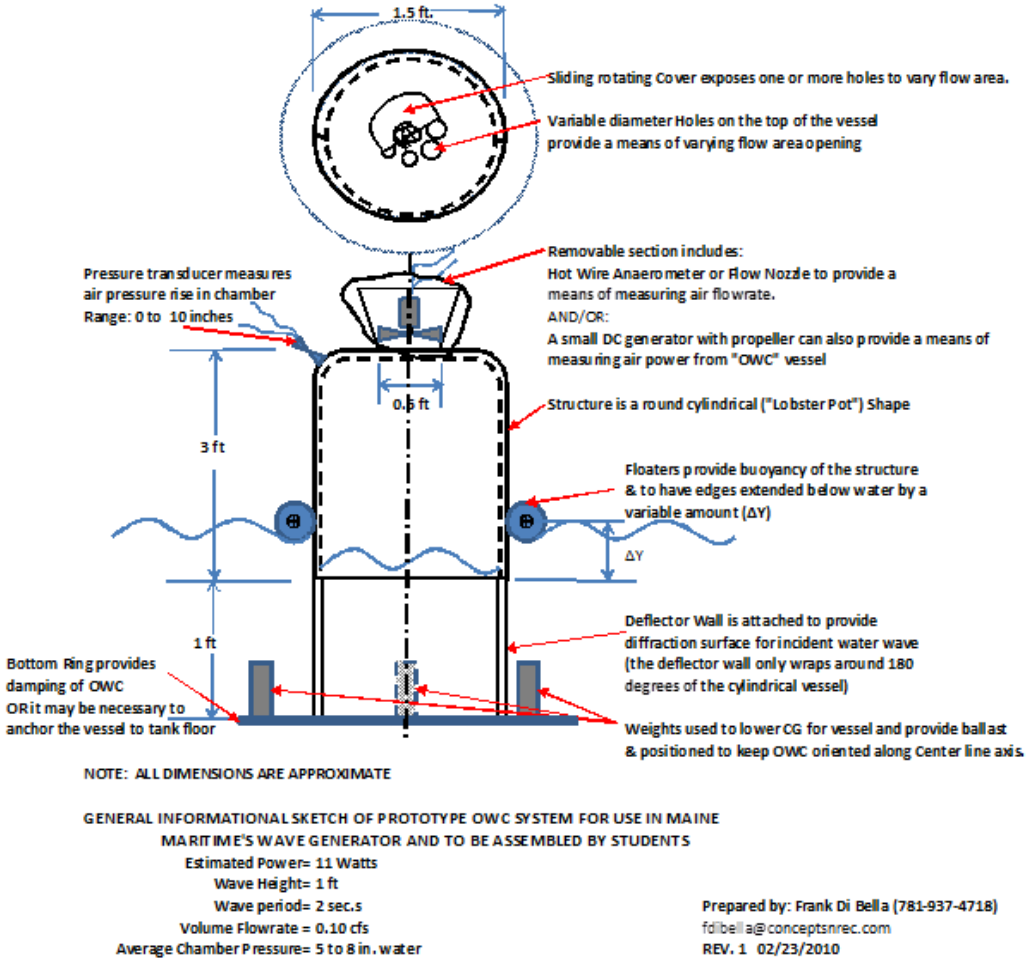

Figure 33. A Very Preliminary Concept for a Laboratory Prototype OWC to Be Tested at the University of Maine

The fabrication of this scaled-up system, with more instrumentation to record the performance of an equivalent turbine shutter system and the effect of OWC height adjustments, was completed by the students at MMA during Phase II. The system helped to validate the OWC numerical modeling, specifically the OWC chamber pressure and volume flow rate transients, as well as the verification of the improvements that are proposed by *CN* based on *CN*'s Phase I and Phase II engineering analyses; including the validation of the controls algorithms that will be a direct result of MMA's and *CN*'s continued OWC numerical modeling. The controls algorithms, i.e., the functional relationship between the timing of the shutter valve and height adjustments of the OWC, and the incident wave frequency and amplitudes, were a major part of the collaborative effort during the first year of Phase I. Certainly it was an important and timely educational tool for the students at MMA as well as the focus of wave energy conversion research.

The Phase I effort succeeded in identifying the most viable advanced wave energy conversion opportunities that can improve the OWC system economics by as much as 30% energy recovery improvement, in addition to reducing the OWC capital costs while confirming the robustness of the system.

Through the work completed in the Phase I effort, the proposed design of a turbine shutter prototype, and validation testing of this technology in Phase II, *CN* has produced a well-documented and established technical foundation from which to incorporate this adaptive turbine technology into the next-generation OWC systems.

The strong commitment from *CN* and MMA, as the principal investigators, served to successfully carry forward the Phase I program and Phase II. Oceanlinx, as the possible entrepreneurial industrial user of the technology, suffered the loss of their OWC test platform in 2010 during a severe storm in Australia. The platform could not be recovered, and thus, Oceanlinx could not continue their participation in Phase II. The Statement of Work given here is a revised version that substitutes a dry test platform for the testing of the Mk3PC OWC turbine, in lieu of testing by Oceanlinx. The testing of the OWC prototype turbine in the University of Maine water wave tank continues as scheduled.

3.2 Phase II Tasks and Work Completed

The text in italics below each task title is content from the original Statement of Work. Please note that figure, section, and table numbers referred to within the text in italics are in the original proposal, not this final report.

3.2.1 Task 1. *CN* Prepares Final OWC and Turbine Specifications for Mk3PC Demonstration Turbine

CN and its project collaborator, the MMA, will review the design specifications of a 100 watt, nominally rated prototype (Mk3PC), oscillating water column-based wave energy converter, for the purpose of defining the specifications suitable for testing in the University of Maine water wave test facility. Based on this review, a specification will be prepared by CN for the purpose of guiding the detailed design of a turbine shutter that can be integrated into the Mk3PC.

Two OWC prototype turbines were conceptualized for the testing at *CN*. The prototypes were developed by *CN* personnel and the University of Maine by MMA researchers. These two turbines were sized for approximately 10 and 50 watts, respectively, and labeled the micro-OWC Wells turbine and the mini-OWC Wells turbine (previously the Mk3PC). The first requirement was to analyze the wave energy available from the University of Maine wave energy facility, in order to determine the size and speed of a mini-Wells turbine. The turbine speed and diameter of the mini-Wells had to match what was commercially available for use with a simple DC motor/generator test. Such motors have speeds of approximately 1000 to 1200 rpm and a diameter that is limited to about 50 to 75 mm and that can match the size of the prototype MMA OWC structure that must fit in the available tow/wave tank. For that purpose, *CN*'s thermo-fluids OWC performance model was used to determine the pressure and air

volume flow rate through this turbine based on a computer model of the estimated 12” x 12” x 12” MMA OWC chamber. The results of this modeling are shown in Figures 34 and 35. The two pressure-air volume flow rate specifications that are shown in Figures 36 and 37 have been derived using a computer model that has been prepared to model the thermo-fluid performance of an OWC system. The thermo-fluids model treats the ascending-descending water wave front as a piston within an open cylinder. However, the opening in the cylinder includes an air turbine which can provide power generation from the transient chamber pressure and air flow rate that the wave front forces through the turbine.

The calculated transient pressure and volume flow rates are dependent on the nature of the obstruction (i.e., the turbine) that is in the opening. Two models have been programmed based on a study of either a variable-pitch turbine (such as available with the Dennis-Auld turbine promoted by Oceanlinx) or a fixed-airfoil, bi-directional air turbine (the type available with a Wells turbine).

A sketch of *CN*’s initial prototype OWC chamber and the integrated mini-Wells turbine could be used with the testing that is planned for the MMA tow/wave tank to achieve some useful results in testing the Phase I hypotheses. That initial conceptual design was shown in Figure 33.

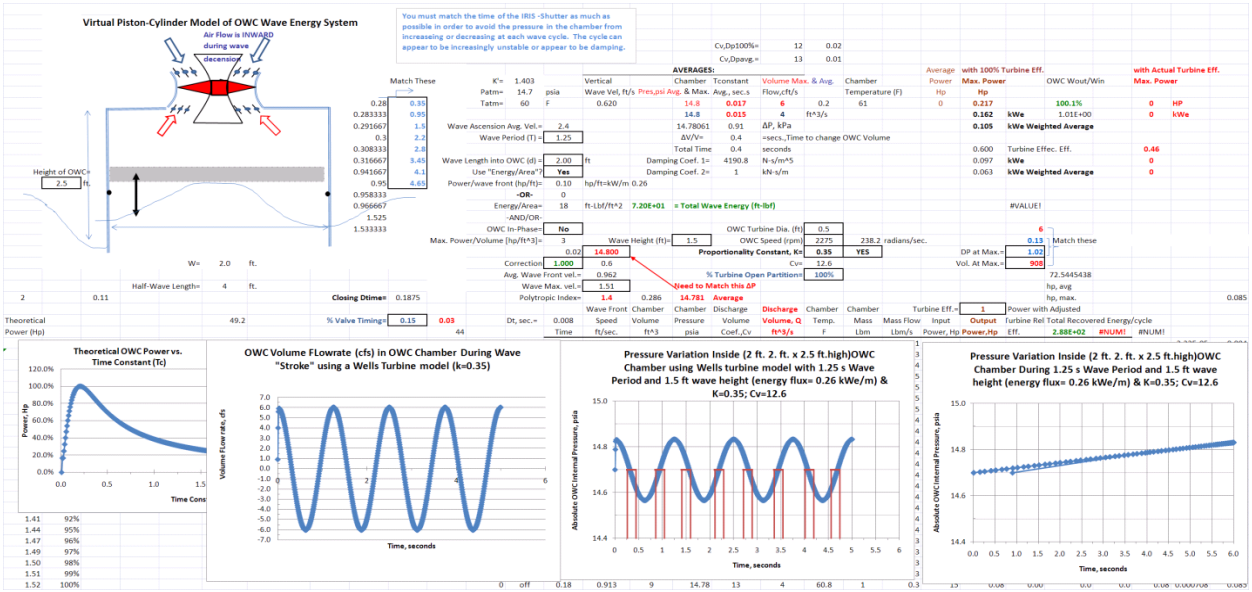

Figure 34. Example of Input Page of *CN*’s Spreadsheet Numerical Model

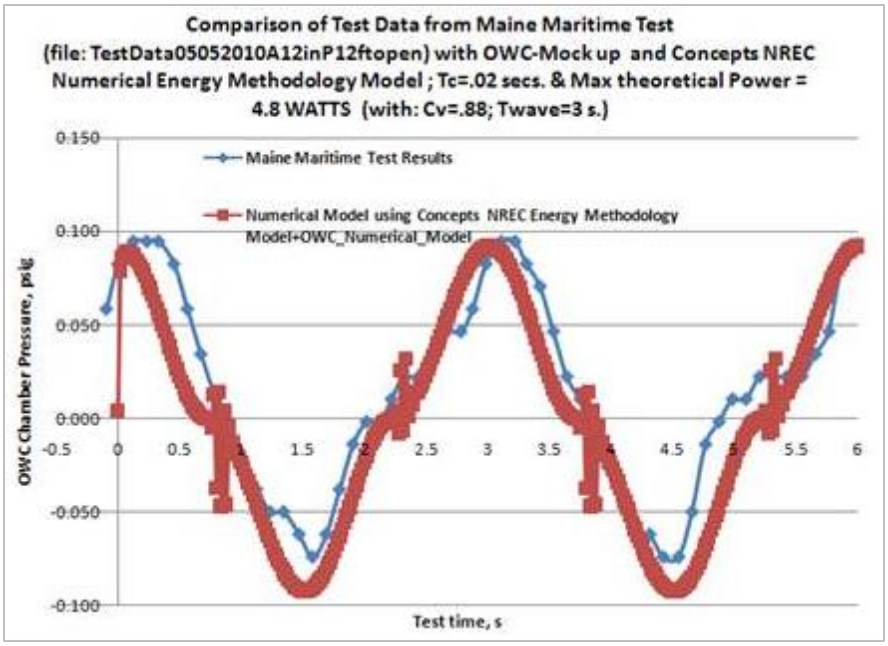

Figure 35. Comparison of *CN*'s Numerical Model Matching the Measured Performance of a Prototype OWC Chamber Constructed and Tested by the MMA

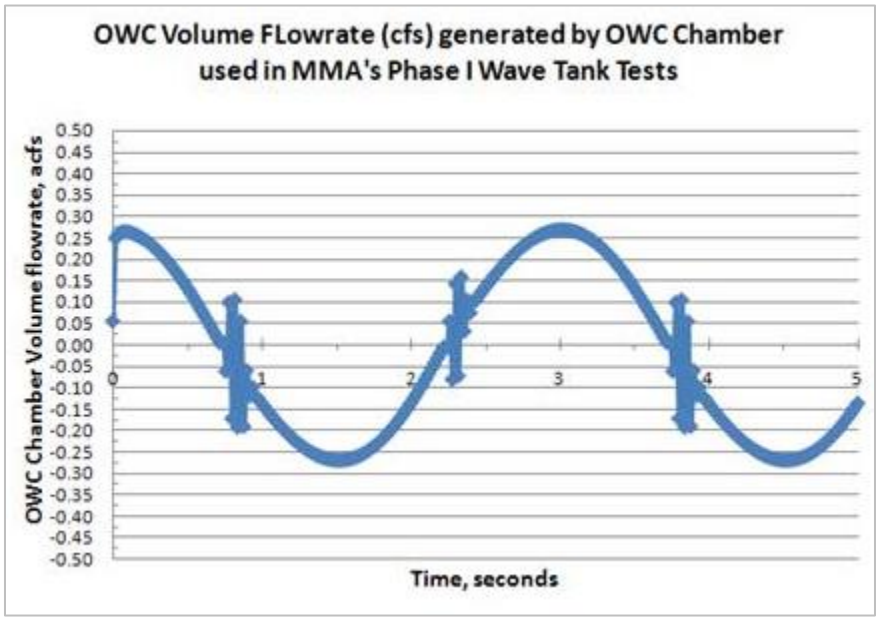

Figure 36. OWC Volume Flow Rate (cft/s) for Micro-OWC Used at the MMA

As stated previously, the primary project objective of the testing of these prototypes was to determine the benefit of two methods of improving the energy recovery potential of an OWC system when water waves of varying amplitude and period are incident upon the OWC structure. The two proposed methods for energy improvement are reviewed in Section 2.6.1 of this final report. The Wells turbine remains the best turbine to be used for these tests, so as to replicate the most common type of turbine used in an actual OWC system. The Wells turbine is the most common choice for an OWC turbine application due to its design simplicity in being able to handle the bi-directional flow that is inherent in OWC wave energy convertors. A 3D rapid prototype "printing" system was used to quickly create a small and light Wells turbine for

this testing. The turbine was installed onto the OWC prototype structure and was used in the wave tank testing performed at the University of Maine.

The variable pitch turbine model assumes a pressure volume relationship based on the following equation:

Volume flow rate (*cfs*) = C_v *x SQRT*[*DP*(*psid*)]; where C_v is a constant and *DP* is the pressure drop across the turbine (based on static chamber pressure). This relationship is similar to the equations governing an orifice with a fixed size or flow obstruction.

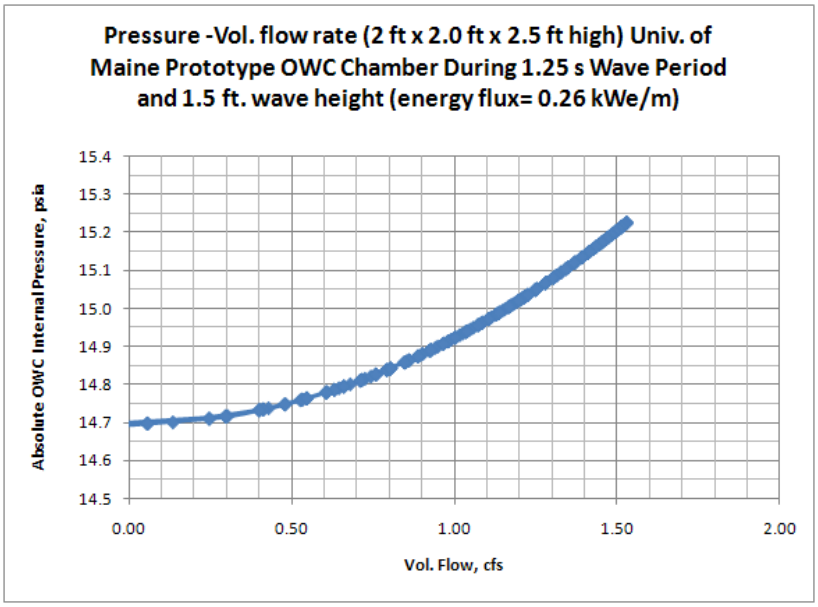

Figure 37. Pressure-Volume Flow Using a Variable Pitch Turbine Model

The Wells turbine is modeled after the technical literature recommendations that the flow coefficient (φ) and load coefficient (Ψ) are proportional with a proportionality constant, *K*, as follows:

$\varphi = K \times \Psi$, where $K = 0.35$ (for the present case study only);

The flow coefficient (φ) is defined as $(Vol.\ flow)/(ND^3)$.

The load coefficient (Ψ) is defined by: $\Delta P\, g_c/(\rho\, N^2 D^2)$.

Figure 38 provides the pressure variation as a function of time for the prototype OWC vessel that was fabricated and tested at the University of Maine.

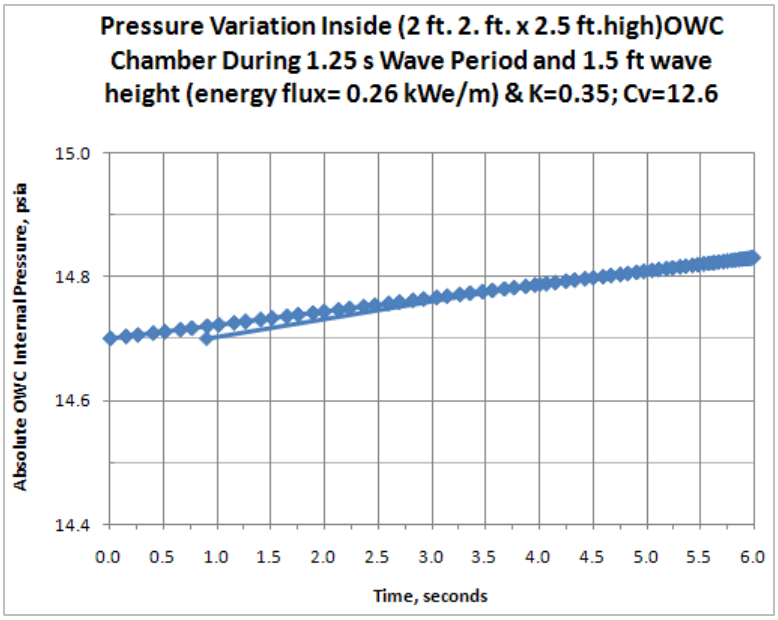

Figure 38. Pressure-Volume Flow Using a Wells Turbine Model

It is interesting to note that the two pressure-volume flow rates are very different in magnitude, depending on the assumed turbine model, but that the maximum potential power generation is the same, or approximately 100 watts (weighted average across the wave stroke). The differences in the pressure-volume flow rate characteristics are a concern, but perhaps the explanation is simply because of the differences in the way different air turbines behave. For example, Figure 37 is more typical of a damping curve that has been observed by CN during previous OWC turbine studies, including tests conducted by MMA during Phase I of this STTR using their very small OWC chamber.

A turbine that obstructs flow in this manner would result in a higher chamber pressure and lower air flow rates. Figure 40 simply displays the linearity between pressure and volume flow rate that is expected, based on the linear relationship of the flow and load coefficients used in the model. However, it must be noted that the turbine speed, N, (and certainly the turbine diameter, D) is kept constant during the OWC modeling used to determine Figure 40. If the speed were allowed to change, the pressure-volume flow rate may be more like that of Figure 40.

Figure 41 provides a more complete presentation of the pressure and volume transients during the cyclic wave intake and exhaust strokes with respect to the same size OWC chamber. Based on Figures 40 and 41, a size estimate for a Wells-type turbine is 0.5 ft in diameter with a speed of 2300 rpm.

Lastly, Figure 42 is provided to demonstrate the sensitivity of the maximum power recovery potential with changes in the system's time constant. The time constant is defined as $T_c = \sqrt{(\Delta P)} \times V/(P \times C_v)$ by CN and is similar to the damping coefficient, D (defined as: ΔP_{avg} $A_{owc}{}^2/Q_{avg}$) as used by other OWC researchers. However, the use of the time constant, T_c, is attractive in analysis and system sizing, because it has been demonstrated by CN that the maximum recoverable power from an incident wave with a period (T) can be found using the equation: T_c @ *max power* $= T/2\pi$.

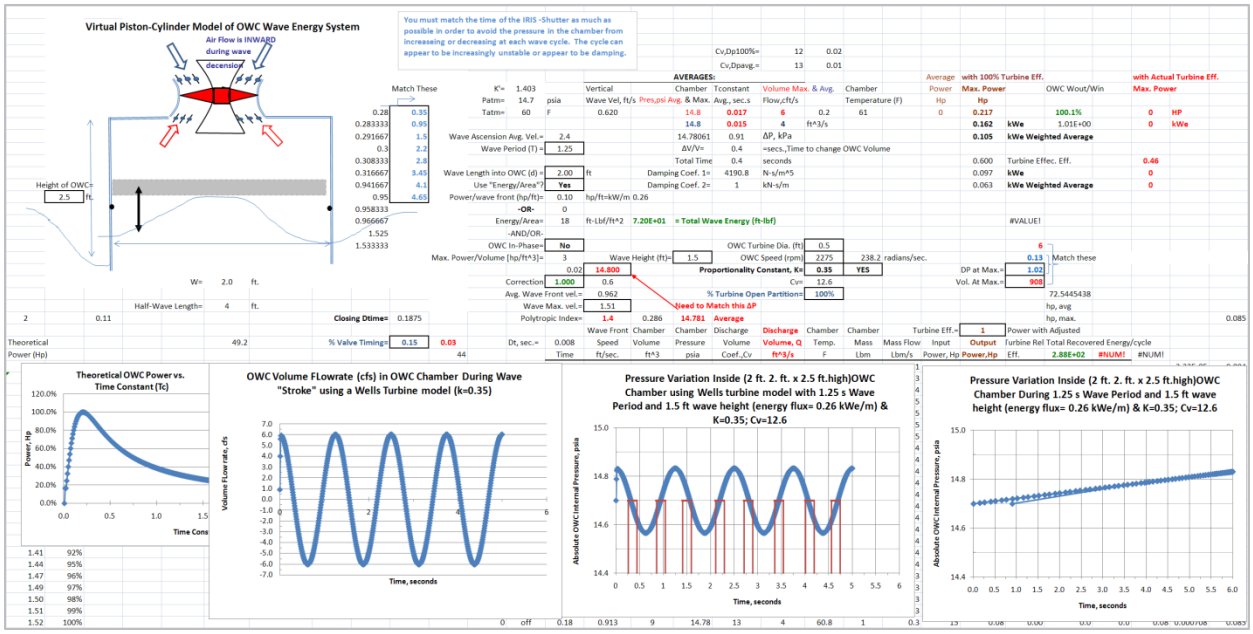

Figure 39. Complete Computer Model Output for Variable Pitch Turbine

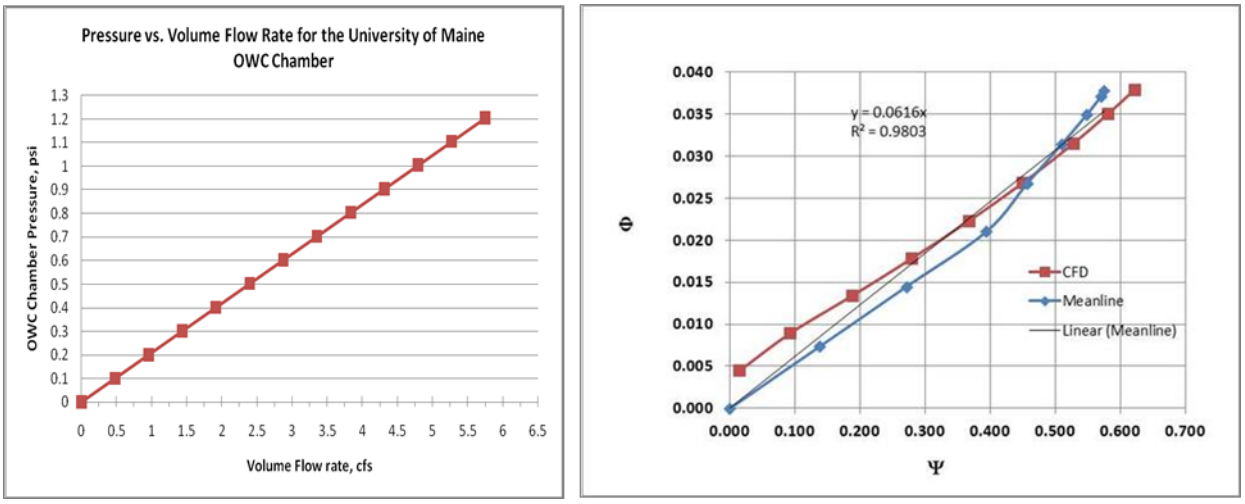

Figure 40. Design Pressure vs. Volume Flow Rate for the Wells Turbine Used in the Mini-OWC Lab Prototype and the Corresponding Wells Turbine Flow Coefficient (φ) and Load Coefficient (Ψ)

CN's numerical model of the OWC system, using the flow coefficient, φ, and load coefficient, ψ, was compared against the numerical model using the flow coefficient, C_v. The results are presented in Figures 43 and 44. Figure 43 is the baseline data for a demonstration, floating OWC that was promoted by an OWC manufacturer. The dimensions of this OWC system were used as input to the *CN* thermo-fluids model that was revised to use the relationship:

$\varphi = K \times \Psi$, where K is a proportionality constant for the Wells turbine.

The result of the comparison is shown in Figure 44, once again demonstrating the validity of *CN*'s numerical model to use either a proportionality constant, K, or the flow coefficient, C_v.

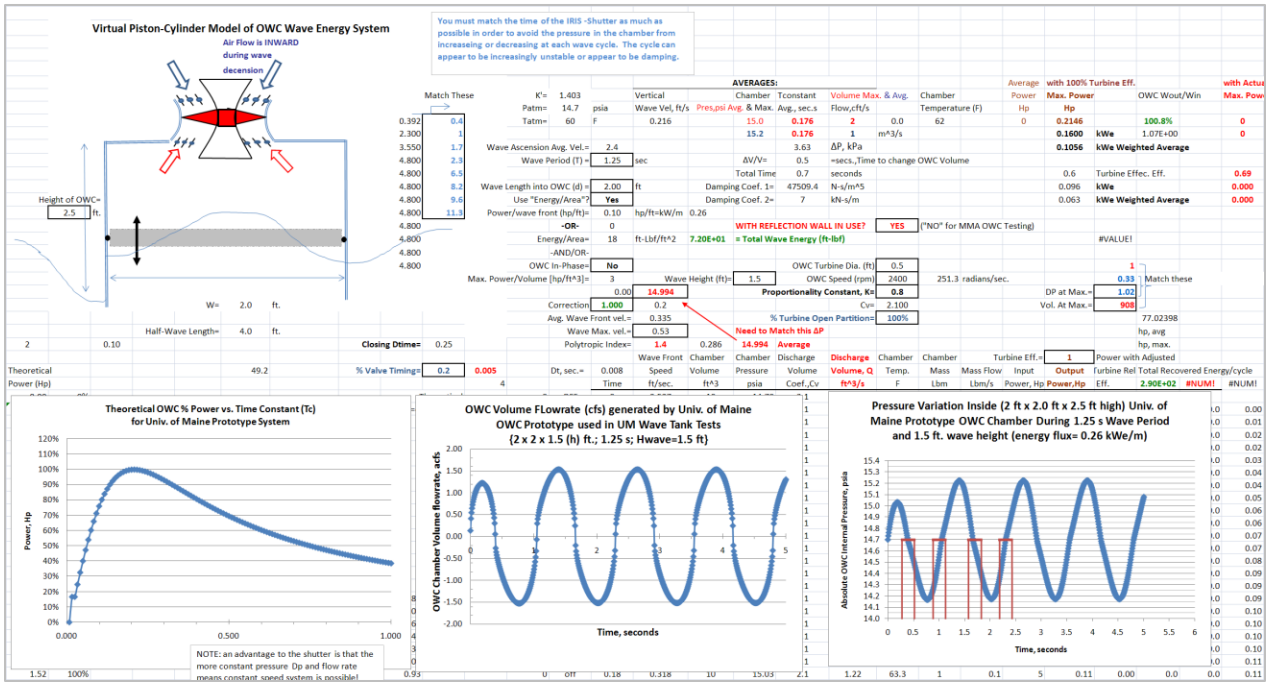

Figure 41. Complete Computer Model Output for Wells Turbine Model

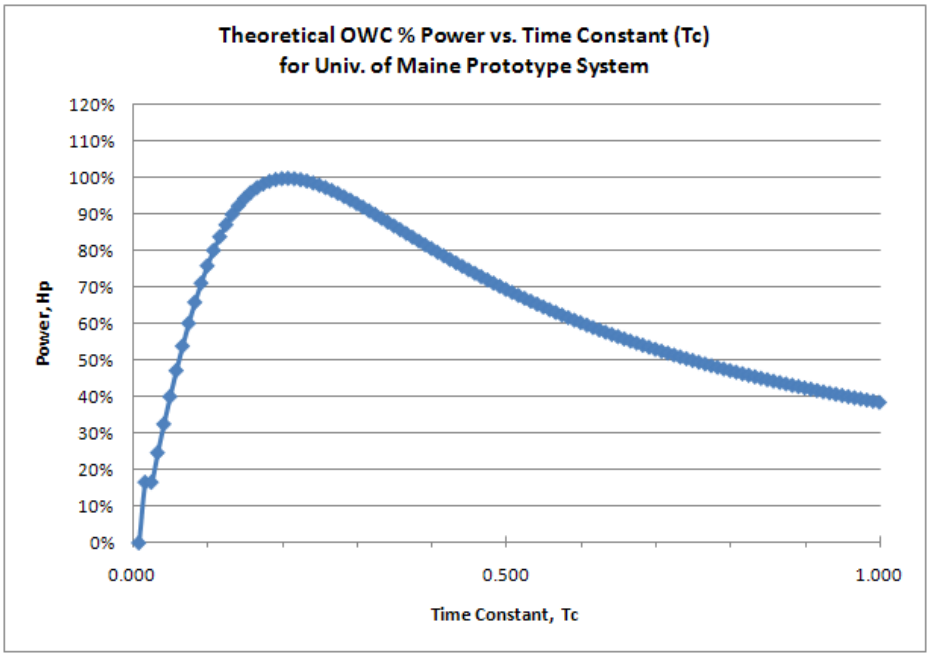

Figure 42. Theoretical OWC Fractional Power from Wells Turbine Model

		Baseline Nominal		Scaled Nominal	
DeltaP	Pa	4563	1700	2500	
Q	m3/s	219.1	5.8	7.27	
rho (standard air)	kg/m3	1.2	1.2	1.2	
nu (standard air)	m/s2	1.51E-05	1.51E-05	1.51E-05	
H	m	388.0102	144.5578	212.585	
Power In	kW	1000	10	18.18	
Power Out	**kW**	**550**	**5.423**	**10**	
Efficiency		0.55	0.55	0.55	
Geometry Scale	**-**	**1.00**	**0.208**	**0.212**	
R - mean	m	1.27	0.264	0.269	
Blade Height	m	0.5	0.104	0.106	
Area	m2	3.990	0.173	0.179	
N	**RPM**	**610**	**1787.950**	**2132.654**	
omega	rad/s	63.87905	187.234	223.331	
V axial	m/s	54.91472	33.523	40.653	
U mean	m/s	81.12639	49.517	60.048	
Specific Speed		**10.816**	**10.816**	**10.816**	<---- Match with rotational speed 1st
Power Coefficient		0.532	0.532	0.532	<---- Other non-dimensional parameters fall out except for Reynolds number
Flow Coefficient		**0.677**	**0.677**	**0.677**	<---- Match with geometry scale 2nd
Reynolds Number		**4.61E+06**	**5.86E+05**	**7.22E+05**	<---- Reynolds number does not match but still high enough that the efficiency will only be impacted a small amount

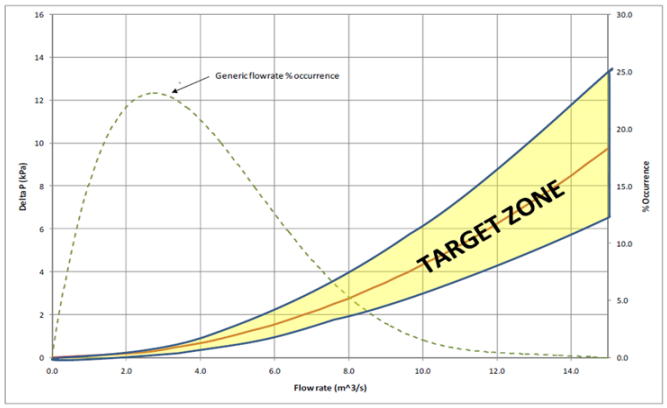

Figure 43. Example of Damping Curve Used in the Sizing of Several Full-scale, OWC Turbines

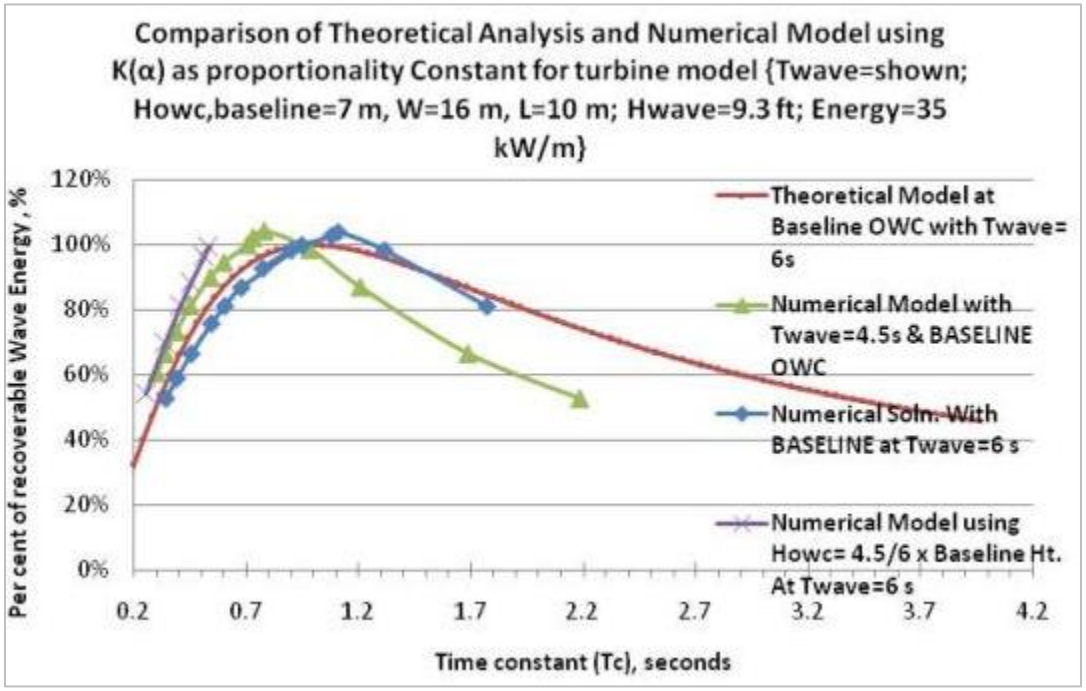

Figure 44. Comparison of Theoretical and Numerical OWC Models Using a Proportionality Constant, $K(\alpha)$, for the Turbine in the Relationship: $\varphi = K \times \Psi$, and not the Flow Coefficient, Cv

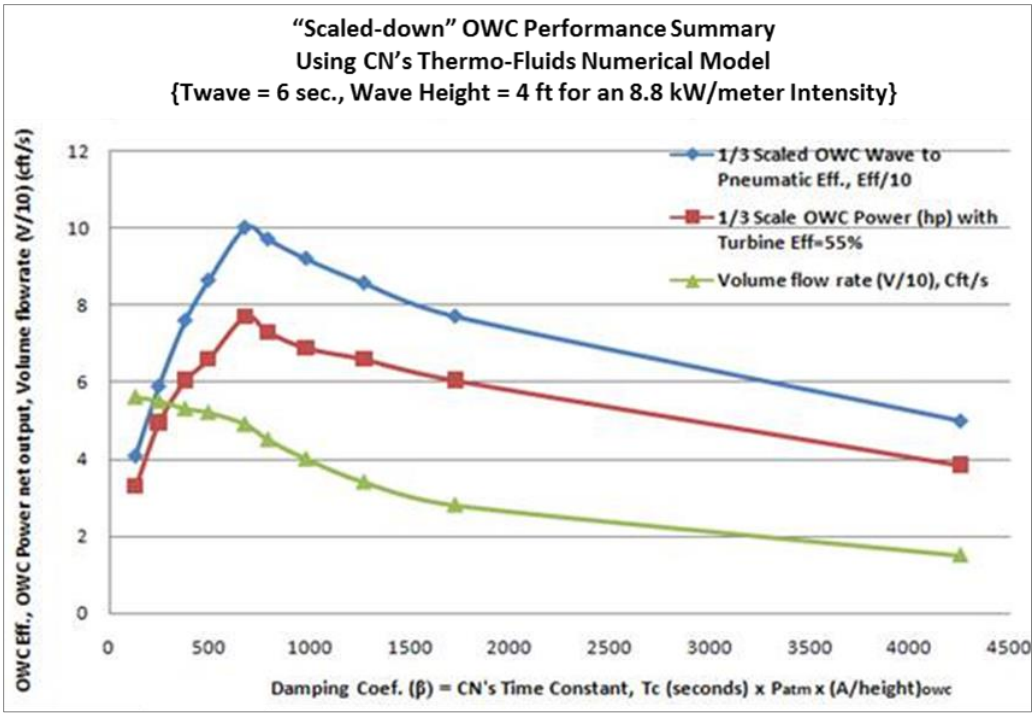

Figure 45. Predicted Power Output for a 1/3 Scaled OWC System, Based on an OWC Manufacturer's Prototype System

3.2.2 Task 2. MMA and CN Continue to Develop OWC Modeling Using Energy Methodology for Modeling the OWC System as Discovered and Developed by CN

The MMA engineering and mathematics professors (Lorenz and Kimball) will continue to refine the mathematical model that was started in Phase I and validated with preliminary testing on a laboratory-scale OWC prototype. The OWC model will now be incorporated with the new energy methodology protocol that was discovered and validated by CN using a spreadsheet computer platform. The MMA analysis will proceed to refine this model and utilize a more sophisticated mathematics platform such as MATLAB®[4] to enable the analysis to support an electrical feedback and control of the turbine shutter actuation. The modeling will facilitate the development of an electrical feedback control system based on the Controls methodology that defines the functional relationship of turbine shutter operation (timing and duration) as well as height adjustments of the OWC as a function of incident wave amplitude and frequency.

CN has developed a more universal model of water wave energy capture by combining these two probability densities. Of particular interest is that the maximum of each function may be associated with the OWC time constant, T_c, which as has been shown previously, is equal to the wave period $(T_w)/2\pi$.

Figure 46 illustrates the graphical relationship of the time constant, wave period, and recoverable wave energy for a given wave amplitude. The technical literature up to this time had reported similar results using an entirely different optimizing parameter called a damping coefficient. However, what is discernible from CN's Figure 46 where the time constant, T_c, is the independent parameter, but is not discernible from using a traditional damping coefficient, is the very conclusive observation that the optimum power recovery is always achieved when the time constant (T_c) is $1/2\pi$ *x the wave period*, T_w. Thus, Figure 46 serves to quickly identify the point of optimum performance of an OWC, given the amplitude of the wave and its period. It is

[4] MATLAB is a registered trademark of The Math Works, Inc.

also clear from Figure 46 that when the time constant (T_c,) is small or very large, there is less potential for pneumatic energy recovery. That is, when the time constant is very large, the OWC acts essentially as a very stiff gas spring, as evidenced by very high air chamber pressures which cause the OWC to "ride" the incident wave, and thus without relative motion between the OWC structure and the wave, there cannot be large recovery of the available wave energy. With very low time constants, there is very little pressure generated within the OWC, and thus little or no power generated.

OWC systems typically operate at low time constants that are to the left of the optimum – usually less than 1.0 seconds. Also apparent from Figure 46 is the effect of different wave periods on the amount of energy that can be recovered once the design point of the OWC system has been selected. For example, if the OWC system is designed for a 4.5-second wave period, the maximum energy recovery is $4.5/2\pi = .72$ seconds. The turbine size and speed, as well as the OWC chamber size, would be designed to accommodate this time constant. But then, as the incident wave energy is changed corresponding to a wave period of 10 seconds, it is clear that the optimum time constant is now $10/2\pi = 1.59$ seconds. More importantly, however, the OWC must continue to operate at a time constant of 0.72 seconds, because all of the system's physical parameters have been fixed by the initial design point. Thus, the recoverable energy is reduced from 100% for the 4.5-second wave to approximately 60% when the 10-second wave is incident to the OWC. Thus, as may be seen from Figure 46 there is considerable unrecovered potential wave energy at time constants of 1–1.5 seconds. In summary, proceeding to the left or the right of the optimum 100% recoverable energy design point, the recovery energy is less than 100%.

CN continues to work on deriving a more universal solution for determining the recoverable energy from different water wave energy densities, with the expectation that the universal solution will aid in the design of OWC systems.

Background of *CN*'s OWC Research and Development

CN's research effort has been focused on the design of an OWC system that can be actively "tuned" to recover more energy from a wider range of water wave energy that may be incident on the OWC system. There are two principal issues that must be addressed when optimizing the water wave energy recovery with an OWC. Both of these issues center on the ability of the OWC air-turbine design to respond to changes in the wave climate. Current OWC systems fail to:

1. Maintain a near constant air flow rate and pressure drop across the turbine. In OWC applications, both the pressure and flow rate through the air turbine cyclically varies from zero to maximum, resulting in a lowering of its overall efficiency.
2. Design the OWC system so that it can be physically "tuned" to accommodate changes in the wave climate that are incident upon it.

In the application of an energy recovery with water wave energy as the energy source, the water wave energy climate is not predictive, and thus a "fixed" OWC system design (i.e., one that is not "tunable" to prevalent energy input) may not operate at its design point optimum as it attempts to recover the most energy from the incident wave. Through analytical and laboratory experimentation, *CN* has started testing these innovations to the design of OWC air turbines: an air shuttering system shown in Figure 43 and the detail of the turbine and shutter valve on the right in its bench-scale configuration to be tested at the University of Maine.

A complete description of the thermo-fluids model of an OWC, developed in Phase I of the project, is given in Section 2.4.2. The analytical basis for these innovations is founded upon an engineering design factor that was analytically derived for the first time by *CN* during the computer modeling of an OWC system during work on Phase I of a DOE STTR (in collaboration with the MMA). This analytical parameter has been identified as a time constant

(T_c) that uniquely couples the OWC air turbine design with the OWC geometry, wave amplitude, and period. The functional relationship between these system parameters provides an analytical basis for engineering the "tuning" of the OWC system for a wide range of incident water wave amplitudes and periods. The functional relationship between the time constant and how it identifies the optimum operating design point is best observed in Figure 46. The optimum time constant has been shown to be exactly equal to the wave period (T_{wave}) divided by 2π. As shown in Figure 46, the time constant for the optimum power from the OWC system shifts if the period of the incident wave climate changes. The time constant relates several critical engineering design parameters, such as the volume of the OWC system (V_{owc}) air space above the water line, the average pressure difference across the turbine, and an air flow coefficient, C_v, in the relationship: $T_c = (\sqrt{\Delta P}/P) \times V_{owc}/C_v$.[5] This relationship enables an engineering methodology to be established for improving the energy capture from a varied wave climate by "tuning" either the flow coefficient (C_v) via variable inlet nozzle vanes that affect partial admission, or articulating blades or the volume (V_{owc}) of the OWC chamber by raising or lowering the OWC vessel. As a result, the OWC system can be tuned to recover more energy from a wide range of incident water wave energy.

Lagrangian Linear Model Development of OWC Dynamics

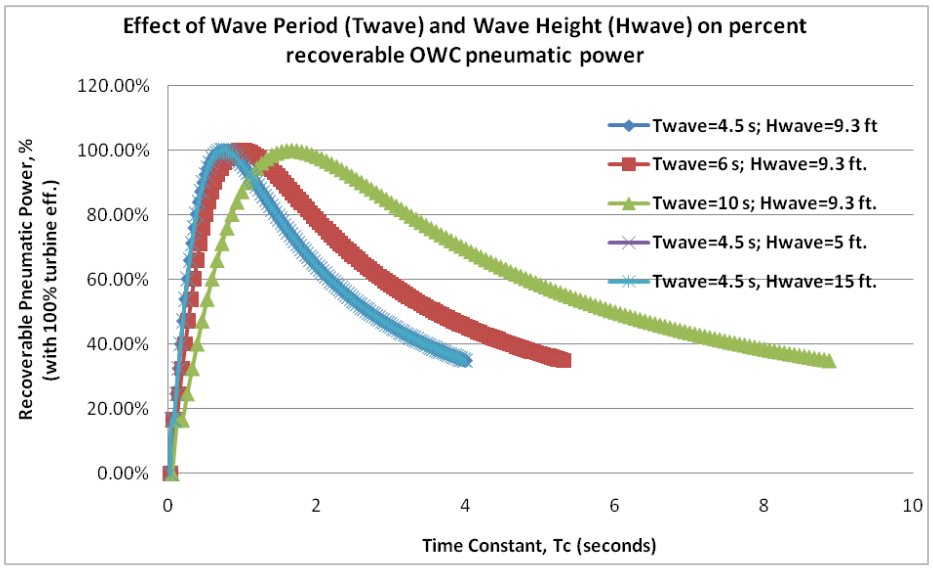

Figure 46. Effect of Wave Period and Wave Height on Percent Recoverable Wave Energy

A new OWC math model proposed by CN may be able to provide more utility as an engineering tool to analyze and design an OWC system (based on Lagrangian dynamics). Professor Pat Lorenz of MMA provided the mathematical solution to the differential equations that were derived by Mr. Frank Di Bella using Lagrangian dynamics.

The sketch shown in Figure 47 depicts the model of an OWC with distances in relation to the seabed floor taken to be the inertial reference: X_1 represents the massless distance of the water wave from the inertial reference into which is an applied exciting non-conservative force ft; X_2 represents the distance of the OWC mass from the inertial reference and includes a non-conservative exciting force, F_b, that is associated with the buoyancy of the OWC mass as the submerged depth of the vessel changes as X_2 responds to changes in X_1; X_3 represents the distance of the virtual joint connecting the spring constant and the damping coefficient The model of the Wells turbine and the air cavity within the OWC is thus modeled using a damping

[5] Where: C_v is similar to the familiar fluid flow coefficient defined by: $Q = C_v \, x \, \sqrt{\Delta P}$ and Q is the volume flow rate (cft/s).

coefficient, C [lbf/(ft/s)], and is thus a non-conservative force for the turbine and a spring constant, K [lbf/ft] for the air cavity.

While the analogy of a damping system that extracts work from the input energy source is reasonable in the model, the use of a spring constant to represent the compression and expansion of the entrapped air may not be as reasonable. In fact, the air within the OWC is not trapped, but rather is pushed through the turbine and is thus not a restorative (conservative) force system as traditionally held. However, the induction of the equivalent amount of air during the descension of the water wave within the OWC chamber does provide some credence to the use of a spring constant to represent the repeated compression and expansion of the air within the chamber, and the derivation of an equation for the spring constant, K, since a function of the OWC geometry can be demonstrated and was used in the analysis presented herein. The overall objective for the analysis is to determine the amount of work extracted from the OWC system via the damping system, with damping constant, C, as a function of the OWC size and the wave period and amplitude to discern how the recovery of the energy from the wave may be improved upon by designing the OWC features when the incident wave changes.

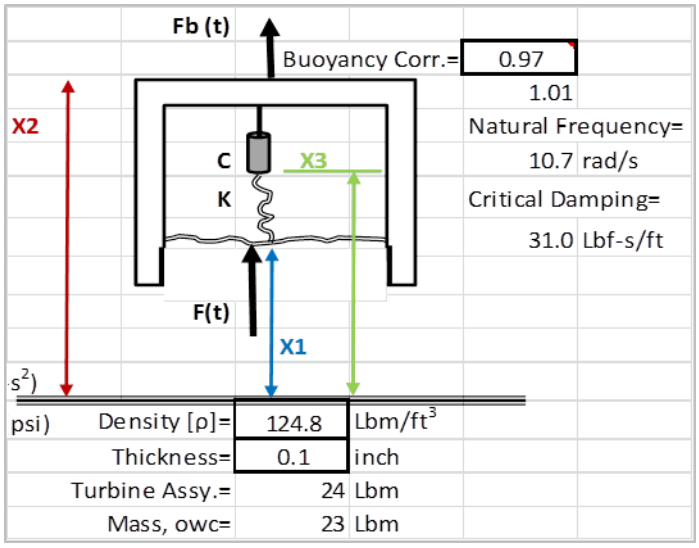

Figure 47. An Illustration of a Floating OWC WEC Used to Construct the Lagrangian Model

The Lagrangian dynamics equations of motion are:

$$① \quad \frac{m}{g_c} x_2'' + \frac{mg_g}{g_c} + C(x_2' - x_3') = \varphi A \left\{ X_1 - NX_{amp} + \frac{mg_g}{g_c \varphi A} \right\}$$

$$② \quad -K(x_3 - x_1) = F(t)$$

$$③ \quad K(x_3 - x_1) = C(x_2' - x_3')$$

The solution to this set of differential equations is as follows:

$$x_1 = C_2 e^{-\sqrt{\frac{\varphi A g_c}{m}}t} + \left(\frac{1}{K} - \frac{\left(\frac{\left(\frac{\varphi A g_c}{m}\right)}{K} + \frac{\left(\frac{C g_c}{m}\right)}{C}\right)}{\left(\frac{\varphi A g_c}{m} + \omega^2\right)} \right) F_{max} \sin(\omega t) - \frac{\frac{\omega}{C}}{\left(\frac{\varphi A g_c}{m} + \omega^2\right)} F_{max} \cos(\omega t)$$

$$x_2 = C_1 + C_2 e^{-\sqrt{\frac{\varphi A g_c}{m}}t} - \frac{\left(\frac{\left(\frac{\varphi A g_c}{m}\right)}{K} + \frac{\left(\frac{C g_c}{m}\right)}{C}\right)}{\left(\frac{\varphi A g_c}{m} + \omega^2\right)} F_{max} \sin(\omega t) + \left(\frac{1}{C\omega} - \frac{\frac{\omega}{C}}{\left(\frac{\varphi A g_c}{m} + \omega^2\right)} \right) F_{max} \cos(\omega t)$$

$$x_3 = C_2 e^{-\sqrt{\frac{\varphi A g_c}{m}}t} - \frac{\left(\frac{\left(\frac{\varphi A g_c}{m}\right)}{K} + \frac{\left(\frac{C g_c}{m}\right)}{C}\right)}{\left(\frac{\varphi A g_c}{m} + \omega^2\right)} F_{max} \sin(\omega t) - \frac{\frac{\omega}{C}}{\left(\frac{\varphi A g_c}{m} + \omega^2\right)} F_{max} \cos(\omega t)$$

Here, we see all three equations are of the form

$$x_i = C_2 e^{-\sqrt{\frac{\varphi A g_c}{m}}t} + A_i \sin(\omega t) + B_i \cos(\omega t) = C_2 e^{-\sqrt{\frac{\varphi A g_c}{m}}t} + E_i \sin(\omega t + \emptyset_i),$$

Where A_i, B_i are obvious, and $E_i^2 = A_i^2 + B_i^2,\ tan(\emptyset_i) = \frac{B_i}{A_i}$

The complete solution using the OWC defined parameters can be shown as follows:

Calculating the E_i, $\emptyset_i$:

$$E_1 = [A_1^2 + B_1^2]^{\frac{1}{2}} = \left[\left(\frac{1}{K} - \frac{\left(\frac{(\varphi A g_c)}{m} + \frac{(C g_c)}{m}\right)}{\left(\frac{\varphi A g_c}{m} + \omega^2\right)}\right)^2 F_{max}^2 + \left(-\frac{\frac{\omega}{C}}{\left(\frac{\varphi A g_c}{m} + \omega^2\right)}\right)^2 F_{max}^2\right]^{\frac{1}{2}} =$$

$$tan(\emptyset_1) = \frac{B_1}{A_1} = \frac{-\frac{\frac{\omega}{C}}{\left(\frac{\varphi A g_c}{m} + \omega^2\right)} F_{max}}{\left(\frac{1}{K} - \frac{\left(\frac{(\varphi A g_c)}{m} + \frac{(C g_c)}{m}\right)}{\left(\frac{\varphi A g_c}{m} + \omega^2\right)}\right) F_{max}} = \frac{-\omega K}{C\left(\omega^2 - \frac{K g_c}{m}\right)} = \frac{-1}{C\left(\frac{\omega}{K} - \frac{g_c}{\omega m}\right)}$$

$$E_2 = [A_2^2 + B_2^2]^{\frac{1}{2}} = \left[\left(-\frac{\left(\frac{(\varphi A g_c)}{m} + \frac{(C g_c)}{m}\right)}{\left(\frac{\varphi A g_c}{m} + \omega^2\right)}\right)^2 F_{max}^2 + \left(\frac{1}{C\omega} - \frac{\frac{\omega}{C}}{\left(\frac{\varphi A g_c}{m} + \omega^2\right)}\right)^2 F_{max}^2\right]^{\frac{1}{2}} =$$

$$tan(\emptyset_2) = \frac{B_2}{A_2} = \frac{\left(\frac{1}{C\omega} - \frac{\frac{\omega}{C}}{\left(\frac{\varphi A g_c}{m} + \omega^2\right)}\right) F_{max}}{\left(-\frac{\left(\frac{(\varphi A g_c)}{m} + \frac{(C g_c)}{m}\right)}{\left(\frac{\varphi A g_c}{m} + \omega^2\right)}\right) F_{max}} = -\frac{\varphi A}{C\omega\left(\frac{\varphi A}{K} + 1\right)} = \frac{-1}{C\left(\frac{\omega}{K} + \frac{\omega}{\varphi A}\right)}$$

$$E_3 = [A_3^2 + B_3^2]^{\frac{1}{2}} = \left[\left(-\frac{\left(\frac{(\varphi A g_c)}{m} + \frac{(C g_c)}{m}\right)}{\left(\frac{\varphi A g_c}{m} + \omega^2\right)}\right)^2 F_{max}^2 + \left(-\frac{\frac{\omega}{C}}{\left(\frac{\varphi A g_c}{m} + \omega^2\right)}\right)^2 F_{max}^2\right]^{\frac{1}{2}}$$

$$tan(\emptyset_3) = \frac{B_3}{A_3} = \frac{\left(-\frac{\frac{\omega}{C}}{\left(\frac{\varphi A g_c}{m} + \omega^2\right)}\right) F_{max}}{\left(-\frac{\left(\frac{(\varphi A g_c)}{m} + \frac{(C g_c)}{m}\right)}{\left(\frac{\varphi A g_c}{m} + \omega^2\right)}\right) F_{max}} = \frac{\frac{\omega}{C}}{\frac{g_c}{m}\left(\frac{\varphi A}{K} + 1\right)}$$

Summary: $x_1(t), x_2(t), x_3(t)$ are similar, but with their own amplitudes $E_1(t), E_2(t), E_3(t)$ and phases $\emptyset_1, \emptyset_2, \emptyset_3$ relative to the force $F(t)$.

The damping constant, *C*, is used to more easily model the extraction of pneumatic energy. The extracted "damping" energy is the energy extracted by a high-speed air turbine with an efficiency, η. Here, of course, the recovered energy is useful and not converted to heat as in typical mass-spring-damper systems. The spring constant, *K*, represents the compressible nature of the air as the air is pushed out of the chamber and through the turbine. The expectation is that this revised model can more easily handle the wave transients that are incident to the OWC chamber than our earlier models and provide more continuous

relationships between the wave energy function, $F(t)$, and the OWC characteristics of K and C. The use of Lagrangian dynamics enables the closed-form solution of the combined equations of motion for the OWC WEC system shown in Figure 47 and thus will be a more accurate model of the interactions of the generalized coordinates: X_1, X_2, and X_3, and therefore the motion of the OWC (from X_2) based on the exciting force applied to the X_1 coordinate. Figures 48 and 49 illustrate the relative, sinusoidal variations of X_1, X_2, and X_3 in response to changes in the major OWC system parameters including: the damping coefficient, C, spring coefficient, K, and the relative mass and size of the OWC system. The mass of the OWC vessel is calculated in the model by selecting a density of the vessel material of construction and the size of the OWC, defined by the footprint, A_{owc}, and OWC height, H_{owc}.

Figures 48, 49, and 50 also begin to demonstrate how there must be constraints that limit the "reality" of the closed-form solutions to the Lagrangian differential equations to comply with the physical limitations of the OWC chamber. For example, the numerical difference between the X_1 and X_2 generalized coordinates in Figures 50 are larger than the displacement in Figure 49 due to the reduction in the spring constant, K. Although the solution to the differential equations is correct mathematically, the numerical difference between X_1 and X_2 is larger than the height of the OWC used in this sample calculation and thus should be avoided. It is also expected that the damping coefficient, C, can more accurately relate changes in the turbine energy extraction optimization criteria by showing a functional relationship with the flow coefficient, C_v, that was defined in the Phases I and II development of the thermo-fluids model of the OWC. Similar constraints are identified in the following inaugural application of the Lagrangian model to the mini-OWC system.

It is also noted that the constant, C_2, in each of the three solutions to the differential equations was set to zero in the analysis and thus only the dynamically stable sinusoidal solutions are presented.

The Lagrangian dynamics equations have been correctly solved, as is evidenced by the verification that the energy into the OWC mass system is equal to the energy output, or in actuality, the damping energy. This is mathematically expressed using the Lagrangian terms:

$$\sum \{ C\,(dX_2/dt - dX_3/dt)\,(\delta X_2 - \delta X_3) \} = \sum \{ F_b(t)\,(\delta X_2) + F_t(t)\,(\delta X_1) \}$$

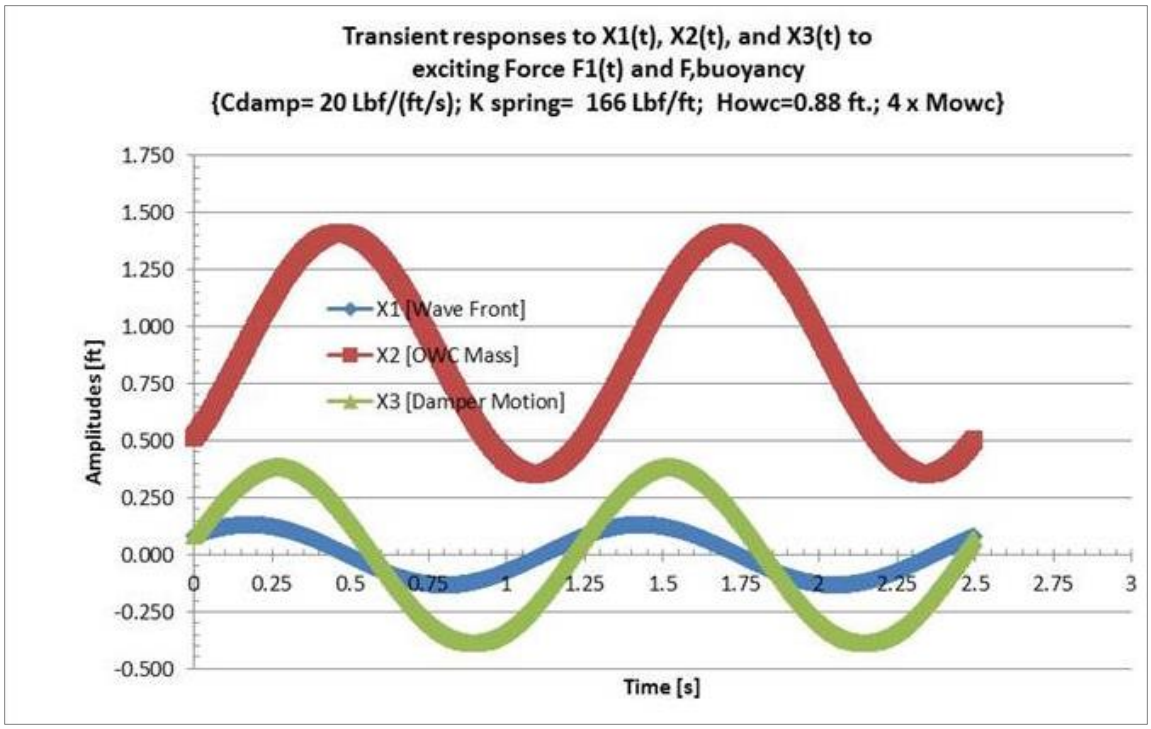

Figure 48. Typical Sinusoidal Transient Response to Wave Energy Incident to an OWC System

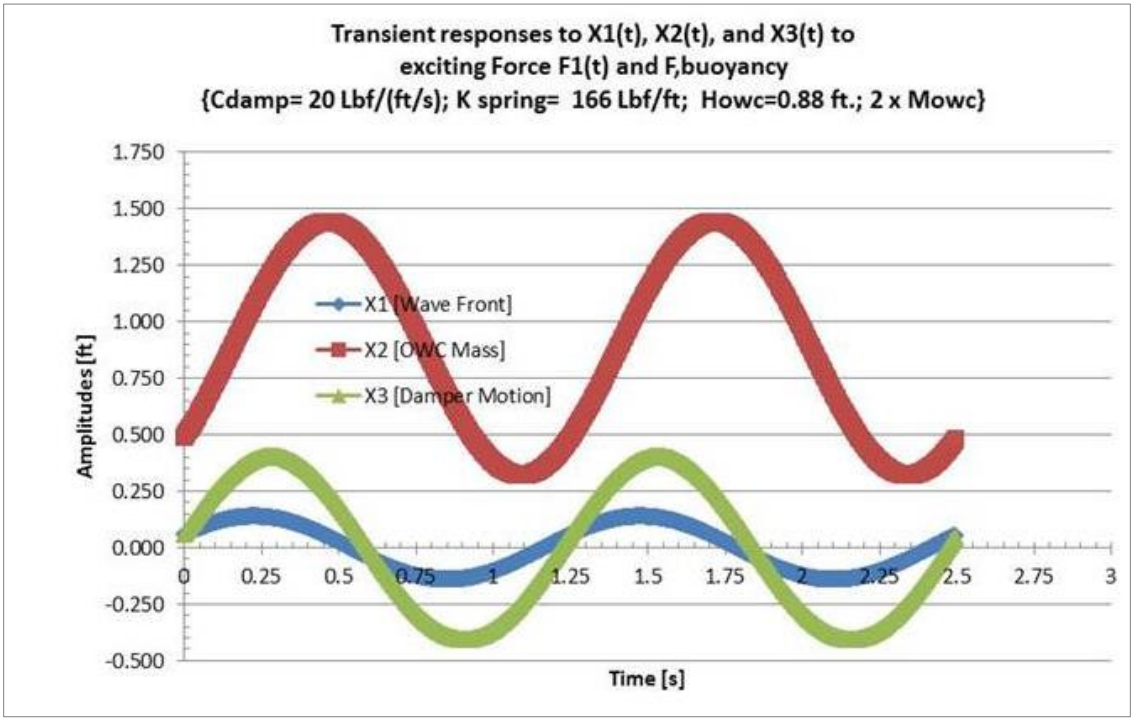

Figure 49. Illustrating Effect of Mass on Dynamic Performance

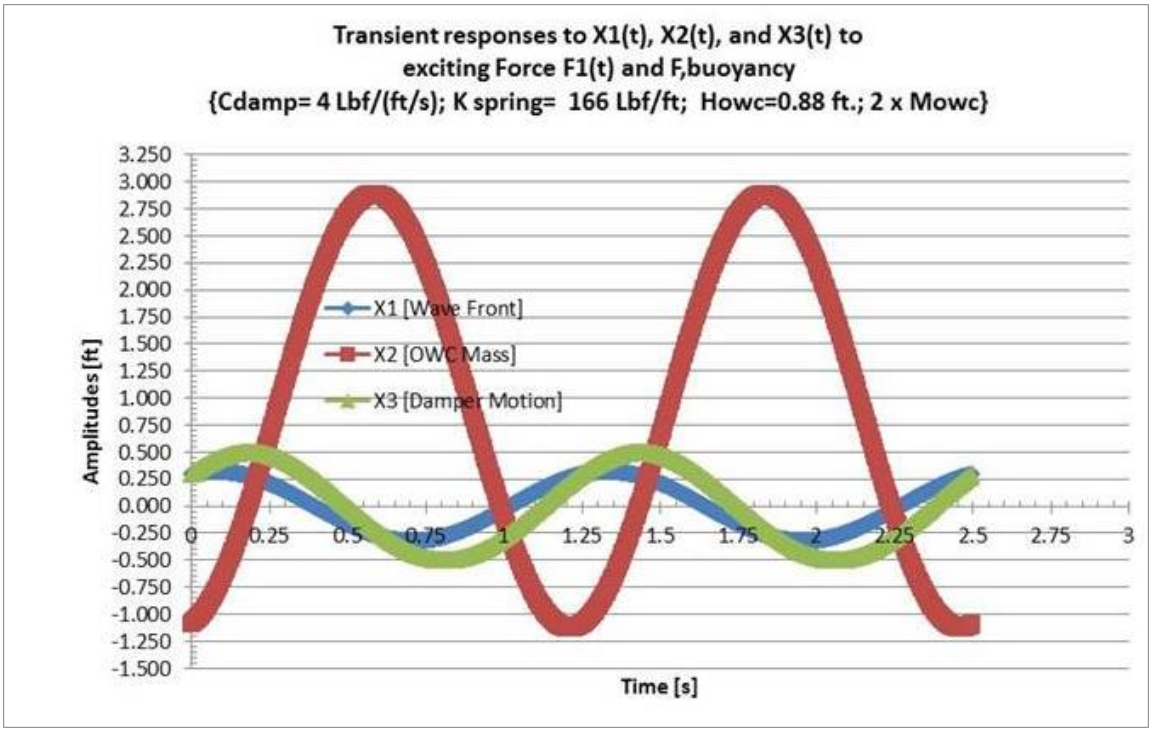

Figure 50. Lagrangian Solution with C_1 and C_2 Constants = 0 for the Generalized Coordinates: X_1, X_2, and X_3 Illustrating Constraint of Lagrangian Solution Exceeding Actual Available Displacements of X_1- $X_2 < H_{wave}$

Results of the Lagrangian Analysis Applied to the Mini-OWC Chamber

An inaugural, parametric analysis has been applied to the mini-OWC system that was constructed for testing at the University of Maine water tank. This sample calculation is thought to test the accuracy but also the overall utility of the Lagrangian solution for characterizing an OWC system by using an OWC system that was previously analyzed using the thermo-fluids OWC model developed in Phase I of the SBIR. A review of this thermo-fluids model is given in Section 2.4.3 of this final report. In summary, the thermo-fluids model uses a numerical solution of the conservation of energy principles as it is applied to the OWC chamber. This technique was successful in identifying a parameter, labeled the time constant, T_c, which is a measure of the magnitude of airflow and pressure that is inducted and exited from the OWC chamber through the turbine. The time constant was shown to identify the optimum flow rate and pressure differential that should be selected for the design point of the Wells turbine. It also enabled a means of quantifying several methods for maximizing the recovery of the wave energy that is incident on the OWC vessel.

The following functional relationships have been derived between the various major design parameters for an OWC system. It is noted that the functional relationships between C_v, $\Delta P_{energy,owc}$, $\Delta P_{geomtery,owc}$, V_{owc}, H_{wave}, and H_{owc} must assume that the change in volume of the OWC vessel is equal to the amount of air that is able to escape from the OWC vessel at each wave "stroke". It is certainly possible that the amount of air mass leaving the OWC vessel is not equal to the relative, geometric displacement of the OWC vessel with respect to the wave front. In that instance, $\Delta P_{energy,owc}$ (defined here as the pressure change in the OWC vessel due to the maximum absorption of wave energy) is not equal to the $\Delta P_{geomtery,owc}$ (defined here as the change in the vessel pressure due to the reduction of the OWC chamber volume due solely to the wave front moving within the OWC vessel and the escape of some air through the turbine). The amount of air passing through the turbine is defined by the flow coefficient, C_v. In a properly tuned OWC, the two chamber pressure changes would be equal.

Variables and Functions Developed for the Thermo-Fluids OWC Analysis Model (Phase I)

- $Energy/Area)_{theory}$ $[E/A, lbf\text{-}ft/ft^2] = (\rho\ (H_{wave})^2\ g_g/g_c)/8$
- $Power/L_{owc}$ $[lbf\text{-}ft/ft] = (\rho\ H_{wave}^2\ g_g^2)\ Tw/(32\ \pi\ g_c)$

Note 1: These two equations are standard wave energy flux and power per unit wave front equations derived by others.

Note 2: The $E/A)_{theory}$ is understood to have equal magnitude potential and kinetic energy per the conventional theory and practice. The OWC system without a reflector plate downstream of the wave front can only capture the potential energy part, and this can be factored into the Lagrangian OWC dynamics by reducing the $E/A)_{theory}$ by ½ where it is used in the derived equations.

- Flow coefficient, $C_v\ [ft^3/s/\sqrt{psi}]$ = turbine vol. flow rate/(chamber $\Delta P_{owc})^{1/2}$
- Time constant, $T_c\ [s] = (\text{chamber } \Delta P_{owc})^{1/2}\ (A_{owc} \times H_{owc})/C_v$
- Incident wave frequency, $\omega_n = 2\pi/T_{wave}$; wave length, $\lambda[ft] = (T^2_{wave})g_g/(2\pi)$; $T_w[s]$ = wave period
- A_{owc} = footprint area of OWC chamber; H_{owc} = height of OWC chamber above static water line

Variables and Functions Developed for the Lagrangian Dynamics OWC Analysis Model

- $Energy/Area)_{Lagrangian\ model\ calc.}\ [E/A_{LMC}, lbf\text{-}ft/ft^2] = \{ C\ (dX_2/dt - dX_3/dt)\ (\delta X_2 - \delta X_3)\} / A_{owc}$
  $= \{ F_b(t)\ (\delta X_2) + F_t(t)\ (\delta X_1)\ \}/ A_{owc}$
- Damping energy (from Lagrangian dynamics) $[E_d, lbf\text{-}ft] = C\ (dX_2/dt - dX_3/dt)\ (\delta X_2 - \delta X_3)$
- Input exciting energy (from Lagrangian dynamics) $[Einput, lbf\text{-}ft] = F_b(t)\ (\delta X_2) + F_t(t)\ (\delta X_1)$
- $Fb(t)$= {buoyancy exciting, non-conservative force} $= \rho \times A_{owc} \times (X_1(t) - NX_{max}) - M_{owc}\ g_g/g_c$
- $Ft(t)$= {incident wave energy exciting, non-conservative force} $= [(E/A)_{theory}\ \lambda/ H_{wave}]\ \sin(\omega_n t)$
- $\omega_n = 2\pi/T_{wave}$; $\lambda = (T^2_{wave})g_g/(2\pi)$
- Chamber $\Delta P_{energy,owc,max.} = (E_d / A_{owc}) / (H_{wave}/2 \times 144 \times 4)$
- Flow coefficient, $C_v\ [ft^3/s/\sqrt{psi}] = E_d / (T_w \times 144 \times (\text{chamber } \Delta P_{energy,owc})^{3/2})$
- or: $C_v\ [ft^3/s/\sqrt{psi}] = (2\sqrt{2}) \times A_{owc} \times (H_{wave}^{3/2}) \times 12/T_w/(E/A)_{LMC}^{1/2}$
- or: $C_v\ [ft^3/s/\sqrt{psi}] = A_{owc} \times (H_{owc}/2)/(T_w/4)/ (\text{chamber } \Delta P_{geometry,owc})^{1/2}$
- Relationship between "old" C_v and "new" damping coefficient C
- $C_v = \{ C\ (dX_2/dt - dX_3/dt)\ (\delta X_2 - \delta X_3)\ \}/ T_w/(\text{chamber } \Delta P_{owc})^{3/2}$
- Spring constant, $K = A_{owc}/H_{wave} \times \{P_{atm} \times 144 - \rho_{air} \times 1545 \times (460+60)/28.966\}$
- $\Delta P_{geomtery,owc} = \Delta V/V_{owc} \times \{P_{atm} \times 144 - \rho_{air} \times 1545 \times (460+60)/28.966\}$

Inputs Required for Lagrangian Analysis Model

The necessary inputs to the Lagrangian OWC analysis model are limited to the following:

- OWC footprint area: $A_{owc}\ [ft2]$
- Wave height (trough to peak): $H_{wave}\ [ft]$
- Wave period: $T_w\ [s]$

- Ratio of wave height (H_{wave}) to OWC height above static water line (H_{owc}): $(H_{wave}/2)/H_{owc}$
- Density of materials of construction for the OWC: ρ_s *[lbm/ft^3]*
- Damping coefficient: *C [lbf/(ft/s)]*

All other operating parameters are outputs based on the solution to the Lagrangian equations.

Physical Constraints Imposed by Geometry of the OWC Structure

The following constraints on the energy and power output of the OWC are based on the physical geometry (A_{owc}, H_{owc}, H_{wave}) that have been used as inputs to the model. It is necessary to impose these "reality" constraints on the solutions calculated by the model because the Lagrangian solution is otherwise unconstrained to calculate an energy per Area $(E/A)_{calc}$, flow coefficient, C_v, relative displacement of X_1 and X_2, for each damping coefficient, C, that is used as an input to the model. For example, an input of any arbitrary value of a damping coefficient, C, will result in the Lagrangian dynamics analysis model to provide a solution that has all of the input energy from the force functions: $F_b(t)$ and $F_t(t)$ to be absorbed in order to maintain steady-state operation; i.e., energy into the mass system is equal to the energy absorbed or dampened. In this model, the energy absorbed is assumed to be the power that could be generated by the turbine, and thus the energy extracted from the Lagrangian mass system. As will be observed in the later figures, a decrease in the damping coefficient, approaching zero causes more energy to be generated and thus dampened out of the system. This is made visually obvious by the large displacements of the generalized coordinates X_1, X_2, and X_3, in addition to the absolute magnitudes of the energy as provided in the output of the model.

I. Maximum OWC chamber pressure differential (Chamber ΔP_{owc}) must be less than the weight of the M_{owc} per unit area or:

$$E/A)_{max.} <= (M_{owc}\, g_g/g_c)\, H_{wave}/A_{owc}$$

II. Maximum relative displacement for the generalized coordinates X_1 and X_2 must not exceed the total depth of the OWC vessel walls which is H_{owc} or:

$$X_2(t) - X_1(t) <= H_{owc}$$

III. Minimum value of the flow coefficient, C_v, is based on the maximum $E/A)_{theory}$ or:

$$C_{v,min.} >= (2\sqrt{2})\, x\, A_{owc}\, x\, (H_{wave}{}^{3/2})x12/T_w/(E/A)_{theory}{}^{1/2}$$

IV. The maximum value of the energy output must be less than the energy available in the wave or:

$$E/A)_{max.IV} <= E/A)_{theory};\ \text{where } E/A)_{theory} = (\rho\, (H_{wave})^2\, g_g/g_c)/8$$

V. The maximum value of the energy output is also dependent upon the maximum achievable chamber ΔP_{owc}. This constraint requires $\Delta P_{energy,owc} = \Delta P_{geomtery,owc}$. Solving for:

$$E/A)_{max.V.} = 4\, x\, f_{,owc}\ x\, (H_{wave}/2)\, x\, \{P_{atm}\, x\, 144 - \rho_{air}\, x\, 1545\, x\, (460+60)/28.966\}$$

See Note 2 above.

VI. The maximum time constant, T_c, is calculated based on the maximum chamber ΔP_{owc} and minimum value of C_v, or:

$$T_c <= (\sqrt{Max.\ Chamber\ \Delta P_{owc}})/14.696\, x\, (A_{owc}\, x\, H_{owc})/C_{v,min}$$

VII. The maximum velocity through the OWC turbine must be less than the sonic velocity of the air or:

$$C_v \times E_d^{1/2} / [\, A_{owc}^{3/2} \times \{2 \times H_{owc} \times 1.4 \times 1545/28.966 \times 32.2 \times (460+60)\}^{1/2} \times 12] << 1$$

Table V and VI identify the outputs from the Lagrangian dynamics analysis model applied to the mini-OWC prototype using the constraints shown above and with the inputs as given above. The transient responses for X_1, X_2, and X_3 are shown in Figure 51.

TABLE V. OUTPUTS FROM LAGRANGIAN DYNAMICS ANALYSIS MODEL FOR MINI-OWC PROTOTYPE

OUTPUTS		INPUTS	
Delta P,energy[psi]=	0.025		
Tc [sec]=	0.00062		
Cv=	61.00		
K,spring [Lbf/ft]=	166.1		
$E/A)_{LCM}$=	10.7	0.882	Howc (ft.)
Delta P,energy[psi]=	0.025	4.0	Aowc (ft^2)
Tc [sec]=	0.00062	47	Mowc (LBm)
Cv=	61.36	1.5	Hwave (ft)
Tc, max. [sec]=	0.00049	1.25	Twave (s)
Cv)minimum=	48.4	30	C,d [Lbf/(ft/s)]
E/A)wave max.>	17.0		
E/A)owc mass max.<	17.4		
Power,theory(Watts)=	74.00		
Power max (Watts)=	75.7		

TABLE VI. THE INPUT PAGE OF THE LAGRANGIAN MODEL SHOWING A SKETCH OF A FLOATING OWC WEC AND THE CONSTANTS TO THE SINUSOIDAL SOLUTIONS TO THE DIFFERENTIAL EQUATIONS

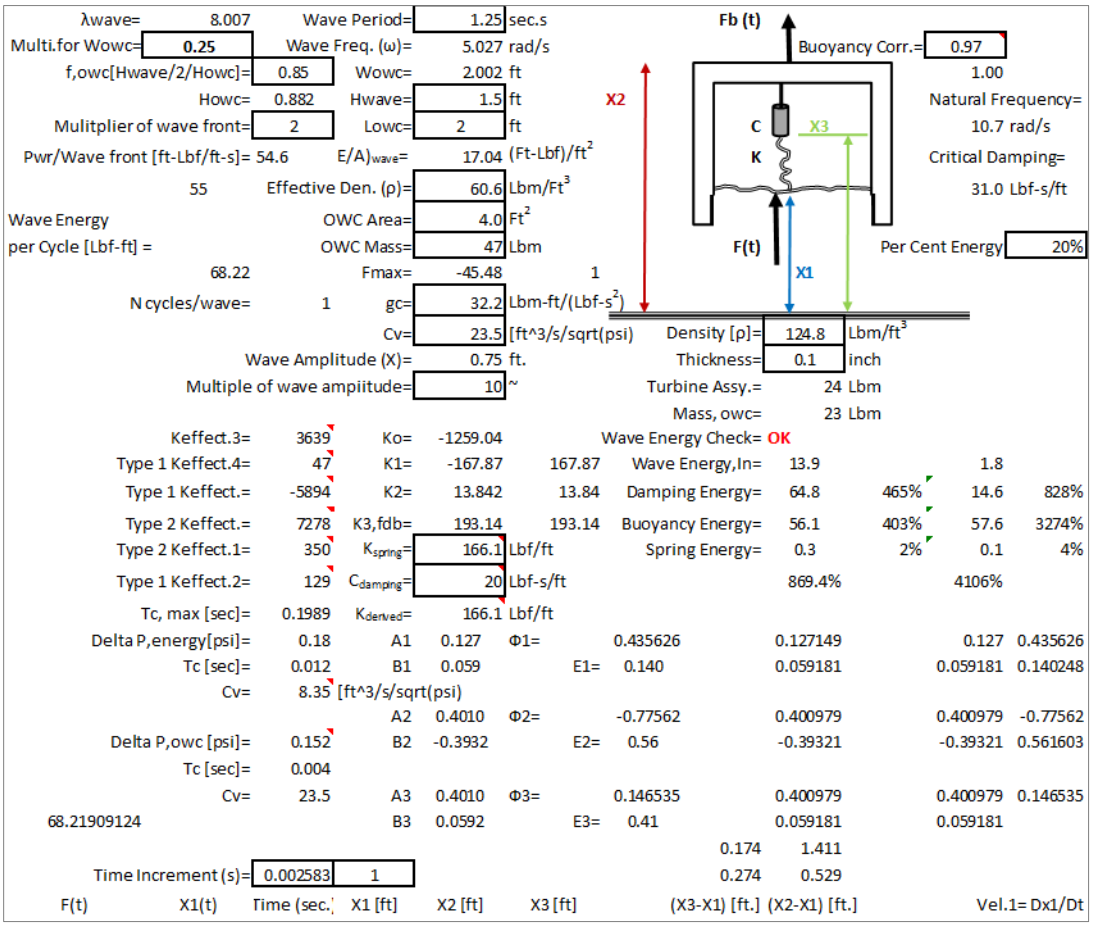

λwave=	8.007	Wave Period=	1.25	sec.s									
Multi.for Wowc=	0.25	Wave Freq. (ω)=	5.027	rad/s									
f,owc[Hwave/2/Howc]=	0.85	Wowc=	2.002	ft									
Howc=	0.882	Hwave=	1.5	ft									
Mulitplier of wave front=	2	Lowc=	2	ft									
Pwr/Wave front [ft-Lbf/ft-s]=	54.6	$E/A)_{wave}$=	17.04	(Ft-Lbf)/ft^2									
	55	Effective Den. (ρ)=	60.6	Lbm/Ft^3									
Wave Energy		OWC Area=	4.0	Ft^2									
per Cycle [Lbf-ft] =		OWC Mass=	47	Lbm									
	68.22	Fmax=	-45.48	1									
N cycles/wave=	1	gc=	32.2	Lbm-ft/(Lbf-s^2)									
		Cv=	23.5	[ft^3/s/sqrt(psi)									
		Wave Amplitude (X)=	0.75	ft.									
		Multiple of wave ampiitude=	10	~									
Keffect.3=	3639	Ko=	-1259.04										
Type 1 Keffect.4=	47	K1=	-167.87	167.87									
Type 1 Keffect.=	-5894	K2=	13.842	13.84									
Type 2 Keffect.=	7278	K3,fdb=	193.14	193.14									
Type 2 Keffect.1=	350	K_{spring}=	166.1	Lbf/ft									
Type 1 Keffect.2=	129	$C_{damping}$=	20	Lbf-s/ft									
Tc, max [sec]=	0.1989	$K_{derived}$=	166.1	Lbf/ft									
Delta P,energy[psi]=	0.18	A1	0.127	Φ1=	0.435626								
Tc [sec]=	0.012	B1	0.059	E1=	0.140								
Cv=	8.35	[ft^3/s/sqrt(psi)											
		A2	0.4010	Φ2=	-0.77562								
Delta P,owc [psi]=	0.152	B2	-0.3932	E2=	0.56								
Tc [sec]=	0.004												
Cv=	23.5	A3	0.4010	Φ3=	0.146535								
68.21909124		B3	0.0592	E3=	0.41								
Time Increment (s)=	0.002583	1											
F(t)	X1(t)	Time (sec.)	X1 [ft]	X2 [ft]	X3 [ft]								

Fb (t)													
Buoyancy Corr.=	0.97												
	1.00												
X2													
C	X3												
K													
Natural Frequency=													
	10.7 rad/s												
Critical Damping=													
	31.0 Lbf-s/ft												
F(t)													
Per Cent Energy	20%												
X1													
Density [ρ]=	124.8	Lbm/ft^3											
Thickness=	0.1	inch											
Turbine Assy.=	24	Lbm											
Mass, owc=	23	Lbm											
Wave Energy Check=	OK												
Wave Energy,In=	13.9			1.8									
Damping Energy=	64.8	465%		14.6	828%								
Buoyancy Energy=	56.1	403%		57.6	3274%								
Spring Energy=	0.3	2%		0.1	4%								
	869.4%			4106%									
	0.127149			0.127	0.435626								
	0.059181			0.059181	0.140248								
	0.400979			0.400979	-0.77562								
	-0.39321			-0.39321	0.561603								
	0.400979			0.400979	0.146535								
	0.059181			0.059181									
0.174	1.411												
0.274	0.529												
(X3-X1) [ft.]	(X2-X1) [ft.]												
	Vel.1= Dx1/Dt												

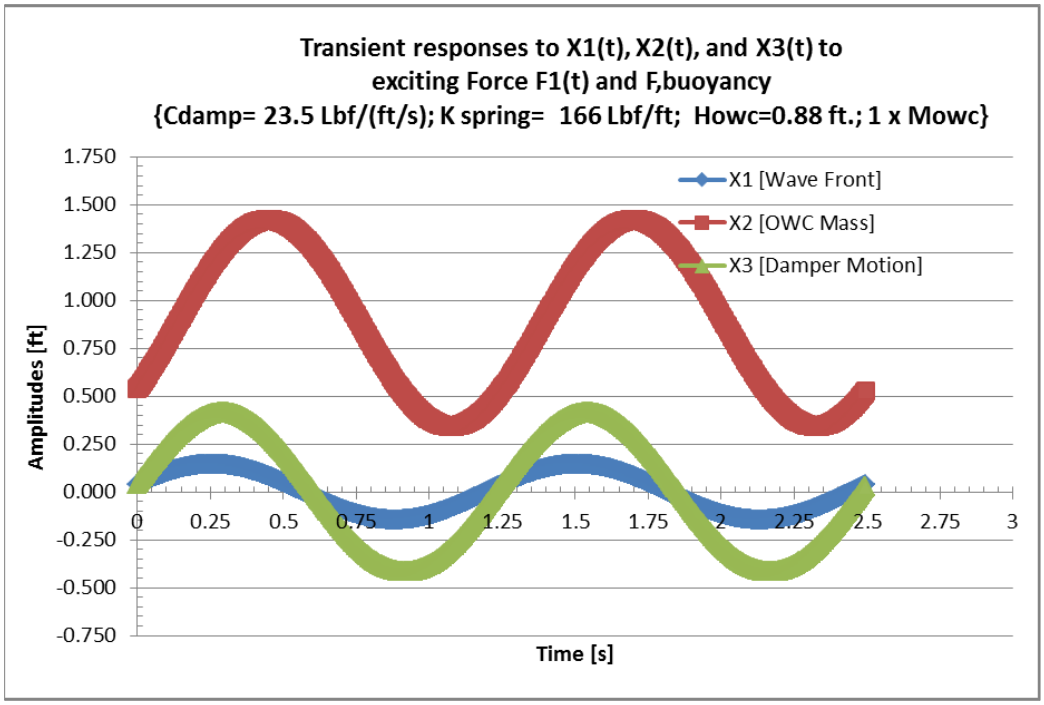

Figure 51. Baseline Transient Response of the Mini-OWC Prototype

While the simple output presentation shown in Table V is a reasonable engineering tool for future OWC analysis, a better and more informative characterization of the OWC is afforded by presenting the first results of a parametric study. In this study, the baseline system with the size characteristics shown in Table VI had the mass, H_{owc}, damping coefficient, C, and spring constant, K, variables changed in order to determine the effect of these parameters on the overall performance of the OWC with respect to energy, power, and E/A.

Although the parametric analysis is still in progress, the first result of this parametric analysis enables some interesting conclusions to be drawn from the observations. These observations are identified for each of the figures.

Functional Relationship Between C_v (Flow) and C (Damping) Coefficients

Figures 52, 53, and 54 present an interesting functional relationship between the flow coefficient and time constant, T_c, as first defined and used in the thermo-fluids model of the Phase I study and the damping coefficient, C. Figure 52 reveals that the functional relationship is not just dependent upon the height (H_{owc}) of the OWC vessel, but also that, for the OWC vessel size used in this case study, the minimum C_v is shown to require a very high damping coefficient to satisfy the physical constraint number III (see page 62). This is consistent with the observation shown in Figure 53, in which the Lagrangian solution indicates that the energy recovery is increasing exponentially while the input energy is increasing unabated, as the damping coefficient is reduced, approaching zero (0).

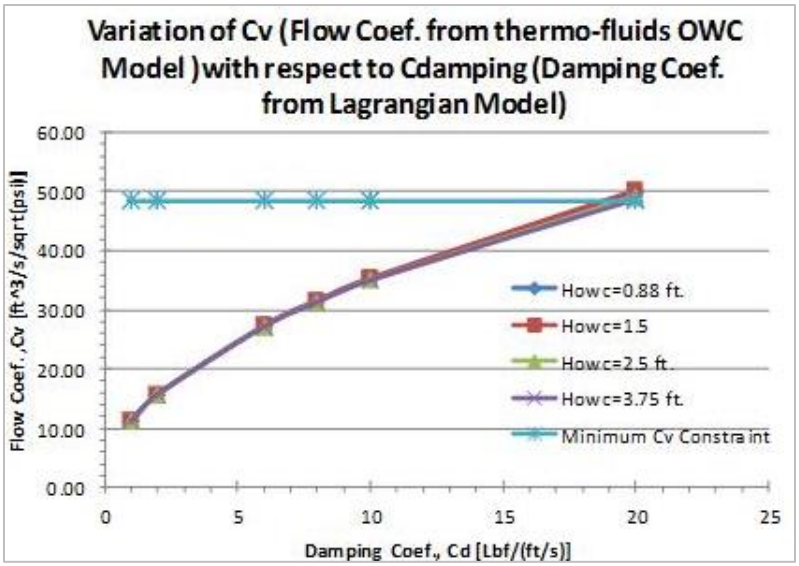

Figure 52. Illustrating Functional Relationships Between Cv, C, and E/A, and Independency on H_{owc} Height

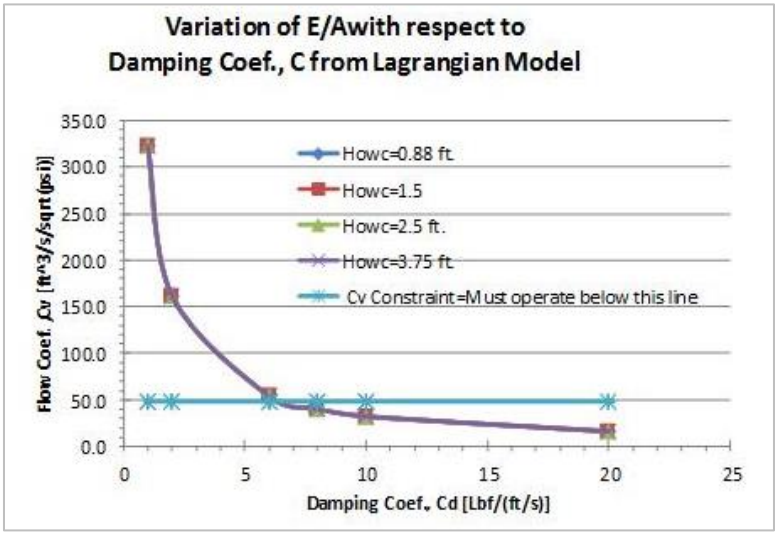

Figure 53. Illustrating Functional Relationships Between Cv, C, and E/A, and Independency on H_{owc} Height

It was understood from the earlier Phase I study using the thermo-fluids model that an exponential relationship exists between the flow coefficient, C_v, and the time constant, T_c. It was also understood that different wave heights and wave periods affect the power recovery optimization for a fixed-OWC vessel geometry. However, it was also predicted that controlling the buoyant height (H_{owc}) of the OWC vessel (i.e., relative to the static water level) will afford an opportunity to optimize the energy recovery of the fixed-OWC design when different water wave amplitudes are incident on the OWC vessel. This was demonstrated in Phase I using the thermo-fluids model, and now this conjecture has been confirmed using the Lagrangian model, as evidenced by Figure 54. Figure 54 illustrates how the T_c can be changed by changing the height of the OWC vessel to maintain the same flow coefficient, C_v, and thus maintain the same flow characteristics for which the turbine has been designed.

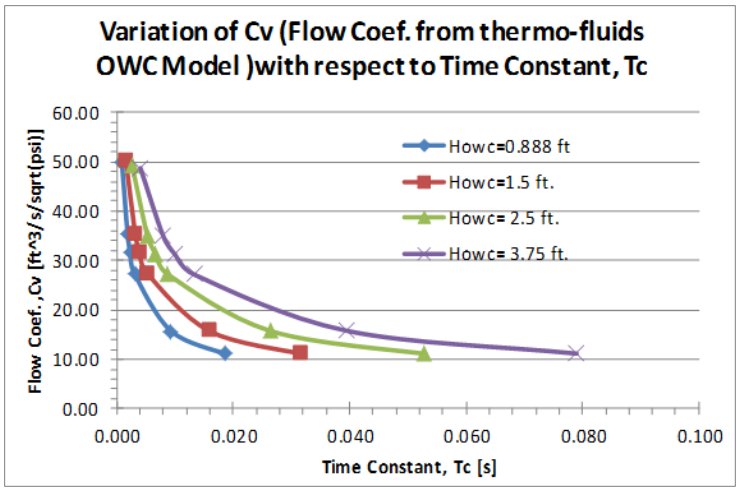

Figure 54. Variation of Flow Coefficient, C_v, with Respect to *CN*'s OWC Design Parameter, Time Constant, T_c

A similar display of dependency of OWC height, but also an independency between the OWC mass with respect to the energy recovery from the wave per unit OWC footprint area $(E/A)_{LMC}$ can be demonstrated from a parametric study using the Lagrangian dynamics OWC model. Figure 55 illustrate the results of the parametric study of this effect. It must be noted that for the results presented in Figures 52–55, the OWC mass was determined by calculating the actual weights of the vessel walls and the turbine assuming a material density (125 lbm/ft^3) applied to the actual dimensions of the vessel used in the case study (A_{owc}= *4 ft*^{2} and H_{owc} as given). The masses shown in the legend were introduced to be at ¼, 1, and 4 times the M_{owc}, baseline mass of 47 lbf that is precisely calculated using the physical dimensions of the mini-OWC system. This was done to be very clear that the height of the OWC system was still affecting the potential energy recovery, while also demonstrating that the mass of the OWC is not similarly affecting the magnitude of the energy recovered. Figure 56 present similar results, if only "zoomed in" to clearly discern the operational range as bounded by the constraints that must be imposed on the system due to the actual OWC physical dimensions assumed for the case study.

It also must be noted however, that the potential and kinetic energies of the floating OWC mass is conserved. That is, any energy stored as a result of the system-exciting forces $F_t(t)$ and $F_b(t)$ will be returned to the mass system as a result of defining the gravity force as a conserving force in the derivation of the Lagrangian dynamics equation of motion.

The spring constant, *K*, was similarly defined as a conserving force, as is the convention in typical Lagrangian dynamics derivations. However, the spring constant, *K*, is perhaps not easily argued to be a conserving force if (as in this case) the entrapped air that would normally constitute a conserving spring force is, at best non-linear, albeit cyclic, and at worst, should be treated as non-conserving to account for the expulsion and induction of air to and from the OWC chamber through the turbine. It is must be noted that the spring constant, *K*, may be considered a conserving force, at least during each expulsion stroke and each induction stroke (with fresh air through the turbine) taken separately as individual events, if not during the inflections that separate the two events to otherwise enable the entire wave cycle to be treated as a continuous process. For this study, an average value for the spring constant was calculated using the equation shown earlier in this report.

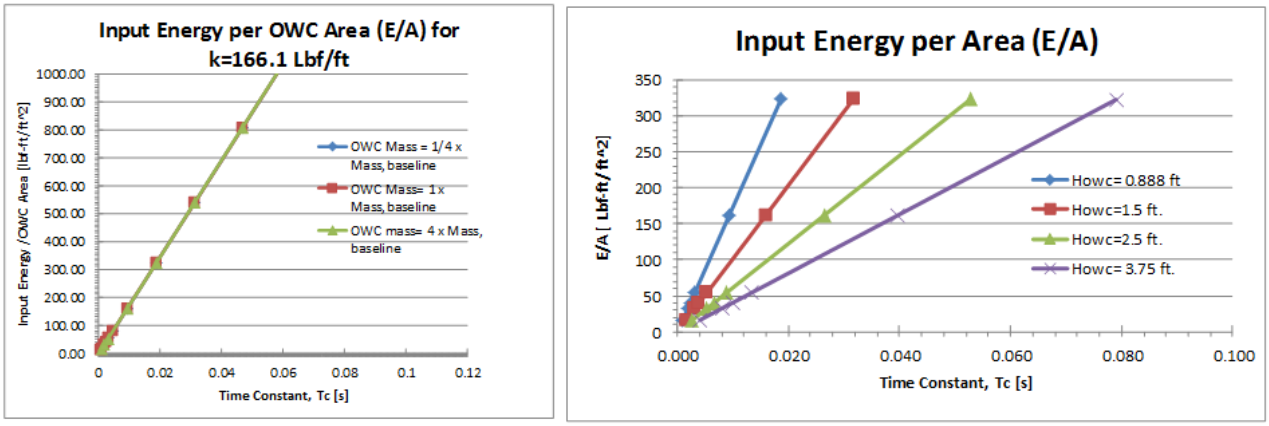

(a) (b)

Figure 55. Illustrations of the Independency of Changes in Mass and Dependency of OWC Height on the Output Range of E/A

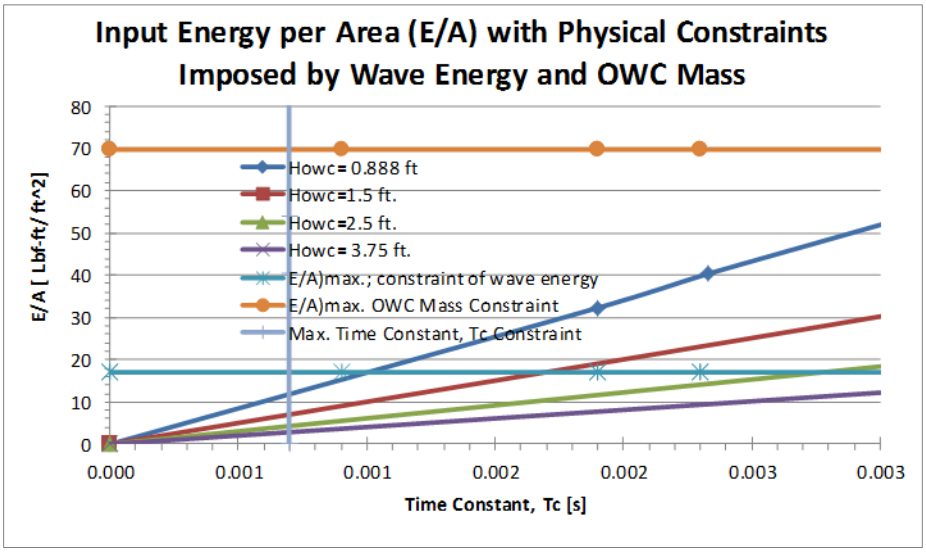

Figure 56. E/A Function with Time Constant, T_c, Using 4 x M_{owc}, Baseline

Figures 57 and 58 provide the range of power output that is available from the OWC system with unconstrained input of damping coefficient, C.

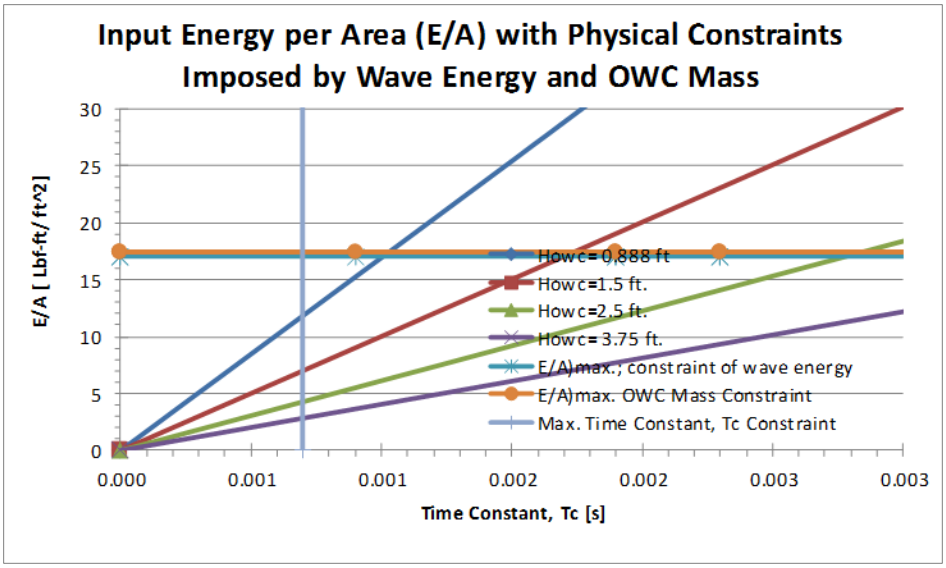

Figure 57. E/A Function with Time Constant, T_c, Using 1 x M_{owc}, Baseline

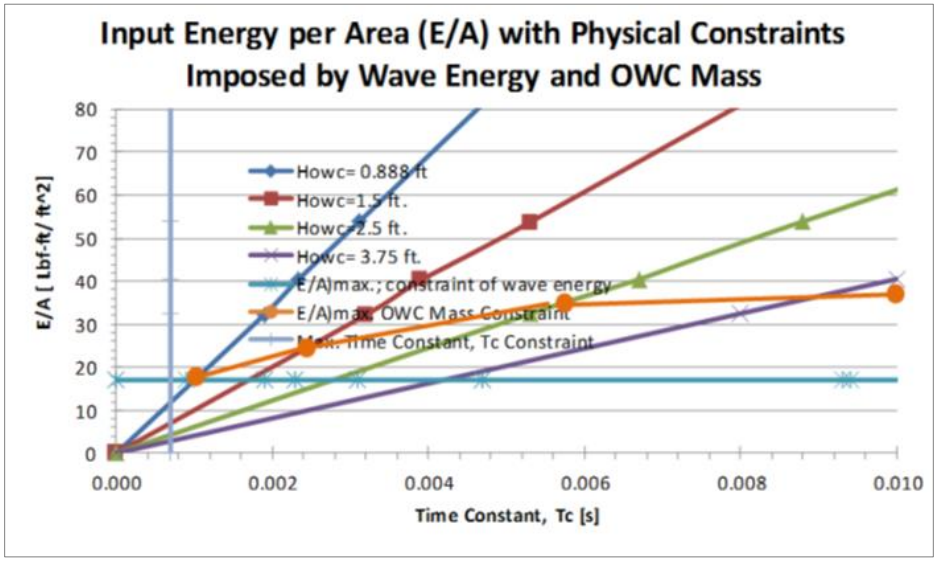

Figure 58. Detail of Relevant Zone of Operation for the Mini-OWC with Respect to the Constraints Imposed by the Physical Size of the OWC

Another result from the analysis using the Lagrangian dynamics model is shown in Figure 61. Figure 61 illustrates the functional relationship of percentage of power recovered as a function of the time constant, T_c. This theoretical result was first confirmed by a numerical solution that has been embodied in what has been labeled as the thermo-fluids model of the OWC system. Both of these models were developed in Phase I of the project. This functional relationship is important because the time constant, T_c, at which the percentage of power is maximum was shown to be equal to the $T_w/2\pi$, which is equal to the inverse of the wave frequency or $\omega = 2\pi/T_w$. This relationship is a very elegant and simple engineering criterion for optimizing the physical sizing of an OWC system with respect to the prevalent wave energy climate that the OWC is intended to serve.

Thus, an important goal of this inaugural study was to demonstrate this or an equivalent relationship between optimum performance and the time constant, T_c. This effort has been shown to be successful, as evidenced by the result shown in Figure 60, and has led,

as was hoped, to further insight into the optimization of the energy recovery from an incident wave with respect to the time constant, T_c, and how it can be used to enable an engineering design tool for OWC systems.

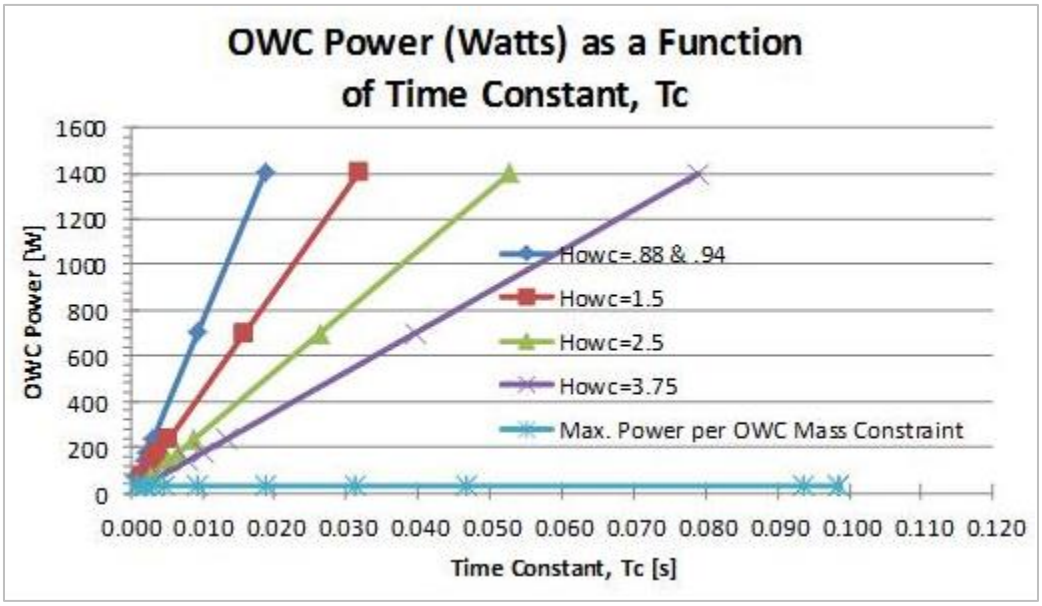

Figure 59. OWC Power (watts) as a Function of Time Constant, T_c, at Different OWC Vessel Heights

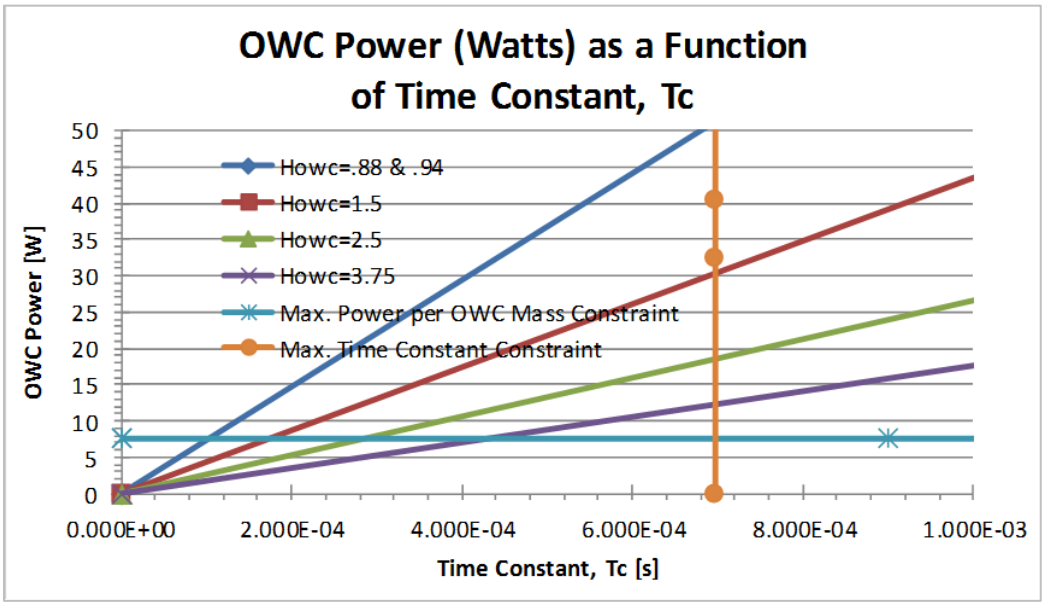

Figure 60. OWC Power (watts) as a Function of *CN*'s OWC Design Parameter, the Time Constant, T_c (seconds)

Shown in Figure 61 is the theoretical solution (see Section 2.4.2) of the OWC system for a single frequency, sinusoidal wave using the conservation of energy and definitions of the flow rate as a function of pressure.

Also shown are the results of two algorithms that have been derived from the Lagrangian dynamics OWC analysis model. The two algorithms provide excellent agreement

with the theoretical solution and, in so doing, provide some additional insight into how the OWC performance is affected by changes in the incident wave energy and the back pressure-flow rate characteristics of the OWC turbine that would be installed in the OWC system.

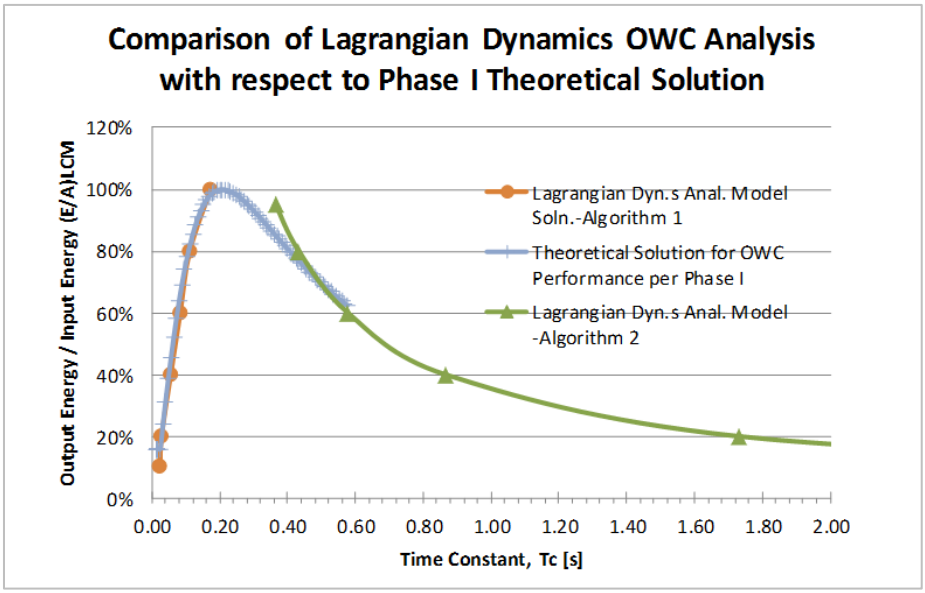

Figure 61. Comparison of the Lagrangian Dynamics OWC Analysis Model Results with the Theoretical Derivation Developed in Phase I of the Project

Derivation of Algorithm No 1

Algorithm No. 1 (for T_c's < $T_{c,optimum}$) is based on determining the change in the volume within the OWC chamber per unit step in time due to the change in the virtual interface between the water wave front and the entrapped air (X_1) with respect to the OWC mass (X_2). This is expressed mathematically as:

$\Delta Vol. = - A_{owc} \times \delta(X_2-X_1)$; that is, the change in the volume of the OWC vessel between the OWC mass as determined by X_2, and the mass-less wave front as determined by X_1, is the negative of the product of the OWC footprint area and $\delta(X_2-X_1)$.

This change in volume per incremental time step is used to determine the incremental change in the pressure for that step using the energy that is also determined for that step, and then the average across the entire sinusoidal period is determined. This can be represented mathematically as:

$$\Delta P_{avg.}\ [psi] = average\ (\{C\ (dX_2/dt - dX_3/dt)\ (\delta X_2-\delta X_3)\}_n \times Wave\ Energy\ Fraction\ (\zeta we))\ /\ \Delta Vol._n/144)$$

Where the wave energy fraction, ζwe = ratio of part load wave energy to full load (design point) wave energy (i.e., 80%, 60%, 40%, …) with respect to the wave intensity, and C is the damping coefficient that has $E/A)_{LCM} = E/A)_{wave}\ (=(\rho\ (H_{wave})^2\ g_g/g_c)/8)$ and is held constant as the variable, ζe, is changed from 0.0 to <1.

The flow coefficient for the complete sinusoidal cycle of the wave is then determined from:

$C_v = \{\Delta Vol./(Tw/4)\}\ /sqrt(\Delta P_{avg})$; this is also used to determine the volume flow rate $(dV/dT) = \Delta Vol./(Tw/4)_n$ for each incremental time step, dT.

The calculation of the time constant, T_c, concludes the derivations and is determined from:

$$T_c = sqrt(\Delta P_{avg}) \times (A_{owc} \times H_{owc})/14.696/(4 \times C_v);$$

Note: $A\ \pi/2$ multiplier converts the ΔP_{avg} to ΔP_{max} for the sinusoidal wave form, and it is used to determine the variation of $\Delta P = (\pi \times \Delta P_{avg}/2) \times \sin(\omega_n t)$.

The derivation of Algorithm No. 1 leads to the understanding that the functional relationship to the left of the T_c, optimum between the fraction of recoverable wave energy with respect to the time constant, T_c, is a maximum when the flow coefficient is held constant at its design point flow rate (i.e., ζ_{cv} = 1.0), a design point that would be selected for use with a specific size OWC system. The insight gained from this algorithm of how the incident wave energy affects the performance of the OWC includes the observation that with C_v not changing, then the flow coefficient, $C_{damping}$ does not change for a fixed OWC turbine design, even as the amount of incident wave energy is reduced below that for which the OWC system was originally designed (i.e., $\zeta_{we} < 1.0$), but with an energy reduction rate that falls off many times faster than if the flow control fraction is reduced (i.e., $\zeta_{cv} < 1.0$) to accommodate a change in the design point incident wave energy.

Consider Figure 62 which is comparable to Figure 62 except there are now two characteristic curves to the right of the $T_{c,optimum}$. Figure 63 illustrates these curves as identical because the energy control fraction, ζ_{we}, is assumed to be equal to 1.0 (i.e., the wave energy of incident wave is the same as the design point wave energy potential), but the flow control fraction, ζ_{cv}, is numerically assumed to be equal to the 1.0, 0.8, 0.6, 0.4, and 0.2 ratio for the data points shown for the curve to the right of the $T_{c,optimum}$. The curve to the left of the $T_{c,optimum}$ uses the wave energy fraction to vary as shown, but the flow control fraction is held at 1.0.

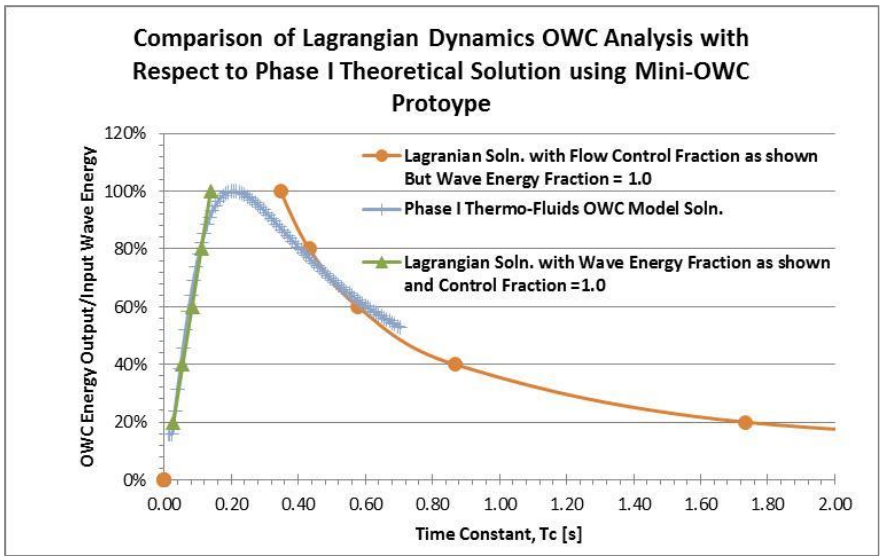

Figure 62. Comparison of Lagrangian Dynamics Numerical Model with the Theoretical Model Developed in Phase I

However, Figure 63 presents the results of the Lagrangian dynamics OWC analysis model with Algorithm No. 2 using the flow control fraction equal to 60% and with the wave energy fraction varying as shown. The left curve shifts toward the right, indicating that if the OWC design point were selected to be 0.2 (= $T_{c,optimum}$ for the original wave energy intensity), that fixed OWC design is likely to return only 40% of the original wave energy as evidenced by the intersection of T_c = 0.2 and the new curve.

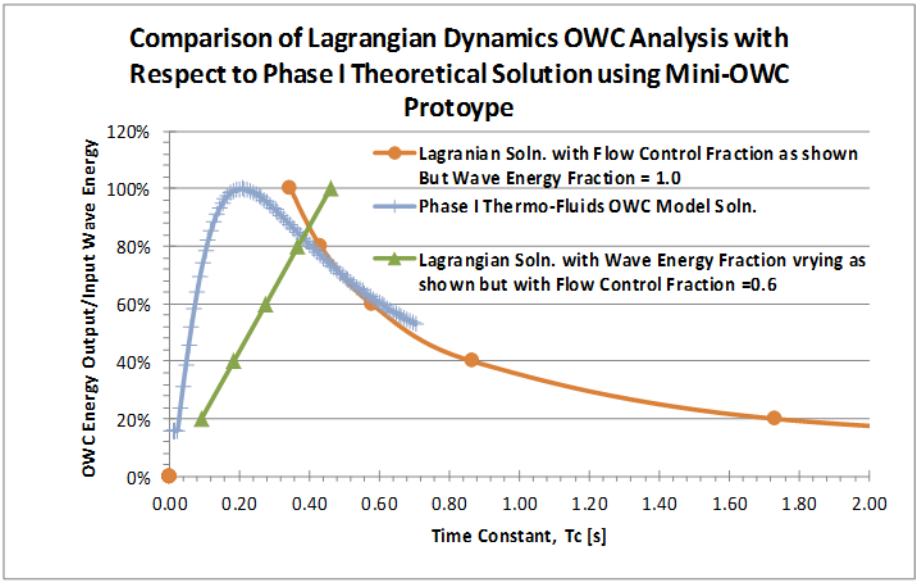

Figure 63. An Illustration of the Changes in the Power Recovery Ratio for an OWC with Changes in the Wave Energy Fraction and the Flow Control Fraction

Derivation of Algorithm No 2

Algorithm No. 2 (for T_c's > $T_{c,optimum}$) is based on fixing the values of $\Delta P_{avg.max}$ and $C_{v,max}$ to be the maximum values as determined with Energy Fraction, ζe =100%.

Then, the time constant, T_c, is calculated by:

$T_c = sqrt(\Delta P_{avg.}@\zeta_{we} \ x \ \pi/2)$ x $(A_{owc} \ x \ H_{owc})/14.696/(2 \ x \ C_v,@\zeta_{we} \ x \ \zeta_{cv})$ with the values of the flow control fraction, ζ_{cv} and ζ_{we} each potentially ranging from 0.0 to <1.0.

Note that the flow control fraction, ζ_{cv}, is a new variable, different from the wave energy fraction ζ_{we} that was used in the derivation of Algorithm No. 1, which enables the flow coefficient to be changed in order to adjust the flow of air through the turbine. For example, flow control of the air through the turbine can be affected by using air shutters, as proposed in Phase I of this project. The derivation of Algorithm No. 2 leads to the understanding that the functional relationship to the right of the $T_{c,optimum}$ between the fraction of recoverable wave energy with respect to the time constant, T_c, is a maximum when the wave energy fraction (ζ_{we}) = 1.0 but with the flow control fraction (ζ_{cv}) < 1.0.

Figures 64 and 65 illustrate this result, where in each of the figures the wave energy fraction, ζ_{we}, is kept at a constant value of 0.6 in Figure 64 and 1.2 in Figure 65, even as the flow control fraction, ζ_{cv}, is varied from 0.0 to 1.0.

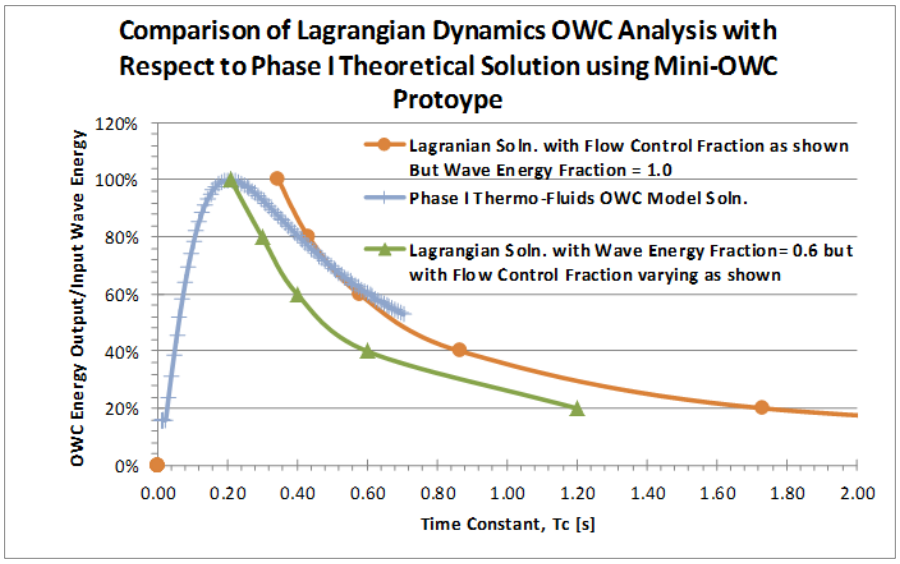

Figure 64. Comparison of Lagrangian Dynamics Solution with Thermo-Fluids Model

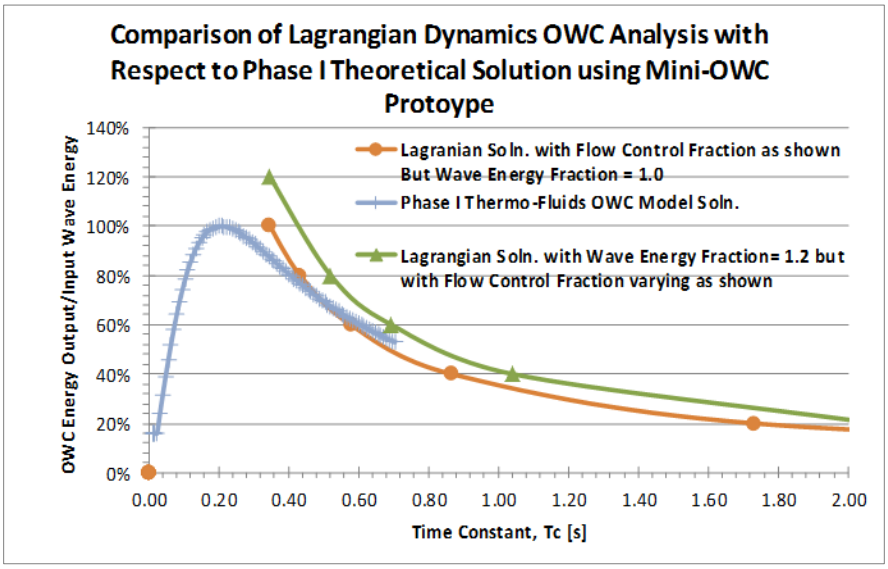

Figure 65. Comparison of Lagrangian Dynamics Solution of OWC Performance with Respect to Time Constant and Effects of Wave Energy Fraction

Derivation of Lagrangian Dynamics-based Engineering Model

The algorithms presented in the previous section provided a reasonably good fit to the theoretical solution derived in Phase I of the project. There is some benefit to using these algorithms in order to provide a consistent methodology for designing an OWC vessel with respect to its theoretical optimum time constant, T_c, which was found to be equal to $Tw/(2\pi)$.

However, another engineering methodology has been derived based solely on the calculations provided by the Lagrangian dynamics OWC model. While the equations are similar, the Lagrangian solution avoids the "curve fit" nature of the previous algorithms, and thus the calculations are more supported by the basic physics associated with power generation. The basic equations to consider are as follows:

$dVn = \Delta Vol. = A_{owc} \; x \; \delta(X_2\text{-}X_1)_n$; this is the incremental change in the OWC chamber at each small time step.

Total volume change (V_{total}) = $\sum dVn$; determined from summing the small incremental volume changes at each step for one complete wave cycle. It is noted that the V_{total} may be much larger than the OWC vessel dimensions that are under consideration for a specific OWC design, and thus, the constraint of the chosen OWC dimensions must limit this volume in any application.

$$\Delta P_{avg.}\ [psi] = (\sum\{ C\ (dX_2/dt - dX_3/dt)\ (\delta X_2 - \delta X_3) \}_n \ x\ \text{wave energy fraction}\ (\zeta we))/\ V_{total}/144)$$

$$C_v = \{V_{total}/(Tw)\} / sqrt(\Delta P_{avg.});$$

$$T_c = sqrt(\Delta P_{avg.})\ x\ (V_{total})/(14.696\ x\ C_v)$$

These equations provide a very similar result to what is produced using Algorithms 1 and 2, as may be observed from Figure 66. However, the peak performance is not at a time constant, T_c, equal to $Tw/(2\pi)$ = 0.2 s. The curves to the right and to the left of the peak performance do have the same derivation. That is, the "left side" of the performance curve with respect to the $T_{c,optimum}$ is characteristic of the OWC performing with the wave energy fraction, ζ_{we} = 1.0, and the flow control fraction, ζ_{cv}, varying from 0.0 to 1.0. The "right side" of the performance curve with respect to the $T_{c,optimum}$ is characteristic of the OWC performing with the flow control fraction, ζ_{cv} =1, and the wave energy fraction, ζ_{we}, varying from 0.0 to 1.0. An interesting effect that the damping coefficient, C, has on the position of the peak time constant, T_c, is shown in Figure 66. The peak approaches a limit as the damping coefficient, C, approaches zero (0).

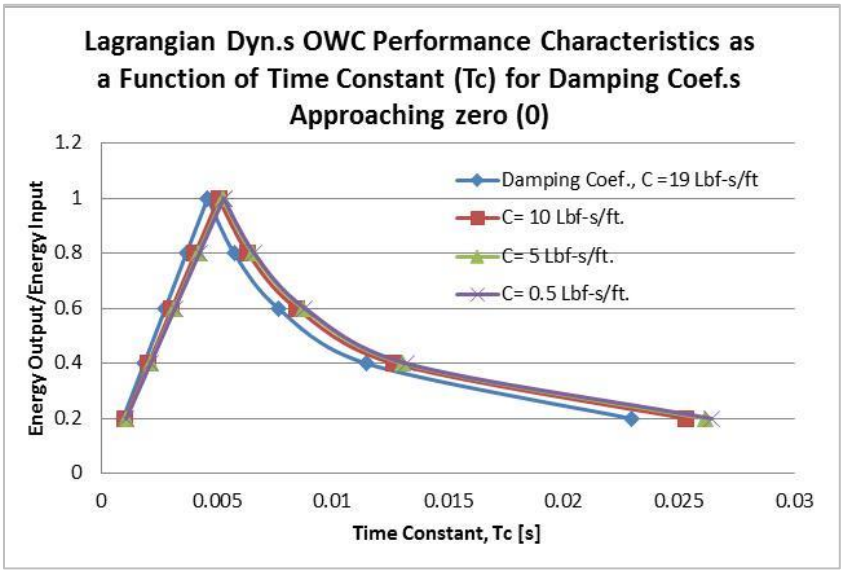

Figure 66. An Illustration of the Effect of the Flow Coefficient Parameter on Percent Power Recovery

Another useful engineering functional relationship is shown in Figure 67. The OWC energy per volume of the OWC is linear with respect to the average OWC pressure change. This is a direct result of the derivation for ΔP_{avg} from the energy per area of wave energy or ΔP_{avg} = $E/\sum V_n$. This straight line functional relationship (with the slope equal to 1/144) is dependent on the K_{spring} of the OWC vessel, but only in that low values of K_{spring} will reduce the value of the ratio of the OWC energy/OWC volume. However the values of *E/Vol.* still lie on the straight line relationship. Also, it can be demonstrated that a larger wave energy intensity (i.e., larger T_{wave} and/or H_{wave}) causes the OWC pressure to increase and the energy per OWC volume to increase, but these points lie on the same straight line.

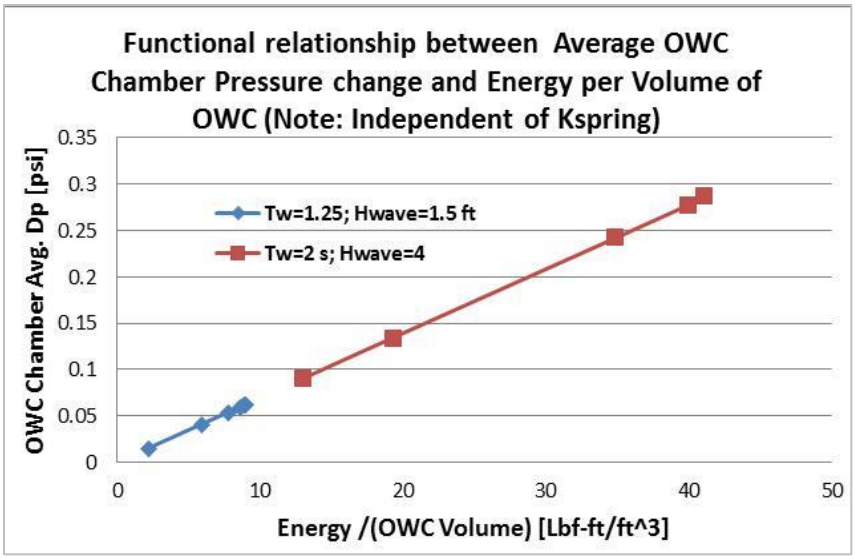

Figure 67. Energy Relationship Between Average OWC Chamber Pressure and Energy per Volume of OWC (note: independent of K_{spring})

Summary

For the first time, and as a direct result of using the Lagrangian dynamics OWC analysis solution, it becomes easier to determine how the OWC performance varies with the two part-load phenomenon, ζ_{we} and ζ_{cv}, occurring either separately or together. The part-load performance scenarios may be determined by the following steps:

1. The incident wave energy to the OWC may be increased or decreased with respect to the design point wave energy for which the OWC system was originally designed. This ratio is represented using the wave energy fraction, ζ_{we}.
2. The ability to affect control of the air flow through the OWC turbine is represented by the flow control fraction, ζ_{cv}. This control is considered to be an active control with the OWC turbine is place.
3. The "right side" of the performance curve with respect to the $T_{c,optimum}$ is characteristic of the OWC performing with the wave energy fraction, ζ_{we}, varying from 0.0 to 1.0 and the flow control fraction, ζ_{cv}, varying from 0.0 to 1.0. That is, the right side of the T_c graph indicates the effect that the flow rate through the turbine has on the wave energy recovery. Although the wave energy may have been mechanically transferred to the entrapped OWC air, the air flow through the turbine may be insufficient to completely convert this mechanical (pressure) energy into rotary mechanical energy. The ability to expel the air through the turbine is a function of the magnitude of the flow coefficient, C_v.
4. The "left side" of the performance curve with respect to the $T_{c,optimum}$ is characteristic of the OWC performing with the flow control fraction, ζ_{cv} = 1 and the wave energy fraction, ζ_{we}, varying from 0.0 to 1.0. That is, the left side of the T_c graph indicates the effect that waves of different potential energy have on the energy recovery, assuming that the flow coefficient, C_v, is unchanged.
5. In the event that the incident wave has a wave energy density less than what the OWC vessel was designed to accommodate, the viable performance area is reduced by the "left side" and "right side" performance curves closing in on each other, effectively reducing the efficient operating range.

Engineering Case Study

The main objective of developing a model of an OWC system, using Lagrangian dynamics, is to provide a means of analyzing and designing an OWC system with respect to the incident wave energy, and thus to optimize the OWC performance. The Lagrangian solution that was demonstrated above, and summarized in the conclusions, provides an opportunity to demonstrate the strength of the Lagrangian dynamics analysis model to design an OWC system. The Lagrangian dynamics model also provides an opportunity to compare the results with previously studied and published research. As an example, Figure 68 identifies the OWC chamber pressure (*Pa*) and the volume flow rate (m^3/s) through the turbine that is installed at the top of the OWC chamber. The relationships shown in Figure 68 are the results from four previously studied and published studies of an engineering analysis performed for a 150 m^2 OWC system. The results are from *CN*'s thermo-fluids OWC model and those provided by an OWC developer. The wave was estimated to have an amplitude of 8 ft and a period of 4 seconds. Other parameters used in the case study are shown below.

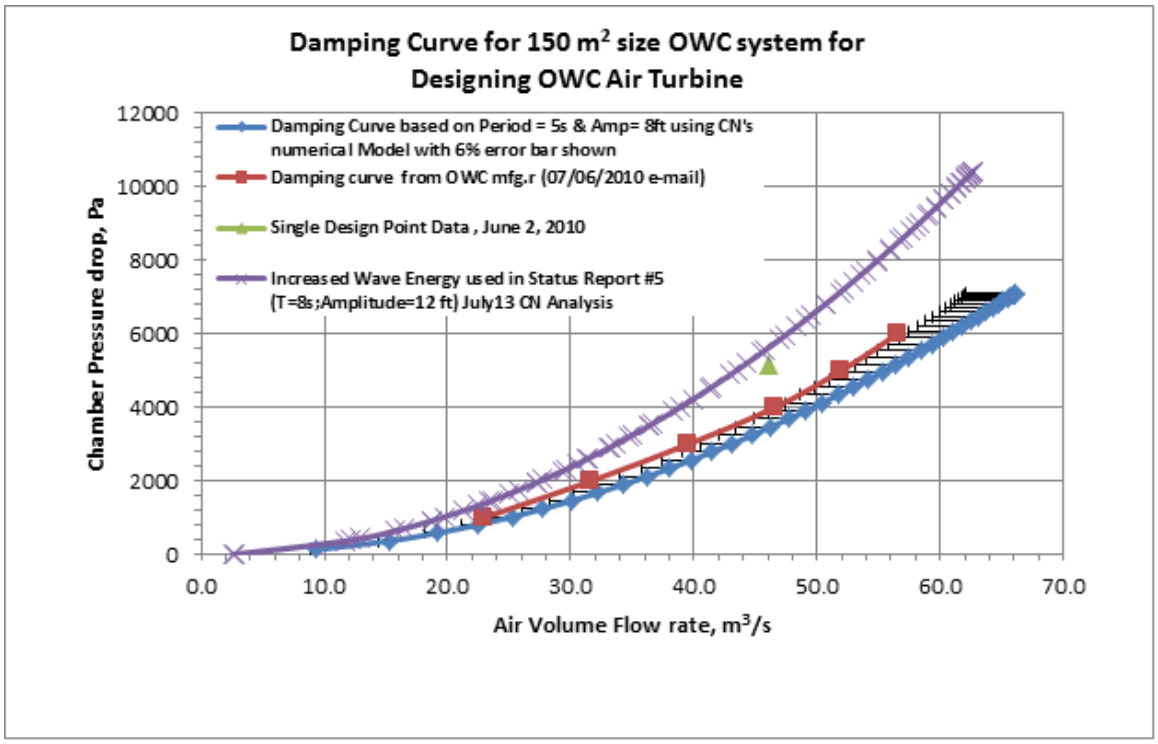

Figure 68. Results of Numerical and Theoretical Models of Damping Curve for Full-scale OWC System

The Lagrangian dynamics analysis solution was applied to the same size OWC system and incident wave energy application. Figure 69 displays a direct comparison of the same OWC chamber pressure and volume flow rate. As may be observed, the modeling from the Lagrangian dynamics algorithms is in excellent agreement with the prior studies.

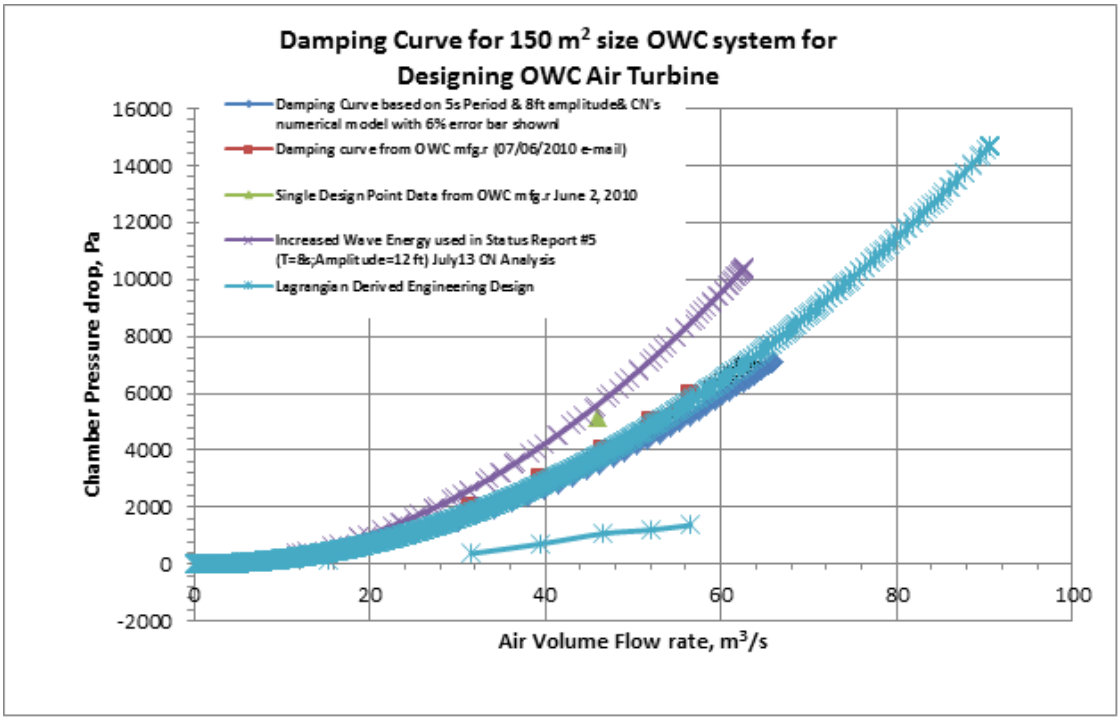

Figure 69. Damping Curve Illustrating Success of Lagrangian Dynamics Model Matching Theoretical and Numerical Model Solutions

OWC Design Algorithm Using Lagrangian Solution

A modification has been made to the design algorithm that was presented previously. The modifications include a correction to the OWC pressure increase to satisfy the conservation of available energy in the incident wave. The following equations are part of the model shown in Figure 70. The equations have been developed and demonstrated to be viable algorithms for designing a floating OWC wave energy conversion system.

The incremental pressure change during each time step is determined from the equation:

$$\Delta P_n\ [psi] = (\sum\{ C\ (dX_2/dt - dX_3/dt)\ (\delta X_2 - \delta X_3)\ \}_n \ x\ \text{wave energy fraction}\ (\zeta we))/\ dV_n/144\ )$$

Where: $dVn = \Delta Vol. = A_{owc}\ x\ \delta(X_2 - X_1)_n$; this is the incremental change in the OWC chamber at each small time step.

$\Delta P_{energy\ \ max.}\ [psi] = [E/A]_{theory}\ /(A_{owc}\ x\ H_{wave}/2)/144$, which determines the maximum chamber pressure change that can be achieved from an energy input $[E/A]_{theory}$ and $volume = /(A_{owc}\ x\ H_{wave}/2)$

$$C_v = \{\ A_{owc}\ x\ (H_{wave}/2)\ /Tw\ \}\ /sqrt(\Delta P_{avg.})$$

where: $(\Delta P_{avg.}) = average \sum\ (\Delta P_{energy\ \ max/(avg.}\ \sum \Delta P_n)\ \ x\ \ (\Delta P_n)\ \ x\ (\text{energy fraction}, \zeta_{we})\ x\ \text{energy correction factor})$

and: $\text{Energy correction factor} = [E/A]_{theory}\ /\ \sum(\Delta P_n\ x\ \text{volume flow rate}\ x\ \Delta T_{,time\ increment})$

but: $\text{Vol. flow rate} = sqrt(\Delta P_n)\ x\ \ C_v$

$T_c = sqrt(\Delta P_{avg.})\ x\ (V_{total})/(14.696\ x\ C_v\ x\ \text{flow rate coefficient factor}, \zeta\ x\ C_v)$

Step I. Match the $E/A)_{LMC}$ with $E/A)_{theory}$ by changing the $C_{damping}$ coefficient.

Step II. Manually transfer (input) the calculated value of ΔP_{avg} from the corrected OWC pressure calculations into the C_v equation.

Step III. Manually type in the recalculated energy correction factor.

Step IV. Choose the correct value of f_{owc} which is used to modify the height of the OWC chamber: H_{owc} until the value of T_c, as calculated from the above equation is equal to: T_c, theory = $Tw/(2 \times \pi)$.

Figures 71 and 72 provide a display of the flow rate as a function of wave period. Figure 72 illustrates the system power as a function of the flow coefficient. Figure 73 is similar to Figure 72; however, Figure 73 shows the effect of height change on the OWC.

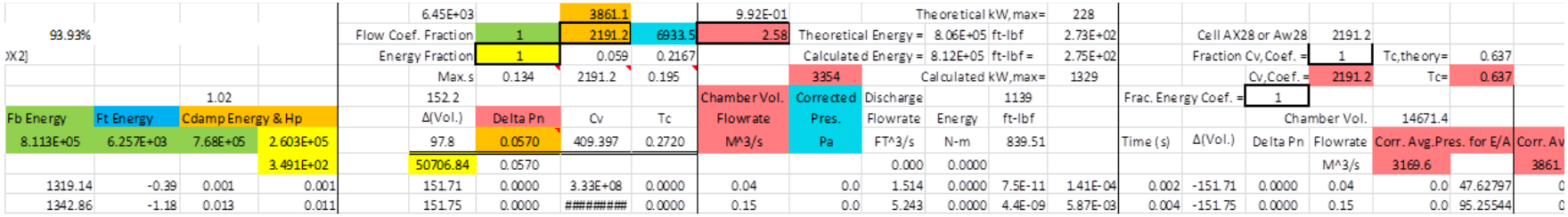

					6.45E+03		3861.1		9.92E-01				Theoretical kW, max=		228																
	93.93%				Flow Coef. Fraction	1	2191.2	6933.5	2.58		Theoretical Energy =	8.06E+05	ft-lbf	2.73E+02				Cell AX28 or Aw28	2191.2												
)X2]					Energy Fraction	1	0.059	0.2167			Calculated Energy =	8.12E+05	ft-lbf =	2.75E+02				Fraction Cv, Coef. =	1	Tc, theory=	0.637										
					Max.s	0.134	2191.2	0.195		3354			Calculated kW, max=		1329				Cv, Coef. =	2191.2	Tc=	0.637										
		1.02			152.2				Chamber Vol.	Corrected	Discharge		1139					Frac. Energy Coef. =	1												
Fb Energy	Ft Energy	Cdamp Energy & Hp			Δ(Vol.)	Delta Pn	Cv	Tc	Flowrate	Pres.	Flowrate	Energy	ft-lbf							Chamber Vol.	14671.4										
8.113E+05	6.257E+03	7.68E+05	2.603E+05		97.8	0.0570	409.397	0.2720	M^3/s	Pa	FT^3/s	N-m	839.51				Time (s)	Δ(Vol.)	Delta Pn	Flowrate	Corr. Avg.Pres. for E/A		Corr. Av								
			3.491E+02		50706.84	0.0570					0.000	0.0000								M^3/s	3169.6		3861.								
1319.14	-0.39	0.001	0.001		151.71	0.0000	3.33E+08	0.0000	0.04	0.0	1.514	0.0000	7.5E-11	1.41E-04			0.002	-151.71	0.0000	0.04	0.0	47.62797	0								
1342.86	-1.18	0.013	0.011		151.75	0.0000	########	0.0000	0.15	0.0	5.243	0.0000	4.4E-09	5.87E-03			0.004	-151.75	0.0000	0.15	0.0	95.25544	0								

					6.45E+03		3861.1																								
	93.93%				Flow Coef. Fraction	1	2191.2	6933.5																							
)X2]					Energy Fraction	1	0.059	0.2167																							
					Max.s	0.134	2191.2	0.195																							
		1.02			152.2																										
Fb Energy	Ft Energy	Cdamp Energy & Hp			Δ(Vol.)	Delta Pn	Cv	Tc																							
8.113E+05	6.257E+03	7.68E+05	2.603E+05		97.8	0.0570	409.397	0.2720																							
			3.491E+02		50706.84	0.0570																									
1319.14	-0.39	0.001	0.001		151.71	0.0000	3.33E+08	0.0000																							
1342.86	-1.18	0.013	0.011		151.75	0.0000	#########	0.0000																							
1366.58	-1.97	0.042	0.037		151.79	0.0000	#########	0.0000																							

9.92E-01				Theoretical kW, max=		228																									
2.58	Theoretical Energy =		8.06E+05	ft-lbf		2.73E+02				Cell AX28 or Aw28		2191.2																			
	Calculated Energy =		8.12E+05	ft-lbf =		2.75E+02				Fraction Cv, Coef. =		1	Tc, theory=		0.637																
	3354		Calculated kW, max=			1329					Cv, Coef. =		2191.2	Tc=		0.637															
Chamber Vol.	Corrected	Discharge		1139					Frac. Energy Coef. =		1																				
Flowrate	Pres.	Flowrate	Energy	ft-lbf								Chamber Vol.		14671.4																	
M^3/s	Pa	FT^3/s	N-m	839.51					Time (s)	Δ(Vol.)	Delta Pn	Flowrate		Corr. Avg.Pres. for E/A		Corr. Avg.Pres. for E/A															
		0.000	0.0000									M^3/s		3169.6		3861.1	0.559867														
0.04	0.0	1.514	0.0000	7.5E-11	1.41E-04		0.002	-151.71	0.0000	0.04		0.0	47.62797		0.00																
0.15	0.0	5.243	0.0000	4.4E-09	5.87E-03		0.004	-151.75	0.0000	0.15		0.0	95.25544		0.04																
0.27	0.1	9.570	0.0000	4.3E-08	3.57E-02		0.006	-151.79	0.0000	0.27		0.1	142.8819		0.13																

Figure 70. Typical Output from Lagrangian Dynamics Solution of OWC Model

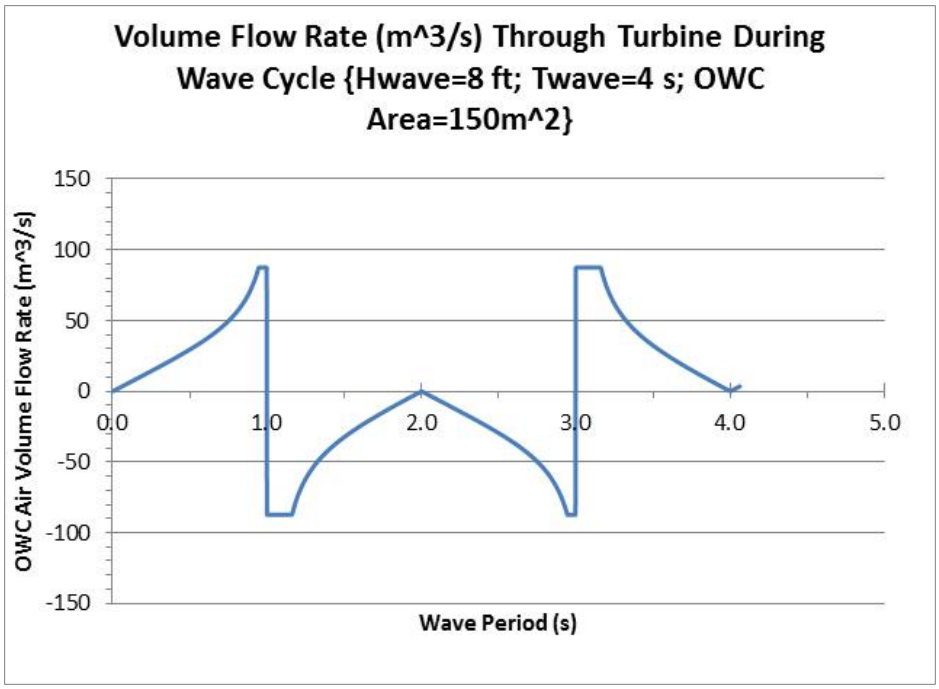

Figure 71. Variation of OWC Flow Rate as a Function of Wave Period

Note: Changing C_v per time increment affects modeling of the damper control on the Wells turbine.

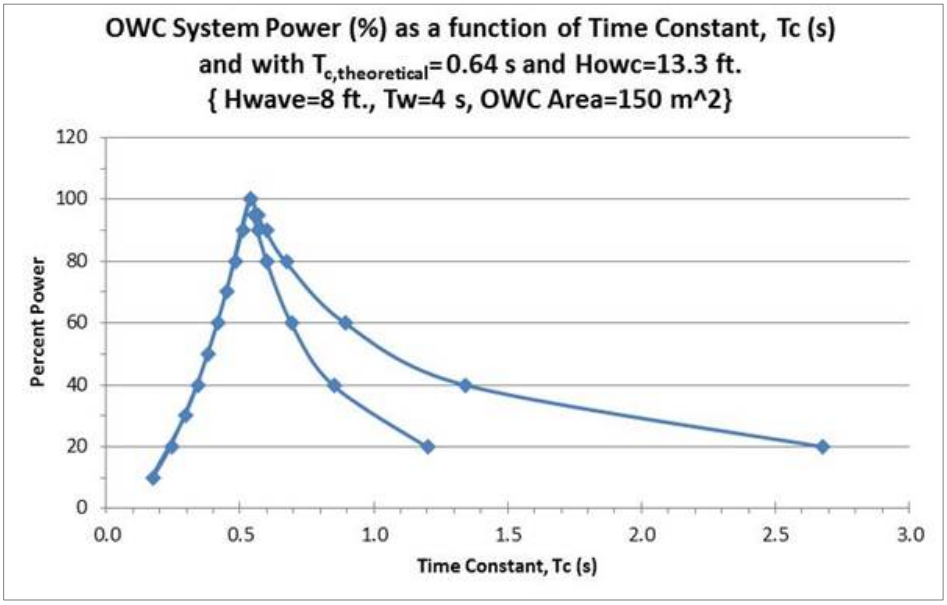

Figure 72. OWC System Power Illustrating Effect of Different Flow Coefficient, C_v, on Optimum OWC Energy Recovery

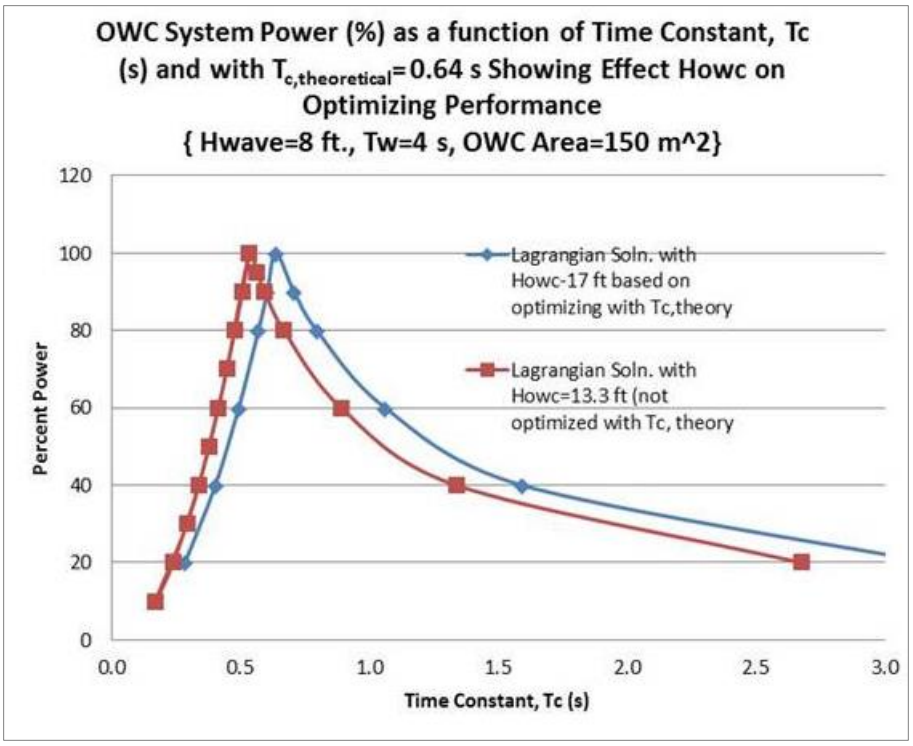

Figure 73. Numerical Solution from the Lagrangian Analysis for Two Different OWC Chamber Heights, Confirming the Project Hypothesis that OWC Chamber Height Can Increase Wave Energy Recovery

Erlang Analysis

Advanced models should also increase the understanding of how water wave energy can be most effectively recovered, independent of the type of electro-mechanical energy recovery system that may be deployed. *CN* continues to research better, more versatile computer models for the prediction of energy recovery from water waves. *CN*'s current research includes the use of two probability distribution functions, the Erlang and the Lognormal, that show some promise of being able to provide a closed-form solution to the amount of energy that can be recovered from an incident wave. For example, Figure 74 displays the graphical display of the Erlang and the Lognormal (Gamma) probability distributions as a function of the time constant parameter that has been used as the independent variable. The Erlang and Lognormal probability functions are used frequently to determine the probability of events that do not behave in the more typical Gaussian (normal) frequency. Applications such as predicting the number of telephone calls which may be made at one time, and the number of simultaneous visits to a web-site, have been successfully modeled using the Erlang probability distribution.

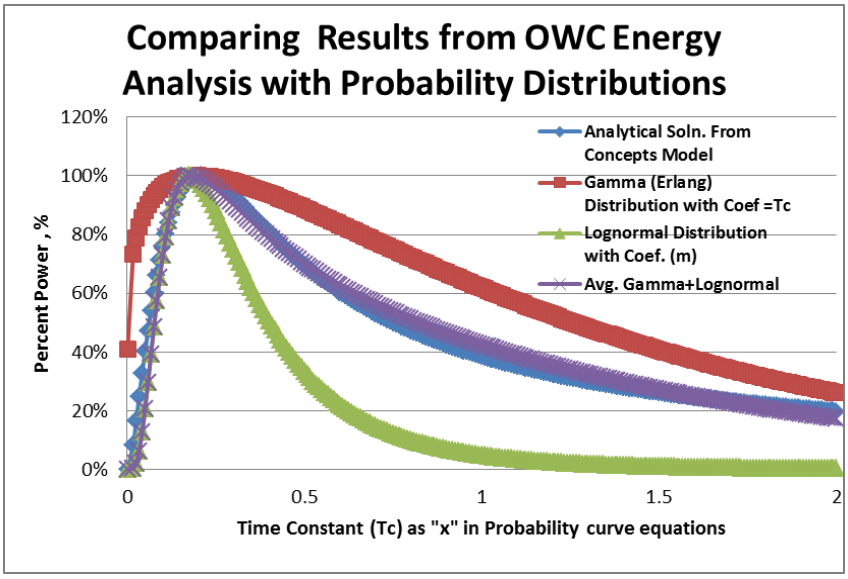

Figure 74. Comparisons of Numerical Analysis Using Lognormal, Erlang, and CN's Thermo-Fluids Model to Model the OWC Wave Energy Conversion

CN is working to develop a more universal model of water wave energy capture by combining these two probability densities. Figure 74 shows one such result, where CN's aforementioned computer model is reproduced almost precisely by simply (in this case) averaging the results from the Erlang and Lognormal distribution curves. Of particular interest, is that the maximum of each function may be associated with the OWC time constant, T_c, which, as has been shown previously, is equal to the wave period $(T_w)/2\pi$.

CN continues to work on deriving a more universal solution for determining the recoverable energy from different water wave energy densities, with the expectation that the universal solution aids in the design of OWC systems.

3.2.3 Task 3. MMA Designs an OWC Prototype for Validating Energy Model of OWC and Energy Recovery Advances

MMA engineering professors and staff, with the assistance and guidance of CN engineering, and Program Managers, will prepare the detailed design of a laboratory-scaled prototype of an OWC-based wave energy converter similar to the preliminary design shown in. The prototype will be scaled to enable it to be used in the wave tank in collaboration with the MMA's Tidal Energy Demonstration and Evaluation Center (TEDEC), a test facility that has been established by the MMA for demonstrating hydrokinetic and water wave energy systems. The prototype will further validate the performance benefits of the proposed turbine shutter system as predicted by the OWC mathematical model, and will verify the operational integrity of the feedback and controls system that must be used to control the turbine shutter during each wave cycle. The prototype OWC will also be used to verify the ability of controlling the height of the OWC above the mean water line to effect an improvement in wave energy recovery, as revealed in CN's Phase I research (Reference Section 2.3.2.3 Result No. 5). As necessary, MMA will engage the use of the wave tank facility operated by the University of Maine, approximately 20 miles from the MMA campus. The University of Maine, like the MMA, is part of the public university system in Maine.

In order to complete the Statement of Work for Phase II, two prototype OWC turbines and two OWC chambers were constructed. The smaller of the two systems was labeled the micro-OWC turbine and the larger system, the mini-OWC turbine (Mk3PC). The micro-OWC system was designed to be tested in the special TEDEC wave tank facilities constructed at the

MMA. The mini-OWC turbine was designed to be tested at the wave energy test facility at the University of Maine. The details of the mini-OWC turbine assembly (Task 5) are given in Section 3.26 of this final report. The micro-OWC turbine is rated at 10 watts and is detailed in Figure 75 based on the *CN* numerical model shown in Figure 76. The diameter of the micro-turbine is 50 mm and it operates at 20,000 rpm. The system is powered at start-up using a miniature electric motor until the wave energy is able to produce power using the micro-Wells turbine. At that time, the permanent magnet electric motor operates as a generator with a speed that is approximately 24,000 rpm. The micro-OWC turbine is constructed of hard plastic and machined using a three-dimensional, SLA printer from RedEye (a business unit of Stratasys, Inc.) Figure 77 displays the results of the structural analysis, validating the structural integrity of the high-speed turbine rotor.

CN also completed the design of the OWC chamber that was used with the micro- and mini-OWC turbines. The initial concepts for the OWC chamber are shown in Figure 78. The designs were constrained by the physical dimensions of the wave energy tanks available from the MMA and the University of Maine.

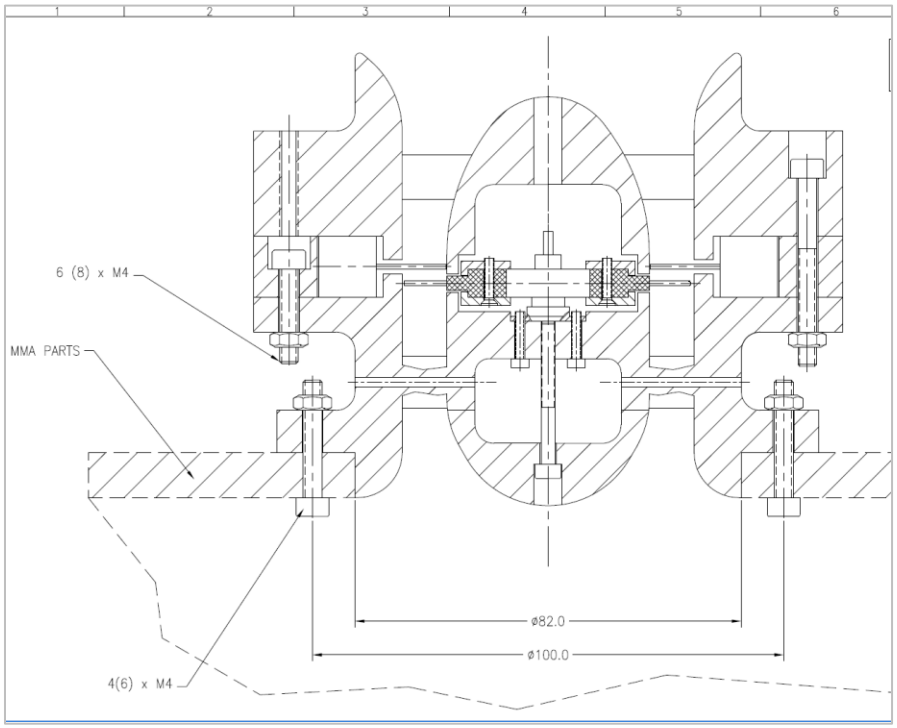

Figure 75. Micro-OWC Turbine Subassembly Turbine Design

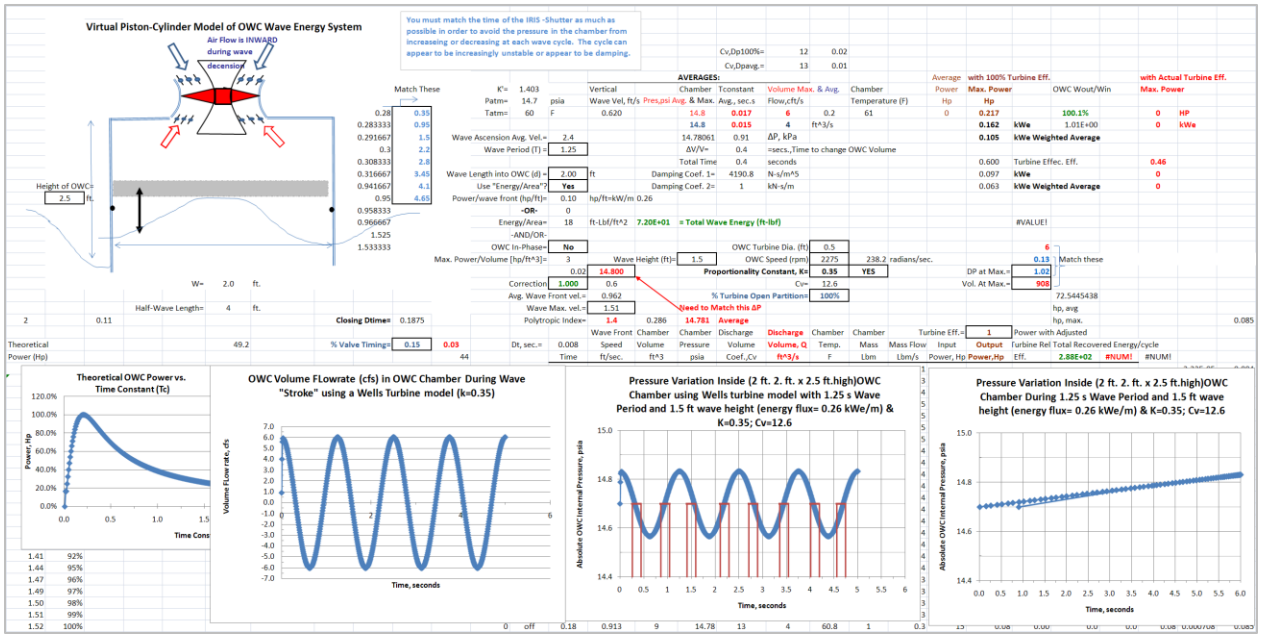

Figure 76. Computer Output from Thermo-Fluids Model of the Micro-OWC Turbine Design

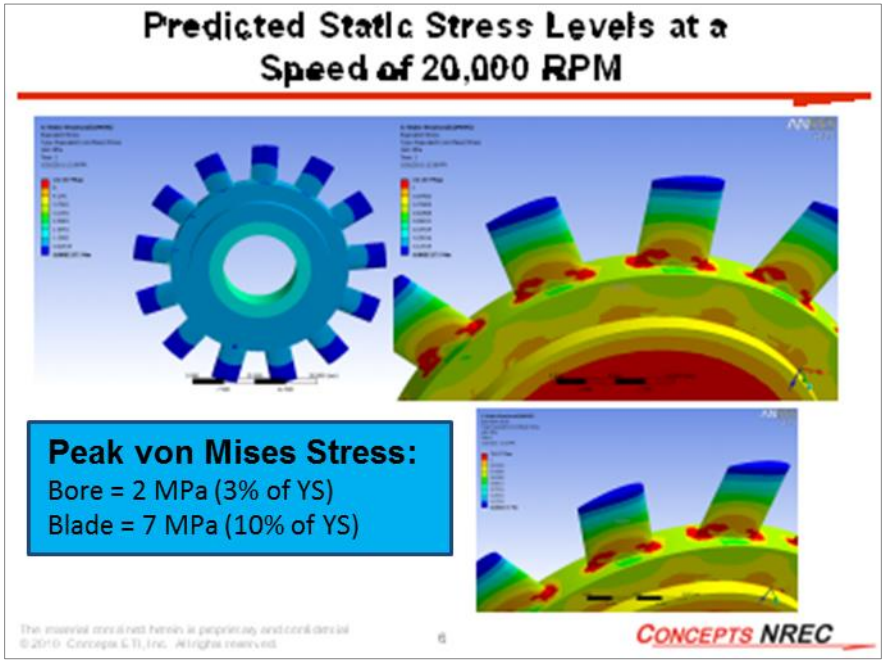

Figure 77. FEA Structural Analysis for 50-mm Diameter Micro-OWC Turbine

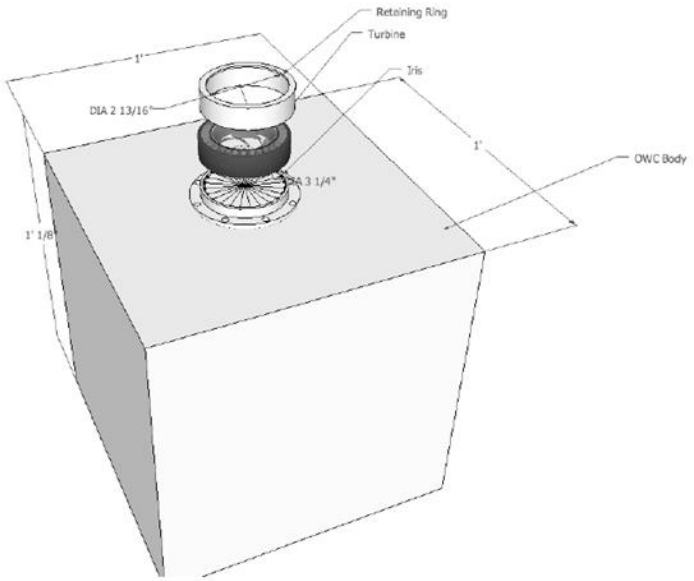

Figure 78. Conceptual Design for the Micro-OWC Chamber Used in the MMA In-Water Testing

The MMA faculty, staff, and students have modified an existing small wave tank at the MMA facility. This tank and the new, small (micro) OWC structure, made from transparent plexi-glass with the torque measuring system attached to the top of the OWC turbine assembly, is shown in Figure 79.

In addition to the wet water testing that was performed at the MMA and University of Maine test facilities, *CN* constructed a dry OWC turbine test apparatus to test the mini-OWC turbine under more controlled conditions. The conceptual design for the dry OWC turbine test system is shown in Figure 80. The completed design is shown in Figure 81. The dry OWC turbine test apparatus consisted of a cylindrical chamber with an opening at the top that could accommodate the mini-PWC turbine assembly. The bottom of the dry OWC turbine test apparatus consisted of an elastomeric membrane that was stretched vertically into and out of the OWC cylindrical chamber by the use of a pneumatic cylinder. The maximum stroke for the cylinder was 10 inches. The purpose of the dry OWC turbine test apparatus is to simulate the ascension and descension of the water wave front as it would enter in a real OWC chamber. The use of an elastomeric membrane in place of the water enabled a more controlled wave energy profile, frequency, and amplitude to be produced while avoiding the cumbersome interaction with water.

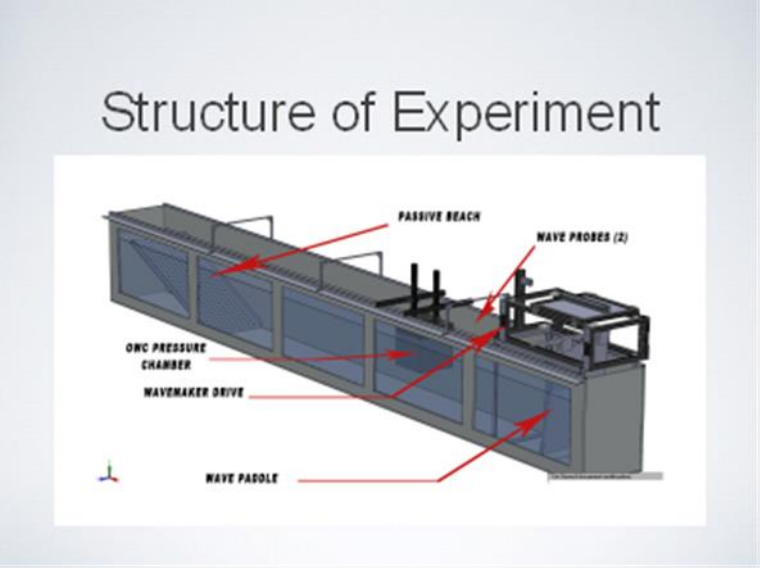

Figure 79. Wave Tank Installed at MMA

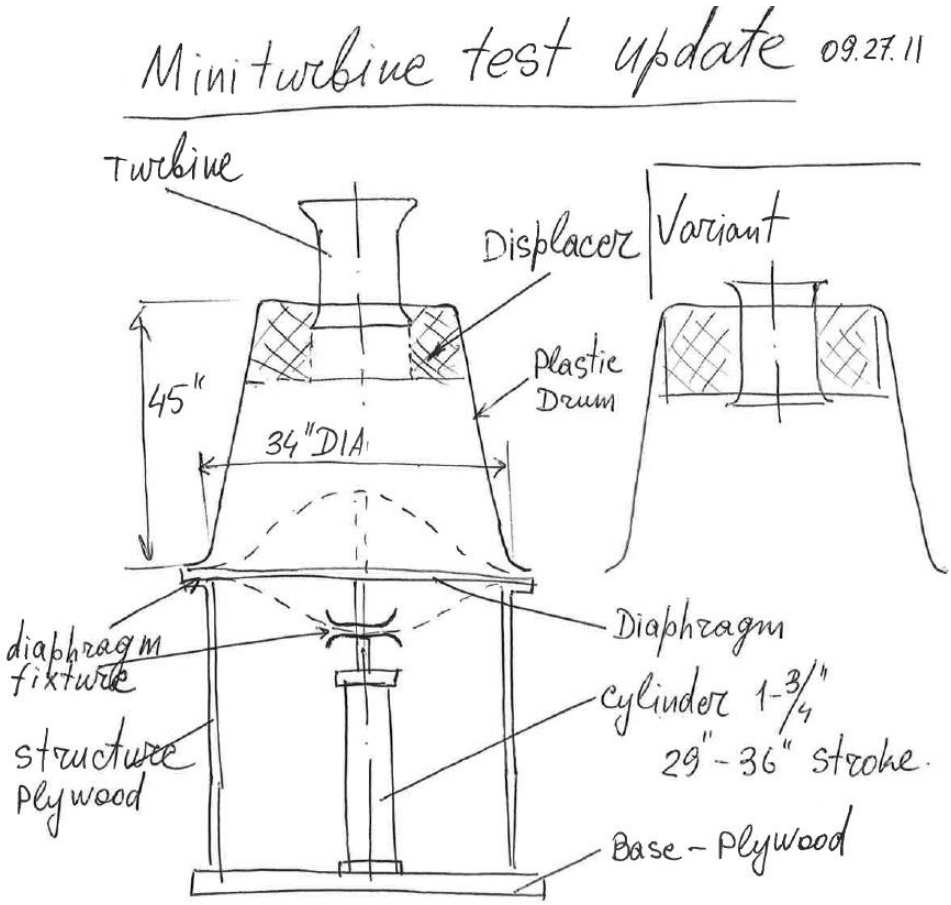

Figure 80. Engineering Conceptual Sketch for a Dry-Turbine Test Apparatus

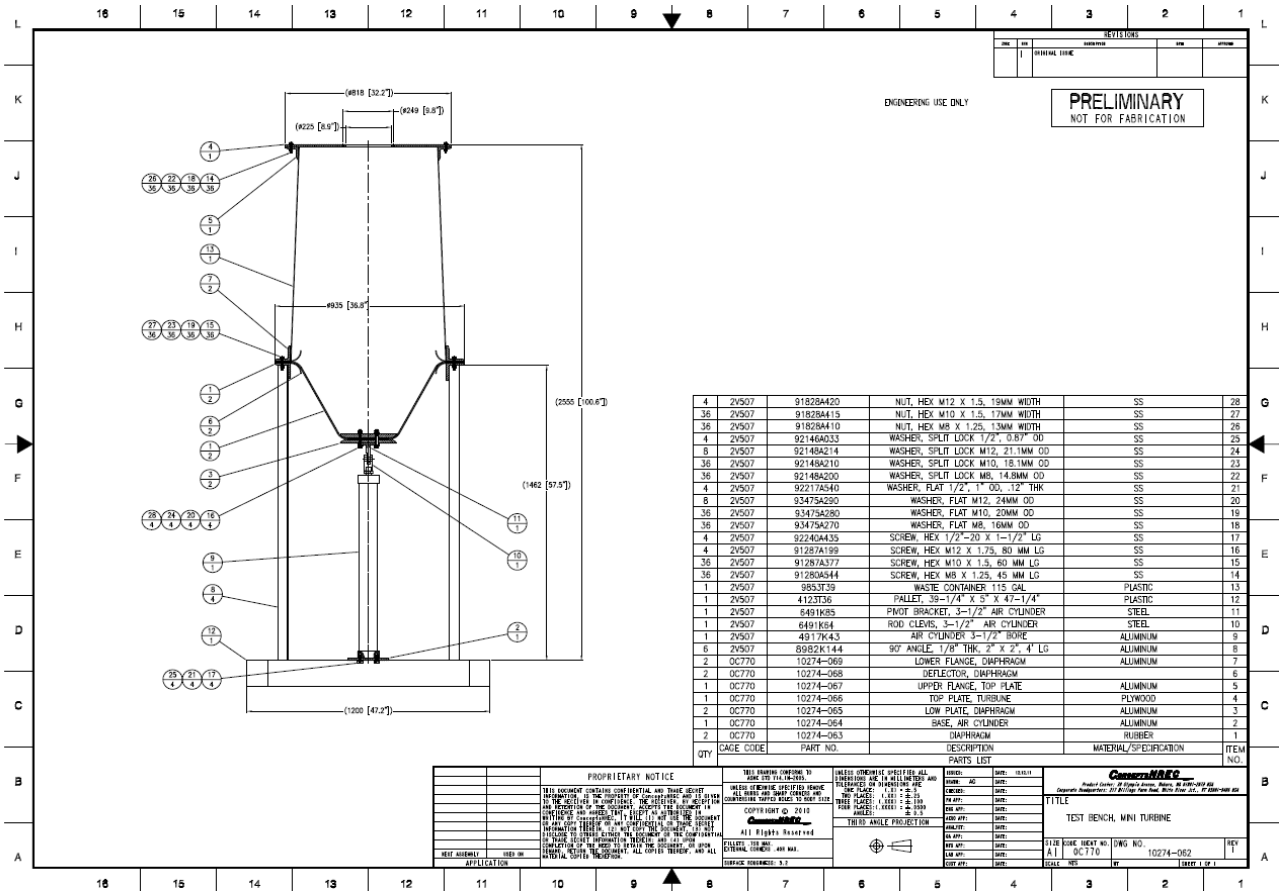

Figure 81. Detail Design Drawing for the Dry-Turbine Test Apparatus

3.2.4 Task 4. MMA Completes Construction of OWC Prototype and Initiates TEDEC Lab Testing

The MMA engineering students and staff will complete the procurement of parts and assemble the laboratory prototype OWC system. Testing of the prototype system will be initiated with CN and MMA personnel and accepted for permanent testing of the turbine shutter energy improvement concept, as well as the feedback and controls necessary for its actuation. The prototype will be fully instrumented with pressure and flow rate measurement devices. It will serve as a permanent laboratory test apparatus in collaboration with MMA's TEDEC facility for the testing of future advances in OWC designs. The purpose of these tests is threefold. The first is to establish a well-documented test protocol and a scaled OWC system for testing all future OWC component improvements using MMA's TEDEC facility. The second is to test the two major improvements that have been identified by CN in the Phase I STTR study, namely the use of a turbine shutter valve and the modulation of the OWC chamber height in order to affect wave energy recovery improvement. The scaled OWC fabricated in Task 4 will enable this to be accomplished. Lastly, the use of the turbine shutter valve is also hypothesized (see Result No. 7 from Phase I STTR) to enable the control of the phasing of the OWC structure with the frequency of the incident wave. This controllability will be tested during the testing with no other requirement than manual control of the turbine shutter valve system that has been installed in the scaled OWC device. The net result of these tests will be to develop a controls algorithm that will be used as the controls methodology for the feedback control system that will time the operation of the shutter valve and height control for the OWC.

The micro-OWC turbine assembly was manufactured and assembled according to the design completed in Task 3. This design included a 50-mm Wells-type micro-turbine and

housing, a 20,000 rpm permanent magnet electric motor/generator, and a shutter valve. Figure 82 illustrates these features for the micro-OWC turbine assembly.

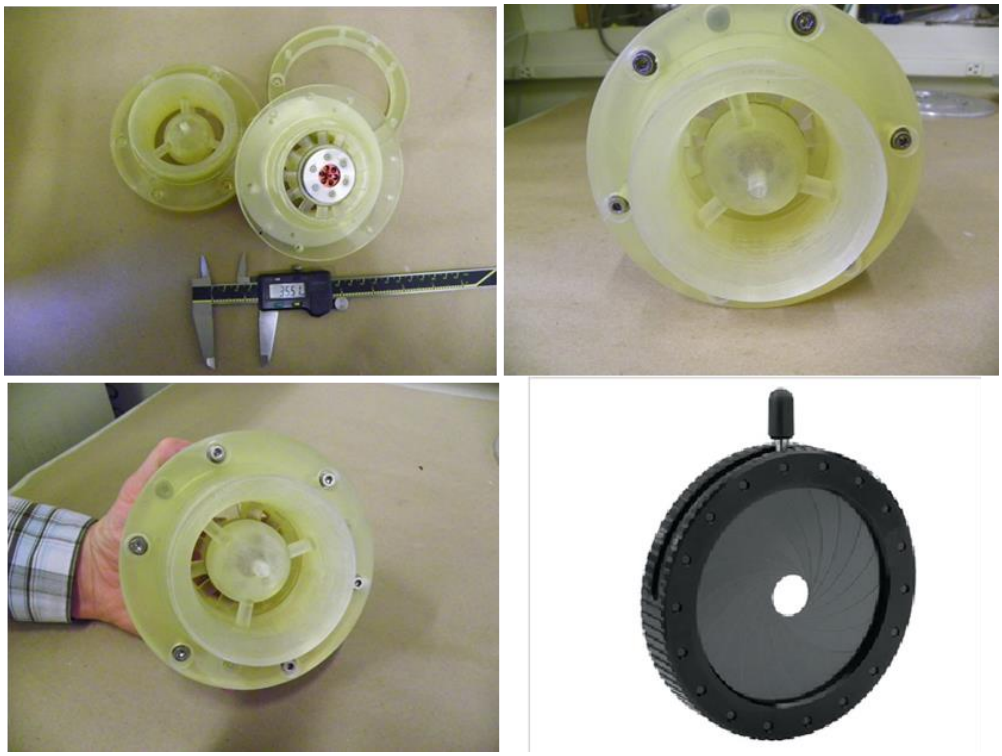

Figure 82. 10-watt Micro-OWC Turbine Prototype
Assembly and Micro-Shutter Valve Used in the MMA In-Water Test

The shutter valve was actuated using an electric solenoid as shown in Figures 83 and 84.

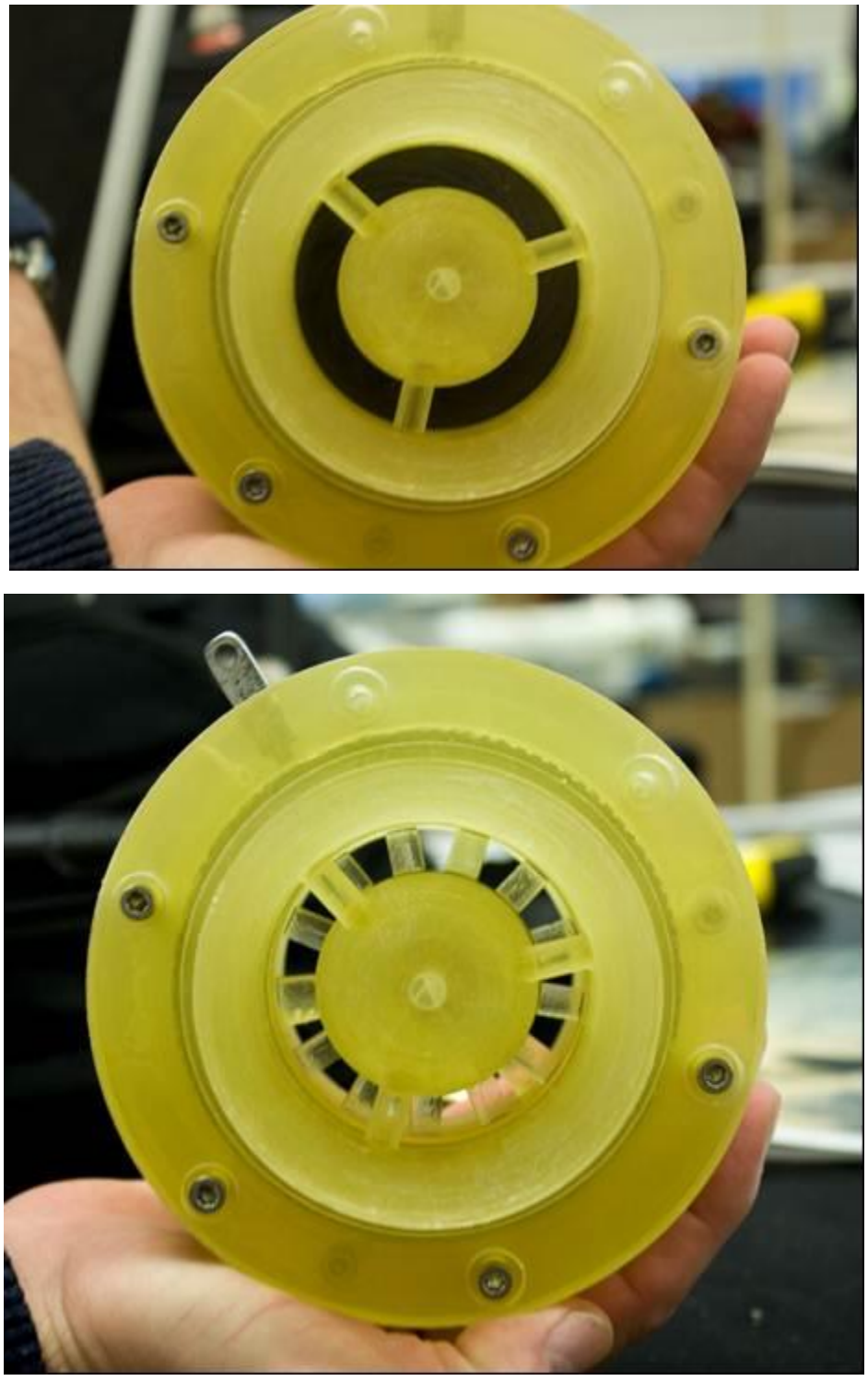

Figure 83. Micro-OWC Turbine Assembly
Used in the MMA In-Water Testing

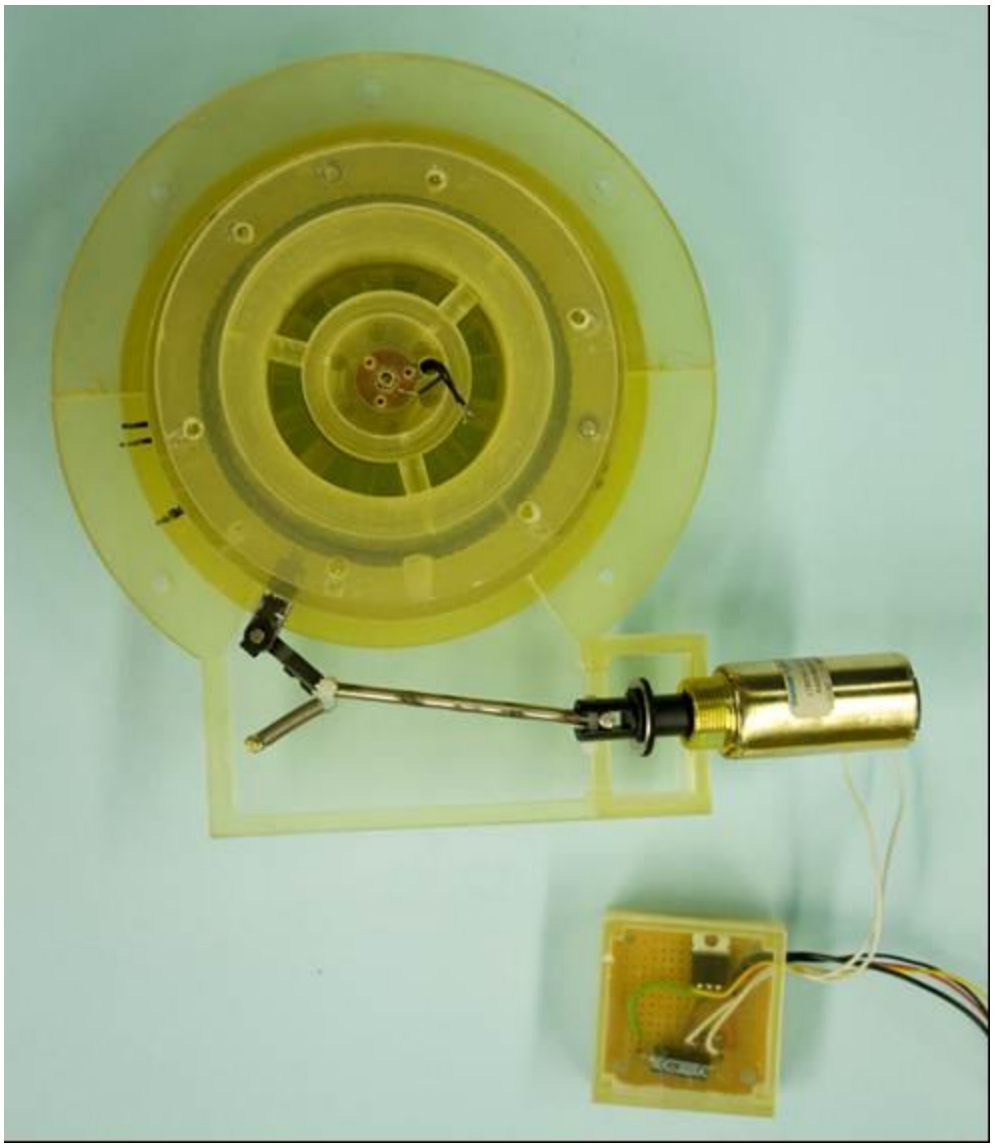

Figure 84. Actuation Solenoid for 10-watt OWC Shutter-Valve System

A torque measuring system, borrowed from MMA, was installed into the micro-OWC turbine and OWC chamber systems (as shown in Figure 85). The torque sensor was programmed using the Data Acquisition (DAQ) software. All of the necessary sensors for operating the torque sensor were wired to the hardware in the DAQ box that interfaces with the LabVIEW™[6] software interface. Unfortunately, MMA was only able to spin up the motor enough to turn the turbine to 10,000 rpm; at that speed, a slight imbalance in the power train was noted. MMA traced this unbalance to the use of two double-expansion couplings on each side of the torque sensor. MMA has a video recording of the testing to provide a record of this observation. As a method of correction, MMA attempted to change the design slightly by placing a rigid coupling above the torque sensor, while a double-expansion coupling absorbed the axial thrust at the shaft of the torque sensor. However, the unbalance persisted, and the torque recording was not possible. MMA decided to devote the remaining project time to characterizing the pressure transients in the OWC chamber at the various positions of the shutter valve. MMA also detected gearbox noise using the current configuration. MMA filtered

[6] LabVIEW is a trademark of National Instruments Corporation.

this noise out, but because this was thought to be a future issue, MMA decided to research a more precise gearing scheme. However, the torquemeter and gearing were abandoned in favor of using *CN*'s electrical motor, electrical controls, and resistor circuit to measure the motor/generator power.

Figure 85. Micro-OWC Chamber with Torque Measuring System at MMA

MMA has discovered that in order to reference box pressure for lowering the throat pressure of the turbine housing, they will need to change out the current pressure transducer from an Omega PX-139 to a PX-655 model, which offers bidirectional capability in a differential mode. Figure 86 shows the GUI interface that controls the DAQ process which logs chamber pressure, turbine rpm, lower throat pressure, upper throat pressure, and torque as a function of time. MMA has the capability of recording data at 10,000 Hz or lower, user-defined sampling rates.

MMA has added two wipers alongside the wave-maker paddle. The wipers help seal the paddle against the edge of the tank, and this acts to prevent eddies forming that act to change the shape of the wave pattern that the paddle produces.

Figure 86 (b and c) shows the DAQ box used to record instrumentation values sent from various sensors on the OWC box. The DAQ box is configured with power supplies, a Xenus motor controller, and two compact DAQ cards used to take channel data from the array of sensors. The box seen in Figure 86 (b) shows the control box used for the wave-maker. This box also has power supplies: two high-speed USB carriers that carry independent cards (one for control channels and one for LVDT feedback channels). Voltage is divided for needed applications using stackable terminal blocks. MMA and *CN* have eliminated the issues with these systems, with the exception of the relays that will control the solenoids operating the iris-shuttering device.

(a)

(b)

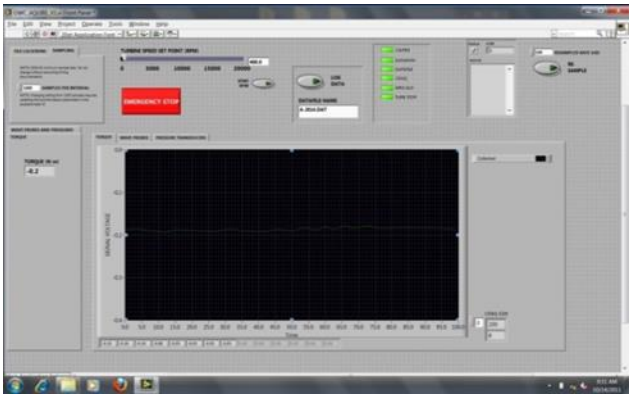

(c)

Figure 86. Test Apparatus Used in the MMA In-Water Testing of the OWC Micro-Chamber

MMA proceeded by first testing the instrumentation and measuring the OWC chamber pressure as a function of wave amplitudes and period, with the iris shutter valve in three positions: 0% open, 50% open, and 100% open, and with 6-inch and 12-inch reflector plates

installed. The results shown in Figure 87 (a and b) are the first results from the testing that was conducted.

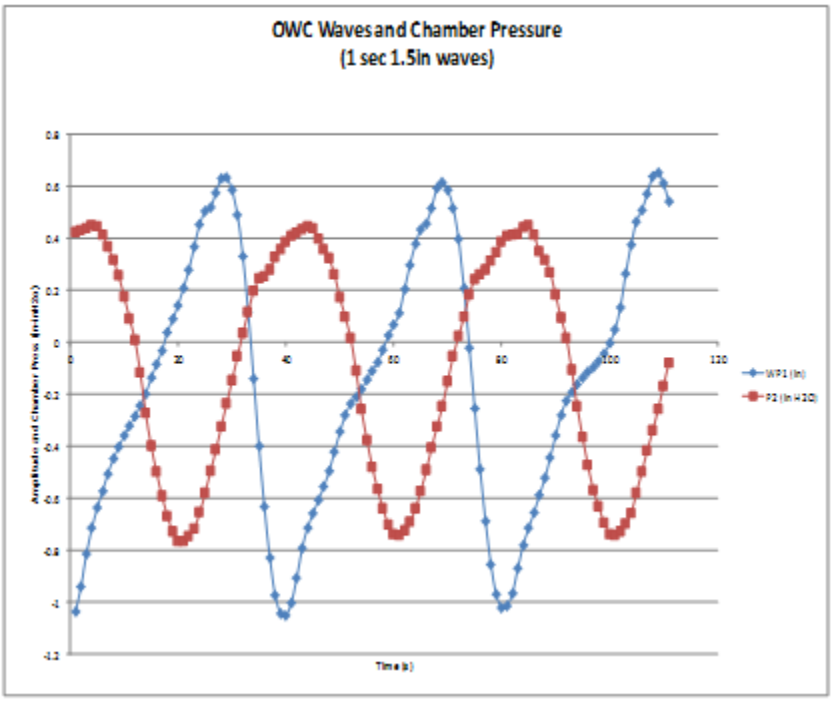

(a)

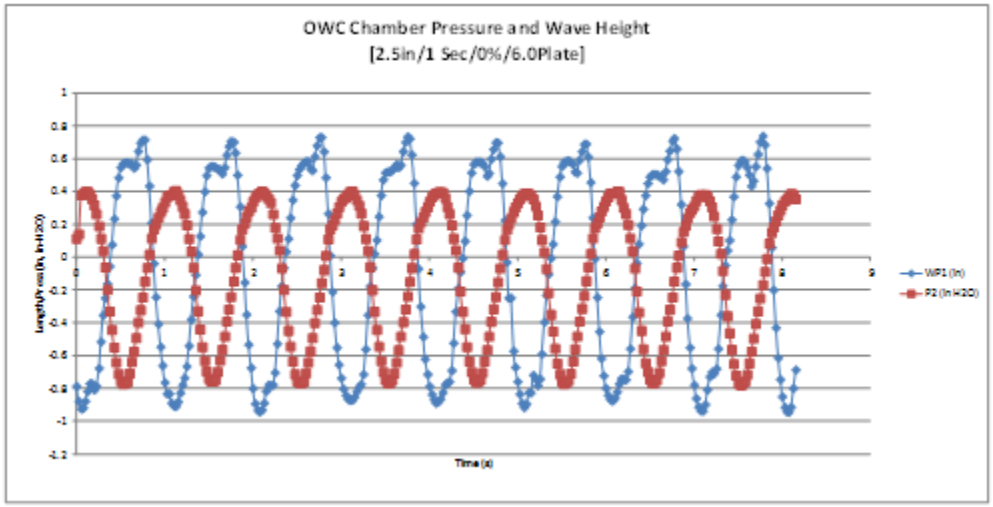

(b)

Figure 87. Presenting First Test Results from the MMA Testing of the Micro-OWC Chamber (as shown in Figure 78) and Tested in the MMA Wave Tank (Figure 79) with Iris Closed (Figure 84)

The following results have been determined from the series of tests that have been conducted at the MMA wave tank facilities on the micro-OWC chamber shown in Figure 88. The supportive data that generated Figure 88 is given in Appendix No. 2 of this final report. The chamber measures 12" x 12" x 14". The basic principle of OWC operation for the MMA test chamber is diagrammed in Figure 33. This chamber also includes a novel approach for the use of a wave reflector plate, which is adjustable inward (under the OWC), in order to capture some

of the kinetic energy stored in the wave. The test results reported are for tests without the micro-turbine in place. The objective of the testing was to measure the rise in the chamber pressure with the turbine aperture at 50% open, and with the wave reflector plate adjusted to three lengths: 0 inches, 6 inches, and 12 inches. The air space above the water line was also adjusted to 8 inches and 5 inches. For several of the tests, the reflector plate was also adjusted to 45-degree and 90-degree positions, from the vertical. The normal (default) position for the reflector plate is 0 degrees for the vertical position.

A measure of the chamber pressure is a direct indication of the amount of wave energy that is recovered from the incident wave. The use of the reflector plate enables, in theory, the total kinetic and potential energy of the wave to be recovered, while the complete absence of a reflector plate would prevent the kinetic fraction of the total wave energy from being recovered.

Figure 88 displays a summary of the testing. In Figure 88, the OWC chamber pressure is shown as a function of the wave period, and it also shows the effect of using a reflector plate and varying the height of the OWC chamber above the level (undisturbed) water line.

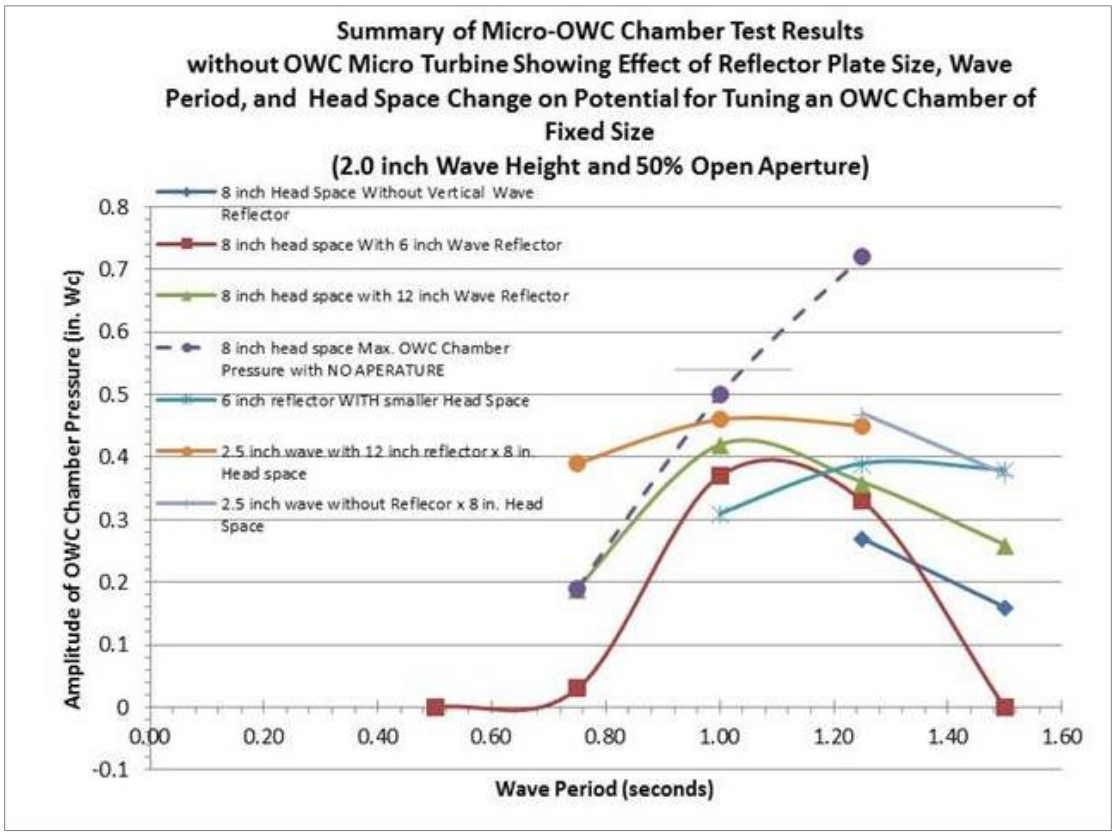

Figure 88. Summary of Test Results of the Micro-OWC Chamber Using the MMA Wave Tank Facility

The measured results lead to the following conclusions:

1. There is clearly a maximum amount of wave energy that can be recovered if the fixed OWC chamber can be tuned to the variation of the wave period. The optimization is similar, although not yet statistically quantified to the analytical solution, as expressed in earlier modeling of the OWC chamber.
2. The 0% open chamber represents the maximum pressure that the OWC chamber can achieve (but would result in zero power recovery). However, the 0% open chamber results can be compared against the results obtained with the

chamber using a 50% aperture, as a reference for determining the precision of the experiment.

3. The results indicate that the longer reflector plate achieves more total wave energy recovery, since it enables some degree of recovery of the kinetic energy from the incident wave. The extent of recovery of the kinetic energy portion of the total wave energy is shown in Figure 89, and is compared to an analytical expression derived independently for the efficiency of the kinetic energy recovery to total wave energy.
4. A comparison of the OWC chamber pressure, as measured with the same wave amplitude but with 8-inch and 5-inch head spaces, indicates that the optimum performance is shifted ("tuned") for the fixed-size OWC chamber (for the wave with the higher wave period).
5. The testing of the reflector plate at 45 and 90 degrees (with respect to the vertical) is not conclusive due to the limited testing that has been completed. The testing of the effectiveness of an angled reflector plate was not attempted during the testing at the University of Maine.

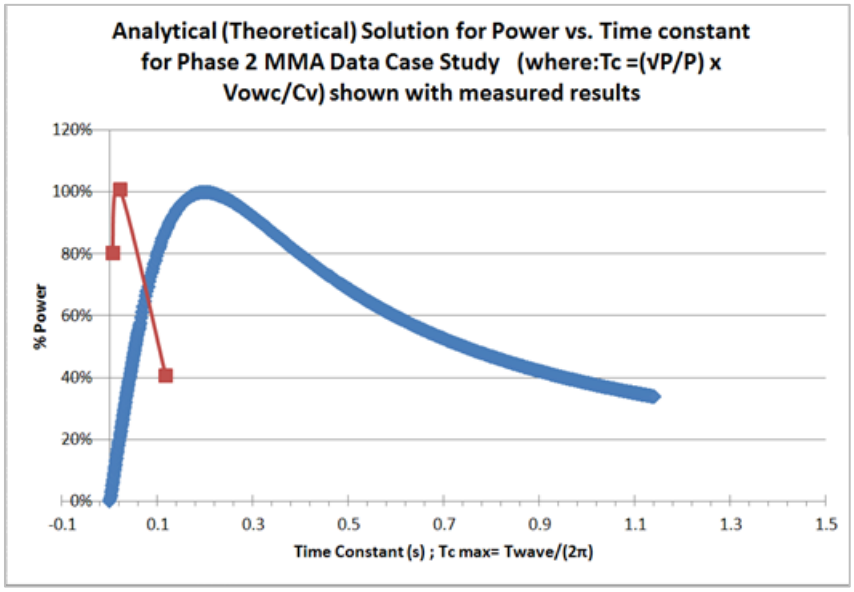

Figure 89. Comparison of the Theoretical Solution for OWC Percent Power Recovery and the Measured Performance Using the Micro-OWC Chamber Tested at the MMA

Figure 90 (a and b) is used to further quantify the amount of energy that may be recovered from the incident wave energy using an OWC chamber with respect to the potential energy available from the incident wave. This figure displays the results (and thus the comparison) of the turbo-fluids model that was developed by *CN* to model the OWC WEC system. Figure 90 (a) illustrates the predicted OWC chamber pressure for an OWC system that does not have a wave reflector plate (an 8-inch head space above the level water line is shown). Thus, a maximum OWC chamber pressure of 1.6 inches of water is predicted if 100% of the potential hydraulic wave energy could be recovered by an air OWC turbine. However, as shown in Figure 90 (b), using the same thermo-fluids model, a match of the measured OWC chamber pressure indicates that as much as 80% of the potential hydraulic energy may still be recoverable if an OWC air turbine were used. This must assume that the air flow rate through the turbine is much higher for the measured performance (i.e., with the lower operating pressure) than what was theoretically predicted for the 100% effective OWC system.

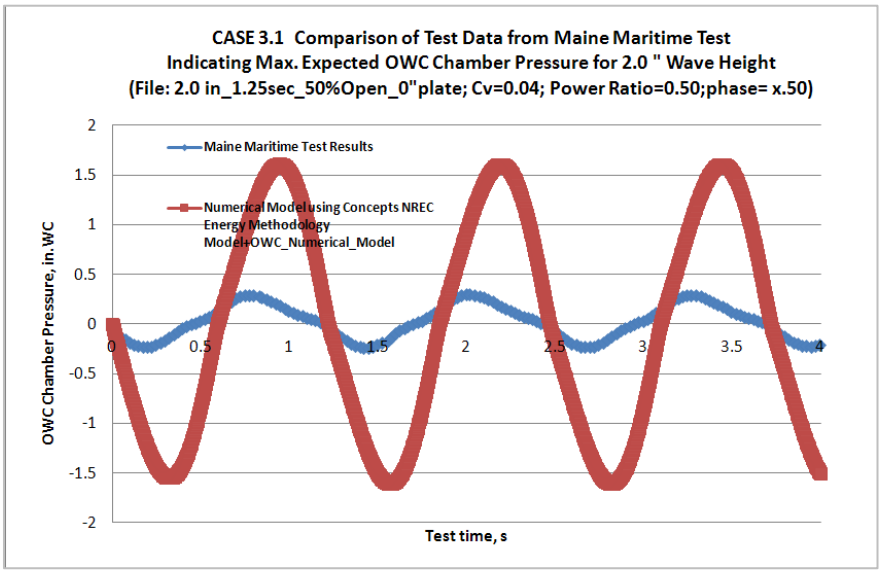

(a)

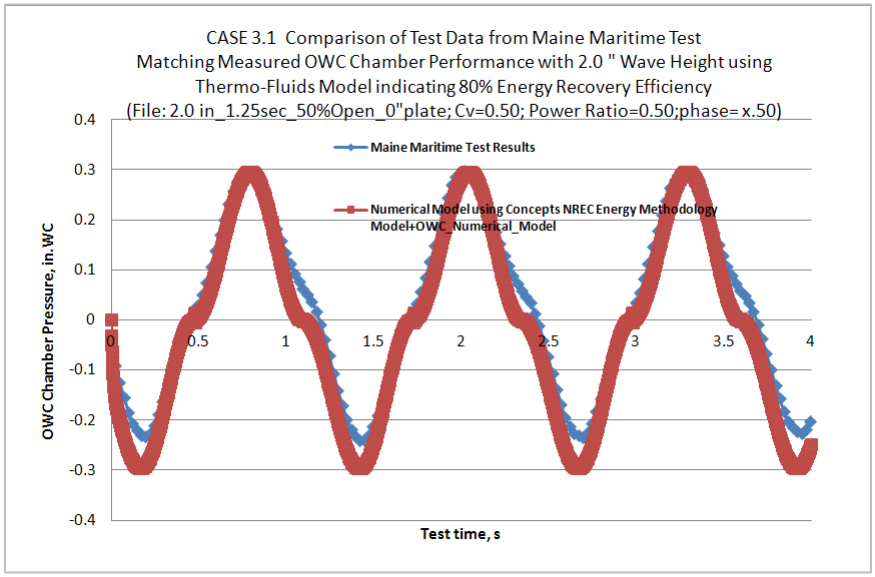

(b)

Figure 90. Comparison of Test Data from the MMA In-Water Testing, Illustrating the Maximum Expected OWC Chamber Pressure and Measured Chamber Pressure

3.2.5 Task 5 (original). Oceanlinx Measures Baseline OWC Performance Using Two OWC Turbines on Mk3PC OWC System

The original SOW required Oceanlinx to prepare a test report using non-proprietary data that baselines the performance of their Mk3PC OWC system that has been used with two different OWC turbines while it is tested in Port Kembla, Australia. The test report would have provided the engineering guidance that is needed to complete the detailed design engineering of the turbine shutter system. This task was cancelled due to the destruction of the OWC test platform and Oceanlinx's decision not to recover the system or provide a substitute during the timeframe for the Phase II project effort. Since this effort was not to be paid for by Phase II

program funds, but rather by Oceanlinx's cost share contribution to the project, the budget was not affected.

3.2.6 Task 5. *CN* Prepares Detailed Design of Advanced Turbine Shutter for Integration into *CN* Dry Test OWC System and University of Maine System

Using the results of the MMA testing and the refined energy methodology model of the OWC, CN will complete the detailed design of its advanced turbine shutter system. The design for manufacturing criteria will focus on system reliability and robustness while also being mindful of the need to be cost-effective in order to maintain its cost benefit for use in OWC systems. The design will carefully integrate the turbine shutter system into the dry test OWC system. The detailed design will also include the necessary feedback and control system required to properly actuate the turbine shutter in response to changes in the wave period.

The prototype OWC structure that was tested in the wave-tow tank facilities at the University of Maine measured approximately 2 ft (L) x 3 ft (W) x 3 ft (H), and will use a mini-turbine assembly that is installed above the shutter assembly. Figures 91 and 92 provide details of the Wells-type turbine rotor using a NACA0015 air foil. The turbine housing and turbine impeller are shown in Figure 92. All of the parts were produced using a rapid-reproduction prototyping technique. The entire assembly has a 10.5-inch diameter (267 mm) and is 2 ft high (610 mm). The assembly will be mounted on the OWC chamber. This mini-turbine assembly uses a Wells-type rotor (permitting bi-directional air to flow) that is approximately 8.5 inches in diameter, and rated for a maximum of 50 watts with a wave that is only 1.5 ft high. The mini-turbine, shutter vanes, and housing were designed and constructed by *CN*, specifically for the University of Maine testing. The adjustable shutter valve is designed to allow either a full or partial admission of air into the turbine, as may be necessary to maintain the air velocity through the turbine that is closest to the design point.

The stages of motion of the turbine shutters are depicted in Figures 93 and 94. The complete turbine module is installed on the top of the OWC chamber over the aperture. The turbine shutter system has been designed for a full-scale turbine (approximately 6 ft in diameter; 350 kWe). An equivalent shutter valve that has been designed for manufacture is shown in Figure 95.

The specially designed turbine shutters will be opened and closed using an electrically powered, linear actuator with the necessary linkages, as shown in Figure 96. The shutter valve can also be kept partially open and/or can be continually adjusted in order to maximize the relative velocity of the air with respect to the Wells turbine airfoil. Keeping the shutter valve partially open and/or continually adjusted is also thought to improve the efficiency of the overall turbine, even as the air flow rate varies from zero to a maximum flow rate when the OWC (i.e., the water wave front) reaches its maximum ascension in the OWC chamber.

The OWC structure has also been designed to include an adjustable length (in the direction of the water wave front) in order to tune the OWC to the different wave lengths that may be incident upon the OWC structure during the testing. A conceptual design of this adjustable OWC structure is shown in Figure 97.

A Wells turbine with stationary air foils was designed for the prototype OWC system. The turbine was designed to provide a maximum of 50 watts at a speed of 5,000 rpm. The Wells turbine model is shown in Figure 98, and the final assembly with the permanent magnetic micro-motor/generator (ready for testing) is shown in Figure 99. The micro-motor/generator serves to provide the initial motoring of the Wells turbine during startup and until the air flow has been established by the ascending and decscending water wave in the OWC chamber. The protoype Wells turbine was manufactured using a high-density plastic and was machined from a three-dimensional stereolothography technique. The geometric characteristics of the Wells turbine, particularly the inertia of the impeller along the three-dimensional axis, is given in Figure 100. In order to ensure the mechanical integrity of the Wells turbine, a complete finite element analysis (FEA) was performed. The result is shown in

Figure 101 and indicated a stress that was only 27% of the yield strength of the plastic material of construction. The flow and head coefficients for the Wells turbine design used in the mini-OWC protoype are shown in Figure 102.

It is also interesting to consider alternate applications of a 50-watt turbine assembly, as shown in Figure 96. For example, the turbine assembly shown is a very viable power generation source for on-board electrical equipment in remote, unmanned, marine-monitoring stations.

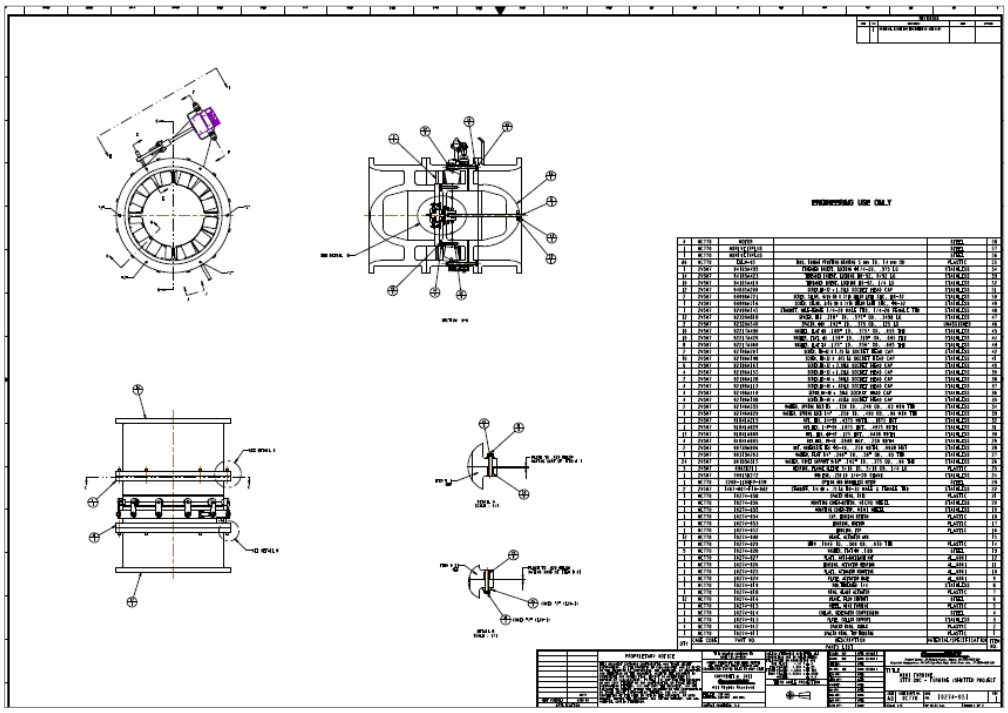

(a)

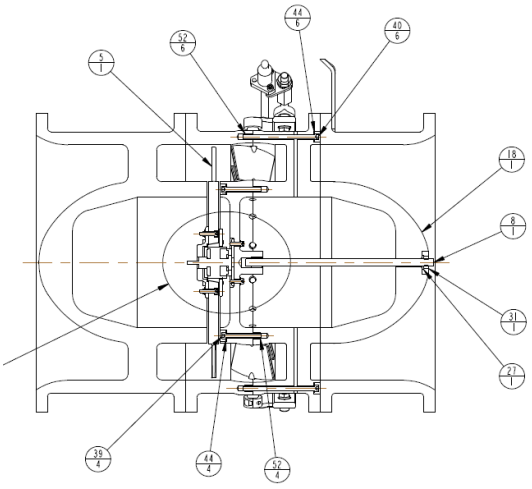

(b)

Figure 91. Detailed Cross-section Design
of the 50-watt Prototype OWC Turbine Assembly

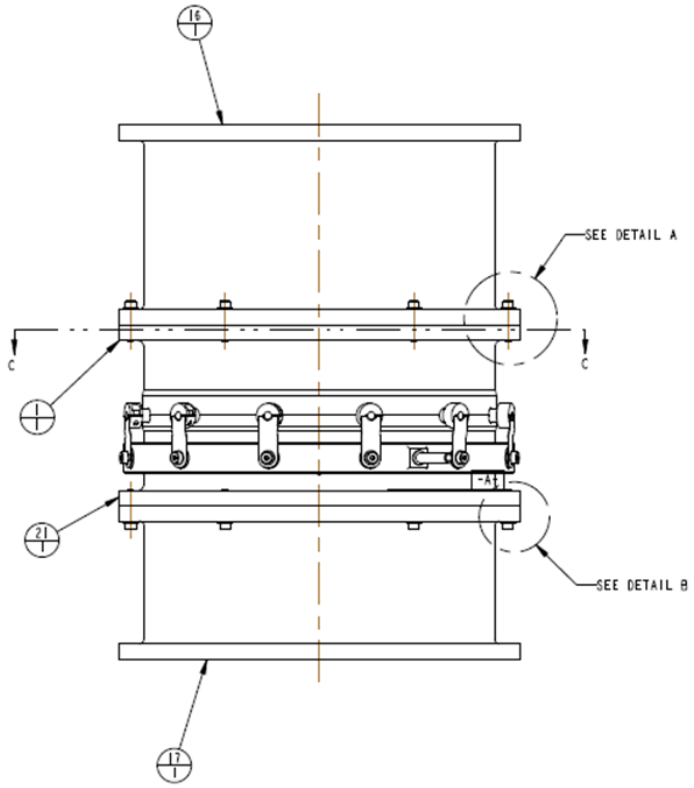

(a)

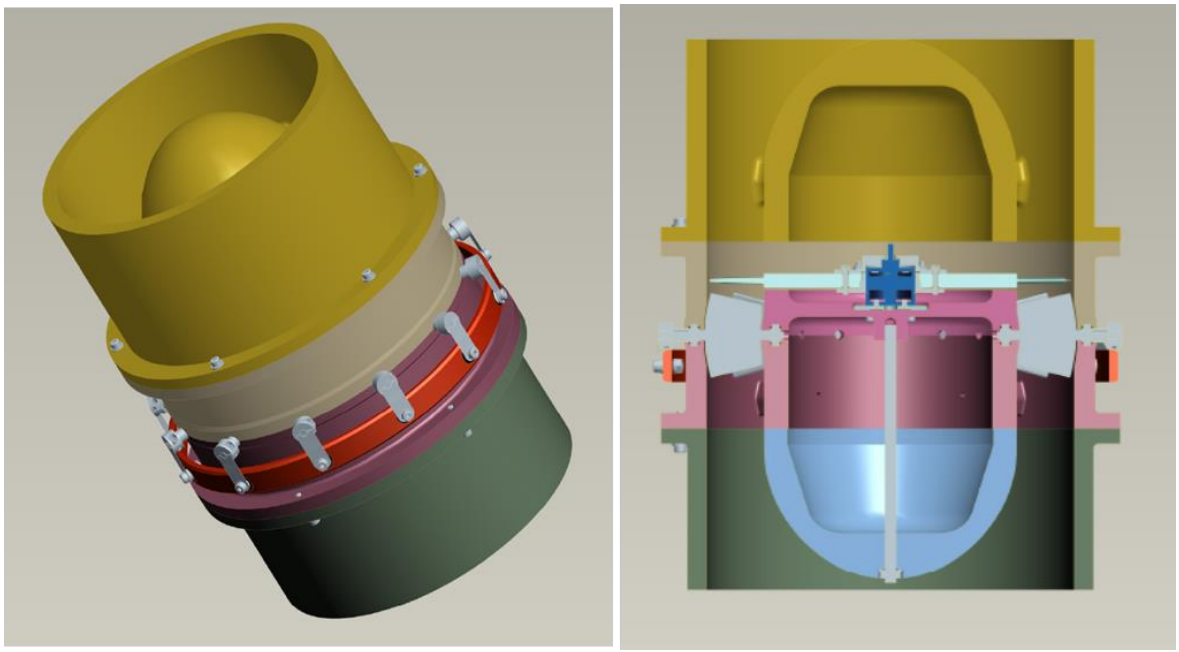

(b)

Figure 92. The Pro/ENGINEER®[7] Model of the Mini-OWC Turbine Assembly Designed for the In-Water and Dry Testing

[7] Pro/ENGINEER is a registered trademark of Parametric Technology Corporation (PTC).

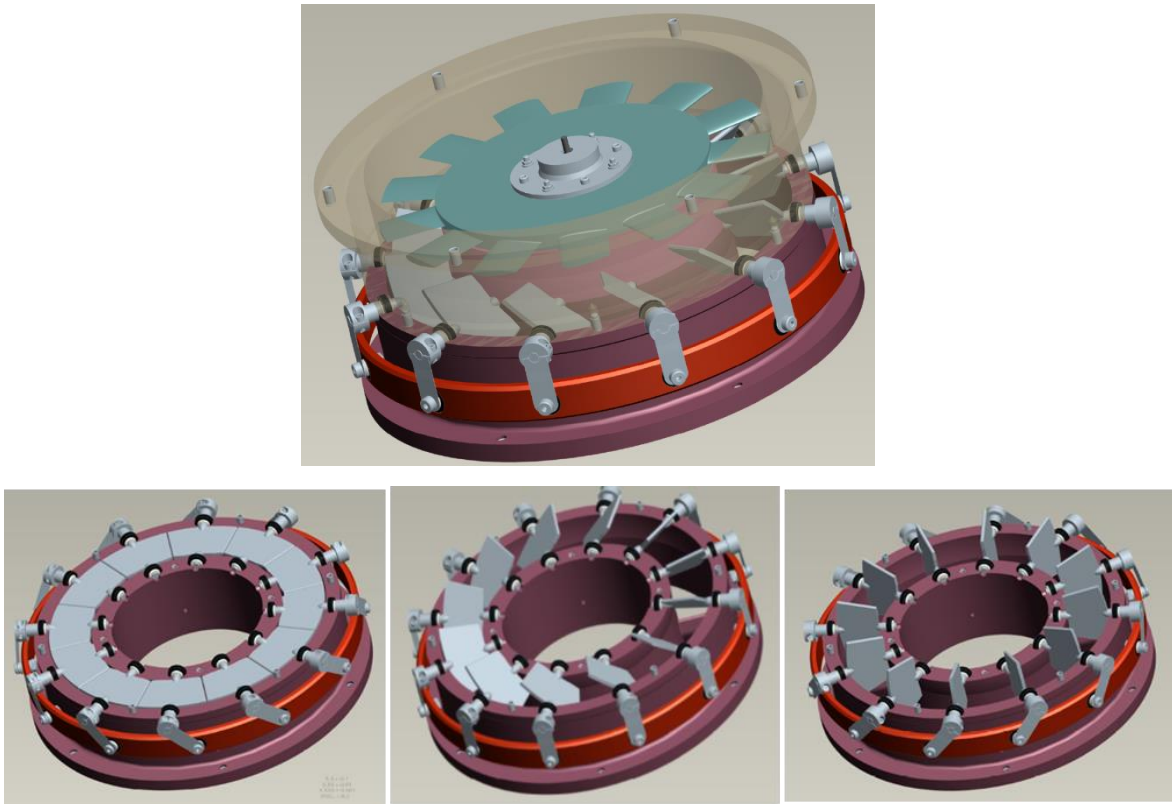

Figure 93. Shutter Valve Shown Installed Below the Wells Turbine and Shown in a Closed, Partially Open, and Completely Open Position

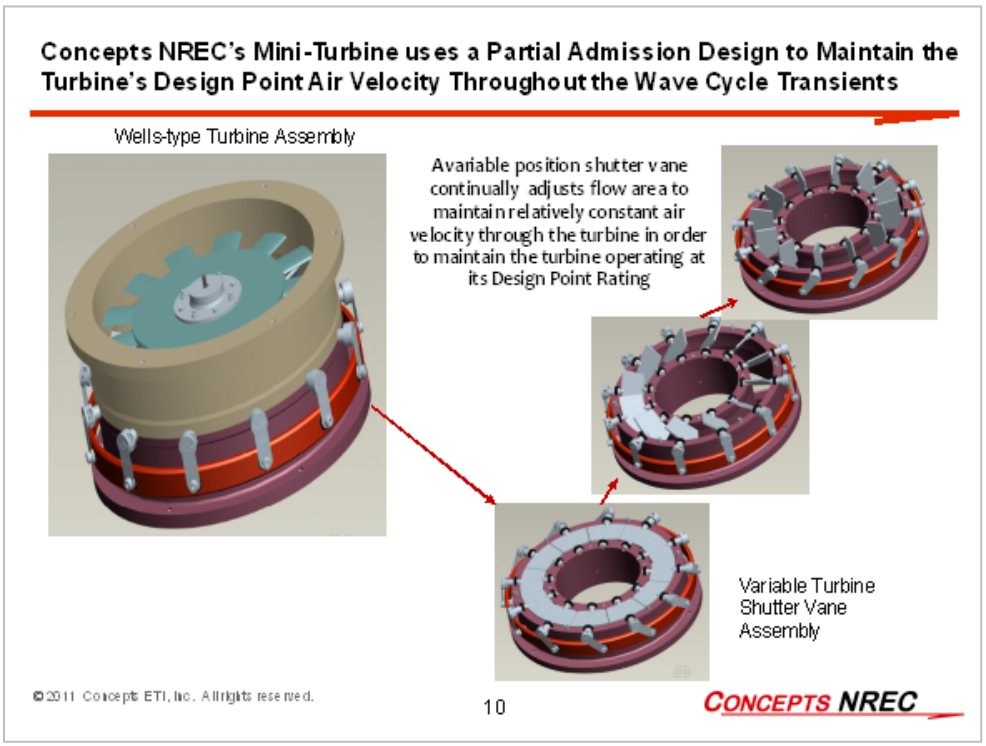

Figure 94. *CN*'s Mini-Turbine, Shown Assembled and with Three Positions of the Shutter as it Proceeds from Fully Closed to Fully Open

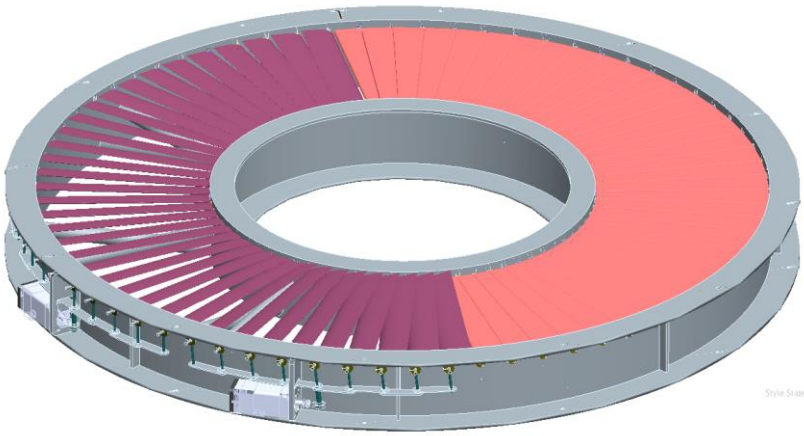

Figure 95. Full-scale Shutter Valve Based on *CN*'s Prototyped Shutter Valve, as Designed in Phase II

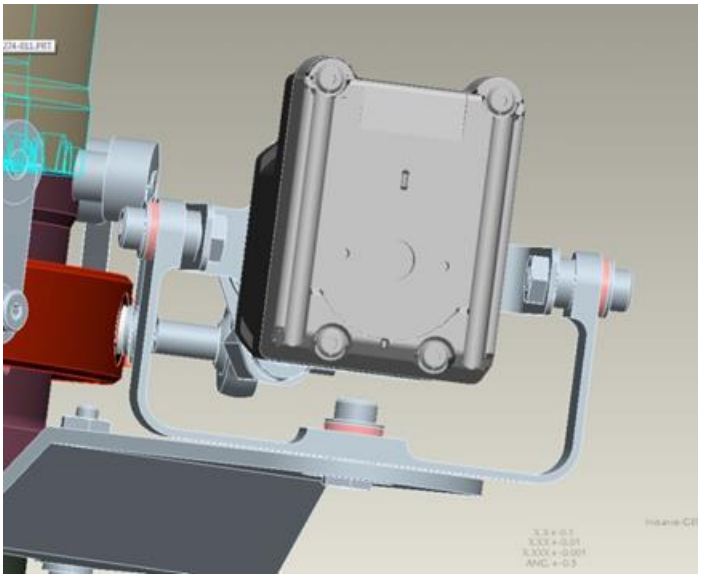

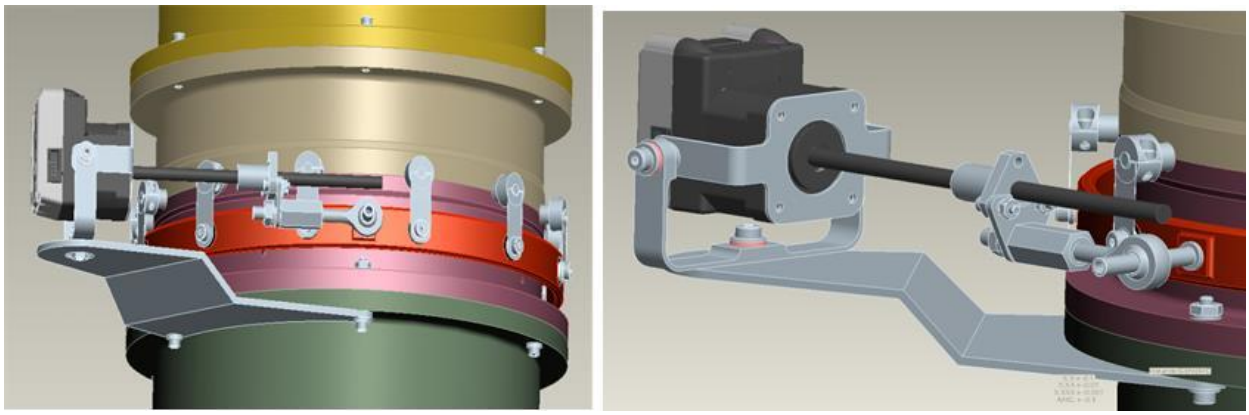

Figure 96. Illustration of the Shutter Actuating Linkage Design and Linear Electrical Actuator

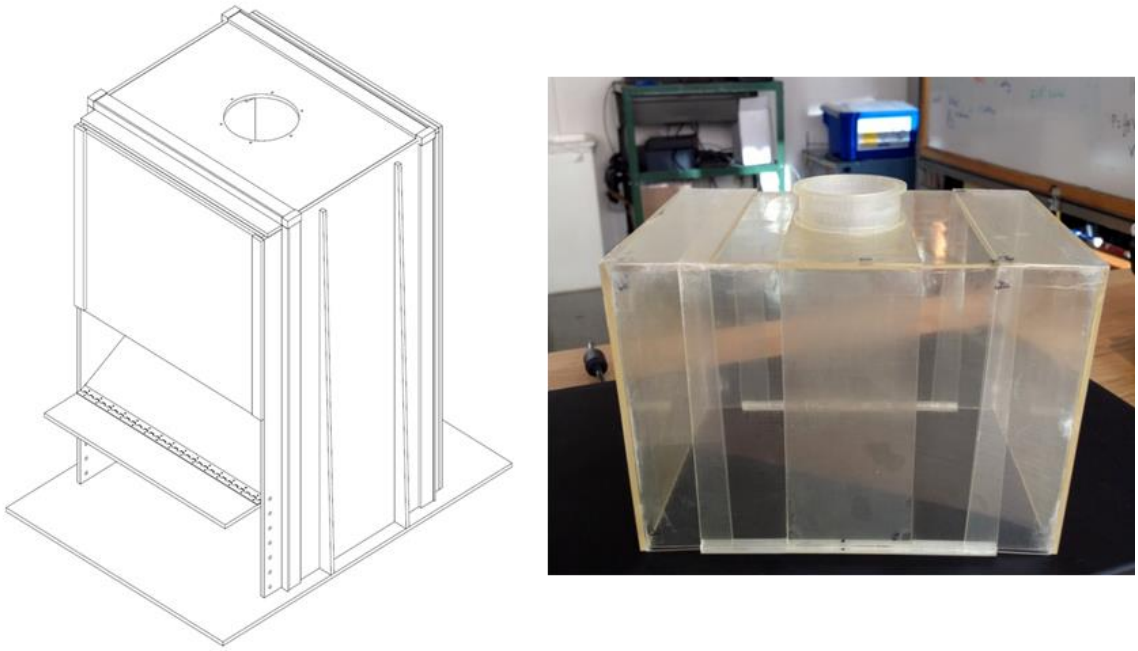

Figure 97. Conceptual Design and Mock-up of OWC Prototype Vessel with Adjustable Sides to Change OWC Volume Used in the Univeristy of Maine Test

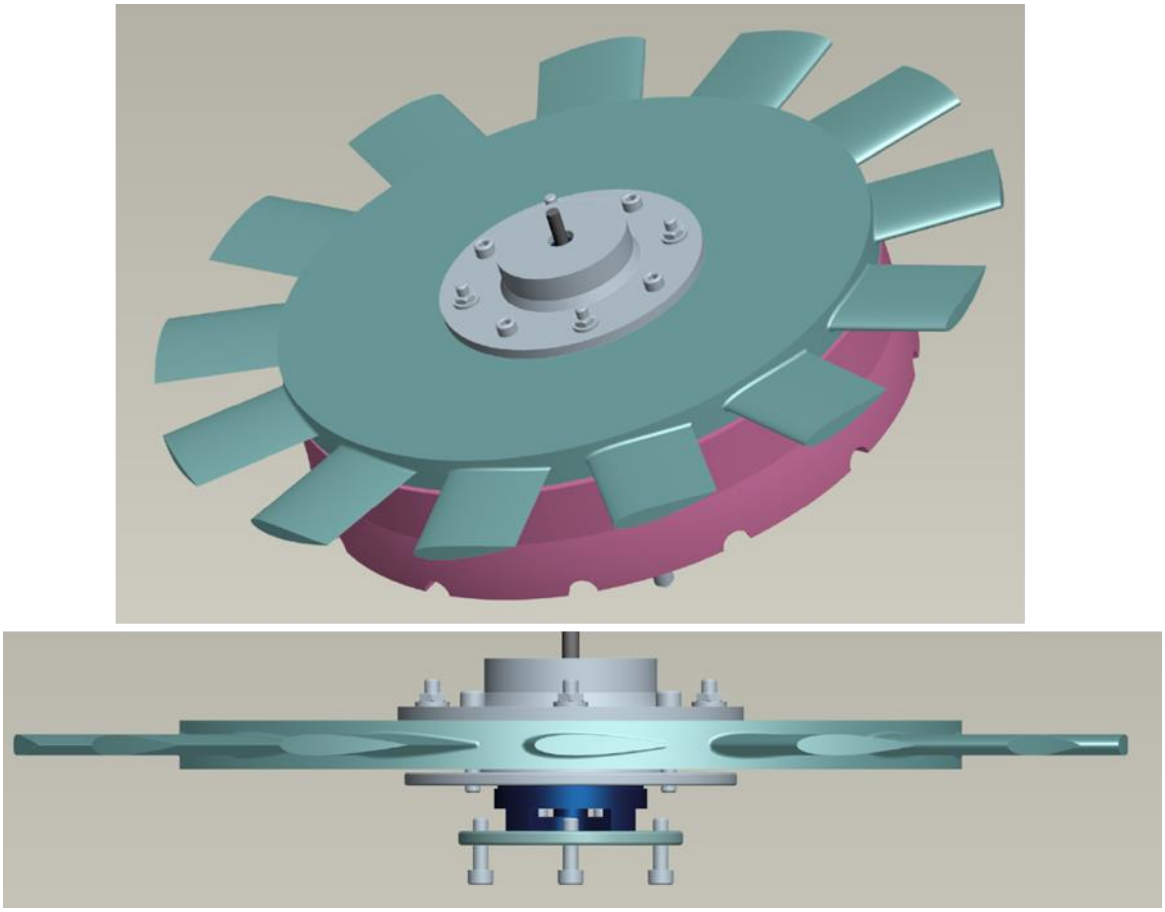

Figure 98. 50-watt Wells-style OWC Turbine (200-mm diameter; 5,000 rpm)

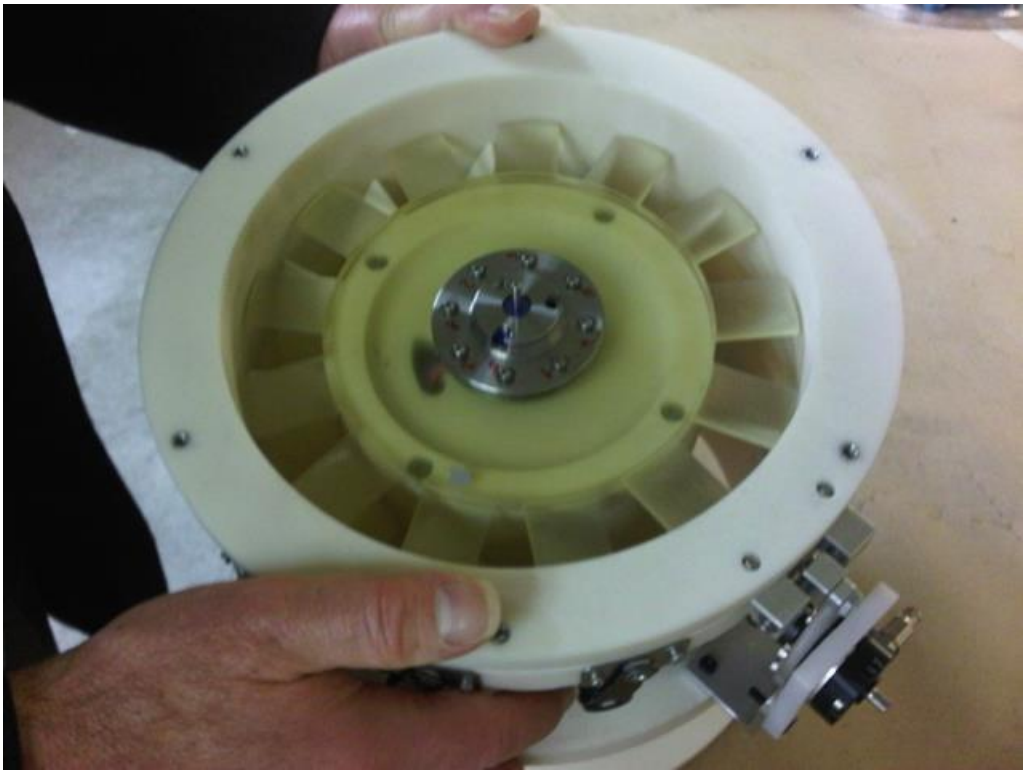

Figure 99. Assembled 50-watt OWC Turbine
(shutter valve not shown)

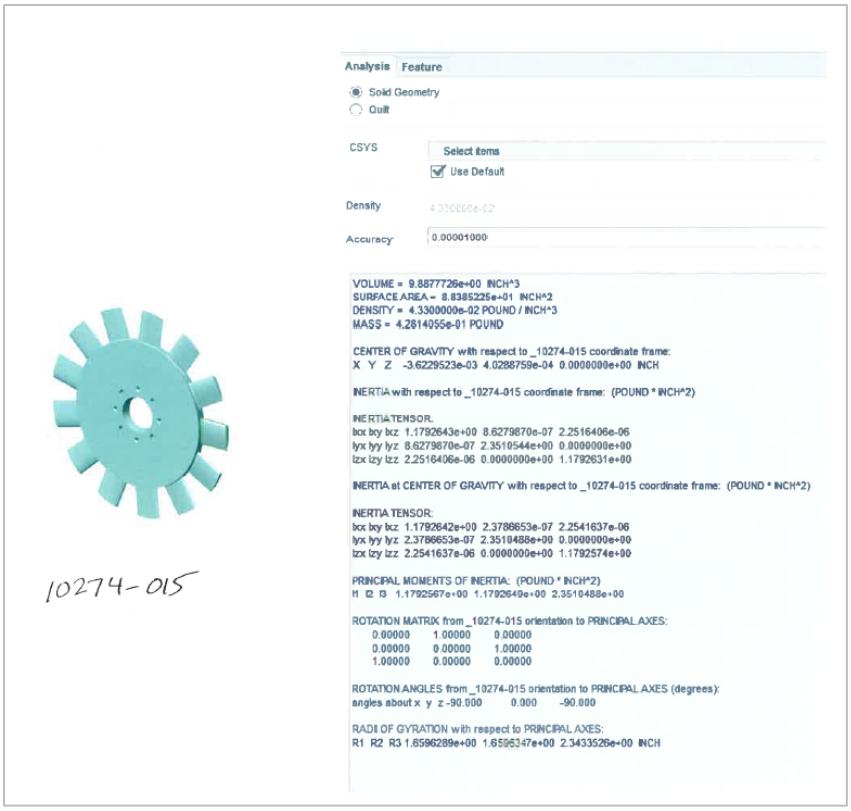

Figure 100. Mass Moment of Inertia for Wells Turbine Used in Determining Applied Torque

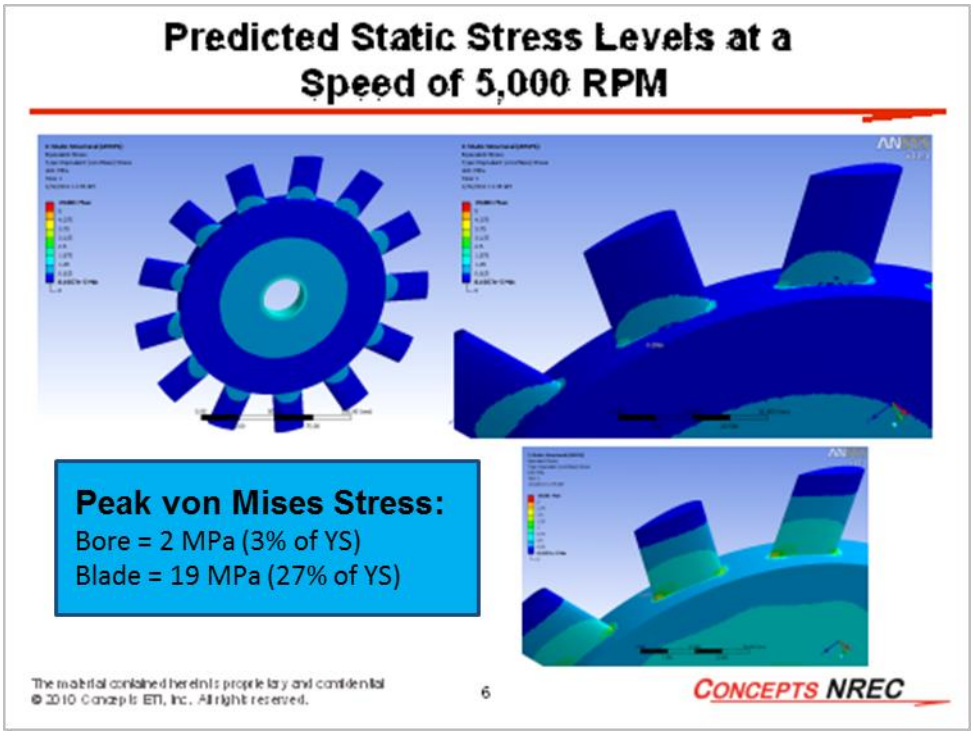

Figure 101. FEA Results of Analysis on 50-watt Wells Turbine

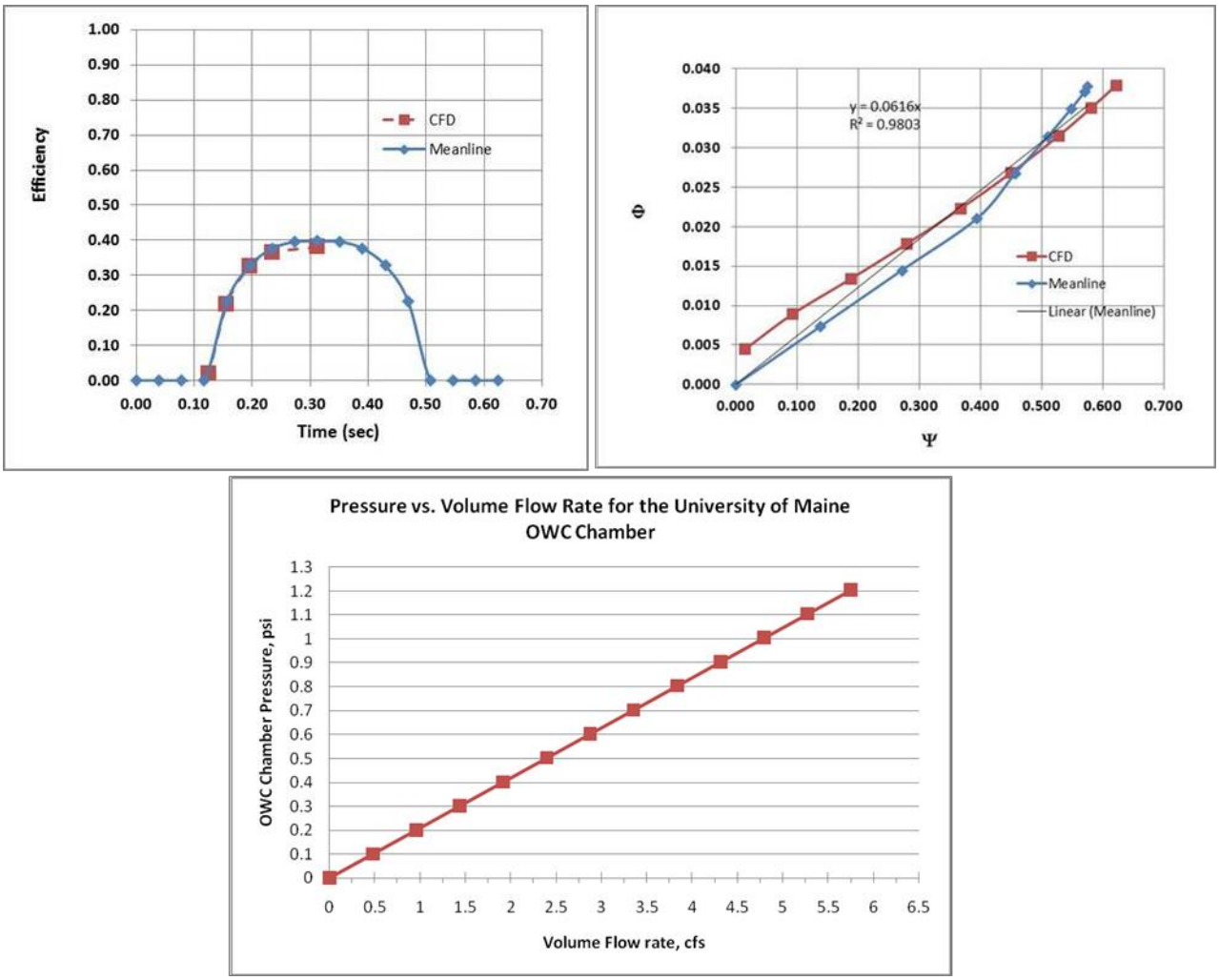

Figure 102. Flow and Head Coefficients for the Wells Turbine Design Used in the Mini-OWC Prototype System

3.2.7 Task 6. CN Constructs Advanced Turbine Shutter System for the Prototype Mk3PC Turbine System

CN will procure the necessary mechanical, electrical, and/or electronic components for assembling and operating a prototype turbine shutter system in trial tests in the laboratory. The operation of the turbine shutter valve system will be checked for mechanical and electrical operational integrity at CN's test facility in Woburn, MA. Based on the operational integrity of the system and the availability schedule of the Oceanlinx Mk3PC demonstration test platform, the shutter valve system will either be shipped to Oceanlinx for installation and testing as detailed in Task 8 or continue cyclic life tests in CN's Woburn test facility. The cyclic tests will help to determine the mean time to failure (MTTF) statistics for the shutter valve until it is ready for use in Oceanlinx's Mk3PC or an equivalent OWC system.

Figure 103. Prototype Wells-type (200-mm) OWC Turbine with Shutter Valve Assembly

3.2.8 Task 7. Oceanlinx and *CN* Install Turbine Shutter System into Mk3PC System or Equivalent

With the concurrence of the DOE Program Manager, and based on the Mk3PC test schedule and location, i.e., the availability of the Oceanlinx Mk3PC or equivalent OWC system, CN personnel will assist Oceanlinx with the installation of the prototype turbine shutter system into one of the eight OWC modules that constitute the Mk3PC OWC system. When possible, and with approval to proceed, the prototype turbine shutter valve system will be installed in the dry test OWC. The side-by-side installation of the modified OWC turbine with the turbine shutter system will provide a fair comparison of the energy recovery potential of the proposed turbine shutter system. If the Mk3PC is not immediately available according to the program plan and schedule, the turbine shutter testing will be postponed until in-water testing can be performed or an equivalent test can be scheduled.

Concurrent to the in-water testing that was done at the MMA and University of New Hampshire water wave tank facility, *CN* constructed a mock-up of an OWC system that would test the 50-watt OWC air turbine without the need for water. An elastomeric diaphragm served as the rising and falling water wave front and thus induced a bidirectional air flow through the air turbine. This experimental OWC chamber and turbine assembly enabled the wave amplitude and period to be adjusted; it also made it easier to measure the effects of the shutter valve system on the turbine power.

In preparation for the testing of the mini-OWC turbine at the University of Maine or University of New Hampshire, *CN* decided to construct a dry-turbine test fixture that could be used to test the OWC turbine performance, without the complication of dealing with scheduling tests at the Universities' wave- and tow-tank facilities. This dry test with the test fixture helped determine the performance of the turbine. A preliminary sketch of the dry-test system is shown in Figure 80 and the corresponding engineering assembly drawing is shown in Figure 81. The dry test rig is composed of a cylindrical OWC chamber with its open end covered by a

flexible elastomeric membrane. The ascending and descending motion of the membrane models the ascending and descending wave as the wave pushes the chamber air through the turbine and out of or into the OWC chamber. The membrane is controlled via a pneumatic piston. The piston stroke and speed has a wider range of operation than is available from the water tank test facility. This test fixture is now part of *CN*'s test facility at the Wilder, Vermont Headquarters and Product Center. Photos of the in-progress assembly are shown in Figures 104 and 105. The parts of the turbine and the turbine housing assembly are shown in Figures 103 and 106 (shown previously in Figures 91 and 92). The turbine housing assembly was installed on top of the OWC chamber.

Preliminary tests with the dry, mini-test system indicated that additional thrust bearing support and rebalancing of the turbine were needed. This was resolved and testing continued. Results indicated a clear benefit from having the shutter vanes statically positioned to increase turbine power recovery; however, additional testing needed to be done to confirm the hypothesis that the cyclic dynamic operation of the shutter vane increases turbine power recovery.

Figure 104. Dry-Turbine Test Apparatus Under Construction in *CN*'s Test Lab (Wilder, VT)

Figure 105. Dry-OWC Turbine Test Apparatus with Diaphragm Timing Circuit and Turbine (installed on top) in *CN*'s Test Facility (Wilder, VT)

Figure 106. Prototype 200-mm Diameter OWC Wells-type Turbine

3.2.9 Task 8. *CN* Provides Start-up Check-out Tests of Modified Turbine System

After the completion of Task 8, and based on the Mk3PC test schedule and location, i.e., the availability of the Mk3PC or equivalent OWC system, CN and Oceanlinx personnel will complete the start-up of the modified OWC turbine with the turbine shutter system. The start-up will be sufficient to demonstrate operational integrity, so that the entire system can be authorized for continuous in-water testing at Port Kembla, Australia, and/or an alternative equivalent site. The effect of an adjustment of the OWC height above the mean water line level can also proceed with or without the turbine shutter valve system using the controls methodology developed by MMA and CN (as a result of Task 3) for the OWC height adjustment strategy.

During Phase II, MMA engineering staff completed a mock-up of an adjustable OWC vessel and prepared the University of Maine tow tank for testing this system with the OWC prototype turbine. The OWC prototype turbine subsystem requires a new control valve to interface with the method of control. Due to the requirements of the prototype tests, it was determined that several modifications would be needed to make the system operational, including a new wave-maker control box built along with the existing wave-maker software, a new control block (lines the porting of the control valve to the hydraulic ram), and a check of the existing LVDT feedback to determine if it was still in operation.

MMA and *CN* project personnel also visited the University of New Hampshire wave tank in order to determine the status. The tank and control systems were all working, but several modifications were required to hold the OWC chamber in the wave tank at the correct position. It was determined that their testing schedule could accommodate the testing required for the OWC system. Software that governs the wave-maker is capable of generating the kinds of waves needed for the scope of research and was fully operational. As a result of these visits, staff interviews, and inspections, *CN* and MMA decided to continue the testing program with the University of New Hampshire wave tank facilities.

Figures 107, 108, and 109 show the OWC test vessel with the turbine assembly installed on top (used in the University of Maine's in-water tank tests). The OWC chamber was designed with an adjustable volume via sliding sides along the major length. This design enabled the testing of one of the hypotheses of how to improve the energy capture from the incident wave, i.e., the changing of the volume via the OWC height. However, the adjustable sides also allowed the tuning of the chamber to match the frequency of the incident wave.

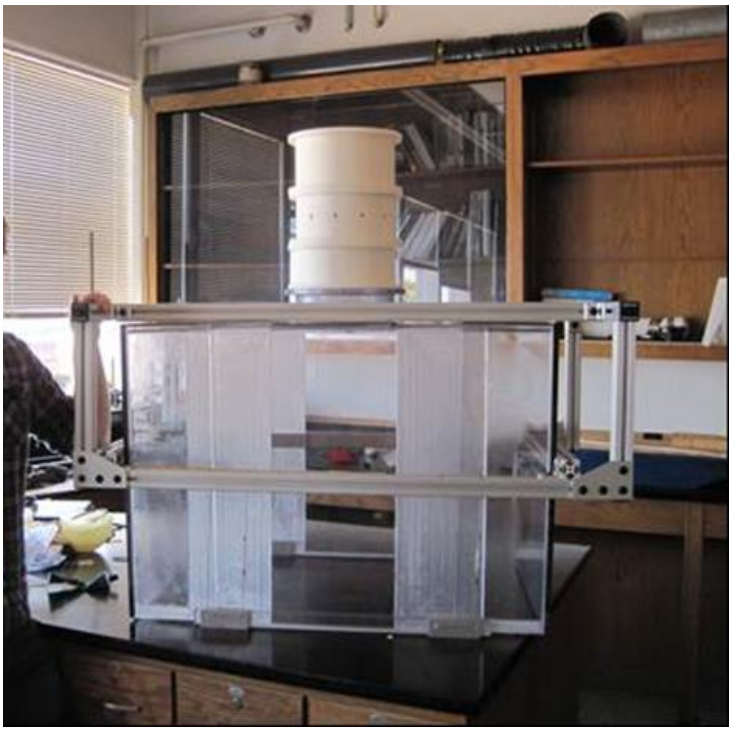

Figure 107. MMA Student Pictured with the Protoype OWC Structure Used with the Mini-OWC Turbine Water Wave Tests at the University of Maine

Figure 108. Prototype OWC with Adjustable End Sections Shown in Perspective with 200-mm Diameter Wells Turbine Rotor

Figure 109. Prototype Mini-OWC Chamber with the Mini-Wells Turbine Assembly Installed at the Top

In the initial trials of the testing of the OWC prototype, it was determined that the wave power was not as high as originally planned, due to limits in the stability of producing large waves by the University of Maine's wave-maker. The torquemeter and the electric motor that were used could not provide a clear electric voltage signal long enough between the opening and closing of the turbine shutters, from which the electric power from the turbine could be determined at low power levels. As a result of the lower energy capacity, it was necessary to use a different method for measuring the net power from the incident wave that actually was converted to electric power by the OWC turbine. The method employed to measure the power captured by the turbine from the incident water wave consisted of measuring the transient and steady-state speed of the turbine as it accelerated from zero to steady-state speed. Using the speed as a function of time, the acceleration of the turbine could be determined, and knowing the mass moment of inertia, the net torque applied to the turbine could be determined using the following equation:

$$Net\ Torque = I/gc\ x\ \alpha$$

In order to determine the maximum power that is recovered from the incident water wave per cycle, the drag and bearing losses (i.e., rolling drag) from the turbine must also be determined. This was determined from a separate test of the turbine during the coast-down from a maximum speed after the water wave action was stopped. The rolling drag torque was then added to the torque determined from Equation A in order to determine the maximum torque generated by the recovered wave energy. Figure 110 (a and b) identifies these two transient torque curves for several water wave periods (T_w).

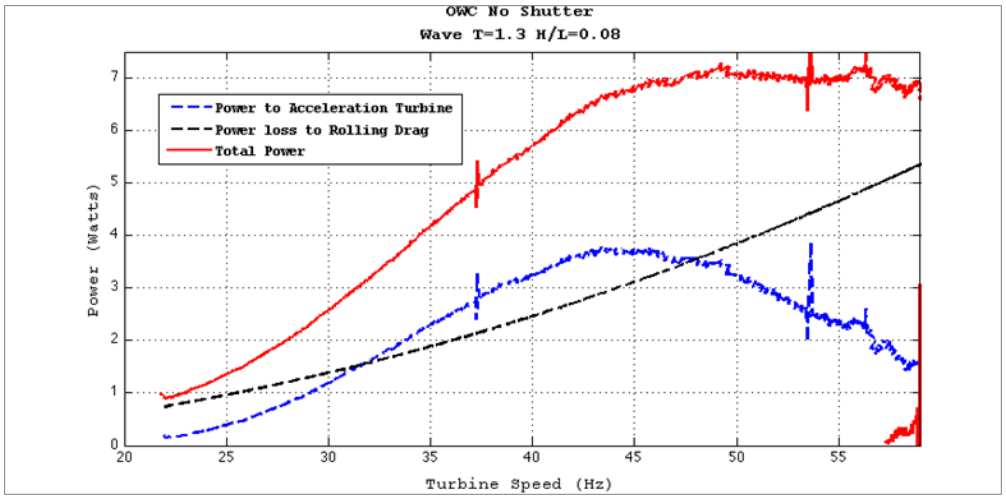

(a)

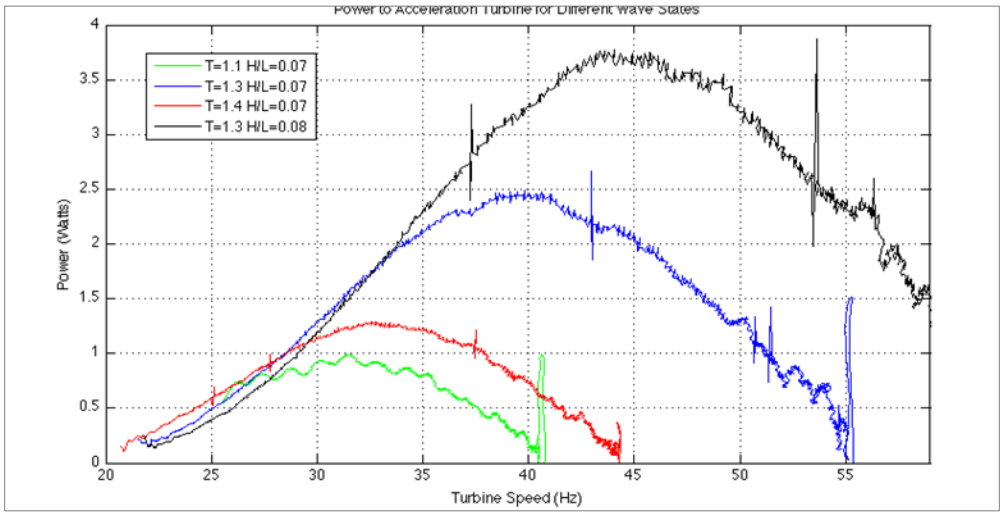

(b)

Figure 110. Measured Power vs. Speed Response and Rolling Drag Friction Power for the Wells Turbine Used in the Prototype OWC Testing

The results from the testing at the University of Maine are summarized in Table VII. The testing was suspended due to damage sustained by the turbine shutter linkage, as shown in Figure 111. The power measurements for the OWC turbine from the water wave testing in the University of Maine's water tank facility are shown in Figures 112 and 113.

Figure 111. View of Damaged Shutter Valve Linkage

The power (watts) and the recovered wave energy (N-m) shown in Figures 112 and 113 were determined from the measured speed transient of the 200-mm diameter Wells turbine during the water wave testing at the University of Maine. The power was determined using a numerical integration of the speed transient function and the inertia (I) of the Wells turbine. The equations include the calculation of the torque using:

$$Torque\ [lbf\text{-}in] = I \times \Delta\omega/\Delta t \times (2\pi/60) \times 12/g_c$$

where: I = 2.3511 lbm-in^2 is the mass moment of inertia for the 200-mm diameter Wells turbine

From this equation the instantaneous power is determined from:

$$Power\ [watts] = Torque \times rpm/5252/12/1.341*1000$$

and the incremental energy recovered from the wave is determined from a numerical integration using the measured transient data such that:

$$Total\ Energy = \sum (Instantaneous\ Power \times \Delta time)$$

Summary

Table VII identifies the wave test by number and includes the duty cycle of the shutter valve (seconds), the wave period (seconds), and the ratio (H/L) of the OWC height (H) of air space above the water line to overall wave length (L). The measured data indicates that a shutter valve cycle of 0.75 seconds, with a wave period of 0.75 seconds, provided the highest instantaneous torque and power. More power was expected to be generated by the Wells turbine. However, as may be observed from Figure 112, the speed of the turbine also did not achieve its design point of 5,000 rpm. The testing was terminated after the actuator linkage shown in Figure 111 failed.

The results shown in Figure 113 reveal one possible conclusion: the power and energy output increased with an increase in the cyclic period of the shutter valve. There is an increase in energy recovered from 36% to 63% for the tests with the longer shutter valve period.

TABLE VII. SUMMARY OF WAVE TESTS

		date: August 4, 2013				
		Note: no turbine data for test 1, 2, 3. Only file of interest is 7.				
	N-m	avg. watts	Test #	Duty Cycle	Period	H/L
OWC216_09_34	22.5	0.108	1	0	2	0.035
OWC216_10_36	22.5	0.096	2	0	2	0.035
OWC216_10_49	26.6	0.128	3	1	2	0.035
OWC216_11_10	27.1	0.112	4	0.25	2	0.035
OWC216_11_29	36.0	0.189	5	0.25	2	0.035
OWC216_11_46	20.8	0.102	6	0.5	2	0.035
OWC216_12_08	22.0	0.126	**7**	**0.5**	**2**	**0.035**
OWC216_12_22	30.6	0.148	8	0.75	2	0.035
			9	0.25	1.8	0.05
			10	0.5	1.8	0.05
			11	0.75	1.8	0.05

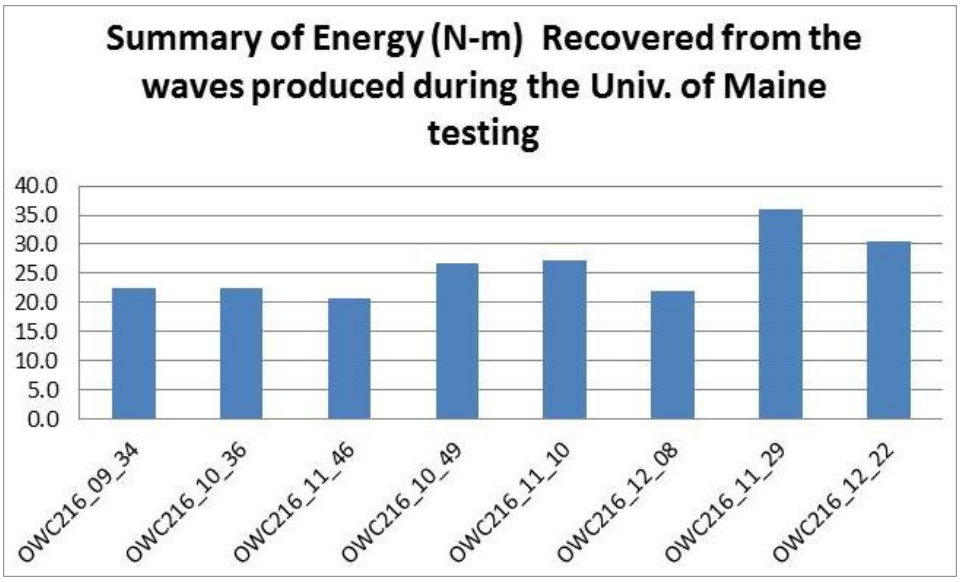

(a)

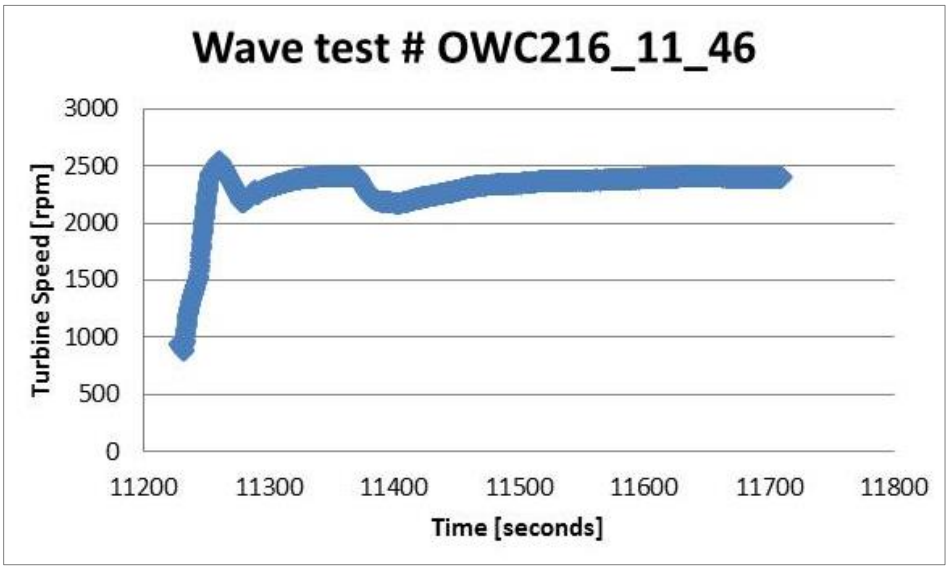

(b)

Figure 112. (a) Summary of Turbine Rotor Energy Test Results (not sorted); (b) An Example of the Typical Rotor Speed Transient Measured During a Test

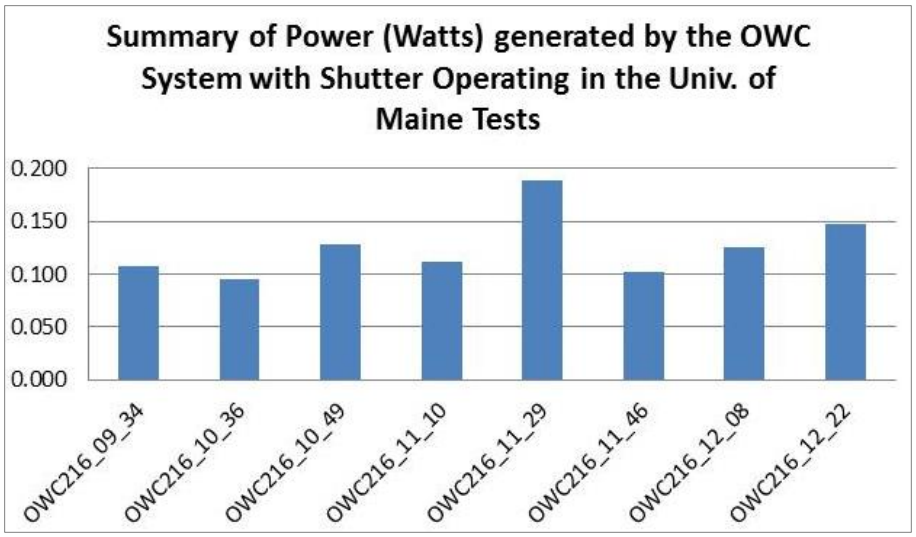

(a)

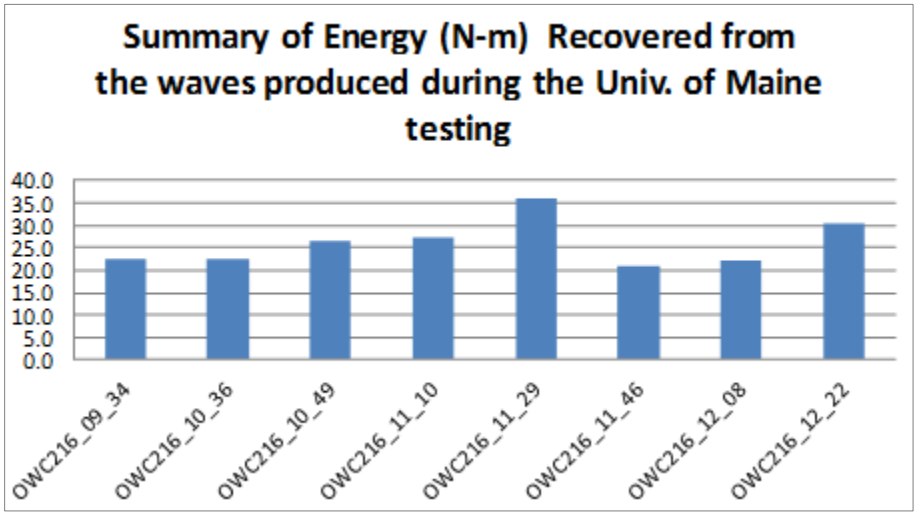

(b)

Figure 113. (a) and (b) – Power (watts) and Energy (N-m) Recovered from the Incident Wave for the Wave Tests Shown, but Sorted by Increasing Order of the Duty Cycle Frequency of the Shutter Valve

3.2.10 Task 9. Program Management (for Years 1 and 2)

CN is the prime contractor for this project and will coordinate the engineering activities for each of the tasks as required to be performed by its project collaborators: Oceanlinx, Ltd., and the MMA engineering professors and staff of the TEDEC facility. During the administration of this program, progress reports will be submitted to the DOE program monitor as required using DOE guidelines. The reports will document the status of each task, problem areas, and proposed courses of action. A final report will be prepared at the end of the program, documenting the results of Phase II and the preparation of the Phase III plan for the further commercialization of the advanced energy recovery improvement system that has been developed and demonstrated during Phase II of the project.

Principal Investigator and Key Personnel

Mr. Francis Di Bella, PE, was the Principal Investigator for the STTR. Mr. Di Bella is the Program Manager for several large renewable energy projects at *CN*, including the development of a high-capacity, centrifugal hydrogen compressor for pipeline applications that can serve the DOE's strategy for the hydrogen economy. Mr. Di Bella has spent over 25 years developing large-scale power generation systems, including cogeneration and waste heat recovery Organic Rankine Cycle (ORC) systems. Mr. Kevin Fairman, a Program Manager for previous Oceanlinx projects, worked with Mr. Di Bella. Mr. Fairman developed a mechanical articulating turbine blade system for Oceanlinx's OWC and was a major contributor to this final report. Professors Patrick Lorenz and Richard Kimball of the MMA worked on the computational solutions of the equations of motion for the OWC.

APPENDIX 1:
MMA MATHEMATICAL MODEL OF OWC-WAVE INTERACTION

In addition to the numerical model developed by Concepts NREC (*CN*), the researchers at the Maine Maritime Academy (MMA) developed a closed-form, mathematical solution to the wave energy problem that is more closely associated with the operation of an OWC and the prediction of recoverable wave energy. This Appendix provides the mathematical solution proposed by the MMA researchers, under the direction of Professor Patrick Lorenz.

The following summary of work completed has been prepared by Professor Patrick Lorenz (Department of Mathematics at MMA). The goal of the mathematical analysis is to provide a theoretical mathematical model of an incident wave as it interacts with the OWC chamber. More specifically, the determination of the wave front speed as it ascends and descends in the chamber will be an input to the thermo-fluids model that has been developed by *CN*. The *CN* model is designed to provide an engineering analysis tool for sizing the OWC structure, specifically the length, width, and height, as well as the relationship of the chamber pressure with the transient flow rate through the turbine. The availability of the wave front speed will enable *CN*'s thermo-fluids model of the OWC system to be more accurate in predicting the available energy that is available from the incident wave.

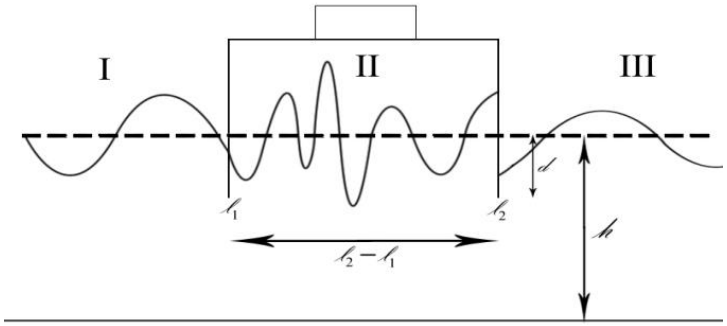

Figure A1-1. A Mathematical Representation of the: I - Incident Wave of the OWC Chamber; II - The Energy Absorbed; and III - The Reflected Wave

The variables used in the analysis are defined using the OWC diagram shown here.

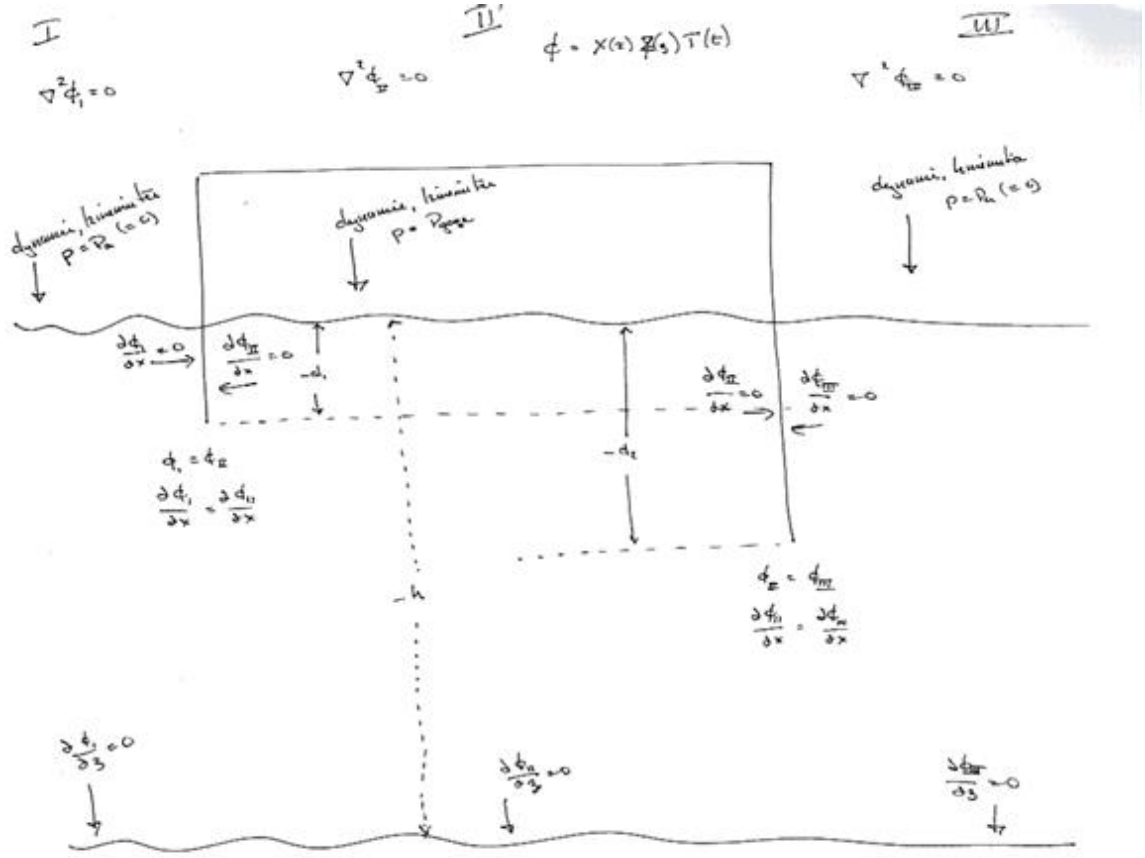

Figure A1-2. OWC Diagram

$$\varphi_I(x,z) = \sum_{n=0}^{\infty}\left[C_I^1 e^{\frac{n\pi}{h}x}\sin\left(\frac{n\pi}{h}z\right)\right] + C_I^2\sin(\mu x)cosh[\mu(z+h)]$$

$$\varphi_{III}(x,z) = \sum_{n=0}^{\infty}\left[C_{III}^1 e^{\frac{-n\pi}{h}(x-L_2)}\sin\left(\frac{n\pi}{h}z\right)\right] + C_{III}^2\sin[\mu(L_2-x)]cosh[\mu(z+h)]$$

$$\varphi_{II}(x,z) = \sum_{n=0}^{\infty}\left\{C_{II}^1\left(g_3(L_2,z)sinh\left(\frac{n\pi}{h}x\right) + g_2(0,z)sinh\left[\frac{n\pi}{h}(L_2-x)\right]\right)sin\left(\frac{n\pi}{h}z\right) + C_{II}^2 sin\left(\frac{n\pi}{L_2}x\right)cosh\left[\frac{n\pi}{L_2}(h+z)\right]\right\} + \frac{iw}{\rho gK}p$$

In all equations

$\mu\ tanh(\mu h) = \frac{w^2}{g} = K$, the dispersion relation

$p = p(z)$

g_2, g_3 are boundary conditions between regions I and II, and II and III, respectively

Oscillating Water Column 2D Model, with the front wall at depth d_1, back wall at d_2
Laplace's Equation applies with boundary conditions f_i, g_i, i = 1, 2… as indicated

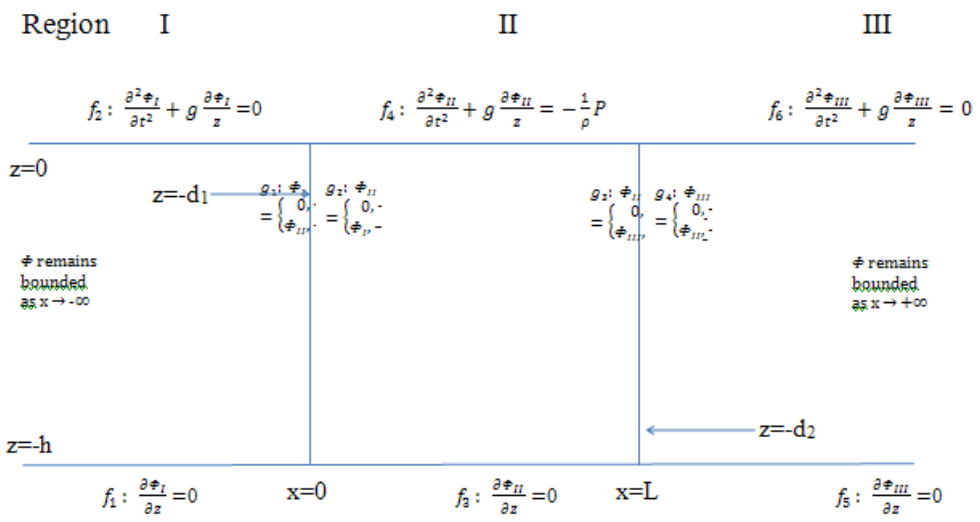

We assume variables separable, and $\Phi = \varphi T = XZT$.

The boundary conditions are all homogeneous except for f_4, which will be handled by making the potential φ_{II} equal to $\nu_{II}+\psi_{II}$, each with their own boundary conditions.

Laplace's Equation is linear, and we may therefore treat each region as the sum of two or more subregions with their own boundary conditions. This allows us to create pairs of boundary conditions — f_1 and f_2, or g_2 and g_3, for example — that are equal to zero in a subregion and thereby solve Laplace's Equation in each subregion.

For example, Region II becomes

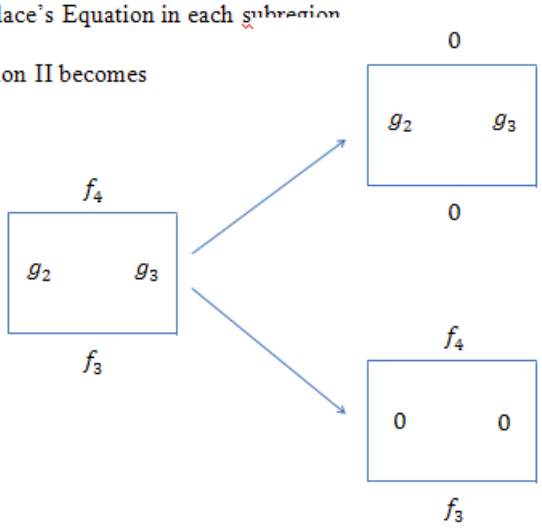

Region I: $\varphi_I = \varphi_{I(0,g)} + \varphi_{I(f,0)}$

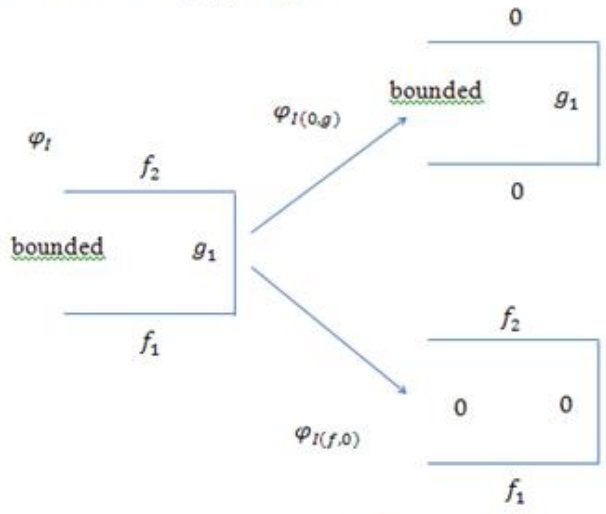

— means trivial solution

means nontrivial solution

$$\lambda = \begin{cases} 0 & — \\ -k_2 & \\ +k_2 & — \end{cases}$$

$\varphi_{I(0,g)}(x,z)$

$$\lambda = \begin{cases} 0 & — \\ -k_2 & \\ +k_2 & — \end{cases}$$

$$\varphi_{I(f,0)}(x,z) = C_I^2 \sin(\mu x) \cosh \mu(z + h)$$

$$\varphi_I = \varphi_{I(0,g)} + \varphi_{I(f,0)} = \sum_{n=0}^{\infty} \left[C_I^1 e^{\frac{n\pi}{h}x} \sin\left(\frac{n\pi}{h} z\right) \right] + C_I^2 \sin(\mu x) \cosh \mu(z + h)$$

Solution for Region I as shown above:

We solve Laplace's Equation for $\varphi_{I(0,g)}$ and $\varphi_{I(f,0)}$ and thereby obtain the result for φ_1.

$$\nabla^2 \varphi_I = \nabla^2 \varphi_{I(0,g)} + \nabla^2 \varphi_{I(f,0)} = 0$$

With appropriate boundary conditions from above, we may also write:

$\varphi_{1(o,g)}$

$$\nabla^2 \varphi_{I(0,g)} = 0$$
$$\nabla^2 \varphi_{I(f,0)} = 0$$

$$\nabla^2 \varphi_{I(0,g)} = 0 \quad \rightarrow \quad X''Z + XZ'' = 0 \quad \rightarrow \quad \frac{x''}{x} + \frac{z''}{z} = 0 \quad \rightarrow \quad \frac{x''}{x} = -\frac{z''}{z} = \lambda = \begin{cases} 0 \\ -k^2 \\ +k^2 \end{cases}$$

Note: The immediate line above recurs similarly in all regions and subregions and will therefore not be repeated when we address these regions and subregions.

$\varphi_{1(0,g)}$, case λ=0:

$$Z'' + \lambda Z = 0 \quad \rightarrow \quad Z = C_1 z + C_2$$

Boundary condition f_2, (i.e., ocean surface boundary condition)

$$\varphi_{I(0,g)}(x,0) = X(x)Z(0) = 0 \quad \rightarrow \quad Z(0) = 0 \quad \rightarrow \quad -C_1(0) + C_2 = 0 \quad \rightarrow \quad C_2 = 0$$

Boundary condition f_1, (i.e., ocean floor boundary condition)

$$\varphi_{I(0,g)}(x,-h) = X(x)Z(-h) = 0 \quad \rightarrow \quad Z(-h) = 0 \quad \rightarrow \quad -C_1 h = 0 \quad \rightarrow \quad C_1 = 0$$

Therefore both C_1 and C_2 are zero. Since $\varphi_{I(0,g)} = XZ = 0$, only the trivial solution exists for $\lambda=0$.

$\Phi_{I(0,g)}$, case $\lambda=-k^2$:

$$Z'' + \lambda Z = 0 \quad \rightarrow \quad Z'' - k^2 Z = 0 \quad \rightarrow \quad Z(z) = C_1 \sinh(kz) + C_2 \cosh(kz)$$

Boundary condition f_2, (i.e., ocean surface boundary condition)

$$\varphi_{I(0,g)}(x,0) = X(x)Z(0) = 0 \quad \rightarrow \quad Z(0) = 0 \quad \rightarrow \quad C_2 = 0$$

Boundary condition f_1, (i.e., ocean floor boundary condition)

$$\varphi_{I(0,g)}(x,-h) = X(x)Z(-h) = 0 \quad \rightarrow \quad Z(-h) = 0 \quad \rightarrow \quad C_1 \sinh(kh) = 0 \quad \rightarrow \quad C_1 = 0$$

Therefore both C_1 and C_2 are zero. Since $\varphi_{I(0,g)} = XZ = 0$, only the trivial solution exists for $\lambda=-k^2$.

$\Phi_{I(0,g)}$, case $\lambda=+k^2$:

$$Z'' + \lambda Z = 0 \quad \rightarrow \quad Z'' + k^2 Z = 0 \quad \rightarrow \quad Z(z) = C_1 \sin(kz) + C_2 \cos(kz)$$

Boundary condition f_2, (i.e., ocean surface boundary condition)

$$\varphi_{I(0,g)}(x,0) = X(x)Z(0) = 0 \quad \rightarrow \quad Z(0) = 0 \quad \rightarrow \quad C_1 \sin(0) + C_2 \cos(0) = 0 \quad \rightarrow \quad C_2 = 0$$

Boundary condition f_1, (i.e., ocean floor boundary condition)

$$\varphi_{I(0,g)}(x,-h) = X(x)Z(-h) = 0 \quad \rightarrow \quad Z(-h) = 0 \quad \rightarrow \quad C_1 \sin(kh) = 0 \quad \rightarrow \quad k = \frac{n\pi}{h},\ n=0,1,\ldots\infty$$

Therefore, $Z(z) = C_1 \sin\left(\frac{n\pi}{h} z\right)$.

Now looking at X(x) under the boundary conditions for this subregion $\varphi_{I(0,g)}$.

$$X'' - \lambda Z = 0 \quad \rightarrow \quad X'' - k^2 X = 0 \quad \rightarrow \quad X(x) = C_3 e^{-kx} + C_4 e^{+kx}$$

Boundary condition f_1, (i.e., far field boundary condition, $x \to -\infty$)

$$\varphi_{I(0,g)}(-\infty, z) = X(x-\infty)Z(z) \text{ is bounded} \quad \to \quad C_3 = 0 \quad \to \quad X(x) = C_4 e^{+kx}$$

Boundary condition g_1, (i.e., front wall boundary condition)

$$\varphi_{I(0,g)}(0, z) \quad \to \quad X(0) = C_4$$

Therefore: (Note: To evaluate C_I^1 requires using the boundary condition g_1, and we will do that later.)

$$\varphi_{I(0,g)}(x, z) = X(x)Z(z) = C_1 C_4 e^{x} \sin\left(\frac{n\pi}{h} z\right) = C_I^1 e^{\frac{n\pi}{h}x} \sin\left(\frac{n\pi}{h} z\right)$$

$\boldsymbol{\varphi_{I(f,0)}}$

$\Phi_{I(f,0)}$, case λ=0:

$$X'' + \lambda X = 0 \quad \to \quad X = C_1 x + C_2$$

Boundary condition g_1, (i.e., front wall boundary condition)

$$\varphi_{I(f,0)}(0, z) = X(0)Z(z) = 0 \quad \to \quad X(0) = 0 \quad \to \quad C_1(0) + C_2 = 0 \quad \to \quad C_2 = 0$$

Boundary condition f_1, (i.e., far field boundary condition)

$$\varphi_{I(0,g)}(-\infty, z) = X(-\infty)Z(z) \text{ is bounded} \quad \to \quad X(-\infty) \text{ is bounded} \quad \to \quad C_1 = 0$$

Therefore both C_1 and C_2 are zero. Since $\varphi_{I(f,0)} = XZ = 0$, only the trivial solution exists for λ=0.

$\Phi_{I(f,0)}$, case $\lambda = -\mu^2$:

$$X'' + \mu^2 X = 0 \quad \to \quad X(x) = C_1 \sin(\mu x) + C_2 \cos(\mu x)$$
$$Z'' - \mu^2 Z = 0 \quad \to \quad Z(z) = C_3 \sinh(\mu z) + C_4 \cosh(\mu z)$$

Boundary condition g_1, (i.e., front wall boundary condition)

$$\varphi_{I(f,0)}(0, z) = X(0)Z(z) = 0 \quad \to \quad X(0) = C_1 \sin(0) + C_2 \cos(0) \quad \to \quad C_1(0) + C_2 = 0$$
$$\to \quad C_2 = 0$$

$$X(x) = C_1 \sin(\mu x)$$

The far field boundary condition is automatically satisfied for the sine function.

Boundary condition f_2, (i.e., ocean surface boundary condition) comes from the following differential equation: for z=0:

$$\frac{\partial^2 \Phi}{\partial t^2} + g\frac{\partial \Phi}{\partial z} = 0$$

$$XZ(0)T'' + gXZ'(0)T = 0$$

$$Z'(0) = \left(-\frac{T''}{gT}\right)Z(0)$$

For the usual sinusoidal wave, $T = e^{i\omega t}$. In this case, we find the usual expression

$$Z'(0) = \frac{\omega^2}{g}Z(0)$$

We will use this expression after evaluating at the f_1 boundary condition.

Boundary condition f_1, (i.e., ocean floor boundary condition) is that $Z'(-h) = 0$
From above:

$$Z(z) = C_3\sinh(\mu z) + C_4\cosh(\mu z)$$
$$Z'(z) = C_3\mu\cosh(\mu z) + C_4\mu\sinh(\mu z)$$
$$Z'(-h) = C_3\mu\cosh(-\mu h) + C_4\mu\sinh(-\mu h) = 0$$

$$C_3 = C_4\frac{\sinh(\mu h)}{\cosh(\mu h)}$$

Note that this also results in $Z(0) = C_4$ and $Z(-h) = \frac{C_4}{\cosh(\mu h)}$

Therefore

$$Z(z) = C_3\sinh(\mu z) + C_4\cosh(\mu z)$$

$$Z(z) = C_4\frac{\sinh(\mu h)}{\cosh(\mu h)}\sinh(\mu z) + C_4\cosh(\mu z)$$

$$Z(z) = \frac{C_4}{\cosh(\mu h)}[\sinh(\mu h)\sinh(\mu z) + \cosh(\mu h)\cosh(\mu z)]$$

$$Z(z) = \frac{C_4}{\cosh(\mu h)}[\cosh\mu(z+h)]$$

Since $Z'(0) = \frac{\omega^2}{g}Z(0)$ from the $\varphi_{1(f,0)}$ f_2 ocean surface boundary condition,

$$Z'(0) = \frac{\omega^2}{g} Z(0)$$

$$\frac{C_4 \mu}{\cosh(\mu h)} \sinh(\mu h) = \frac{\omega^2}{g} C_4 \frac{\cosh(\mu h)}{\cosh(\mu h)}$$

$$\mu \sinh(\mu h) = \frac{\omega^2}{g} = K$$

This is the well-known dispersion relation. Note that there is only one μ from this relation.

$\Phi_{I(f,0)}$, case $\lambda = +\mu_2$

$$X'' - \mu^2 X = 0 \quad \rightarrow \quad X(x) = C_1 e^{\mu x} + C_2 e^{-\mu x}$$

From the far field boundary condition, X(x) as x →-∞ must remain bounded. Therefore

$$C_2 = 0$$

From the front wall boundary condition, X(0) = 0, and therefore

$$X(0) = 0 \quad \rightarrow \quad C_1 = 0$$

Only the trivial solution exists for $\varphi_{I(f,0)}$, case $\lambda = +\mu_2$

The solution for the subregion is therefore

$$\varphi_{I(f,0)}(x,z) = X(x)Z(z) = C_1 \sin(\mu x) \frac{C_4}{\cosh(\mu h)} [\cosh \mu(z+h)] = C_I^2 \sin(\mu x) \cosh \mu(z+h)$$

As before for C_I^1, we will need to later apply the g1 boundary condition to find C_I^2.

Region III: $\varphi_{III} = \varphi_{III(0,g)} + \varphi_{III(f,0)}$

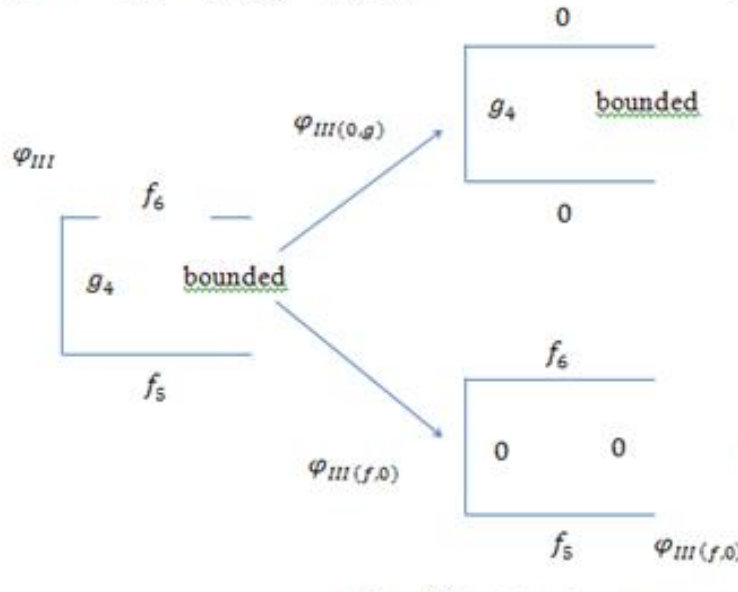

— means trivial solution
means nontrivial

$$\lambda = \begin{cases} 0 & — \\ -k_2 & — \\ +k_2 & \end{cases}$$

$\varphi_{III(0,g)}(x,z)$

$$\lambda = \begin{cases} 0 & — \\ -k_2 & \\ +k_2 & — \end{cases}$$

$\varphi_{III(f,0)}(x,z) = C_{III}^2 \sin[\mu(L_2 - x)] \cosh \mu(z + h)$

$$\varphi_{III} = \varphi_{III(0,g)} + \varphi_{III(f,0)} = \sum_{n=0}^{\infty} \left[C_{III}^1 e^{\frac{n\pi}{h}[L_2 - x]} \sin\left(\frac{n\pi}{h} z\right) \right] + C_{III}^2 \sin[\mu(L_2 - x)] \cosh \mu(z + h)$$

Solution for Region III as shown above:

From symmetry considerations, we see that φ_{III} is similar to φ_I with the following change:

$$x \rightarrow L_2 - x$$

- Far field boundary condition is satisfied. φ_{III} is bounded as $x \rightarrow \infty$.
- Back wall boundary condition g_4 is satisfied.
- By accounting for the horizontal length L2 of the OWC chamber, we are also enabling Region II to be solved. There will be a series of equations relating all solution coefficients.

Note that we could have combined the constant part of $e^{\frac{n\pi}{h}[L_2 - x]} = e^{\frac{n\pi}{h}[L_2]} e^{\frac{n\pi}{h}[x]} = Ce^{\frac{n\pi}{h}[x]}$
Into the coefficient C_{III}^1, but we chose not to at this time.

Note also that the infinite series for Regions I and III could begin at n = 1 instead of n = 0 because of the sine term in the series.

Consider the velocity potentials determined for the regions before, in, and after the OWC chamber – regions I, II and III respectively. In particular, consider ϕ_{II}. The previous analysis assumed that the chamber gage pressure P was constant in order to get a first-order approximation to the needed A coefficients. While useful to develop the methodology, it is unrealistic. In particular, it ignores the obvious relationship between flow and gage pressure, where gage pressure creates a flow through the wells turbine prototype on top of the OWC chamber. The unphysical nature of this assumption becomes even more apparent when one realizes that the A coefficients can be determined for region II without considering the boundary conditions related to the back wall of the OWC chamber. Therefore, under the assumption of constant P, the length of the back wall is immaterial to the analysis.

$$\varphi_I = (\eta_0 e^{-ik_0(x-l_1)} + A_0 e^{ik_0(x-l_1)}) \frac{\cosh k_0(z+h)}{\cosh k_0 h} + \sum_1^\infty A_n e^{k_n(x-l_1)} \frac{\cos k_n(z+h)}{\cos k_n h}$$

$$\phi_{II} = v(x,z) + \psi(z)$$

$$= i(-\eta_0 + A_0) \frac{\cos k_0(x-l_2)}{\sin k_0(l_2-l_1)} \frac{\cosh k_0(z+h)}{\cosh k_0 h} - \sum_1^\infty A_n \frac{\cosh k_n(x-l_2)}{\sinh k_n(l_2-l_1)} \frac{\cos k_n(z+h)}{\cos k_n h} + \frac{iwP}{\rho g K}$$

$$\varphi_{III} = (\eta_{III} e^{-ik_0(x-l_2)} + A_{III} e^{-ik_0(x-l_2)}) \frac{\cosh k_0(z+h)}{\cosh k_0 h} + \sum_1^\infty A_n e^{-k_n(x-l_2)} \frac{\cos k_n(z+h)}{\cos k_n h}$$

Conceptual approach to functionalize gage pressure P. We will achieve the functionalization of gage pressure P in two ways:

1. Approach #1: Use Bernoulli's equation to get a functional relationship between P and v through the OWC chamber. This approach is reasonable as the frequencies of the water waves in the OWC chamber are relatively low and we will not be anywhere near Mach 1. That is, we can consider a homogeneous compression of the air inside the chamber, from the water level to the top of the OWC chamber. This is the most analytical approach of the two approaches, but will require a term for energy loss due to the Wells turbine prototype and other losses from air flow through the connecting annulus. We will estimate these until we get sufficient data to measure the losses.

Consider Bernoulli's Equation connecting inside the chamber (subscript 1) and in the annulus just outside the chamber exit (subscript 2).

$$\frac{P_1}{\rho g} + Z_1 + \frac{v_1^2}{2g} - \text{energy loss terms} = \frac{P_2}{\rho g} + Z_2 + \frac{v_2^2}{2g}$$

We can ignore the insignificant contributions from Z_1 and Z_2, the air depth differences in the OWC

chamber, set the atmospheric pressure P_2 to zero, calculate v_1 and v_2 from the known volumes of the OWC chamber and the annulus, estimate or measure the energy losses, and thereby arrive at a P gage pressure equation to be used in the ϕ_{II} velocity potential equation.

2. Approach #2: Do controlled experiments to generate a curve of P versus flow rate for the OWC chamber, and then fit the curve with an appropriate function. This experimentally-determined function will be used to generate the appropriate P pressure function to be used in the ϕ_{II} velocity potential equation. In practice, we will first generate a set of curves for different constant rotation speeds of the turbine blades with the diaphragm completely open. We will then allow the turbine blades to free spin under varying differential pressure values and generate the P vs flow curve.

Both approaches require measurements to get experimentally-determined, *ad hoc* values for the best P equation. The Bernoulli's equation approach, approach #1, requires early estimation of some parameters, but this is only a temporary measure until the necessary data is obtained to determine the *ad hoc* values.

Having functionalized gage pressure P, we anticipate that determination of the A coefficients and the ultimate solution of the velocity potential equations will be appropriately sensitive to the OWC chamber back wall depth into the water.

Review of the earlier results indicated the following issues:

1. Finding the solution of the flow potentials in regions I and II did not require any information about region III. In other words, the boundary conditions between regions II and III were irrelevant. This could not be correct.

2. A careful analysis of the region I flow potential indicated that the incident and diffracted waves were of the same height. This again is inconsistent with reality, as energy is transmitted past region I into regions II and III, necessarily making the diffracted wave height lower than the incident wave height.

3. The earlier analysis assumed a fixed gage pressure inside the OWC chamber; i.e., in region II. This could not be correct, as it should have a dependence on the depth of the chamber walls into the water. Note that this does not include time dependence as that part of the solution was separated out.

I went back and reconsidered my assumptions, and made the following changes.

4. Boundary conditions on the walls must be treated in their entirety, not using part of the condition as done previously. For example, on the wall that the incident wave strikes, one of the boundary conditions is:

$$g(z) = \begin{cases} 0 & -d_1 < z < 0 \\ \varphi_1 = \varphi_2 & -h < z < -d_1 \end{cases}$$

This is correctly handled by expressing g(z) as a Fourier Series, and not just using the g(z)=0 part of the boundary condition.

5. Use the OWC chamber geometry and Bernoulli's equation and find an expression of gage pressure as a function of the:
   a. average flow rate in the OWC chamber, and,
   b. the flow rate through the annulus on the top of the chamber.

Progress to date:

6. Preliminary Fourier series expression found for $g_1(z)$. Other boundary conditions are near the same preliminary state of completion.
7. Preliminary gage pressure expression found.

The next phase includes refinement and evaluation of the expressions. This will require significant automation support, mainly MATLAB programming.

The logic now requires that the boundary conditions be expressed as Fourier series on the front and back walls of regions I and III, respectively. This avoids the logical inconsistencies identified and detailed in previous documents. Namely, that the reflected wave amplitude always equaled the incident wave amplitude, and also that the back wall plate depth did not affect the solutions for the wave potential. These observations indicated that logical inconsistencies were in the model.
The general approach is to solve the Laplace equation in the three regions I, II, and III with the indicated boundary conditions. The significant difference is in the expression of the aforementioned boundary conditions as Fourier series.

Region I:

$$\nabla^2\varphi = 0 \xrightarrow{yields} X''Z + XZ'' = 0 \xrightarrow{yields} \frac{X''}{X} + \frac{Z''}{Z} = 0 \xrightarrow{yields} \frac{X''}{X} = -\frac{Z''}{Z} = \lambda, where\ \lambda = \begin{cases} 0 & case\ 1 \\ -k^2 & case\ 2 \\ +k^2 & case\ 3 \end{cases}$$

In other words, $X'' - \lambda X = 0$, and $Z'' + \lambda Z = 0$ are the two equations of interest
We will see that only case 2, $\lambda = -k^2$ has nontrivial solutions.

Case 1: $\lambda = 0$ has only trivial roots

$Z'' = 0 \xrightarrow{yields} Z = C_3 + C_4 Z \xrightarrow{yields} Z'(-h) = C_4 = 0$ By floor boundary condition

Type equation here.

Therefore, $Z = C_3$, and therefore we have $Z' = 0$ for all z. (This is used immediately below.)
But because of the surface boundary condition

$\frac{\partial^2 \Phi}{\partial t^2} + g\frac{\partial \Phi}{\partial z} = 0$, where $= XZT = \varphi T$,

We have

$$\frac{\partial^2 XZT}{\partial t^2} + g\frac{\partial XZT}{\partial z} = 0 \xrightarrow{yields} XZT'' + gXZ'T = 0 \xrightarrow{yields} Z' = \left(-\frac{T''}{gT}\right)Z = 0 \xrightarrow{yields} Z(z) = 0.$$

Thus only the trivial solution exists for case I.

Note: the other possibility is that $\left(-\frac{T''}{gT}\right) = 0$, but this is easily seen to not be the case. Take a sinusoidal wave for example. Then $\Phi = XZT = \varphi T = \mathrm{Ze}^{-\mathrm{ikx+iwt}}$, and $\left(-\frac{T''}{gT}\right) = \frac{w^2}{g}$, which is only 0 if the angular frequency w is 0. Therefore Case I has only the trivial solution. Similarly,

Case 3: $\lambda = k^2$ has only trivial roots. We will not show this at this time, but it has been shown in our earlier documents.

Case 2: $\lambda = -k^2$ has meaningful roots.

$$X'' + k^2X = 0 \xrightarrow{yields} \begin{cases} X = C_1 sinkx + C_2 coskx, \\ X = C_3 e^{-ikx} + C_4 e^{ikx} \end{cases}$$

$$Z'' - k^2Z = 0 \xrightarrow{yields} \begin{cases} Z = C_5 \sinh(kz) + C_6 \cosh(kz) \\ Z = C_7 e^{-kz} + C_8 e^{kz} \end{cases}$$

Working first with the Z equations: Applying Z floor and surface boundary conditions:

Floor boundary condition: $Z'(-h) = 0 \xrightarrow{yields} C_5 \cosh(-kh) + C_6 \sinh(-kh) = 0$

$\xrightarrow{yields} C_5 \cosh(kh) - C_6 \sinh(kh) = 0 \xrightarrow{yields} C_5 = C_6 \frac{\sinh(kh)}{\cosh(kh)}$

Placing this result for C_5 back into the equation for Z:

$$Z(z) = C_6 \frac{\sinh(kh)}{\cosh(kh)} \sinh(kz) + C_6 \cosh(kz)$$

$$= \frac{C_6}{\cosh(kh)} [\sinh(kh)\sinh(kz) + \cosh(kh)\cosh(kz)]$$

$$= \frac{C_6}{\cosh(kh)} \cosh[k(z+h)]$$

By letting $z = -h$, or z=0 in the above expression, we can write the alternative equations

$$Z(z) = \frac{C_6}{\cosh(kh)} \cosh[k(z+h)] = Z(-h)\cosh[k(z+h)] = \frac{Z(0)}{\cosh(kh)} \cosh[k(z+h)]$$

Surface boundary condition: The equation $\frac{\partial^2 \Phi}{\partial t^2} + g\frac{\partial \Phi}{\partial z} = 0 \xrightarrow{yields} Z'(0) = \left(-\frac{T''}{gT}\right) Z(0) = KZ(0)$, and using the above expression for Z(z), we get the well-known **dispersion relation**

$$Z'(0) = KZ(0) \xrightarrow{yields} \frac{C_6}{\cosh(kh)} \mathrm{k}\sinh(kh) = K\frac{C_6}{\cosh(kh)} \cosh(kh) \xrightarrow{yields} k\tanh(kh) = K$$

The dispersion relation will be used to determine the allowed eigenvalues of k to be used in the ultimate solution. Note that $= \frac{w^2}{g}$, as usual, when the incoming wave is sinusoidal. This was mentioned previously in this document.

Now we work with the X equations. This requires using the "new" boundary value equations expressed as Fourier series.

The first boundary condition expressed as a Fourier series is the **front wall boundary** between regions I and II, and is

$$g_1(z) = \begin{cases} \frac{\partial \varphi_I}{\partial x} = 0 & -d_1 < z < h \\ \frac{\partial \varphi_I}{\partial x} = \frac{\partial \varphi_{II}}{\partial x} & -h < z < -d_1 \end{cases} \quad \text{Where}$$

$$\frac{\partial \varphi_I}{\partial x} = \frac{dX}{dx} Z = X'(0)Z = \frac{X'(0)C_4}{cosh(kh)} \cosh[k(h+z)]$$

Note that $X' = X'(x = l_1) = X'(0)$, and is used for convenience throughout.

And the Fourier series representation is

$$g_1(z) = \frac{a_0}{2} + \sum_{n=1}^{\infty} a_n cos\left(n\pi/_h\right) z + \sum_{n=1}^{\infty} b_n sin\left(n\pi/_h\right) z$$

Where

$$a_0 = \frac{1}{h}\int_{-h}^{h} g_1(z)\, dz = \frac{1}{h}\int_{-h}^{-d_1} \frac{\partial \varphi_I}{\partial x}\, dz = \frac{1}{h}\int_{-h}^{-d_1} \frac{\partial \varphi_I}{\partial x}\, dz$$

$$= \frac{1}{h}\int_{-h}^{-d_1} \frac{X'(0)C_4}{cosh(kh)} \cosh\left(k(h+z)\right) dz$$

Therefore

$$a_0 = \frac{1}{h}\frac{X'(0)C_4}{cosh(kh)}\int_{-h}^{-d_1} \cosh\left(k(h+z)\right) dz$$

Similarly

$$a_n = \frac{1}{h}\frac{X'(0)C_4}{cosh(kh)}\int_{-h}^{-d_1} \cosh\left(k(h+z)\right) cos\left(n\pi/_h\right) z\ dz$$

and

$$b_n = \frac{1}{h}\frac{X'(0)C_4}{cosh(kh)}\int_{-h}^{-d_1} \cosh\left(k(h+z)\right) sin\left(n\pi/_h\right) z\ dz$$

We therefore arrive at the values for the Fourier series coefficients:

$$a_0 = -\frac{1}{hk}\frac{X'(0)C_4}{cosh(kh)} sinh\left(k(h-d_1)\right)$$

$$a_n = \frac{1}{h}\frac{X'(0)C_4 C}{cosh(kh)}\left[\left(\frac{hk}{n\pi}\right)A - B\right]$$

$$b_n = -\frac{1}{h}\frac{X'(0)C_4 C}{cosh(kh)}\left[D + \left(\frac{hk}{n\pi}\right)E\right]$$

The following integrals were evaluated and used in determining the above (see appendix A)

$$\int_{-h}^{-d_1} \cosh\left(k(h+z)\cos\left(\frac{n\pi}{h}z\right)\right) dz = C\left[\left(\frac{hk}{n\pi}\right)A - B\right]$$

$$\int_{-h}^{-d_1} \sinh\left(k(h+z)\sin\left(\frac{n\pi}{h}z\right)\right) dz = -C\left[A + \left(\frac{hk}{n\pi}\right)B\right]$$

$$\int_{-h}^{-d_1} \cosh\left(k(h+z)\sin\left(\frac{n\pi}{h}z\right)\right) dz = -C\left[D + \left(\frac{hk}{n\pi}\right)E\right]$$

$$\int_{-h}^{-d_1} \sinh\left(k(h+z)\cos\left(\frac{n\pi}{h}z\right)\right) dz = C\left[\left(\frac{hk}{n\pi}\right)D - E\right]$$

Where

$$C = \frac{hk/n\pi}{k\left[1 + \left(hk/n\pi\right)^2\right]}$$

$$A = sinh(k[h - d_1])cos\left(\frac{n\pi}{h}\right)d_1$$

$$B = cosh(k[h - d_1])sin\left(\frac{n\pi}{h}\right)d_1$$

$$D = cosh(k[h - d_1])cos\left(\frac{n\pi}{h}\right)d_1 - (-1)^n$$

$$E = sinh(k[h - d_1])sin\left(\frac{n\pi}{h}\right)d_1$$

Notes: By using trigonometric identities, we can simplify the Fourier series as follows:

$$g_1(z) = \frac{a_0}{2} + \sum_{n=1}^{\infty}\left\{\frac{1}{h}\frac{X'(0)C_4C}{cosh(kh)}\left[\left(\frac{hk}{n\pi}\right)A - B\right]cos\left(n\pi/_h\right)z - \frac{1}{h}\frac{X'(0)C_4C}{cosh(kh)}\left[D + \left(\frac{hk}{n\pi}\right)E\right]sin\left(n\pi/_h\right)z\right\}$$

$$g_1(z) = \frac{a_0}{2} + \frac{1}{h}\frac{X'(0)C_4C}{cosh(kh)}\sum_{n=1}^{\infty}\left\{\left[\left(\frac{hk}{n\pi}\right)A - B\right]cos\left(n\pi/_h\right)z - \left[D + \left(\frac{hk}{n\pi}\right)E\right]sin\left(n\pi/_h\right)z\right\}$$

$$g_1(z) = \frac{a_0}{2} + \frac{1}{h}\frac{X'(0)C_4C}{\cosh(kh)}\sum_{n=1}^{\infty}\left\{\left(\frac{hk}{n\pi}\right)\left[A\cos\left(n\pi/_h\right)z - E\sin\left(n\pi/_h\right)z\right] - \left[B\cos\left(n\pi/_h\right)z + D\sin\left(n\pi/_h\right)z\right]\right\}$$

$$g_1(z) = \frac{a_0}{2} + \frac{1}{h}\frac{X'(0)C_4C}{\cosh(kh)}\sum_{n=1}^{\infty}\left\{\left(\frac{hk}{n\pi}\right)\sinh(k[h - d_1])\left(\cos\left(\frac{n\pi}{h}\right)d_1\cos\left(n\pi/_h\right)z - \sin\left(\frac{n\pi}{h}\right)d_1\sin\left(n\pi/_h\right)z\right) - \cosh(k[h - d_1])\left[\sin\left(\frac{n\pi}{h}\right)d_1\cos\left(n\pi/_h\right)z + \left(\cos\left(\frac{n\pi}{h}\right)d_1 - (-1)^n\right)\sin\left(n\pi/_h\right)z\right]\right\}$$

$$g_1(z) = \frac{a_0}{2} + \frac{1}{h}\frac{X'(0)C_4C}{\cosh(kh)}\sum_{n=1}^{\infty}\left\{\left(\frac{hk}{n\pi}\right)\sinh(k[h - d_1])\cos\left(\left(n\pi/_h\right)(d_1 + z)\right) - \cosh(k[h - d_1])\left(\sin\left(\left(n\pi/_h\right)(d_1 + z)\right) + (-1)^n\sin\left(n\pi/_h\right)z\right)\right\}$$

APPENDIX 2:
OWC DATA TAKEN AT TEDEC (MMA) USING MICRO-OWC CHAMBER AND TURBINE

TABLE A2-1. TRANSCRIPTION OF TEST DATA FROM MMA TESTING IN SUMMER 2011

		1	2			3	4
DP at CLOSED OWC		Head Space= 8				Head Space= 5	
	Reflector Plate Length= 0				Reflector Plate Length= 6		
		MAX. OWC Pressure (in. wc)				MAX. OWC Pressure (in. wc)	
		Wave Amplitude (inch)		DP max with		Wave Amplitude (inch)	
	Time (s)	2.0	2.5	0% OPEN OWC at 2.5 inch	Time (s)	2.0	2.5
	0.75		0.04		0.75		
	1		0.46		1		
	1.25	0.27	1.01 ???		1.25		0.47
	1.5	0.16			1.5		0.373
	Reflector Plate Length= 6				Reflector Plate Length= 6		
DP at CLOSED OWC= 0.6		MAX. OWC Pressure (in. wc)				MAX. OWC Pressure (in. wc)	
		Wave Amplitude (inch)		DP max with		Wave Amplitude (inch)	
	Time (s)	2.0	2.5	0% OPEN OWC at 2.5 inch	Time (s)	2.0	2.5
	0.50	0			0.75		
	0.75	0.03			1	0.31	0.59
	1.0	0.37	0.59	0.59	1.25	0.39	
	1.25	0.33			1.5	0.38	
	1.5	0					
	Reflector Plate Length= 12				Reflector Plate Length= 12		
		MAX. OWC Pressure (in. wc)				MAX. OWC Pressure (in. wc)	
DP max with		Wave Amplitude (inch)		DP max with		Wave Amplitude (inch)	
0% OPEN OWC at 2.0 inch	Time (s)	2.0	2.5	0% OPEN OWC at 2.5 inch	Time (s)	2.0	2.5
0.19	0.75	0.19	0.39		0.75		
	1	0.42	0.46		1		
0.72	1.25	0.36	0.45		1.25		0.50
	1.5	0.26			1.5		
				Summary of results using 2.0 inch Wave			
		8 inch Head Space				5 inch Head Space	
		0 Reflector	6 inch reflecto	12 inch.	0 Reflector	6 inch reflecto	12 inch.
	0.50		0				
	0.75		0.03	0.19	0.19		
	1.0		0.37	0.42	0.5	0.31	
	1.25	0.27	0.33	0.36	0.72	0.39	
	1.5	0.16	0	0.26		0.38	
	0.50						
	0.75	0.04		0.39			
	1.0	0.46	0.59	0.46		0.59	
	1.25			0.45	0.47		0.50
	1.5				0.373		

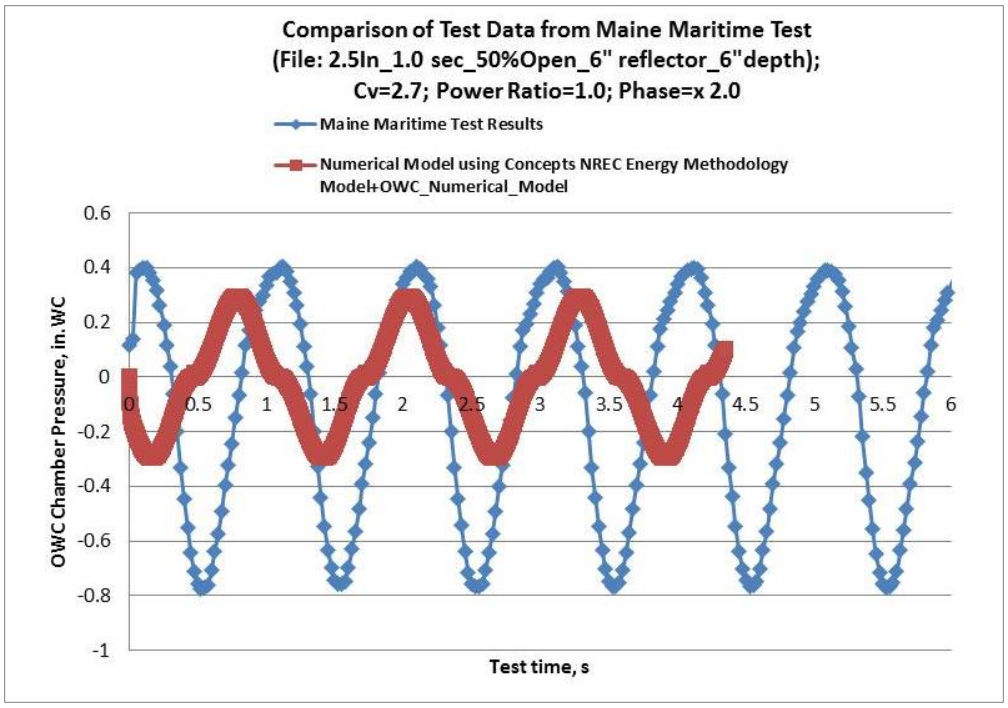

Figure A2-1. Comparison of Numerical Model with Test Results Measured at MMA

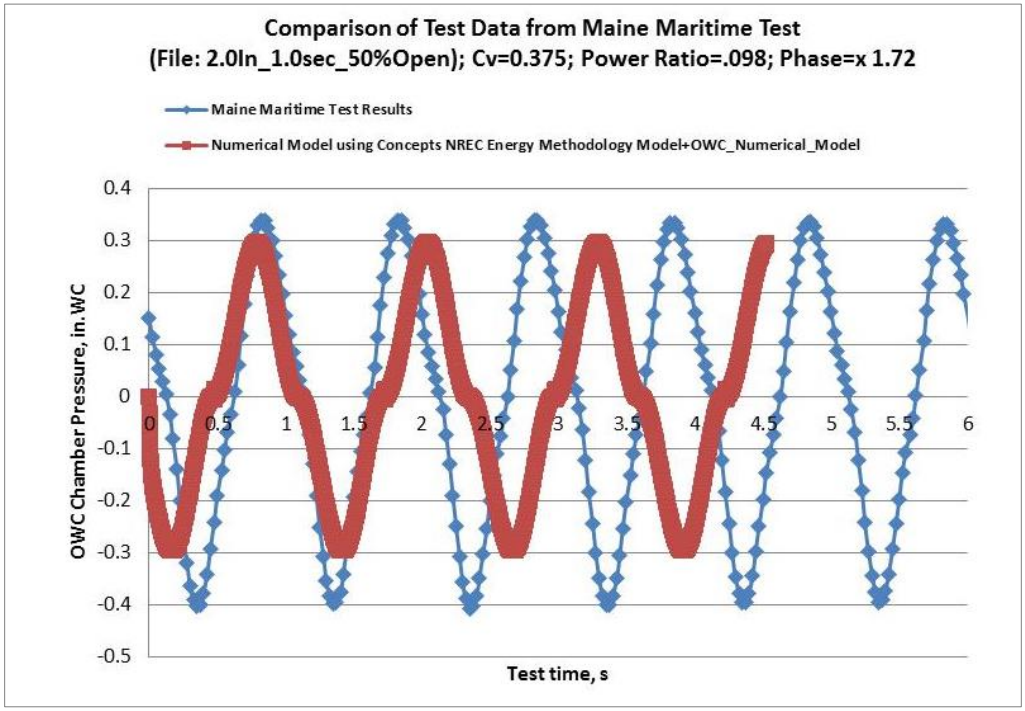

Figure A2-2. Comparison of Numerical Model with Test Results Measured at MMA

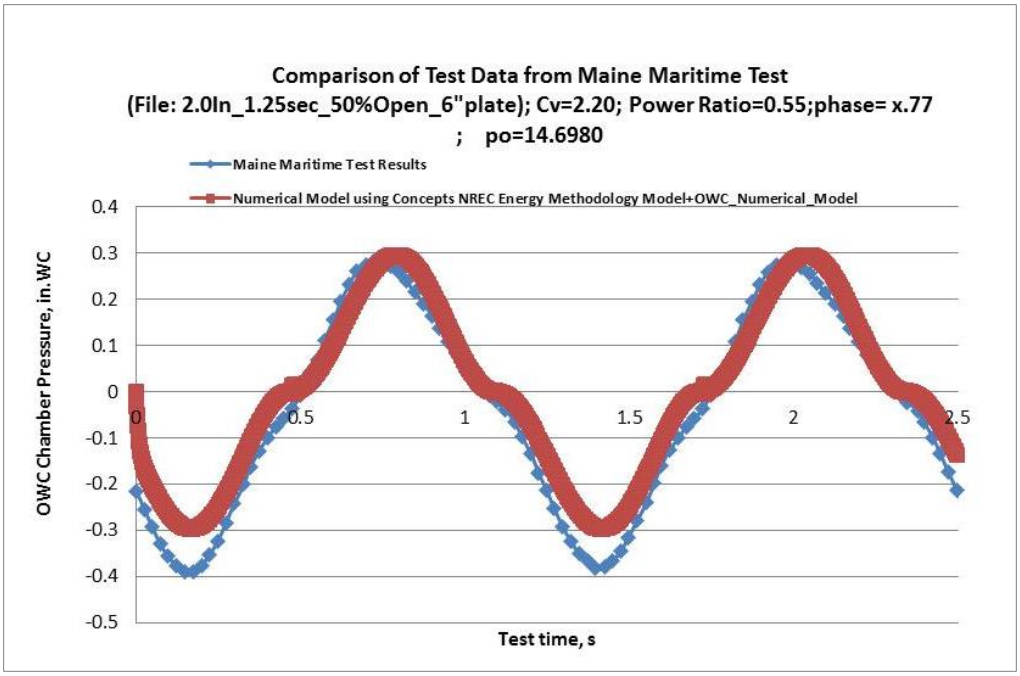

Figure A2-3. Comparison of Numerical Model with Test Results Measured at MMA

APPENDIX 3:
REFERENCES

[1] Falnes, J., "Optimum Control of Oscillation of Wave-Energy Converters," *Intl. J. of Offshore and Polar Engineering*, **12** (2), 2002, ISSN 1053-5381.

[2] "Oscillating Water Column Wave Energy Converter Evaluation Report," The Carbon Trust, Marine Energy Challenge, Arup Energy, 2005.

[3] WaveNet, "Technical Summary Report: Results from the Work of the European Thematic Network on Wave Energy," Energy, Environment and Sustainable Development, ERK5-CT-1999-20001, March 2003.

[4] Evans, D. V., and Porter, R., "Hydrodynamic Characteristics of an Oscillating Water Column Device," *Applied Ocean Research*, Vol. 17, Issue 3, pp. 155–164, 1995, Elsevier Ltd., DOI: 10.1016/0141-1187(95)00008-9.

[5] Suzuki, M., and Arakawa, C., "Design Method of Wave Power Generating System with Wells Turbine," *Int. J. of Offshore and Polar Engineering*, **14** (3), 2004, ISSN: 1053-5381.

[6] Sarmento, A. J. N. A., and de O. Falcão, A. F., "Wave Generation by an Oscillating Surface-Pressure and Its Application in Wave-Energy Extraction," *J. of Fluid Mechanics*, Cambridge University Press, **150**: 467–485, 1985, DOI: 10.1017/S0022112085000234.

[7] de O. Falcão, A. F., and Justino, P. A. P., "OWC Wave Energy Devices with Air Flow Control," *Ocean Engineering*, **26** (12): 1275–1295, 1999, DOI: 10.1016/S0029-8018(98)00075-4.

[8] Tease, W. K., Lees, J., and Hall, A., "Advances in Oscillating Water Column Air Turbine Development," *Proceedings of the 7th European Wave and Tidal Energy Conference*, Porto, Portugal, 2007.

[9] Budal, K., and Falnes, J., "A Resonant Point Absorber of Ocean-Wave Power," *Nature*, **256**: 478–479, 1975. Corrigendum in **257**: 626.

[10] Khaligh, A., and Onar, O. C., *Energy Harvesting: Solar, Wind, and Ocean Energy Conversion Systems*, Chapter 4: Ocean Wave Energy Harvesting, CRC Press, 2009, ISBN-13: 978-1439815083.

[11] Anand, S., Jayashankar, V., Nagata, S., Toyota, K., Takao, M, and Setoguchi, T., "Turbines for Wave Energy Plants," *Proceedings of the 8th International Symposium on Experimental and Computational Aerothermodynamics of Internal Flows*, Paper ISAIF8-31, Lyon, July 2007.

[12] Corsini, A., and Rispoli, F., "Modeling of Wave Energy Conversion with an Oscillating Water Column Device," Dipartimento di Meccanica e Aeronautica, Università di Roma "La Sapienza," Roma, Italy.

[13] Sarmento, A. J. N. A., Gato, L. M. C., de O. Falcão, A. F., "Wave-Energy Absorption by an OWC Device with Blade-Pitch-Controlled Air-Turbine," *Proceedings of the 6th International Offshore Mechanics and Arctic Engineering Symposium*, ASME, **2**: 465–473.

[14] Falnes, J., Principles for Capture of Energy from Ocean Waves. Phase Control and Optimum Oscillation," Department of Physics, NTNU, N-7034 Trondheim, Norway, 1997.

[15] de O. Falcão, A. F., "Control of an Oscillating-Water-Column Wave Power Plant for Maximum Energy Production," *Applied Ocean Research*, **24**: 73–82, 2002.

[16] El-Wakil, M. M., *Powerplant Technology*, McGraw-Hill, Chapter 15: Energy from Oceans, 2002, ISBN: 0-07-287102-4.

[17] Lee, C.-H., and Newman, J. N., "Wave Interactions with an Oscillating Water Column," *Proceedings of the Sixth International Offshore and Polar Engineering Conference*, Los Angeles, California, USA, May 26–31, 1996.

[18] Suzuki, M., and Arakawa, C., "Numerical Methods to Predict Characteristics of Oscillating Water Column for Terminator-type Wave Energy Converter," *The Int. Society of Offshore and Polar Engineers*, **15** (4): 292–299, 2005, ISOPE-05-15-4-292.

[19] Suzuki, M., Kuboki, T., Arakawa, C., and Nagata, S., "Numerical Analysis on 2-D Optimal Profile of Floating Device with OWC-type Wave Energy Converter," *The Int. Society of Offshore and Polar Engineers*, **16** (4): 297–304, 2006, ISOPE-06-16-4-297.

[20] Holmes, P., "Professional Development Programme: Coastal Infrastructure Design, Construction and Maintenance; A Course in Coastal Defense Systems I; Chapter 5 – Coastal Processes: Waves," July 2001.[8]

http://www.oas.org/cdcm_train/courses/course21/chap_05.pdf

[21] Gato, L. M. C., Eça, L. R. C., and de O. Falcão, A. F., Performance of the Wells Turbine with Variable Pitch Rotor Blades," *Journal of Energy Resources Technology*, **113**, September 1991.

OTHER RESOURCES THAT MAY BE OF INTEREST TO THE READER

Arlitt, R. G. H., Tease, K., Starzmann, R., and Lees, J., "Dynamic System Modeling of an Oscillating Water Column Wave Power Plant Based on Characteristic Curves Obtained by Computational Fluid Dynamics to Enhance Engineered Reliability," *7th European Wave and Tidal Energy Conference*, Porto, Portugal, 2007.

de O. Falcão, A. F., and Rodrigues, R. J. A., "Stochastic Modelling of OWC Wave Power Plant Performance," *Applied Ocean Research*, **24** (2): 59–71, 2002, DOI: 10.1016/S0141-1187(02)00022-6.

Boyle, G., "Renewable Energy: Power for a Sustainable Future," Oxford University Press; Third Edition, p. 298, 2012, ISBN-13: 978-0199545339.

Dorrell, D., "Considerations on Wave Energy in Scotland, Department of Electronics and Electrical Engineering, The Sustainable Development of Renewable Energy," Wolfson Medical Building, University of Glasgow,

Evans, D. V., "The Oscillating Water Column Wave-energy Device," *IMA J. of Applied Mathematics*, **22** (4): 423–433, 1978, DOI: 10.1093/imamat/22.4.423.

Finnigan, T., and Auld, D., "Model Testing of a Variable-Pitch Aerodynamic Turbine," *Proceedings of The Thirteenth International Offshore and Polar Engineering Conference*, Honolulu, Hawaii, USA, May 25–30, 2003.

Hansen, T., "Catching a Wave," *Power Engineering*, 2005, http://www.power-eng.com/articles/print/volume-109/issue-9/features/catching-a-wave.html.

Martins-rivas, H., and Mei, C. C., "Wave Power Extraction from an Oscillating Water Column along a Straight Coast," *Ocean Engineering*, **36** (6–7): 426–433, 2009, DOI: 10.1016/j.oceaneng.2009.01.009.

Setoguchi, T., Takao, M., and Kaneko, K., "A Comparison of Performances of Turbines for Wave Power Conversion," *Int. J. of Rotating Machinery*, **6** (2): 129–134, 2000.

Suzuki, M., and Arakawa, C., "Influence of Blade Profiles on Flow around Wells Turbine," *Int. J. of Fluid Machinery and Systems*, **1** (1), October–December 2008.

[8] This is a course that has developed the solution to all of the mathematics of water wave energy, including the Velocity potential function (φ), wave velocity (Ux, Vy), the probability mathematics for varying wave amplitude and frequency, and defining spectra functions.

Suzuki, M., Takao, M., Satoh, E., Nagata, S., Toyota, K., and Setoguchi, T., "Performance Prediction of OWC Type Small Size Wave Power Device with Impulse Turbine," *J. of Fluid Science and Technology*, **3** (3): 466–475, 2008, DOI: 10.1299/jfst.3.466.

Whitham, G. B., *Linear and Nonlinear Waves*, Wiley-Interscience, 1st edition, 1999, ISBN-13: 978-0471359425.

"Electric Power from Ocean Waves," Wavemill Energy Corporation, 2005, www.wavemill.com.

"Options for the Development of Wave Energy in Ireland: A Public Consultation Document," Marine Institute and Sustainable Energy Ireland, 2002.